

Drivers of plant nutrient acquisition and allocation strategies and their influence  
on plant responses to environmental change

by

Evan A. Perkowski, B.S.

A Dissertation

In

Biological Sciences

Submitted to the Graduate Faculty  
of Texas Tech University in  
Partial Fulfillment of  
the Requirements for  
the Degree of

Doctor of Philosophy

Approved

Nicholas G. Smith, Ph.D.  
Chair of Committee

Aimée T. Classen, Ph.D.

Natasja van Gestel, Ph.D.

Lindsey C. Slaughter, Ph.D.

Dylan W. Schwilk, Ph.D.

Mark Sheridan, Ph.D.  
Dean of the Graduate School

May 2023

Copyright 2023, Evan A. Perkowski

## Acknowledgements

Placeholder for text

**Table of Contents**

<b>Acknowledgements . . . . .</b>	ii
<b>Abstract . . . . .</b>	vii
<b>List of Tables . . . . .</b>	viii
<b>List of Figures . . . . .</b>	x
<b>1. Introduction . . . . .</b>	1
<b>2. Structural carbon costs to acquire nitrogen are determined by nitrogen and light availability in two species with different nitrogen acquisition strategies . . . . .</b>	8
2.1    Introduction . . . . .	8
2.2    Methods . . . . .	12
2.2.1 <i>Experiment setup</i> . . . . .	12
2.2.2 <i>Plant measurements and calculations</i> . . . . .	13
2.2.3 <i>Statistical analyses</i> . . . . .	14
2.3    Results . . . . .	16
2.3.1 <i>Carbon costs to acquire nitrogen</i> . . . . .	16
2.3.2 <i>Whole plant nitrogen biomass</i> . . . . .	19
2.3.3 <i>Root carbon biomass</i> . . . . .	21
2.3.4 <i>Root nodule biomass</i> . . . . .	23
2.4    Discussion . . . . .	27
2.4.1 <i>Carbon costs to acquire nitrogen increase with light availability and decrease with fertilization</i> . . . . .	27
2.4.2 <i>Modeling implications</i> . . . . .	29
2.4.3 <i>Study limitations</i> . . . . .	31
2.4.4 <i>Conclusions</i> . . . . .	33
<b>3. Soil nitrogen availability modifies leaf nitrogen economies in mature temperate deciduous forests: a direct test of photosynthetic least-cost theory . . . . .</b>	35
3.1    Introduction . . . . .	35

3.2 Methods . . . . .	39
3.2.1 <i>Study site description</i> . . . . .	39
3.2.2 <i>Experimental design</i> . . . . .	40
3.2.3 <i>Leaf gas exchange and trait measurements</i> . . . . .	40
3.2.4 $A_{net}/C_i$ curve-fitting and parameter estimation . . . . .	43
3.2.5 Proportion of leaf nitrogen allocated to photosynthesis and structure . . . . .	45
3.2.6 Tradeoffs between nitrogen and water use . . . . .	46
3.2.7 Soil nitrogen availability and pH . . . . .	47
3.2.8 Statistical analyses . . . . .	49
3.3 Results . . . . .	51
3.3.1 Leaf N content . . . . .	51
3.3.2 Net photosynthesis and leaf biochemistry . . . . .	54
3.3.3 Leaf N allocation . . . . .	57
3.3.4 Tradeoffs between nitrogen and water use . . . . .	60
3.4 Discussion . . . . .	63
3.4.1 Soil nitrogen availability modifies tradeoffs between nitrogen and water use . . . . .	64
3.4.2 Soil pH did not modify tradeoffs between nitrogen and water usage . . . . .	66
3.4.3 Species identity explains a large amount of variation in leaf and whole plant traits . . . . .	67
3.4.4 Implications for photosynthetic least-cost theory model development . . . . .	68
3.4.5 Conclusions . . . . .	70
4. The relative cost of resource use for photosynthesis drives variance in leaf nitrogen content across climate and soil resource availability gradients . . . . .	71
4.1 Introduction . . . . .	71
4.2 Methods . . . . .	77
4.2.1 Site descriptions and sampling methodology . . . . .	77

4.2.2	<i>Leaf trait measurements</i>	77
4.2.3	<i>Site climate data</i>	83
4.2.4	<i>Site edaphic characteristics</i>	83
4.2.5	<i>Plant functional group assignments</i>	85
4.2.6	<i>Data analysis</i>	86
4.3	Results	88
4.3.1	<i>Cost to acquire nitrogen relative to water (<math>\beta</math>)</i>	88
4.3.2	<i>Leaf <math>C_i:C_a</math> (<math>\chi</math>)</i>	92
4.3.3	<i>Leaf nitrogen content</i>	95
4.3.4	<i>Structural equation model</i>	99
4.4	Discussion	102
4.4.1	<i>Negative effects of <math>\chi</math> on <math>N_{\text{area}}</math> are driven by reductions in <math>M_{\text{area}}</math>, not <math>N_{\text{mass}}</math></i>	102
4.4.2	<i>Soil nitrogen availability increases <math>N_{\text{area}}</math> through changes in the cost to acquire nitrogen</i>	104
4.4.3	<i>Soil moisture increases <math>N_{\text{area}}</math> by facilitating increases in soil nitrogen availability</i>	105
4.4.4	<i>Indirect effects of climate on <math>N_{\text{area}}</math> are mediated through changes in leaf <math>C_i:C_a</math> and <math>\beta</math></i>	106
4.4.5	<i>Species identity traits modify effects of the environment on <math>\beta</math>, <math>\chi</math>, and <math>N_{\text{area}}</math></i>	106
4.4.6	<i>Next steps for optimality model development</i>	108
4.4.7	<i>Conclusions</i>	109
5.	<b>Optimal resource investment to photosynthetic capacity maximizes nutrient allocation to whole plant growth under elevated CO<sub>2</sub></b>	110
5.1	Introduction	110
5.2	Methods	115
5.2.1	<i>Seed treatments and experimental design</i>	115
5.2.2	<i>Growth chamber conditions</i>	116
5.2.3	<i>Leaf gas exchange measurements</i>	118

5.2.4 <i>Leaf trait measurements</i> . . . . .	119
5.2.5 <i>A/C<sub>i</sub> curve fitting and parameter estimation</i> . . . . .	121
5.2.6 Stomatal limitation . . . . .	121
5.2.7 <i>Proportion of leaf nitrogen allocated to photosynthesis and structure</i> . . . . .	122
5.2.8 <i>Whole plant traits</i> . . . . .	124
5.2.9 <i>Statistical analyses</i> . . . . .	126
5.3 Results . . . . .	128
5.3.1 <i>Leaf nitrogen and chlorophyll content</i> . . . . .	128
5.3.2 <i>Leaf biochemistry and stomatal conductance</i> . . . . .	132
5.3.3 <i>Leaf nitrogen allocation</i> . . . . .	136
5.3.4 <i>Whole plant traits</i> . . . . .	140
5.3.5 <i>Nitrogen fixation</i> . . . . .	144
5.4 Discussion . . . . .	148
5.4.1 <i>Soil nitrogen fertilization has divergent effects on leaf and whole plant acclimation responses to CO<sub>2</sub></i> . . . . .	149
5.4.2 <i>Implications for future model development</i> . . . . .	153
5.4.3 <i>Study limitations and future directions</i> . . . . .	154
5.4.4 <i>Conclusions</i> . . . . .	156
6. Conclusions . . . . .	158
References . . . . .	160

**Abstract**

## List of Tables

2.1 Analysis of variance results exploring species-specific effects of light availability, nitrogen fertilization, and their interactions on carbon costs to acquire nitrogen ( $N_{\text{cost}}$ ), whole-plant nitrogen biomass ( $N_{\text{wp}}$ ), and root carbon biomass ( $C_{\text{bg}}$ ) . . . . .	17
2.2 Analysis of variance results exploring effects of light availability, nitrogen fertilization, and their interactions on <i>G. max</i> root nodule biomass and the ratio of root nodule biomass to root biomass* . . . . .	24
2.3 Slopes of the regression line describing the relationship between each dependent variable and nitrogen fertilization at each light level* . . . . .	25
3.1 Effects of soil N availability, soil pH, and species on leaf N content per unit leaf area ( $N_{\text{area}}$ ), leaf N content per unit leaf mass ( $N_{\text{mass}}$ ), and leaf mass per unit leaf area ( $M_{\text{area}}$ ) . . . . .	52
3.2 Effects of soil N availability, soil pH, species, and $N_{\text{area}}$ on leaf biochemistry . . . . .	55
3.3 Effects of soil N availability, soil pH, and species on the proportion of leaf nitrogen content allocated to photosynthesis, Rubisco, bioenergetics, and structure . . . . .	58
3.4 Effects of soil N availability, soil pH, species, and $N_{\text{area}}$ on tradeoffs between nitrogen and water use . . . . .	61

4.1	Site locality information, sampling year(s), 2006-2020 mean annual precipitation (MAP; mm), mean annual temperature (MAT; °C), and water holding capacity (WHC; mm)* . . . . .	81
4.2	Effects of soil moisture, soil nitrogen availability, and plant functional group on $\beta$ . . . . .	90
4.3	Effects of soil moisture, soil nitrogen availability, and plant functional group on $\chi^*$ . . . . .	93
4.4	Effects of soil nitrogen fertilization, inoculation, and CO <sub>2</sub> treatments on $N_{\text{area}}$ , $N_{\text{mass}}$ , and $M_{\text{area}}$ . . . . .	97
4.5	Structural equation model results investigating direct effects of climatic and soil resource availability on $N_{\text{area}}$ , $N_{\text{mass}}$ , $M_{\text{area}}$ , $\chi$ , and $\beta$ . . . . .	100
5.1	Effects of soil nitrogen fertilization, inoculation, and CO <sub>2</sub> treatments on $N_{\text{area}}$ , $N_{\text{mass}}$ , $M_{\text{area}}$ , and $Chl_{\text{area}}$ . . . . .	130
5.2	Effects of soil nitrogen fertilization, inoculation, and CO <sub>2</sub> on leaf biochemistry . . . . .	134
5.3	Effects of soil N availability, soil pH, species, and $N_{\text{area}}$ on leaf nitrogen allocation . . . . .	138
5.4	Effects of soil N availability, soil pH, species, and $N_{\text{area}}$ on total leaf area, whole plant biomass, and carbon costs to acquire nitrogen . .	142
5.5	Effects of soil N availability, soil pH, species, and $N_{\text{area}}$ on root nodule biomass and plant investments in symbiotic nitrogen fixation	146

## List of Figures

2.1 Relationships between soil nitrogen fertilization and light availability on carbon costs to acquire nitrogen in <i>G. hirsutum</i> and <i>G. max</i> . . . . .	18
2.2 Relationships between soil nitrogen fertilization and light availability on whole-plant nitrogen biomass in <i>G. hirsutum</i> and <i>G. max</i> . . . . .	20
2.3 Relationships between soil nitrogen fertilization and light availability on root carbon biomass in <i>G. hirsutum</i> and <i>G. max</i> . . . . .	22
2.4 Effects of shade cover and nitrogen fertilization on root nodule biomass and the ratio of root nodule biomass to root biomass in <i>G. max</i> . . . . .	26
3.1 Effects of soil N availability and species on leaf N content per unit leaf area, leaf nitrogen content per unit leaf biomass, and leaf mass per leaf area . . . . .	53
3.2 Effects of soil N availability, species, and leaf N content leaf biochemistry . . . . .	56
3.3 Effects of soil N availability, species, and leaf N content on the fraction of leaf nitrogen allocated to photosynthesis and structure	59
3.4 Effects of soil N availability, species, and leaf N content on tradeoffs between nitrogen and water use . . . . .	62
4.1 Maps that detail site locations along 2006-2020 mean annual precipitation and mean annual temperature gradients in Texas, USA.	82

4.2 Effects of soil nitrogen availability and soil moisture on the unit cost ratio $\beta$	91
4.3 Effects of 4-day mean vapor pressure deficit, 2-day soil moisture (per water holding capacity), and soil nitrogen availability on $\chi$	94
4.4 Effects of $\chi$ , soil nitrogen availability, and soil moisture on leaf nitrogen content per unit leaf area, leaf nitrogen content per unit leaf biomass, and leaf mass per area.	98
4.5 Structural equation model results exploring direct and indirect drivers of $N_{\text{area}}$	101
5.1 Effects of $\text{CO}_2$ , fertilization, and inoculation on leaf nitrogen per unit leaf area, leaf nitrogen content, leaf mass per unit leaf area, and chlorophyll content per unit leaf area.	131
5.2 Effects of $\text{CO}_2$ , fertilization, and inoculation on maximum rate of Rubisco carboxylation, the maximum rate of RuBP regeneration, and the ratio of the maximum rate of RuBP regeneration to the maximum rate of Rubisco carboxylation leaf mass per unit leaf area, dark respiration, stomatal conductance, and stomatal limitation.	135
5.3 Effects of $\text{CO}_2$ , fertilization, and inoculation on the relative fraction of leaf nitrogen allocated to photosynthesis and the fraction of leaf nitrogen allocated to structure.	139
5.4 Effects of $\text{CO}_2$ , fertilization, and inoculation on total leaf area, total biomass, and structural carbon costs to acquire nitrogen.	143

5.5 Effects of CO <sub>2</sub> , fertilization, and inoculation on nodule biomass, nodule: root biomass, and percent nitrogen fixed from the atmo- sphere. . . . .	147
--	-----

# 1 Chapter 1

## 2 Introduction

3 Photosynthesis represents the largest carbon flux between the atmosphere  
4 and biosphere, and is regulated by complex ecosystem carbon and nutrient cy-  
5 cles (Hungate et al. 2003; IPCC 2021). As a result, the inclusion of robust,  
6 empirically tested representations of photosynthetic processes is critical in order  
7 for terrestrial biosphere models to accurately and reliably simulate carbon and  
8 nutrient fluxes between the atmosphere and terrestrial biosphere (Wieder et al.  
9 2015; Smith and Dukes 2013; Prentice et al. 2015; Oreskes et al. 1994). Despite  
10 evidence that the inclusion of coupled carbon and nutrient cycles can improve  
11 model uncertainty, widespread divergence in predicted carbon and nutrient fluxes  
12 is still apparent across model products (Arora et al. 2020; Friedlingstein et al.  
13 2014; Davies-Barnard et al. 2020). Divergence in predicted carbon and nutrient  
14 fluxes across terrestrial biosphere models may be due to an incomplete under-  
15 standing of how plants acclimate to changing environments (Smith and Dukes  
16 2013; Davies-Barnard et al. 2020), as terrestrial biosphere models are sensitive to  
17 the formulation of photosynthetic processes (Ziehn et al. 2011; Bonan et al. 2011;  
18 Booth et al. 2012; Smith et al. 2016; Smith et al. 2017; Rogers et al. 2017).

Many terrestrial biosphere models predict leaf-level photosynthesis through linear relationships between area-based leaf nitrogen content and the maximum rate of Ribulose-1,5-bisphosphate carboxylase/oxygenase ("Rubisco"), following from the idea that large fractions of leaf nitrogen content are allocated to the construction and maintenance of Rubisco and other photosynthetic enzymes (Evans

24 1989). The inclusion of coupled carbon and nutrient cycles in terrestrial biosphere  
25 models (Shi et al. 2016; Braghieri et al. 2022) allows for the prediction of leaf ni-  
26 trogen content through soil nitrogen availability, which causes models to indirectly  
27 predict photosynthetic processes through shifts in soil nitrogen availability (Smith  
28 et al. 2014; Lawrence et al. 2019). While these patterns are commonly observed  
29 in ecosystems globally (Brix 1971; Evans 1989; Liang et al. 2020; Firn et al. 2019),  
30 this formulation of photosynthetic processes does not allow for the prediction of  
31 leaf and whole plant acclimation responses to changing environments (Smith and  
32 Dukes 2013; Rogers et al. 2017; Harrison et al. 2021), and suggests that con-  
33 stant leaf nitrogen-photosynthesis relationships are ubiquitous across ecosystems.  
34 Incorporating leaf and whole plant acclimation schemes in terrestrial biosphere  
35 models is important (Smith and Dukes 2013), particularly because recent work  
36 indicates that variance in leaf nitrogen content and leaf photosynthesis across en-  
37 vironmental gradients may be better explained as an integrated product of leaf  
38 acclimation responses to changing climates and soil nitrogen availability than soil  
39 nitrogen availability alone (Dong et al. 2017; Dong et al. 2020; Smith et al. 2019;  
40 Querejeta et al. 2022; Dong et al. 2022; Westerband et al. 2023).

41 Photosynthetic least-cost theory (Prentice et al. 2014; Wang et al. 2017;  
42 Smith et al. 2019; Scott and Smith 2022; Harrison et al. 2021) provides a con-  
43 temporary framework for predicting leaf and whole plant acclimation responses  
44 to environmental change. The theory, which unifies photosynthetic optimal coor-  
45 dination (Chen et al. 1993; Maire et al. 2012) and least-cost (Wright et al. 2003)  
46 theories, posits that plants optimize photosynthetic processes by minimizing the  
47 summed cost of nitrogen and water use (referred to here and in the rest of this dis-

48 sertation as  $\beta$ ). The minimized summed cost of nitrogen and water use is dictated  
49 by the ratio of intercellular CO<sub>2</sub> to atmospheric CO<sub>2</sub> (referred to here and in the  
50 rest of this dissertation as leaf C<sub>a</sub>:C<sub>a</sub>, or  $\chi$ ), which is determined by factors that  
51 influence leaf nitrogen demand, such as CO<sub>2</sub>, temperature, vapor pressure deficit,  
52 and light availability (Prentice et al. 2014; Smith et al. 2019; Stocker et al. 2020;  
53 Wang et al. 2017). Photosynthetic processes are optimized such that nitrogen  
54 is allocated to photosynthetic enzymes in to allow net photosynthesis rates to be  
55 equally co-limited by the maximum rate of Rubisco carboxylation and the max-  
56 imum rate of Ribulose-1,5-bisphosphate (RuBP) regeneration (Chen et al. 1993;  
57 Maire et al. 2012). The theory indicates that costs of nitrogen and water use  
58 are substitutable such that, in a given environment, optimal photosynthesis rates  
59 can be achieved by sacrificing inefficient use of a relatively more abundant (and  
60 less costly to acquire) resource for more efficient use of a relatively less abundant  
61 (and more costly to acquire) resource. These predictions imply that acclimation  
62 responses to changing environments may be partially driven by trade-offs between  
63 nitrogen and water use, though empirical tests of the theory are sparse.

64 Optimality models leveraging patterns expected from photosynthetic least-  
65 cost theory have been developed for both C<sub>3</sub> (Wang et al. 2017; Smith et al. 2019;  
66 Stocker et al. 2020) and more recently for C<sub>4</sub> species (Scott and Smith 2022). Such  
67 models show broad agreement with patterns observed across environmental gradi-  
68 ents (Paillassa et al. 2020; Querejeta et al. 2022; Smith et al. 2019; Westerband  
69 et al. 2023), and are capable of reconciling dynamic leaf nitrogen-photosynthesis  
70 relationships and acclimation responses to elevated CO<sub>2</sub>, temperature, light avail-  
71 ability, and vapor pressure deficit (Dong et al. 2017; Dong et al. 2020; Dong et al.

72 2022; Dong et al. 2022; Smith and Keenan 2020; Luo et al. 2021; Peng et al. 2021;  
73 Querejeta et al. 2022; Westerband et al. 2023). Current versions of optimality  
74 models that invoke patterns expected from photosynthetic least-cost theory hold  
75  $\beta$  constant across growing environments. As growing evidence suggests that costs  
76 of nitrogen use change across resource availability and climatic gradients in species  
77 with different nutrient acquisition strategies (Fisher et al. 2010; Brzostek et al.  
78 2014; Allen et al. 2020; Terrer et al. 2018), one might expect that  $\beta$  should  
79 dynamically change across environments and in species with different acquisition  
80 strategies. However, manipulative experiments that test mechanisms underlying  
81 nitrogen-water use trade-offs and leaf nitrogen-photosynthesis relationships pre-  
82 dicted from theory across soil resource availability and climatic gradients are rare.  
83 Furthermore, no study has related shifts in  $\beta$  to nitrogen-water use trade-offs or  
84 leaf nitrogen-photosynthesis relationships. Understanding the dynamic nature of  
85  $\beta$  across different environmental contexts and impacts of  $\beta$  on patterns expected  
86 from theory are critical for further optimality model development, and is the cen-  
87 tral motivation for the experiments presented in this dissertation.

88 In this dissertation, I use four experiments to quantify nutrient acquisition  
89 and allocation responses under different environmental conditions and in species  
90 with different nutrient acquisition strategies. These experiments provide impor-  
91 tant empirical data needed to evaluate patterns expected from photosynthetic  
92 least-cost theory and test mechanisms that drive such patterns. In the first ex-  
93 perimental chapter, I re-analyze data from a greenhouse experiment that grew  
94 *Glycine max* L. (Merr) and *Gossypium hirsutum* seedlings under full-factorial  
95 combinations of four light treatments and four fertilization treatments. This re-

96 analysis examined the effect of soil nitrogen availability and light availability on  
97 structural carbon costs to acquire nitrogen in a species capable of forming associa-  
98 tions with symbiotic nitrogen-fixing bacteria (*G. max*) and a species not capable  
99 of forming such associations (*G. hirsutum*). I find strong evidence suggesting that  
100 increasing light availability increases structural carbon costs to acquire nitrogen  
101 and that increasing soil nitrogen fertilization decreases structural carbon costs to  
102 acquire nitrogen.

103 In the second experimental chapter, I measure leaf physiological traits in  
104 the upper canopy of mature trees growing in a 9-year nitrogen-by-pH field manip-  
105 ulation experiment to assess whether changes in soil nitrogen availability or soil  
106 pH modify nitrogen-water use trade-offs expected from photosynthetic least-cost  
107 theory. I find strong nitrogen-water use trade-offs in response to increasing soil ni-  
108 trogen availability, indicated by a strong negative relationship between leaf  $C_i:C_a$   
109 (referred to here and in the rest of this dissertation as  $\chi$ ) and leaf nitrogen content,  
110 as well as a strong increase in leaf nitrogen content per unit leaf  $\chi$  with increas-  
111 ing soil nitrogen availability. Interestingly, I also find a null effect of soil pH on  
112 nitrogen-water use trade-offs. These patterns provide strong support for patterns  
113 expected from photosynthetic least-cost theory across soil nitrogen availability  
114 gradients, and indicate that previous studies which note strong nitrogen-water  
115 use trade-offs in response to soil pH may be driven by covariation between soil  
116 nitrogen availability and soil pH (Paillassa et al. 2020; Westerband et al. 2023).

117 In the third experimental chapter, I leverage a broad precipitation and soil  
118 nutrient availability gradient in Texan grasslands to investigate primary drivers of  
119 leaf nitrogen content. In this chapter, I directly quantify  $\beta$  and  $\chi$  using leaf  $\delta^{13}\text{C}$  to

120 examine primary drivers of leaf nitrogen content and find that leaf nitrogen content  
121 is driven through a negative relationship with  $\chi$ . I also show that soil nitrogen  
122 availability is negatively associated with  $\beta$ , and that  $\beta$  is positively associated  
123 with  $\chi$ . I show strong support for patterns expected from theory, showing for  
124 the first time that positive effects of increasing soil nitrogen availability on leaf  
125 nitrogen content are mediated by changes in  $\beta$ .

126 In the fourth experimental chapter, I use reach-in growth chambers to  
127 quantify leaf and whole plant acclimation responses to CO<sub>2</sub> across a soil nitro-  
128 gen fertilization gradient, while also manipulating nutrient acquisition strategy  
129 by controlling whether seedlings were able to form associations with symbiotic  
130 nitrogen-fixing bacteria. Specifically, I measure leaf physiological and whole plant  
131 growth responses of 7-week *G. max* seedlings grown under one of two CO<sub>2</sub> treat-  
132 ments, one of nine fertilization treatments, and one of two inoculation treatments  
133 in a full factorial design. I find a down-regulation in leaf nitrogen content and  
134 leaf photosynthesis under elevated CO<sub>2</sub>, a pattern that is not modified across  
135 the fertilization gradient or between inoculation treatments. However, I also find  
136 strong stimulation in total leaf area and whole plant growth under elevated CO<sub>2</sub>  
137 that are enhanced with increasing fertilization. There was no observable effect of  
138 inoculation in modifying whole plant growth responses to CO<sub>2</sub>, which I speculate  
139 is the result of a down-regulation in plant investments to nitrogen fixation with  
140 increasing fertilization. Results from this experiment provide strong evidence sug-  
141 gesting that leaf acclimation responses to CO<sub>2</sub> were controlled by optimal resource  
142 investment to photosynthetic capacity, following patterns expected from photo-  
143 synthetic least-cost theory, and suggest divergent roles of soil nitrogen fertilization

144 in modifying leaf and whole plant acclimation responses to CO<sub>2</sub>.

145 Throughout the four experimental chapters, I find strong and consistent  
146 patterns supportive of patterns expected from photosynthetic least-cost theory.  
147 Specifically, I find strong nitrogen-water use trade-offs in response to changing  
148 climates and soil resources, that shifts in soil nitrogen availability have strong  
149 negative impacts on costs of nitrogen acquisition, and therefore tend to increase  
150  $\beta$ , and that constant leaf nitrogen-photosynthesis relationships only occur in sys-  
151 tems where nitrogen is limiting. In a final conclusion chapter, I summarize ma-  
152 jor findings from each of the four experimental chapters and synthesize common  
153 mechanisms that drive leaf and whole plant responses to changing environmen-  
154 tal conditions. I conclude this dissertation with brief dialogue on lessons learned  
155 throughout experimental chapters, and propose future experiments that will tar-  
156 get additional uncertainties in photosynthetic least-cost theory responses across  
157 environmental gradients.

158

## Chapter 2

159

Structural carbon costs to acquire nitrogen are determined by  
160 nitrogen and light availability in two species with different nitrogen  
161 acquisition strategies

162 2.1 Introduction

163

Carbon and nitrogen cycles are tightly coupled in terrestrial ecosystems.

164

This tight coupling influences photosynthesis (Walker et al. 2014; Rogers et al.

165

2017), net primary productivity (LeBauer and Treseder 2008; Thomas et al. 2013),

166

decomposition (Cornwell et al. 2008; Bonan et al. 2013; Sulman et al. 2019), and

167

plant resource competition (Gill and Finzi 2016; Xu-Ri and Prentice 2017). Ter-

168

restrial biosphere models are beginning to include connected carbon and nitrogen

169

cycles to improve the realism of their simulations (Fisher et al. 2010; Brzostek

170

et al. 2014; Wieder et al. 2015; Shi et al. 2016; Zhu et al. 2019). Simula-

171

tions from these models indicate that coupling carbon and nitrogen cycles can

172

drastically influence future biosphere-atmosphere feedbacks under global change,

173

such as elevated carbon dioxide or nitrogen deposition (Thornton et al. 2007;

174

Goll et al. 2012; Wieder et al. 2015; Wieder et al. 2019). Nonetheless, there

175

are still limitations in our quantitative understanding of connected carbon and

176

nitrogen dynamics (Thomas et al. 2015; Meyerholt et al. 2016; Rogers et al.

177

2017; Exbrayat et al. 2018; Shi et al. 2019), forcing models to make potentially

178

unreliable assumptions.

179

Plant nitrogen acquisition is a process in terrestrial ecosystems by which

180

carbon and nitrogen are tightly coupled (Vitousek and Howarth 1991; Delaire

181

et al. 2005; Brzostek et al. 2014). Plants must allocate photosynthetically de-

182 rived carbon belowground to produce and maintain root systems or exchange with  
183 symbiotic soil microbes in order to acquire nitrogen (Högberg et al. 2008; Hög-  
184 berg et al. 2010). Thus, plants have an inherent carbon cost associated with  
185 acquiring nitrogen, which can include both direct energetic costs associated with  
186 nitrogen acquisition and indirect costs associated with building structures that  
187 support nitrogen acquisition (Gutschick 1981; Rastetter et al. 2001; Vitousek  
188 et al. 2002; Menge et al. 2008). Model simulations (Fisher et al. 2010; Brzostek  
189 et al. 2014; Shi et al. 2016; Allen et al. 2020) and meta-analyses (Terrer et al.  
190 2018) suggest that these carbon costs vary between species, particularly those  
191 with different nitrogen acquisition strategies. For example, simulations using iter-  
192 ations of the Fixation and Uptake of Nitrogen (FUN) model indicate that species  
193 that acquire nitrogen from non-symbiotic active uptake pathways (e.g. mass flow)  
194 generally have larger carbon costs to acquire nitrogen than species that acquire  
195 nitrogen through symbiotic associations with nitrogen-fixing bacteria (Brzostek  
196 et al. 2014; Allen et al. 2020).

197 Carbon costs to acquire nitrogen likely vary in response to changes in soil  
198 nitrogen availability. For example, if the primary mode of nitrogen acquisition  
199 is through non-symbiotic active uptake, then nitrogen availability could decrease  
200 carbon costs to acquire nitrogen as a result of increased per-root nitrogen up-  
201 take (Franklin et al. 2009; Wang et al. 2018). However, if the primary mode of  
202 nitrogen acquisition is through symbiotic active uptake, then nitrogen availabil-  
203 ity may incur additional carbon costs to acquire nitrogen if it causes microbial  
204 symbionts to shift toward parasitism along the parasitism–mutualism continuum  
205 (Johnson et al. 1997; Hoek et al. 2016; Friel and Friesen 2019) or if it reduces

206 the nitrogen acquisition capacity of a microbial symbiont (van Diepen et al. 2007;  
207 Soudzilovskaia et al. 2015; Muñoz et al. 2016). Species may respond to shifts in  
208 soil nitrogen availability by switching their primary mode of nitrogen acquisition  
209 to a strategy with lower carbon costs to acquire nitrogen in order to maximize  
210 the magnitude of nitrogen acquired from a belowground carbon investment and  
211 outcompete other individuals for soil resources (Rastetter et al. 2001; Menge et al.  
212 2008).

213 Environmental conditions that affect demand to acquire nitrogen to sup-  
214 port new and existing tissues could also be a source of variance in plant carbon  
215 costs to acquire nitrogen. For example, an increase in plant nitrogen demand could  
216 increase carbon costs to acquire nitrogen if this increases the carbon that must be  
217 allocated belowground to acquire a proportional amount of nitrogen (Kulmatiski  
218 et al. 2017; Noyce et al. 2019). This could be driven by a temporary state of  
219 diminishing return associated with investing carbon toward building and main-  
220 taining structures that are necessary to support enhanced nitrogen uptake, such  
221 as fine roots (Matamala and Schlesinger 2000; Norby et al. 2004; Arndal et al.  
222 2018), mycorrhizal hyphae (Saleh et al. 2020), or root nodules (Parvin et al. 2020).  
223 Alternatively, if the environmental factor that increases plant nitrogen demand  
224 causes nitrogen to become more limiting in the system (e.g. atmospheric CO<sub>2</sub>;  
225 Luo et al. (2004), LeBauer and Treseder (2008), Vitousek et al. (2010), Liang  
226 et al. (2016)), species might switch their primary mode of nitrogen acquisition to  
227 a strategy with lower relative carbon costs to acquire nitrogen in order to gain a  
228 competitive advantage over species with either different or more limited modes of  
229 nitrogen acquisition (Ainsworth and Long 2005; Taylor and Menge 2018).

230 Using a plant economics approach, I examined the influence of plant ni-  
231 trogen demand and soil nitrogen availability on plant carbon costs to acquire  
232 nitrogen. This was done by growing a species capable of forming associations  
233 with nitrogen-fixing bacteria (*Glycine max* L. (Merr)) and a species not capable  
234 of forming these associations (*Gossypium hirsutum* L.) under four levels of light  
235 availability (plant nitrogen demand proxy) and four levels of soil nitrogen fertil-  
236 ization (soil nitrogen availability proxy) in a full-factorial, controlled greenhouse  
237 experiment. I used this experimental set-up to test the following hypotheses:

- 238 1. An increase in plant nitrogen demand due to increasing light availability will  
239 increase carbon costs to acquire nitrogen through a proportionally larger  
240 increase in belowground carbon than whole-plant nitrogen acquisition. This  
241 will be the result of an increased investment of carbon toward belowground  
242 structures that support enhanced nitrogen uptake, but at a lower nitrogen  
243 return.
- 244 2. An increase in soil nitrogen availability will decrease carbon costs to acquire  
245 nitrogen as a result of increased per root nitrogen uptake in *G. hirsutum*.  
246 However, soil nitrogen availability will not affect carbon costs to acquire  
247 nitrogen in *G. max* because of the already high return of nitrogen supplied  
248 through nitrogen fixation.

**249** 2.2 Methods

**250** 2.2.1 *Experiment setup*

**251** *Gossypium hirsutum* and *G. max* were planted in individual 3 liter pots  
**252** (NS-300; Nursery Supplies, Orange, CA, USA) containing a 3:1 mix of unfertil-  
**253** ized potting mix (Sungro Sunshine Mix #2, Agawam, MA, USA) to native soil  
**254** extracted from an agricultural field most recently planted with *G. max* at the  
**255** USDA-ARS Laboratory in Lubbock, TX, USA (33.59°N, -101.90°W). The field  
**256** soil was classified as Amarillo fine sandy loam (75% sand, 10% silt, 15% clay).  
**257** Upon planting, all *G. max* pots were inoculated with *Bradyrhizobium japonicum*  
**258** (Verdesian N-Dure™ Soybean, Cary, NC, USA) to stimulate root nodulation. In-  
**259** dividuals of both species were grown under similar, unshaded, ambient greenhouse  
**260** conditions for 2 weeks to germinate and begin vegetative growth. Three blocks  
**261** were set up in the greenhouse, each containing four light treatments created us-  
**262** ing shade cloth that reduced incoming radiation by either 0 (full sun), 30, 50,  
**263** or 80%. Two weeks post-germination, individuals were randomly placed in the  
**264** four light treatments in each block. Individuals received one of four nitrogen fer-  
**265** tilization doses as 100ml of a modified Hoagland solution (Hoagland and Arnon  
**266** 1950) equivalent to either 0, 70, 210, or 630 ppm N twice per week within each  
**267** light treatment. Nitrogen fertilization doses were received as topical agents to  
**268** the soil surface. Each Hoagland solution was modified to keep concentrations of  
**269** other macro- and micronutrients equivalent (Supplementary Table S1). Plants  
**270** were routinely well watered to eliminate water stress.

**271** 2.2.2 *Plant measurements and calculations*

**272** Each individual was harvested after 5 weeks of treatment, and biomass  
**273** was separated by organ type (leaves, stems, and roots). Nodules on *G. max*  
**274** roots were also harvested. Except for the 0% shade cover and 630 ppm N treat-  
**275** ment combination, all treatment combinations in both species had lower average  
**276** dry biomass:pot volume ratios than the 1:1 ratio recommended by Poorter et al.  
**277** (2012) to minimize the likelihood of pot volume-induced growth limitation (Sup-  
**278** plementary Tables S2, S3; Supplementary Fig. S1). All harvested material was  
**279** dried, weighed, and ground by organ type. Carbon and nitrogen content ( $\text{g g}^{-1}$ )  
**280** was determined by subsampling from ground and homogenized biomass of each  
**281** organ type using an elemental analyzer (Costech 4010; Costech, Inc., Valencia,  
**282** CA, USA). We scaled these values to total leaf, stem, and root carbon and ni-  
**283** trogen biomass (g) by multiplying dry biomass of each organ type by carbon or  
**284** nitrogen content of each corresponding organ type. Whole-plant nitrogen biomass  
**285** (g) was calculated as the sum of total leaf (g), stem (g), and root (g) nitrogen  
**286** biomass. Root nodule carbon biomass was not included in the calculation of root  
**287** carbon biomass; however, relative plant investment toward root or root nodule  
**288** standing stock was estimated as the ratio of root biomass to root nodule biomass  
**289** ( $\text{g g}^{-1}$ ), following similar metrics to those adopted by Dovrat et al. (2018) and  
**290** Dovrat et al. (2020).

**291** Carbon costs to acquire nitrogen ( $N_{\text{cost}}$ ;  $\text{gC gN}^{-1}$ ) were estimated as the  
**292** ratio of total root carbon biomass ( $C_{\text{bg}}$ ;  $\text{gC}$ ) to whole-plant nitrogen biomass  
**293** ( $N_{\text{wp}}$ ;  $\text{gN}$ ). This calculation quantifies the relationship between carbon spent on  
**294** nitrogen acquisition and whole-plant nitrogen acquisition by using root carbon

295 biomass as a proxy for estimating the magnitude of carbon allocated toward ni-  
296 trogen acquisition. This calculation therefore assumes that the magnitude of root  
297 carbon standing stock is proportional to carbon transferred to root nodules or my-  
298 corrhizae, or lost through root exudation or turnover. The assumption has been  
299 supported in species that associate with ectomycorrhizal fungi (Hobbie 2006; Hob-  
300 bie and Hobbie 2008), but is less clear in species that acquire nitrogen through  
301 non-symbiotic active uptake or symbiotic nitrogen fixation. It is also unclear  
302 whether relationships between root carbon standing stock and carbon transfer to  
303 root nodules are similar in magnitude to carbon lost through exudation or when  
304 allocated toward other active uptake pathways. Thus, because of the way mea-  
305 surements were calculated, proximal values of carbon costs to acquire nitrogen are  
306 underestimates.

307 2.2.3 *Statistical analyses*

308 I explored the effects of light and nitrogen availability on carbon costs to ac-  
309 quire nitrogen using separate linear mixed-effects models for each species. Models  
310 included shade cover, nitrogen fertilization, and interactions between shade cover  
311 and nitrogen fertilization as continuous fixed effects, and also included block as a  
312 random intercept term. Three separate models for each species were built with  
313 this independent variable structure for three different dependent variables: (i)  
314 carbon costs to acquire nitrogen ( $\text{gC gN}^{-1}$ ); (ii) whole plant nitrogen biomass (de-  
315 nominator of carbon cost to acquire nitrogen;  $\text{gN}$ ); and (iii) belowground carbon  
316 biomass (numerator of carbon cost to acquire nitrogen;  $\text{gC}$ ). I constructed two  
317 additional models for *G. max* with the same model structure described above to

318 investigate the effects of light availability and nitrogen fertilization on root nodule  
319 biomass (g) and the ratio of root nodule biomass to root biomass (unitless).

320 I used Shapiro–Wilk tests of normality to determine whether species spe-  
321 cific linear mixed-effects model residuals followed a normal distribution. None of  
322 our models satisfied residual normality assumptions when models were fit using  
323 untransformed data (Shapiro–Wilk:  $p < 0.05$  in all cases). I attempted to satisfy  
324 residual normality assumptions by first fitting models using dependent variables  
325 that were natural-log transformed. If residual normality assumptions were still  
326 not met (Shapiro–Wilk:  $p < 0.05$ ), then models were fit using dependent variables  
327 that were square root transformed. All residual normality assumptions were satis-  
328 fied when models were fit with either a natural-log or square root transformation  
329 (Shapiro–Wilk:  $p > 0.05$  in all cases). Specifically, I natural-log transformed *G.*  
330 *hirsutum* carbon costs to acquire nitrogen and *G. hirsutum* whole-plant nitrogen  
331 biomass. I also square root transformed *G. max* carbon costs to acquire nitrogen,  
332 *G. max* whole-plant nitrogen biomass, root carbon biomass in both species, *G.*  
333 *max* root nodule biomass, and the *G. max* ratio of root nodule biomass to root  
334 biomass. I used the ‘lmer’ function in the ‘lme4’ R package (Bates et al. 2015) to  
335 fit each model and the ‘Anova’ function in the ‘car’ R package (Fox and Weisberg  
336 2019) to calculate Wald’s  $\chi^2$  to determine the significance ( $\alpha = 0.05$ ) of each fixed  
337 effect coefficient. Finally, I used the ‘emmeans’ R package (Lenth 2019) to conduct  
338 post-hoc comparisons of our treatment combinations using Tukey’s tests. Degrees  
339 of freedom for all Tukey’s tests were approximated using the Kenward–Roger ap-  
340 proach (Kenward and Roger 1997). All analyses and plots were conducted in R  
341 version 4.0.1 (R Core Team 2021).

**342** 2.3 Results

**343** 2.3.1 *Carbon costs to acquire nitrogen*

**344** Carbon costs to acquire nitrogen in *G. hirsutum* increased with increasing  
**345** light availability ( $p < 0.001$ ; Table 2.1; Fig. 2.1) and decreased with increasing  
**346** nitrogen fertilization ( $p < 0.001$ ; Table 2.1; Fig. 2.1). There was no interaction  
**347** between light availability and nitrogen fertilization ( $p = 0.486$ , Table 2.1; Fig.  
**348** 2.1).

**349** Carbon costs to acquire nitrogen in *G. max* also increased with increasing  
**350** light availability ( $p < 0.001$ , Table 2.1; Fig. 2.1) and decreased with increasing  
**351** nitrogen fertilization ( $p < 0.001$ ; Table 2.1; Fig. 2.1). There was no interaction  
**352** between light availability and nitrogen fertilization ( $p = 0.261$ , Table 2.1; Fig.  
**353** 2.1).

**Table 2.1.** Analysis of variance results exploring species-specific effects of light availability, nitrogen fertilization, and their interactions on carbon costs to acquire nitrogen ( $N_{\text{cost}}$ ), whole-plant nitrogen biomass ( $N_{\text{wp}}$ ), and root carbon biomass ( $C_{\text{bg}}$ )

	df	$N_{\text{cost}}$			$N_{\text{wp}}$			$C_{\text{bg}}$		
		Coefficient	$\chi^2$	p	Coefficient	$\chi^2$	p	Coefficient	$\chi^2$	p
<i>G. hirsutum</i>										
Intercept		1.594	-	-	-3.232	-	-	0.432	-	-
Light (L)	1	-1.09E-02	56.494	<0.001	-6.41E-03	91.275	<0.001	-2.62E-03	169.608	<0.001
Nitrogen (N)	1	-1.34E-03	54.925	<0.001	1.83E-03	118.784	<0.001	1.15E-04	2.901	0.089
L*N	1	3.88E-06	0.485	0.486	-1.34E-05	10.721	0.001	-1.67E-06	3.140	0.076
<i>G. max</i>										
Intercept		1.877	-	-	0.239	-	-	0.438	-	-
Light (L)	1	-7.67E-03	174.156	<0.001	-6.72E-04	39.799	<0.001	-2.55E-03	194.548	<0.001
Nitrogen (N)	1	-2.35E-04	21.948	<0.001	1.55E-04	70.771	<0.001	2.52E-04	19.458	<0.001
L*N	1	-2.89E-06	1.262	0.261	-6.32E-07	1.435	0.231	-3.16E-06	10.803	0.001

354 \*Significance determined using Wald's  $\chi^2$  tests ( $P = 0.05$ ).  $P$ -values  $< 0.05$  are in bold and  $p$ -values between 0.05 and  
 355 0.1 are italicized. Negative coefficients for light treatments indicate a positive effect of increasing light availability  
 356 on all response variables, as light availability is treated as percent shade cover in all linear mixed-effects models.

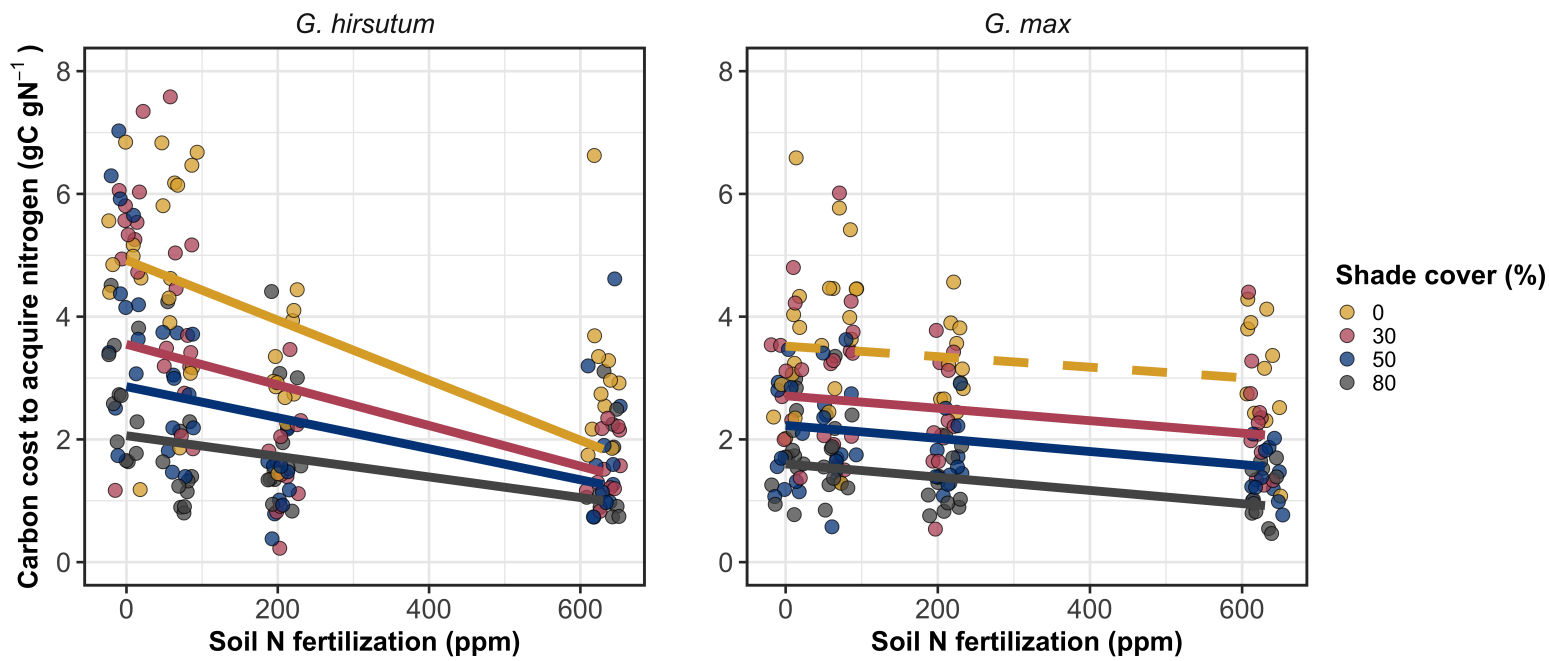


**Figure 2.1.** Relationships between soil nutrient fertilization and light availability on carbon costs to acquire nitrogen in *G. hirsutum* and *G. max*. Nitrogen fertilization treatments are represented on the x-axis. Shade cover treatments are represented through colored points and trendlines. Trendlines were created by back-transforming marginal mean slopes and intercepts from species-specific linear mixed-effects models. These values were calculated using the ‘emtrends’ and ‘emmmeans’ functions in the ‘emmeans’ R package (Lenth, 2019). Yellow points and trendlines represent the 0% shade cover treatment, red points and trendlines represent the 30% shade cover treatment, blue points and trendlines represent the 50% shade cover treatment, and gray points and trendlines represent the 80% shade cover treatment. Solid trendlines indicate slopes that are significantly different from zero (Tukey:  $p < 0.05$ ), while dashed trendlines indicate slopes that are not statistically different from zero.

**357** 2.3.2 *Whole plant nitrogen biomass*

**358** Whole-plant nitrogen biomass in *G. hirsutum* was driven by an interaction  
**359** between light availability and nitrogen fertilization ( $p = 0.001$ ; Table 2.1; Fig.  
**360** 2.2). This interaction indicated a greater stimulation of whole-plant nitrogen  
**361** biomass by nitrogen fertilization as light levels increased (Table 2.1; Fig. 2.2).

**362** Whole-plant nitrogen biomass in *G. max* increased with increasing light  
**363** availability ( $p < 0.001$ ) and nitrogen fertilization ( $p < 0.001$ ), with no interaction  
**364** between light availability and nitrogen fertilization ( $p = 0.231$ ; Table 2.1; Fig.  
**365** 2.2).

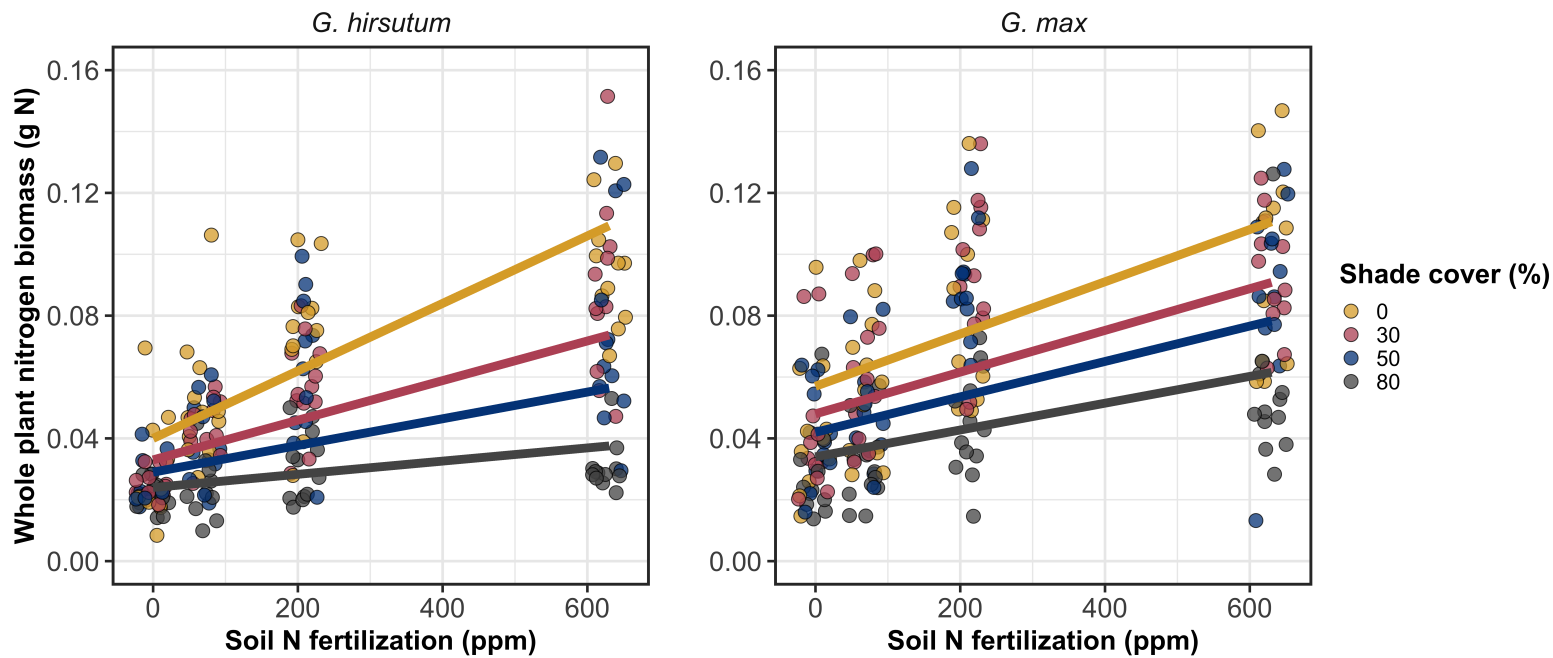


**Figure 2.2.** Relationships between soil nutrient fertilization and light availability on whole-plant nitrogen biomass in *G. hirsutum* and *G. max*. Whole-plant nitrogen biomass is the denominator of the carbon cost to acquire nitrogen calculation. Nitrogen fertilization treatments are represented on the x-axis. Shade cover treatments are represented through colored points and trendlines. Trendlines were created by back-transforming marginal mean slopes and intercepts from species-specific linear mixed-effects models. These values were calculated using the ‘emtrends’ and ‘emmeans’ functions in the ‘emmeans’ R package (Lenth 2019). Points are jittered for visibility. Colored points and trendlines are as explained in Fig. 2.1. Solid trendlines indicate slopes that are significantly different from zero (Tukey:  $p < 0.05$ ), while dashed trendlines indicate slopes that are not statistically different from zero.

**366** 2.3.3 *Root carbon biomass*

**367** Root carbon biomass in *G. hirsutum* significantly increased with increasing  
**368** light availability ( $p < 0.001$ ; Table 2.1; Fig. 2.3) and marginally increased with  
**369** nitrogen fertilization ( $p = 0.089$ ; Table 2.1; Fig. 2.3). There was also a marginal  
**370** interaction between light availability and nitrogen fertilization ( $p = 0.076$ ; Table  
**371** 2.1), driven by an increase in the positive response of root carbon biomass to  
**372** increasing nitrogen fertilization as light availability increased. This resulted in  
**373** significantly positive trends between root carbon biomass and nitrogen fertilization  
**374** in the two highest light treatments (Tukey:  $p < 0.05$  in both cases; Table 2.3;  
**375** Fig. 2.3) and no effect of nitrogen fertilization in the two lowest light treatments  
**376** (Tukey:  $p > 0.05$  in both cases; Table 2.3; Fig. 2.3).

**377** There was an interaction between light availability and nitrogen fertiliza-  
**378** tion on root carbon biomass in *G. max* ( $p = 0.001$ ; Table 2.1; Fig. 2.3). Post-hoc  
**379** analyses indicated that the positive effects of nitrogen fertilization on *G. max* root  
**380** carbon biomass increased with increasing light availability (Table 2.3; Fig. 2.3).  
**381** There were also positive individual effects of increasing nitrogen fertilization ( $p <$   
**382**  $0.001$ ) and light availability ( $p < 0.001$ ) on *G. max* root carbon biomass (Table  
**383** 2.1; Fig. 2.3).

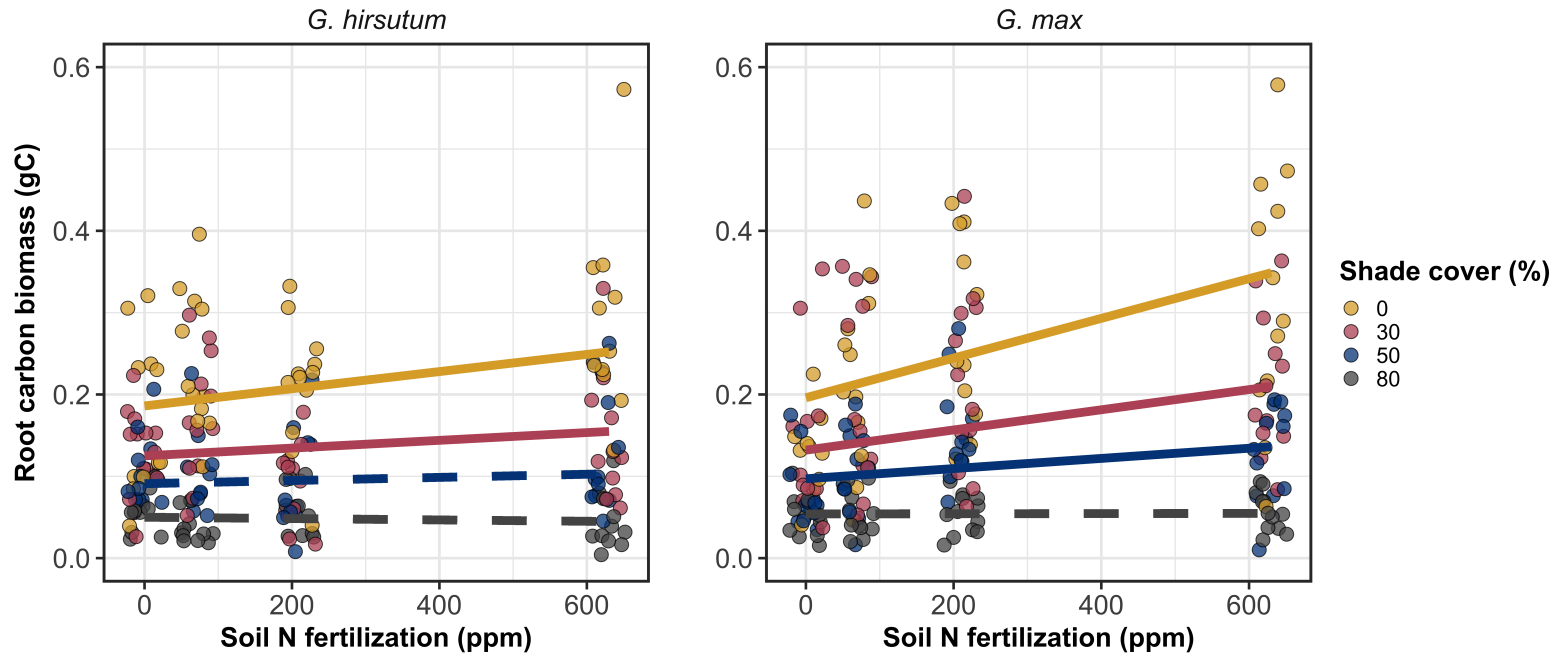


**Figure 2.3.** Relationships between soil nutrient fertilization and light availability on root carbon biomass in *G. hirsutum* and *G. max*. Root carbon biomass is the numerator of the carbon cost to acquire nitrogen calculation. Nitrogen fertilization treatments are represented on the x-axis. Shade cover treatments are represented through colored points and trendlines. Trendlines were created by back-transforming marginal mean slopes and intercepts from species-specific linear mixed-effects models. These values were calculated using the ‘emtrends’ and ‘emmmeans’ functions in the ‘emmeans’ R package (Lenth 2019). Points are jittered for visibility. Colored points and trendlines are as explained in Fig. 2.1.

Yellow points and trendlines represent the 0% shade cover treatment, blue points and trendlines represent the 30% shade cover treatment, green points and trendlines represent the 50% shade cover treatment, and purple points and trendlines represent the 80% shade cover treatment. Solid trendlines indicate slopes that are significantly different from zero (Tukey:  $p < 0.05$ ), while dashed trendlines indicate slopes that are not statistically different from zero.

**384** 2.3.4 *Root nodule biomass*

**385** Root nodule biomass in *G. max* increased with increasing light availability  
**386** ( $p < 0.001$ ; Table 2.2; Fig. 2.4A) and decreased with increasing nitrogen fertiliza-  
**387** tion ( $p < 0.001$ ; Table 2.2; Fig. 2.4A). There was no interaction between nitrogen  
**388** fertilization and light availability ( $p = 0.133$ ; Table 2.2; Fig. 2.4A). The ratio of  
**389** root nodule biomass to root biomass did not change in response to light avail-  
**390** ability ( $p = 0.481$ ; Table 2.2; Fig. 2.4B) but decreased with increasing nitrogen  
**391** fertilization ( $p < 0.001$ ; Table 2.2; Fig. 2.4B). There was no interaction between  
**392** nitrogen fertilization and light availability on the ratio of root nodule biomass to  
**393** root biomass ( $p = 0.621$ ; Table 2.2; Fig. 2.4B).

**Table 2.2.** Analysis of variance results exploring effects of light availability, nitrogen fertilization, and their interactions on *G. max* root nodule biomass and the ratio of root nodule biomass to root biomass\*

	Nodule biomass			Nodule biomass: root biomass			<i>p</i>
	df	Coefficient	$\chi^2$	<i>p</i>	Coefficient	$\chi^2$	
(Intercept)		0.302	-	-	0.448	-	-
Light (L)	1	-1.81E-03	72.964	<b>&lt;0.001</b>	-8.76E-05	0.496	0.481
Nitrogen (N)	1	-2.83E-04	115.377	<b>&lt;0.001</b>	-5.09E-04	156.476	<b>&lt;0.001</b>
L*N	1	1.14E-06	2.226	0.133	-7.30E-07	0.244	0.621

394 \*Significance determined using Wald's  $\chi^2$  tests ( $\alpha = 0.05$ ). *P*-values less than 0.05 are in bold. Negative coefficients  
 395 for light treatments indicate a positive effect of increasing light availability on all response variables, as light avail-  
 396 ability is treated as percent shade cover in all linear mixed-effects models. Root nodule biomass and nodule biomass:  
 397 root biomass models were only constructed for *G. max* because *G. hirsutum* was not inoculated with *B. japonicum*  
 398 and is not capable of forming root nodules.

**Table 2.3.** Slopes of the regression line describing the relationship between each dependent variable and nitrogen fertilization at each light level\*

Shade cover	Carbon cost to acquire nitrogen	Whole plant N biomass	Belowground C biomass	Root nodule biomass	Nodule biomass: root biomass
<i>G. hirsutum</i>					
0%	<b>-1.34E-03<sup>a</sup></b>	<b>1.83E-03<sup>a</sup></b>	<b>1.15E-04<sup>b</sup></b>	-	-
30%	<b>-1.22E-03<sup>a</sup></b>	<b>1.43E-03<sup>a</sup></b>	<b>1.17E-04<sup>b</sup></b>	-	-
50%	<b>-1.14E-03<sup>a</sup></b>	<b>1.17E-03<sup>a</sup></b>	3.12E-05 <sup>b</sup>	-	-
80%	<b>-1.02E-03<sup>a</sup></b>	<b>7.66E-04<sup>a</sup></b>	-1.89E-06 <sup>b</sup>	-	-
<i>G. max</i>					
0%	-2.35E-04 <sup>b</sup>	<b>1.55E-05<sup>b</sup></b>	<b>2.51E-04<sup>b</sup></b>	<b>-2.83E-04<sup>b</sup></b>	<b>-5.09E-04<sup>b</sup></b>
30%	<b>-3.22E-04<sup>b</sup></b>	<b>1.35E-05<sup>b</sup></b>	<b>1.57E-04<sup>b</sup></b>	<b>-2.49E-04<sup>b</sup></b>	<b>-5.31E-04<sup>b</sup></b>
50%	<b>-3.80E-04<sup>b</sup></b>	<b>1.23E-05<sup>b</sup></b>	<b>9.37E-05<sup>b</sup></b>	<b>-2.26E-04<sup>b</sup></b>	<b>-5.45E-04<sup>b</sup></b>
80%	<b>-4.66E-04<sup>b</sup></b>	<b>1.04E-05<sup>b</sup></b>	-9.95E-07 <sup>b</sup>	<b>-1.92E-04<sup>b</sup></b>	<b>-5.67E-04<sup>b</sup></b>

25

399 \*Slopes represent estimated marginal mean slopes from linear mixed-effects models described in the Methods. Slopes  
 400 were calculated using the ‘emmeans’ R package (Lenth 2019). Superscripts indicate slopes fit to natural-log (<sup>a</sup>) or  
 401 square root (<sup>b</sup>) transformed data. Slopes statistically different from zero (Tukey:  $p < 0.05$ ) are indicated in bold.  
 402 Marginally significant slopes (Tukey:  $0.05 < p < 0.1$ ) are italicized.

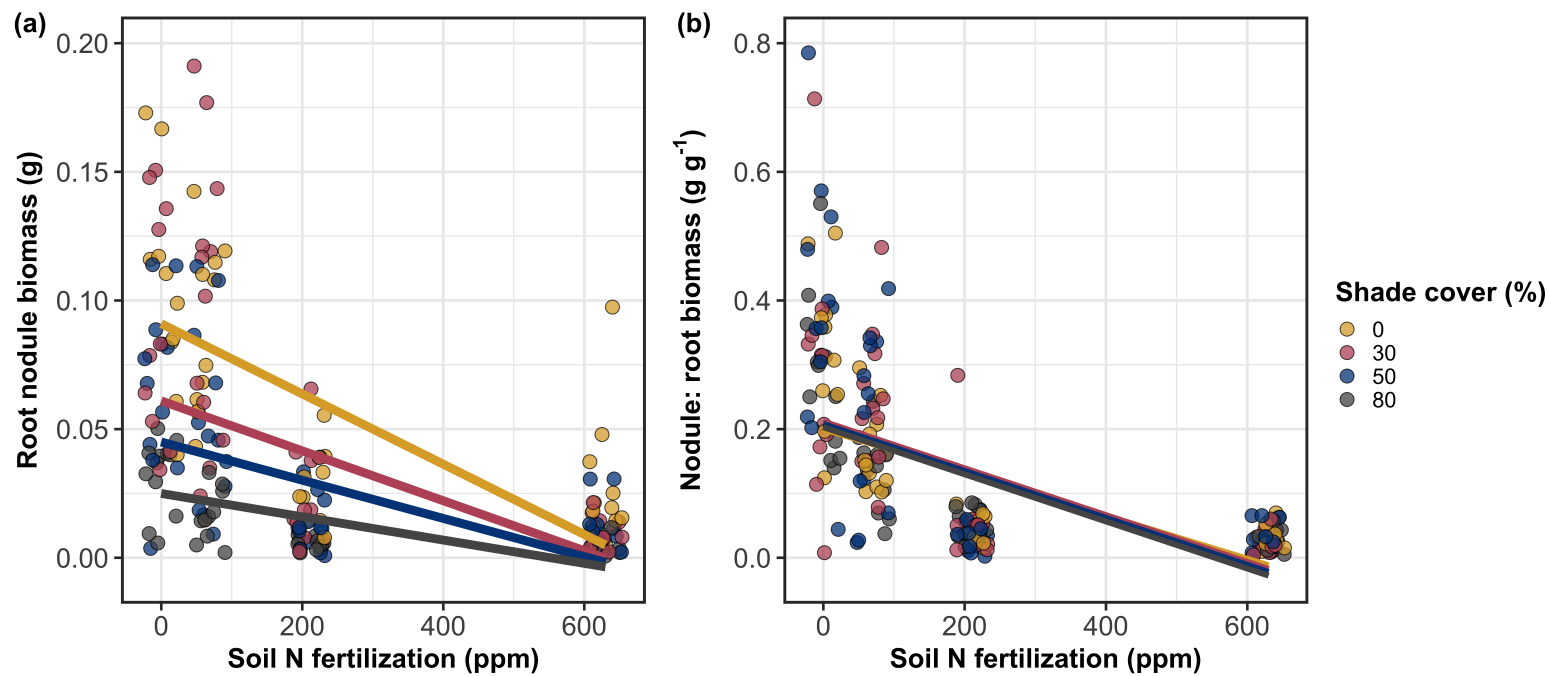


**Figure 2.4.** Effects of shade cover and nitrogen fertilization on root nodule biomass (A) and the ratio of root nodule biomass to root biomass (B) in *G. max*. Nitrogen fertilization treatments are represented on the x-axis. Shade cover treatments are represented through colored points and trendlines. Trendlines were created by back-transforming marginal mean slopes and intercepts from species-specific linear mixed-effects models. These values were calculated using the ‘emtrends’ and ‘emmeans’ functions in the ‘emmeans’ R package (Lenth 2019). Points are jittered for visibility. Yellow points and trendlines represent the 0% shade cover treatment, blue points and trendlines represent the 30% shade cover treatment, green points and trendlines represent the 50% shade cover treatment, and purple points and trendlines represent the 80% shade cover treatment. Solid trendlines indicate slopes that are significantly different from zero (Tukey:  $p < 0.05$ ), while dashed trendlines indicate slopes that are not statistically different from zero.

**403** 2.4 Discussion

**404** In this chapter, I determined the effects of light availability and soil ni-  
**405** trogen fertilization on root mass carbon costs to acquire nitrogen in *G. hirsutum*  
**406** and *G. max*. In support of my hypotheses, I found that carbon costs to acquire  
**407** nitrogen generally increased with increasing light availability and decreased with  
**408** increasing soil nitrogen fertilization in both species. These findings suggest that  
**409** carbon costs to acquire nitrogen are determined by factors that influence plant  
**410** nitrogen demand and soil nitrogen availability. In contrast to my second hypothe-  
**411** sis, root nodulation data suggested that *G. max* and *G. hirsutum* achieved similar  
**412** directional carbon cost responses to nitrogen fertilization despite a likely shift in  
**413** *G. max* allocation from nodulation to root biomass along the nitrogen fertilization  
**414** gradient (Fig. 2.4B).

**415** 2.4.1 *Carbon costs to acquire nitrogen increase with light availability and*  
**416** *decrease with fertilization*

**417** Both *G. max* and *G. hirsutum* experienced an increase in carbon costs to  
**418** acquire nitrogen due to increasing light availability. These patterns were driven by  
**419** a larger increase in root carbon biomass than whole-plant nitrogen biomass. In-  
**420** creases in root carbon biomass due to factors that increase plant nitrogen demand  
**421** are a commonly observed pattern, as carbon allocated belowground provides sub-  
**422** strate needed to produce and maintain structures that satisfy aboveground plant  
**423** nitrogen demand (Nadelhoffer and Raich 1992; Giardina et al. 2005; Raich et al.  
**424** 2014). Findings suggest that plants allocate relatively more carbon for acquiring  
**425** nitrogen when demand increases over short temporal scales, which may cause a

426 temporary state of diminishing return due to asynchrony between belowground  
427 carbon and whole-plant nitrogen responses to plant nitrogen demand (Kulmatiski  
428 et al. 2017; Noyce et al. 2019). These responses might be attributed to a temporal  
429 lag associated with producing structures that enhance nitrogen acquisition. For  
430 example, fine roots (Matamala and Schlesinger 2000; Norby et al. 2004; Arndal  
431 et al. 2018) and root nodules (Parvin et al. 2020) take time to build and first  
432 require the construction of coarse roots. Thus, full nitrogen returns from these  
433 investments may not occur immediately (Kayler et al. 2010; Kayler et al. 2017),  
434 and may vary by species acquisition strategy. I speculate that increases in ni-  
435 trogen acquisition from a given carbon investment may occur beyond the 5-week  
436 scope of this experiment. A similar study conducted over a longer temporal scale  
437 would address this.

438 Increasing soil nitrogen fertilization generally decreased carbon costs to  
439 acquire nitrogen in both species. These patterns were driven by a larger increase  
440 in whole-plant nitrogen biomass than root carbon biomass. In *G. hirsutum*, re-  
441 ductions in carbon costs to acquire nitrogen may have been due to an increase in  
442 per-root nitrogen uptake, allowing individuals to maximize the amount of nitro-  
443 gen acquired from a belowground carbon investment. Interestingly, increased soil  
444 nitrogen fertilization increased whole-plant nitrogen biomass in *G. max* despite  
445 reductions in root nodule biomass that likely reduced the nitrogen-fixing capac-  
446 ity of *G. max* (Andersen et al. 2005; Muñoz et al. 2016). While reductions in  
447 root nodulation due to increased soil nitrogen availability are commonly observed  
448 (Gibson and Harper 1985; Fujikake et al. 2003), root nodulation responses were  
449 observed in tandem with increased root carbon biomass, implying that *G. max*

450 shifted relative carbon allocation from nitrogen fixation to soil nitrogen acquisition  
451 (Markham and Zekveld 2007; Dovrat et al. 2020). This was likely because  
452 there was a reduction in the carbon cost advantage of acquiring fixed nitrogen  
453 relative to soil nitrogen, and suggests that species capable of associating with  
454 symbiotic nitrogen-fixing bacteria shift their relative nitrogen acquisition path-  
455 way to optimize nitrogen uptake (Rastetter et al. 2001). Future studies should  
456 further investigate these patterns with a larger quantity of phylogenetically re-  
457 lated species, or different varieties of a single species that differ in their ability to  
458 form associations with symbiotic nitrogen-fixing bacteria to more directly test the  
459 impact of nitrogen fixation on the patterns observed in this study.

460 2.4.2 *Modeling implications*

461 Carbon costs to acquire nitrogen are subsumed in the general discussion of  
462 economic analogies to plant resource uptake (Bloom et al. 1985; Rastetter et al.  
463 2001; Vitousek et al. 2002; Phillips et al. 2013; Terrer et al. 2018; Henneron et al.  
464 2020). Despite this, terrestrial biosphere models rarely include costs of nitrogen  
465 acquisition within their framework for predicting plant nitrogen uptake. There  
466 is currently one plant resource uptake model, FUN, that quantitatively predicts  
467 carbon costs to acquire nitrogen within a framework for predicting plant nitrogen  
468 uptake for different nitrogen acquisition strategies (Fisher et al. 2010; Brzostek  
469 et al. 2014). Iterations of FUN are currently coupled to two terrestrial biosphere  
470 models: the Community Land Model 5.0 and the Joint UK Land Environment  
471 Simulator (Shi et al. 2016; Lawrence et al. 2019; Clark et al. 2011). Recent work  
472 suggests that coupling FUN to CLM 5.0 caused a large overprediction of plant

473 nitrogen uptake associated with nitrogen fixation (Davies-Barnard et al. 2020)  
474 compared to other terrestrial biosphere model products. Thus, empirical data  
475 from manipulative experiments that explicitly quantify carbon costs to acquire  
476 nitrogen in species capable of associating with nitrogen-fixing bacteria across dif-  
477 ferent environmental contexts is an important step toward identifying potential  
478 biases in models such as FUN.

479 My findings broadly support the FUN formulation of carbon costs to ac-  
480 quire nitrogen in response to soil nitrogen availability. FUN calculates carbon  
481 costs to acquire nitrogen based on the sum of carbon costs to acquire nitrogen  
482 via nitrogen fixation, mycorrhizal active uptake, non-mycorrhizal active uptake,  
483 and retranslocation (Fisher et al. 2010; Brzostek et al. 2014). Carbon costs to  
484 acquire nitrogen via mycorrhizal or non-mycorrhizal active uptake pathways are  
485 derived as a function of nitrogen availability, root biomass, and two parameterized  
486 values based on nitrogen acquisition strategy (Brzostek et al. 2014). Due to this,  
487 FUN simulates a net decrease in carbon costs to acquire nitrogen with increasing  
488 nitrogen availability for mycorrhizal and non-mycorrhizal active uptake pathways,  
489 assuming constant root biomass. This was a pattern I observed in *G. hirsutum*  
490 regardless of light availability. In contrast, FUN would not simulate a net change  
491 in carbon costs to acquire nitrogen via nitrogen fixation due to nitrogen avail-  
492 ability. This is because carbon costs to acquire nitrogen via nitrogen fixation are  
493 derived from a well established function of soil temperature, which is independent  
494 of soil nitrogen availability (Houlton et al. 2008; Fisher et al. 2010). I observed  
495 a net reduction in carbon costs to acquire nitrogen in *G. max*, except when in-  
496 dividuals were grown under 0% shade cover (Fig. 2.1). While a net reduction of

497 carbon costs in response to nitrogen fertilization runs counter to nitrogen fixa-  
498 tion carbon costs simulated by FUN, these patterns were likely because *G. max*  
499 individuals switched their primary mode of nitrogen acquisition from symbiotic  
500 nitrogen fixation to a non-symbiotic active uptake pathway (Fig. 2.4B).

501 2.4.3 *Study limitations*

502 It should be noted that the metric used in this study to determine carbon  
503 costs to acquire nitrogen has several limitations. Most notably, this metric uses  
504 root carbon biomass as a proxy for estimating the amount of carbon spent on  
505 nitrogen acquisition. While it is true that most carbon allocated belowground has  
506 at least an indirect structural role in acquiring soil resources, it remains unclear  
507 whether this assumption holds true for species that acquire nitrogen via symbi-  
508 otic nitrogen fixation. I also cannot quantify carbon lost through root exudates  
509 or root turnover, which may increase due to factors that increase plant nitrogen  
510 demand (Tingey et al. 2000; Phillips et al. 2011), and can increase the magni-  
511 tude of available nitrogen from soil organic matter through priming effects on soil  
512 microbial communities (Uselman et al. 2000; Bengtson et al. 2012). It is also not  
513 clear whether these assumptions hold under all environmental conditions, such  
514 as those that shift belowground carbon allocation toward a different mode of ni-  
515 trogen acquisition (Taylor and Menge 2018; Friel and Friesen 2019) or between  
516 species with different acquisition strategies. In this study, increasing soil nitrogen  
517 fertilization increased carbon investment to roots relative to carbon transferred  
518 to root nodules (Fig. 2.4B). By assuming that carbon allocated to root carbon  
519 was proportional to carbon allocated to root nodules across all treatment com-

520 binations, these observed responses to soil nitrogen fertilization were likely to be  
521 overestimated in *G. max*. I encourage future research to quantify these carbon  
522 fates independently.

523 Researchers conducting pot experiments must carefully choose pot volume  
524 to minimize the likelihood of growth limitations induced by pot volume (Poorter  
525 et al. 2012). Poorter et al. (2012) indicate that researchers are likely to avoid  
526 growth limitations associated with pot volume if measurements are collected when  
527 the plant biomass:pot volume ratio is less than 1 g L<sup>-1</sup>. In this experiment, all  
528 treatment combinations in both species had biomass:pot volume ratios less than  
529 1 g L<sup>-1</sup> except for *G. max* and *G. hirsutum* that were grown under 0% shade  
530 cover and had received 630 ppm N. Specifically, *G. max* and *G. hirsutum* had  
531 average respective biomass:pot volume ratios of 1.24±0.07 g L<sup>-1</sup> and 1.34±0.13 g  
532 L<sup>-1</sup>, when grown under 0% shade cover and received 630 ppm N (Supplementary  
533 Tables S2, S3; Supplementary Fig. S1). If growth in this treatment combination  
534 was limited by pot volume, then individuals may have had larger carbon costs  
535 to acquire nitrogen than would be expected if they were grown in larger pots.  
536 This pot volume induced growth limitation could cause a reduction in per-root  
537 nitrogen uptake associated with more densely packed roots, which could reduce  
538 the positive effect of nitrogen fertilization on whole-plant nitrogen biomass relative  
539 to root carbon biomass (Poorter et al. 2012).

540 Growth limitation associated with pot volume provides a possible explana-  
541 tion for the marginally insignificant effect of increasing nitrogen fertilization on *G.*  
542 *max* carbon costs to acquire nitrogen when grown under 0% shade cover (Table  
543 2.3; Fig. 2.1). This is because the regression line describing the relationship be-

544 tween carbon costs to acquire nitrogen and nitrogen fertilization in *G. max* grown  
545 under 0% shade cover would have flattened if growth limitation had caused larger  
546 than expected carbon costs to acquire nitrogen in the 0% shade cover, 630 ppm  
547 N treatment combination. This may have been exacerbated by the fact that *G.*  
548 *max* likely shifted relative carbon allocation from nitrogen fixation to soil nitrogen  
549 acquisition, which could have increased the negative effect of more densely packed  
550 roots on nitrogen uptake. These patterns could have also occurred in *G. hirsutum*  
551 grown under 0% shade cover; however, there was no change in the effect of nitro-  
552 gen fertilization on *G. hirsutum* carbon costs to acquire nitrogen grown under 0%  
553 shade cover relative to other shade cover treatments. Regardless, the possibility  
554 of growth limitation due to pot volume suggests that effects of increasing nitro-  
555 gen fertilization on carbon costs to acquire nitrogen in both species grown under  
556 0% shade cover could have been underestimated. Follow-up studies using a simi-  
557 lar experimental design with a larger pot volume would be necessary in order to  
558 determine whether these patterns were impacted by pot volume-induced growth  
559 limitation.

#### 560 2.4.4 *Conclusions*

561 In conclusion, this chapter provides empirical evidence that carbon costs to  
562 acquire nitrogen are influenced by light availability and soil nitrogen fertilization  
563 in a species capable of acquiring nitrogen via symbiotic nitrogen fixation and a  
564 species not capable of forming such associations. We show that carbon costs to  
565 acquire nitrogen generally increase with increasing light availability and decrease  
566 with increasing nitrogen fertilization. This chapter provides important empirical

567 data needed to evaluate the formulation of carbon costs to acquire nitrogen in  
568 terrestrial biosphere models, particularly carbon costs to acquire nitrogen that  
569 are associated with symbiotic nitrogen fixation. My findings broadly support the  
570 general formulation of these carbon costs in the FUN biogeochemical model in  
571 response to shifts in nitrogen availability. However, there is a need for future  
572 studies to explicitly quantify carbon costs to acquire nitrogen under different en-  
573 vironmental contexts, over longer temporal scales, and using larger selections of  
574 phylogenetically related species. In addition, I suggest that future studies mini-  
575 mize the limitations associated with the metric used here by explicitly measuring  
576 belowground carbon fates independently.

577

## Chapter 3

578     Soil nitrogen availability modifies leaf nitrogen economies in mature  
579     temperate deciduous forests: a direct test of photosynthetic least-cost  
580     theory

581     3.1     Introduction

582                 Photosynthesis represents the largest carbon flux between the atmosphere  
583     and land surface (IPCC 2021), and plays a central role in biogeochemical cycling  
584     at multiple spatial and temporal scales (Vitousek and Howarth 1991; LeBauer and  
585     Treseder 2008; Kaiser et al. 2015; Wieder et al. 2015). Therefore, carbon and  
586     energy fluxes simulated by terrestrial biosphere models are sensitive to the formu-  
587     lation of photosynthetic processes (Ziehn et al. 2011; Bonan et al. 2011; Booth  
588     et al. 2012; Smith et al. 2016; Smith et al. 2017) and must be represented using  
589     robust, empirically tested processes (Prentice et al. 2015; Wieder et al. 2019).  
590     Current formulations of photosynthesis vary across terrestrial biosphere models  
591     (Smith and Dukes 2013; Rogers et al. 2017), which causes variation in modeled  
592     ecosystem processes (Knorr 2000; Knorr and Heimann 2001; Bonan et al. 2011;  
593     Friedlingstein et al. 2014) and casts uncertainty on the ability of these models to  
594     accurately predict terrestrial ecosystem responses and feedbacks to global change  
595     (Zaehle et al. 2005; Schaefer et al. 2012; Davies-Barnard et al. 2020).

596                 Terrestrial biosphere models commonly represent C<sub>3</sub> photosynthesis th-  
597     rough variants of the Farquhar et al. (1980) biochemical model (Smith and Dukes  
598     2013; Rogers 2014; Rogers et al. 2017). This well-tested photosynthesis model  
599     estimates leaf-level carbon assimilation, or photosynthetic capacity, as a function  
600     of the maximum rate of Ribulose-1,5-bisphosphate carboxylase-oxygenase (Ru-

601 bisco) carboxylation ( $V_{cmax}$ ) and the maximum rate of Ribulose-1,5-bisphosphate  
602 (RuBP) regeneration ( $J_{max}$ ) (Farquhar et al. 1980). Many terrestrial biosphere  
603 models predict these model inputs based on plant functional group specific linear  
604 relationships between leaf nutrient content and  $V_{cmax}$  (Smith and Dukes 2013;  
605 Rogers 2014; Rogers et al. 2017) under the tenet that a large fraction of leaf  
606 nutrients, and nitrogen (N) in particular, are partitioned toward building and  
607 maintaining enzymes that support photosynthetic capacity, such as Rubisco (Brix  
608 1971; Gulmon and Chu 1981; Evans 1989; Kattge et al. 2009; Walker et al. 2014).  
609 Terrestrial biosphere models also predict leaf nutrient content from soil nutrient  
610 availability based on the assumption that increasing soil nutrients generally in-  
611 creases leaf nutrients (Firn et al. 2019; Li et al. 2020; Liang et al. 2020) which, in  
612 the case of N, generally corresponds with an increase in photosynthetic processes  
613 (Li et al. 2020; Liang et al. 2020).

614       Recent work calls the generality of relationships between soil nutrient avail-  
615 ability, leaf nutrient content, and photosynthetic capacity into question, suggest-  
616 ing instead that leaf nutrients and photosynthetic capacity are better predicted as  
617 an integrated product of aboveground climate, leaf traits, and soil nutrient avail-  
618 ability, rather than soil nutrient availability alone (Dong et al. 2017; Dong et al.  
619 2020; Dong et al. 2022; Firn et al. 2019; Smith et al. 2019; Peng et al. 2021).  
620 It has been reasoned that this result is because plants allocate added nutrients to  
621 growth and storage rather than alterations in leaf chemistry (Smith et al. 2019),  
622 perhaps as a result of nutrient limitation of primary productivity (LeBauer and  
623 Treseder 2008; Fay et al. 2015). Additionally, recent work suggests that relation-  
624 ships between leaf nutrient content and photosynthesis vary across environments,

625 and that the proportion of leaf nutrient content allocated to photosynthetic tis-  
626 sue varies over space and time with plant acclimation and adaptation responses  
627 to light availability, vapor pressure deficit, soil pH, soil nutrient availability, and  
628 environmental factors that influence leaf mass per area (Pons and Pearcy 1994;  
629 Niinemets and Tenhunen 1997; Evans and Poorter 2001; Hikosaka and Shigeno  
630 2009; Ghimire et al. 2017; Onoda et al. 2017; Luo et al. 2021). The use of linear  
631 relationships between leaf nutrient content and Vcmax to predict photosynthetic  
632 capacity, as commonly used in terrestrial biosphere models (Rogers 2014), is not  
633 capable of detecting such responses.

634 Photosynthetic least-cost theory provides an alternative framework for un-  
635 derstanding relationships between soil nutrient availability, leaf nutrient content,  
636 and photosynthetic capacity (Harrison et al. 2021). Leveraging a two-input mi-  
637 croeconomics approach (Wright et al. 2003), the theory posits that plants accli-  
638 mate to a given environment by optimizing leaf photosynthesis rates at the lowest  
639 summed cost of using nutrients and water (Prentice et al. 2014; Wang et al. 2017;  
640 Smith et al. 2019; Paillassa et al. 2020). Across resource availability gradients,  
641 the theory predicts that optimal photosynthetic rates can be achieved by trading  
642 less efficient use of a resource that is less costly to acquire (or more abundant)  
643 for more efficient use of a resource more costly to acquire (or less abundant). For  
644 example, an increase in soil nutrient availability should reduce the cost of acquir-  
645 ing and using nutrients (Bae et al. 2015; Eastman et al. 2021; Perkowski et al.  
646 2021), which could increase leaf nutrient investments in photosynthetic proteins to  
647 allow similar photosynthetic rates to be achieved with higher nutrient use (lower  
648 nutrient use efficiency) but lower water use (greater water use efficiency). The

649 theory suggests similar tradeoffs in response to increasing soil pH (Paillassa et al.  
650 2020), specifically, that increasing soil pH should reduce the cost of acquiring soil  
651 nutrients due to an increase in plant-available nutrient concentration (Paillassa  
652 et al. 2020; Dong et al. 2022). The theory is also capable of reconciling dynamic  
653 leaf nutrient-photosynthesis relationships at global scales (Luo et al. 2021).

654 Patterns expected from photosynthetic least-cost theory have recently re-  
655 ceived empirical support both in global environmental gradient (Smith et al.  
656 2019; Paillassa et al. 2020; Luo et al. 2021; Querejeta et al. 2022; Wester-  
657 band et al. 2023) and local manipulative invasion (Bialic-Murphy et al. 2021)  
658 studies. However, nutrient addition experiments that directly examine nutrient-  
659 water use tradeoffs expected from the theory are rare (Guerrieri et al. 2011), and  
660 only global gradient studies testing the theory have considered soil pH in their  
661 analyses. As a result, there is a need to use nutrient addition and soil pH manu-  
662 lation experiments to test mechanisms driving responses predicted by the theory.  
663 Such experiments would also be useful to detect whether patterns expected from  
664 theory translate to finer spatial scales.

665 In this study, we measured leaf responses to soil N availability in five decid-  
666 uous tree species growing in the upper canopy of mature closed canopy temperate  
667 forests in the northeastern United States. Soil N availability and pH were manipu-  
668 lated through an N-by-pH field manipulation experiment with treatments applied  
669 since 2011, eight years prior to measurement. Two different soil N treatments  
670 were applied to increase N availability with opposing effects on soil pH. An addi-  
671 tional N-free acidifying treatment was expected to decrease soil pH. I hypothesized  
672 that increased soil N availability would enable plants to increase nutrient uptake

673 and create more photosynthetic enzymes per leaf, allowing similar photosynthetic  
674 rates achieved with lower leaf C<sub>i</sub>:C<sub>a</sub> and increased leaf N content allocated to  
675 photosynthetic leaf tissue. I expected that this response would be driven by a  
676 reduction in the cost of acquiring N, which would cause trees to sacrifice efficient  
677 N use to enable more efficient use of other limiting resources (i.e., water). Finally,  
678 I hypothesized similar leaf responses to increasing soil pH.

679 3.2 Methods

680 3.2.1 *Study site description*

681 We conducted this study in summer 2019 at three stands located within  
682 a 20-km radius of Ithaca, NY, USA (42.444 °N, 76.502 °W). All stands contain  
683 mature, closed-canopy forests dominated by deciduous tree species. Stands con-  
684 tained abundant sugar maple (*Acer saccharum* Marshall), American beech (*Fagus*  
685 *grandifolia* Ehrh.), and white ash (*Fraxinus americana* L.), accounting for 43%,  
686 15%, and 17% of the total aboveground biomass across the three stands, respec-  
687 tively, with less frequent red maple (*Acer rubrum* L.; 9% of total aboveground  
688 biomass) and red oak occurrences (*Quercus rubra* L.; 10% of total aboveground  
689 biomass). Soils at each site were broadly classified as a channery silt loam Incep-  
690 tisols using the USDA NRCS Web Soil Survey data product (Soil Survey Staff  
691 2022). Between 2006 and 2020, study sites averaged 972 mm of precipitation per  
692 year and had an average temperature of 7.9 °C per a weather station located near  
693 the Cornell University campus (42.449 °N, 76.449 °W) part of the NOAA NCEI  
694 Global Historical Climatology Network (Menne et al. 2012).

**695** 3.2.2 *Experimental design*

**696** Four 40 m x 40 m plots were set up at each site in 2009, each with an  
**697** additional 10 m buffer along plot perimeters (60 m x 60 m total). The plots  
**698** were set up as a nitrogen-by-pH field manipulation experiment, with one each of  
**699** four treatments at each site. Two nitrogen treatments were applied, both at 50  
**700** kg N ha<sup>-1</sup> yr<sup>-1</sup>, as either sodium nitrate (NaNO<sub>3</sub>) to raise soil pH, or ammonium  
**701** sulfate ((NH<sub>4</sub>)<sub>2</sub>SO<sub>4</sub>) to acidify; an elemental sulfur treatment was selected to acid-  
**702** ify without N, applied at the same rate of S addition (57 kg S ha<sup>-1</sup> yr<sup>-1</sup>); and  
**703** control plots received no additions. All amendments were added in pelletized form  
**704** using hand-held fertilizer spreaders to both the main plots and buffers. Amend-  
**705** ments were divided into three equal doses distributed across the growing season  
**706** from 2011-2017 and added as a single dose from 2018 onward. During 2019, plots  
**707** were fertilized during the week of May 20.

**708** 3.2.3 *Leaf gas exchange and trait measurements*

**709** We sampled one leaf each from 6 to 10 individuals per plot between June  
**710** 25 and July 12, 2019 for gas exchange measurements (Table S1). Leaves were  
**711** collected from deciduous broadleaf trees represented across all sites and plots  
**712** and were replicated in efforts to mimic the species abundance of each plot at  
**713** each site. We also attempted to collect leaves from the upper canopy to reduce  
**714** differential shading effects on leaf physiology. Leaves were accessed by pulling  
**715** down small branches using an arborist's slingshot and weighted beanbag attached  
**716** to a throw line. Branches were immediately recut under deionized water and  
**717** remained submerged to reduce stomatal closure and avoid xylem embolism (as in

718 Smith & Dukes, 2018) until gas exchange data were collected.

719 Randomly selected leaves with little to no visible external damage were  
720 attached to a Li-COR LI-6800 (Li-COR Bioscience, Lincoln, Nebraska, USA)  
721 portable photosynthesis machine to measure net photosynthesis ( $A_{\text{net}}$ ;  $\mu\text{mol m}^{-2}$   
722  $\text{s}^{-1}$ ), stomatal conductance ( $g_{\text{sw}}$ ;  $\text{mol m}^{-2} \text{s}^{-1}$ ), and intercellular  $\text{CO}_2$  concentra-  
723 tion ( $C_i$ ;  $\mu\text{mol mol}^{-1}$ ) at different reference  $\text{CO}_2$  concentrations ( $C_a$ ;  $\mu\text{mol mol}^{-1}$ )  
724 concentrations (i.e., an  $A_{\text{net}}/C_i$  curve) under saturating light conditions (2,000  
725  $\mu\text{mol m}^{-2} \text{s}^{-1}$ ). Reference  $\text{CO}_2$  concentrations followed the sequence: 400, 300,  
726 200, 100, 50, 400, 400, 600, 800, 1000, 1200, 1500, and 2000  $\mu\text{mol mol}^{-1} \text{CO}_2$ . Leaf  
727 temperatures were not controlled in the cuvette and ranged from 21.8 °C to 31.7  
728 °C (mean±SD:  $27.2 \pm 2.2$  °C). A linear and second order log-polynomial nonlinear  
729 regression suggested no effect of temperature on stomatal conductance measured  
730 at 400  $\mu\text{mol mol}^{-1} \text{CO}_2$  or net photosynthesis measured at  $\mu\text{mol mol}^{-1} \text{CO}_2$  (Ta-  
731 ble S2-3; Fig. S1). All  $A_{\text{net}}/C_i$  curves were generated within one hour of branch  
732 severance.

733 Leaf morphological and chemical traits were collected on the same leaf used  
734 to generate each  $A_{\text{net}}/C_i$  curve. Images of each leaf were taken using a flat-bed  
735 scanner to determine fresh leaf area using the ‘LeafArea’ R package (Katabuchi  
736 2015), which automates leaf area calculations using ImageJ software (Schneider  
737 et al. 2012). Each leaf was dried at 65°C for at least 48 hours, weighed, and  
738 ground using a Retsch MM200 ball mill grinder (Verder Scientific, Inc., Newtown,  
739 PA, USA) until homogenized. Leaf mass per area ( $M_{\text{area}}$ ,  $\text{g m}^{-2}$ ) was calculated  
740 as the ratio of dry leaf biomass to fresh leaf area. Using a subsample of ground and  
741 homogenized leaf biomass, leaf N content ( $N_{\text{mass}}$ ;  $\text{gN g}^{-1}$ ) and leaf  $\delta^{13}\text{C}$  (‰, rela-

**742** tive to VPDB) were measured at the Cornell Stable Isotope Lab with an elemental  
**743** analyzer (NC 2500, CE Instruments, Wigan, UK) interfaced to an isotope ratio  
**744** mass spectrometer (Delta V Isotope Ratio Mass Spectrometer, ThermoFisher Sci-  
**745** entific, Waltham, MA, USA). Leaf N content per unit leaf area ( $N_{\text{area}}$ ; gN m<sup>-2</sup>)  
**746** was calculated by multiplying  $N_{\text{mass}}$  by  $M_{\text{area}}$ .

**747** We used leaf  $\delta^{13}\text{C}$  values to estimate  $\chi$  (unitless), which is an isotope-  
**748** derived estimate of the leaf  $C_i:C_a$  ratio. While intercellular and atmospheric CO<sub>2</sub>  
**749** concentrations were directly measured during each  $A_{\text{net}}/C_i$  curve, deriving  $\chi$  from  
**750**  $\delta^{13}\text{C}$  provides a more integrative estimate of the  $C_i:C_a$  over an individual leaf's  
**751** lifespan. We derived  $\chi$  following the approach of Farquhar et al. (1989) described  
**752** in Cernusak et al. (2013):

$$\chi = \frac{\Delta^{13}\text{C} - a}{b - a} \quad (3.1)$$

**753** where  $\Delta^{13}\text{C}$  represents the relative difference between leaf  $\delta^{13}\text{C}$  (‰) and air  $\delta^{13}\text{C}$   
**754** (‰), and is calculated from the following equation:

$$\Delta^{13}\text{C} = \frac{\delta^{13}\text{C}_{\text{air}} - \delta^{13}\text{C}_{\text{leaf}}}{1 + \delta^{13}\text{C}_{\text{leaf}}} \quad (3.2)$$

**755** where  $\delta^{13}\text{C}_{\text{air}}$  is assumed to be -8‰ (Keeling et al. 1979; Farquhar et al. 1989), a  
**756** represents the fractionation between <sup>12</sup>C and <sup>13</sup>C due to diffusion in air, assumed  
**757** to be 4.4‰, and b represents the fractionation caused by Rubisco carboxylation,  
**758** assumed to be 27‰ (Farquhar et al. 1989).

**759** 3.2.4  $A_{\text{net}}/C_i$  curve-fitting and parameter estimation

**760** We fit  $A_{\text{net}}/C_i$  curves of each individual using the ‘fitaci’ function in the  
**761** ‘plantecophys’ R package (Duursma 2015). This function estimates the maxi-  
**762** mum rate of Rubisco carboxylation ( $V_{\text{cmax}}$ ;  $\mu\text{mol m}^{-2} \text{s}^{-1}$ ) and maximum rate  
**763** of electron transport for RuBP regeneration ( $J_{\text{max}}$ ;  $\mu\text{mol m}^{-2} \text{s}^{-1}$ ) based on the  
**764** Farquhar, von Caemmerer, and Berry biochemical model of C<sub>3</sub> photosynthesis  
**765** (Farquhar et al. 1980). For each curve fit, we included triose phosphate uti-  
**766** lization (TPU) limitation to avoid underestimating  $J_{\text{max}}$  (Gregory et al. 2021).  
**767** Curves were visually examined to confirm the likely presence of TPU limitation.

**768** We determined Michaelis-Menten coefficients for Rubisco affinity to CO<sub>2</sub>  
**769** ( $K_c$ ;  $\mu\text{mol mol}^{-1}$ ) and O<sub>2</sub> ( $K_o$ ;  $\mu\text{mol mol}^{-1}$ ), and the CO<sub>2</sub> compensation point  
**770** ( $\Gamma^*$ ;  $\mu\text{mol mol}^{-1}$ ) using leaf temperature and equations described in Medlyn et al.  
**771** (2002) and derived in Bernacchi et al. (2001). Specifically,  $K_c$  and  $K_o$  were  
**772** calculated as:

$$K_c = 404.9 * \exp^{\frac{79430(T_k - 298)}{298RT_k}} \quad (3.3)$$

**773** and

$$K_o = 278.4 * \exp^{\frac{36380(T_k - 298)}{298RT_k}} \quad (3.4)$$

**774** while  $\Gamma^*$  was calculated as:

$$\Gamma^* = 42.75 * \exp^{\frac{37830(T_k - 298)}{298RT_k}} \quad (3.5)$$

**775** In all three equations,  $T_k$  is the leaf temperature (in Kelvin) during each  $A_{\text{net}}/C_i$

**776** curve and R is the universal gas constant ( $8.314 \text{ J mol}^{-1} \text{ K}^{-1}$ ).

**777** We standardized  $V_{\text{cmax}}$  and  $J_{\text{max}}$  estimates to  $25^\circ\text{C}$  using a modified Ar-

**778** rhenius equation (Kattge and Knorr 2007):

$$k_{25} = \frac{k_{\text{obs}}}{e^{\frac{H_a(T_{\text{obs}} - T_{\text{ref}})}{T_{\text{ref}}RT_{\text{obs}}}} * \frac{1+e^{\frac{T_{\text{ref}}\Delta S - H_d}{T_{\text{obs}}}}}{1+e^{\frac{T_{\text{obs}}\Delta S - H_d}{T_{\text{obs}}}}}} \quad (3.6)$$

**779**  $k_{25}$  represents the standardized  $V_{\text{cmax}}$  or  $J_{\text{max}}$  rate at  $25^\circ\text{C}$ ,  $k_{\text{obs}}$  represents

**780** the  $V_{\text{cmax}}$  or  $J_{\text{max}}$  estimate at the average leaf temperature measured inside the

**781** cuvette during the  $A_{\text{net}}/C_i$  curve.  $H_a$  is the activation energy of  $V_{\text{cmax}}$  ( $71,513$

**782**  $\text{J mol}^{-1}$ ) Kattge and Knorr (2007) or  $J_{\text{max}}$  ( $49,884 \text{ J mol}^{-1}$ ) (Kattge and Knorr

**783** 2007).  $H_d$  represents the deactivation energy of both  $V_{\text{cmax}}$  and  $J_{\text{max}}$  ( $200,000 \text{ J}$

**784**  $\text{mol}^{-1}$ ) (Medlyn et al. 2002), and R represents the universal gas constant ( $8.314$

**785**  $\text{J mol}^{-1} \text{ K}^{-1}$ ).  $T_{\text{ref}}$  represents the standardized temperature of  $298.15 \text{ K}$  ( $25^\circ\text{C}$ )

**786** and  $T_{\text{obs}}$  represents the mean leaf temperature (in K) during each  $A_{\text{net}}/C_i$  curve.

**787**  $\Delta S$  is an entropy term that (Kattge and Knorr 2007) derived as a linear relation-

**788** ship with average growing season temperature ( $T_g$ ;  $^\circ\text{C}$ ), where:

$$\Delta S_{v_{\text{cmax}}} = -1.07 T_g + 668.39 \quad (3.7)$$

**789** and

$$\Delta S_{j_{\text{max}}} = -0.75 T_g + 659.70 \quad (3.8)$$

**790** We estimated  $T_g$  in Equations 3.7 and 3.8 based on mean daily (24-hour) air  
**791** temperature of the 30 days leading up to the day of each sample collection using  
**792** the same weather station reported in the site description. We then used  $V_{cmax25}$   
**793** and  $J_{max25}$  estimates to calculate the ratio of  $J_{max25}$  to  $V_{cmax25}$  ( $J_{max25}:V_{cmax25}$ ;  
**794** unitless).

**795** 3.2.5 *Proportion of leaf nitrogen allocated to photosynthesis and structure*

**796** We used equations from Niinemets and Tenhunen (1997) to estimate the  
**797** proportion of leaf N content allocated to Rubisco and bioenergetics. The propor-  
**798** tion of leaf N allocated to Rubisco ( $\rho_{rub}$ ; gN gN $^{-1}$ ) was calculated as a function  
**799** of  $V_{cmax25}$  and  $N_{area}$ :

$$\rho_{rubisco} = \frac{V_{cmax25} N_r}{V_{cr} N_{area}} \quad (3.9)$$

**800** where  $N_r$  is the amount of nitrogen in Rubisco, set to 0.16 gN (gN in Rubisco) $^{-1}$   
**801** and  $V_{cr}$  is the maximum rate of RuBP carboxylation per unit Rubisco protein,  
**802** set to 20.5  $\mu$ mol CO $_2$  (g Rubisco) $^{-1}$ . The proportion of leaf nitrogen allocated to  
**803** bioenergetics ( $\rho_{bioe}$ ; gN gN $^{-1}$ ) was similarly calculated as a function of  $J_{max25}$  and  
**804**  $N_{area}$ :

$$\rho_{bioe} = \frac{J_{max25} N_b}{J_{mc} N_{area}} \quad (3.10)$$

**805** where  $N_b$  is the amount of nitrogen in cytochrome f, set to 0.12407 gN ( $\mu$ mol  
**806** cytochrome f) $^{-1}$  assuming a constant 1: 1: 1.2 cytochrome f: ferredoxin NADP  
**807** reductase: coupling factor molar ratio (Evans and Seemann 1989; Niinemets and

808 Tenhunen 1997), and  $J_{mc}$  is the capacity of electron transport per cytochrome f,  
809 set to  $156 \mu\text{mol electron} (\mu\text{mol cytochrome f})^{-1}\text{s}^{-1}$ .

810 We estimated the proportion of leaf N content allocated to photosynthetic  
811 tissue ( $\rho_{photo}$ ;  $\text{gN gN}^{-1}$ ) as the sum of  $\rho_{rub}$  and  $\rho_{bioe}$ . This calculation is an un-  
812 derestimate of the proportion of leaf N allocated to photosynthetic tissue because  
813 it does not include N allocated to light harvesting proteins. This leaf N pool was  
814 not included because we did not perform chlorophyll extractions on focal leaves.  
815 However, the proportion of leaf N content allocated to light harvesting proteins  
816 tends to be small relative to  $\rho_{rub}$  and  $\rho_{bioe}$ , and may scale with changes in  $\rho_{rub}$   
817 and  $\rho_{bioe}$  (Niinemets and Tenhunen 1997).

818 Finally, we estimated the proportion of leaf N content allocated to struc-  
819 tural tissue ( $\rho_{str}$ ;  $\text{gN gN}^{-1}$ ) using an empirical equation from Onoda et al. (2017):

$$N_{cw} = 0.000355 * M_{area}^{1.39} \quad (3.11)$$

820 where  $N_{cw}$  is the leaf N content allocated to cell walls ( $\text{gN m}^{-2}$ ).  $\rho_{str}$  was estimated  
821 by dividing  $N_{cw}$  by  $N_{area}$ .

### 822 3.2.6 *Tradeoffs between nitrogen and water use*

823 Photosynthetic nitrogen use efficiency (PNUE;  $\mu\text{mol CO}_2 \text{ mol}^{-1} \text{ N s}^{-1}$ )  
824 was calculated by dividing  $A_{net}$  by  $N_{area}$ , first converting  $N_{area}$  to  $\text{mol N m}^{-2}$   
825 using the molar mass of N ( $14 \text{ g mol}^{-1}$ ). We used  $\chi$  as an indicator of water  
826 use efficiency, which exploratory analyses suggest had similar responses to soil N  
827 availability and pH as intrinsic water use efficiency measured from gas exchange

828 ( $A_{\text{net}}/g_s$ ). Tradeoffs between nitrogen and water use were determined by cal-  
829 culating the ratio of  $N_{\text{area}}$  to  $\chi$  ( $N_{\text{area}}:\chi$ ; g N m<sup>-2</sup>) and  $V_{\text{cmax25}}$  to  $\chi$  ( $V_{\text{cmax25}}:\chi$ ;  
830  $\mu\text{mol m}^{-2} \text{s}^{-1}$ ). This approach is similar to tradeoff calculations in which nitrogen-  
831 water use tradeoffs are measured as the ratio of  $N_{\text{area}}$  or  $V_{\text{cmax25}}$  to  $g_s$  (Paillassa  
832 et al. 2020; Bialic-Murphy et al. 2021). In this study, we quantify these re-  
833 lationships using  $\chi$  in lieu of  $g_s$  because  $g_s$  rapidly changes with environmental  
834 conditions and therefore may have been altered by recent tree branch severance  
835 and/or placement in the cuvette.

836 3.2.7 *Soil nitrogen availability and pH*

837 To characterize soil N availability at the time of our leaf gas exchange  
838 measurements, we used mixed bed resin bags to quantify mobile ammonium-N  
839 and nitrate-N concentrations in each plot. Lycra mesh bags were filled with 5 g  
840 of Dowex® Marathon MR-3 hydrogen and hydroxide form resin (MilliporeSigma,  
841 Burlington, MA USA) and sealed with a zip tie. Each bag was activated by  
842 soaking in 0.5 M HCl for 20 minutes, then in 2 M NaCl until pH of the saline  
843 solution stabilized, as described in Allison et al. (2008). Five resin bags were  
844 inserted about 10 cm below the soil surface at each plot on June 25, 2019: one  
845 near each of the four plot corners and one near the plot center. All resin bags  
846 were collected 24 days later on July 19, 2019 and were frozen until extracted.

847 Prior to anion and cation extraction, each resin bag was rinsed with ul-  
848 trapure water (MilliQ IQ 7000; Millipore Sigma, Burlington, MA) to remove any  
849 surface soil residues. Anions and cations were extracted from surface-cleaned resin  
850 bags by individually soaking and shaking each bag in 100 mL of a 0.1 M HCl/2.0

851 M NaCl matrix for one hour. Using a microplate reader (Biotek Synergy H1;  
852 Biotek Instruments, Winooski, VT USA), nitrate-N concentrations were quanti-  
853 fied spectrophotometrically at 540 nm with the end product of a single reagent  
854 vanadium (III) chloride reaction (Doane and Horwáth 2003), and ammonium-N  
855 concentrations quantified at 650 nm with the end product of a modified phenol-  
856 hypochlorite reaction (Weatherburn 1967; Rhine et al. 1998). Both the single  
857 reagent vanadium (III) chloride and modified phenol-hypochlorite methodologies  
858 have been well established for determining nitrate-N and ammonium-N concen-  
859 trations in resin bag extracts (Arnone 1997; Allison et al. 2008). We used a  
860 series of negative and positive controls throughout each well plate to verify the  
861 accuracy and precision of our measurements, assaying each resin bag extract and  
862 control in triplicate. Soil N availability was estimated as the sum of the nitrate-N  
863 and ammonium-N concentration in each resin bag, normalized per g of resin and  
864 duration in the field ( $\mu\text{g N g}^{-1} \text{ resin d}^{-1}$ ), then subsequently averaged across all  
865 resin bags in a plot for a plot-level mean.

866 Soil pH was measured on 0-10 cm mineral soil samples collected prior to  
867 fertilization in 2019. Near each of the four plot corners, three 5.5 cm diameter soil  
868 cores were collected after first removing the forest floor where present. Each set  
869 of three cores was placed in a plastic bag, and later composited by hand mixing  
870 and sieved to 4mm. Soil pH was determined for a 1:2 soil:water slurry (10 g field-  
871 moist soil to 20 mL DI water) of each sample using an Accumet AB15 pH meter  
872 with flushable junction probe (Fisher Scientific; Hampton, NH, USA), and was  
873 estimated at the plot level as the mean soil pH within each plot.

**874** 3.2.8 *Statistical analyses*

**875** We built two separate series of linear mixed-effects models to explore effects  
**876** of soil N availability, soil pH, species, and leaf N content on leaf physiological  
**877** traits. In the first series of linear mixed-effects models, we explored the effect  
**878** of soil N availability, soil pH, and species on leaf N content, leaf photosynthesis,  
**879** stomatal conductance, and nitrogen-water use tradeoffs. Models included plot-  
**880** level soil N availability and plot-level soil pH as continuous fixed effects, species  
**881** as a categorical fixed effect, and site as a categorical random intercept term.  
**882** Interaction terms between fixed effects were not included due to the small number  
**883** of experimental plots. We built a series of separate models with this independent  
**884** variable structure to quantify individual effects of soil N availability, soil pH,  
**885** and species on  $N_{\text{area}}$ ,  $M_{\text{area}}$ ,  $N_{\text{mass}}$ ,  $A_{\text{net}}$ ,  $V_{\text{cmax25}}$ ,  $J_{\text{max25}}$ ,  $J_{\text{max25}}:V_{\text{cmax25}}$ ,  $\rho_{\text{rubisco}}$ ,  
**886**  $\rho_{\text{bioenergetics}}$ ,  $\rho_{\text{photo}}$ ,  $\rho_{\text{structure}}$ ,  $\chi$ , PNUE,  $N_{\text{area}}:\chi$ , and  $V_{\text{cmax25}}:\chi$ .

**887** A second series of linear mixed-effects models were built to investigate  
**888** relationships between leaf N content and photosynthetic parameters. Statistical  
**889** models included  $N_{\text{area}}$  as a single continuous fixed effect with species and site des-  
**890** ignated as individual random intercept terms. We used this independent variable  
**891** structure to quantify individual effects of leaf N content on  $A_{\text{net}}$ ,  $V_{\text{cmax25}}$ ,  $J_{\text{max25}}$ ,  
**892**  $J_{\text{max25}}:V_{\text{cmax25}}$ , and  $\chi$ .

**893** For all linear mixed-effects models, we used Shapiro-Wilk tests of normal-  
**894** ity to determine whether linear mixed-effects models satisfied residual normality  
**895** assumptions. If residual normality assumptions were not met, then models were  
**896** fit using dependent variables that were natural log transformed. If residual nor-  
**897** mality assumptions were still not met (Shapiro-Wilk:  $p < 0.05$ ), then models were

898 fit using dependent variables that were square root transformed. All residual nor-  
899 mality assumptions for both sets of models that did not originally satisfy residual  
900 normality assumptions were met with either a natural log or square root data  
901 transformation (Shapiro-Wilk:  $p > 0.05$  in all cases).

902 In the first series of models, models for  $N_{\text{area}}$ ,  $M_{\text{area}}$ ,  $N_{\text{mass}}$ ,  $V_{\text{cmax25}}$ ,  $J_{\text{max25}}$ ,  
903  $\chi$ ,  $N_{\text{area}}:\chi$ , and  $V_{\text{cmax25}}:\chi$ ,  $\rho_{\text{rubisco}}$ ,  $\rho_{\text{bioenergetics}}$ ,  $\rho_{\text{photo}}$ ,  $\rho_{\text{structure}}$  satisfied residual  
904 normality assumptions without data transformations (Shapiro-Wilk:  $p > 0.05$  in  
905 all cases). The model for  $J_{\text{max25}}:V_{\text{cmax25}}$  satisfied residual normality assumptions  
906 with a natural log data transformation, while models for  $A_{\text{net}}$  and PNUE each  
907 satisfied residual normality assumptions with square root data transformations.  
908 In the second series of models, models for  $V_{\text{cmax25}}$ ,  $J_{\text{max25}}$ ,  $\chi$ , and  $V_{\text{cmax25}}:\chi$  satisfied  
909 residual normality assumptions without data transformations (Shapiro-Wilk:  $p$   
910  $> 0.05$  in all cases). The model for  $J_{\text{max25}}:V_{\text{cmax25}}$  required a natural log data  
911 transformation and the model for  $A_{\text{net}}$  required a square root data transformation  
912 (Shapiro-Wilk:  $p > 0.05$  in both cases).

913 In all models, we used the ‘lmer’ function in the ‘lme4’ R package (Bates  
914 et al. 2015) to fit each model and the ‘Anova’ function in the ‘car’ R package (Fox  
915 and Weisberg 2019) to calculate Type II Wald’s  $\chi^2$  and determine the significance  
916 level ( $\alpha = 0.05$ ) of each fixed effect coefficient. Finally, we used the ‘emmeans’  
917 R package (Lenth, 2019) to conduct post-hoc comparisons using Tukey’s tests,  
918 where degrees of freedom were approximated using the Kenward-Roger approach  
919 (Kenward and Roger 1997). All analyses and plots were conducted in R version  
920 4.1.1 (R Core Team 2021). All figure regression lines and associated 95% confi-  
921 dence interval error bars were plotted using predictions generated across the soil

**922** nitrogen availability gradient using the ‘emmeans’ R package (Lenth 2019).

**923** 3.3 Results

**924** 3.3.1 *Leaf N content*

**925** Increasing soil N availability generally increased  $N_{\text{area}}$  (Table 3.1; Fig.  
**926** 3.1a). This pattern was driven by an increase in  $N_{\text{mass}}$  (Table 3.1; Fig. 3.1c)  
**927** and a marginal increase in  $M_{\text{area}}$  (Table 3.1; Fig. 3.1e) with increasing soil N  
**928** availability. There was no effect of soil pH on  $N_{\text{area}}$ ,  $N_{\text{mass}}$ , or  $M_{\text{area}}$  (Table 3.1);  
**929** however, we did observe strong differences in  $N_{\text{area}}$  (Fig. 3.1b),  $N_{\text{mass}}$  (Fig. 3.1d),  
**930** and  $M_{\text{area}}$  (Fig. 3.1e) between species (Table 3.1).

**Table 3.1.** Effects of soil N availability, soil pH, and species on leaf N content per unit leaf area ( $N_{\text{area}}$ ), leaf N content per unit leaf mass ( $N_{\text{mass}}$ ), and leaf mass per unit leaf area ( $M_{\text{area}}$ )

	$N_{\text{area}}$			$N_{\text{mass}}$			$M_{\text{area}}$			
	df	Coefficient	$\chi^2$	p	Coefficient	$\chi^2$	p	Coefficient	$\chi^2$	p
Intercept	-	9.03E-01	-	-	1.68E+00	-	-	4.60E+01	-	-
Soil N	1	1.68E-02	11.990	<b>0.001</b>	1.25E-02	6.902	<b>0.009</b>	4.87E-01	4.143	<b>0.042</b>
Soil pH	1	9.28E-02	0.836	0.361	8.08E-02	0.663	0.415	4.05E+00	0.653	0.419
Species	4	-	72.128	<b>&lt;0.001</b>	-	35.074	<b>&lt;0.001</b>	-	29.869	<b>&lt;0.001</b>

931 \*Significance determined using Type II Wald  $\chi^2$  tests ( $\alpha = 0.05$ ). P-values  $< 0.05$  are in bold.

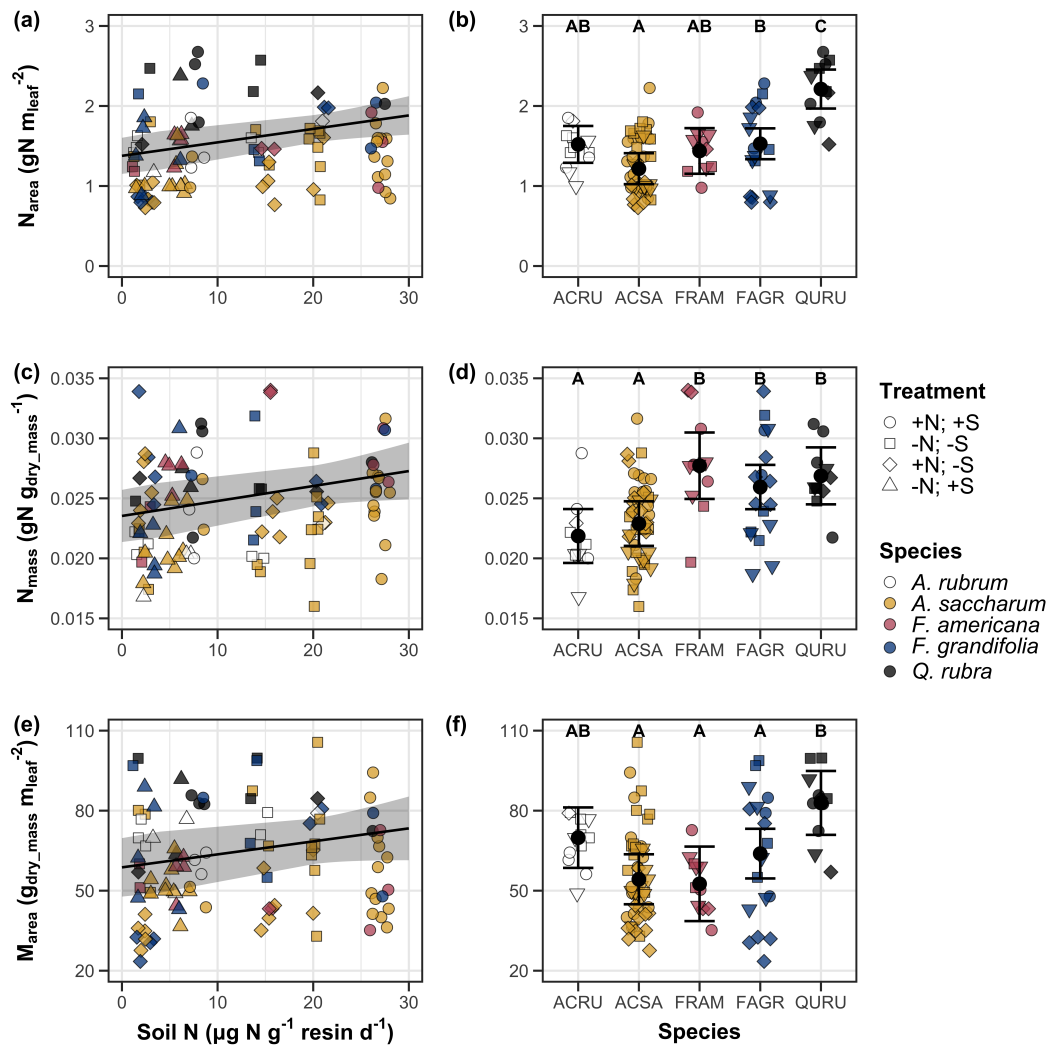


**Figure 3.1.** Effects of soil N availability and species on leaf N content per unit leaf area (a-b), leaf nitrogen content per unit leaf biomass (c-d), and leaf mass per leaf area (e-f). Soil N availability is represented on the x-axis in the left column of panels, while species is represented on the x-axis in the right column of panels. Tree species are represented as colored points and treatment plots are represented as shaped points, jittered for visibility. Species are abbreviated in the right column of panels through their assigned NRCS PLANTS Database symbol (USDA NRCS 2022), grouped along the x-axis per common mycorrhizal association, where the first three species commonly associate with arbuscular mycorrhizae (ACRU, ASCA, FAGR) and the second two species with ectomycorrhizae (FAGR, QURU). Trendlines are only included when the regression slope is statistically different from zero ( $p < 0.05$ ).

**932** 3.3.2 *Net photosynthesis and leaf biochemistry*

**933** Increasing soil N availability generally had no effect on  $A_{\text{net}}$ ,  $V_{\text{cmax25}}$ ,  $J_{\text{max25}}$ ,  
**934** or  $J_{\text{max25}}:V_{\text{cmax25}}$  (Table 3.2, Figs. 3.2a, 3.2d, 3.2g). We also observed strong  
**935** species effects on all measured leaf photosynthetic traits (Table 3.2; Figs. 3.2b,  
**936** 3.2e, 3.2h). Increasing soil pH had a marginal negative effect on  $A_{\text{net}}$ , but had no  
**937** effect on  $V_{\text{cmax25}}$ ,  $J_{\text{max25}}$ , or  $J_{\text{max25}}:V_{\text{cmax25}}$  (Table 3.2). There was a weak positive  
**938** effect of increasing  $N_{\text{area}}$  on  $A_{\text{net}}$  (Fig. 3.2c), but quite strong positive effects of  
**939** increasing  $N_{\text{area}}$  on  $V_{\text{cmax25}}$  and  $J_{\text{max25}}$  (Table 3.2; Fig. 3.2f and 3.2i).

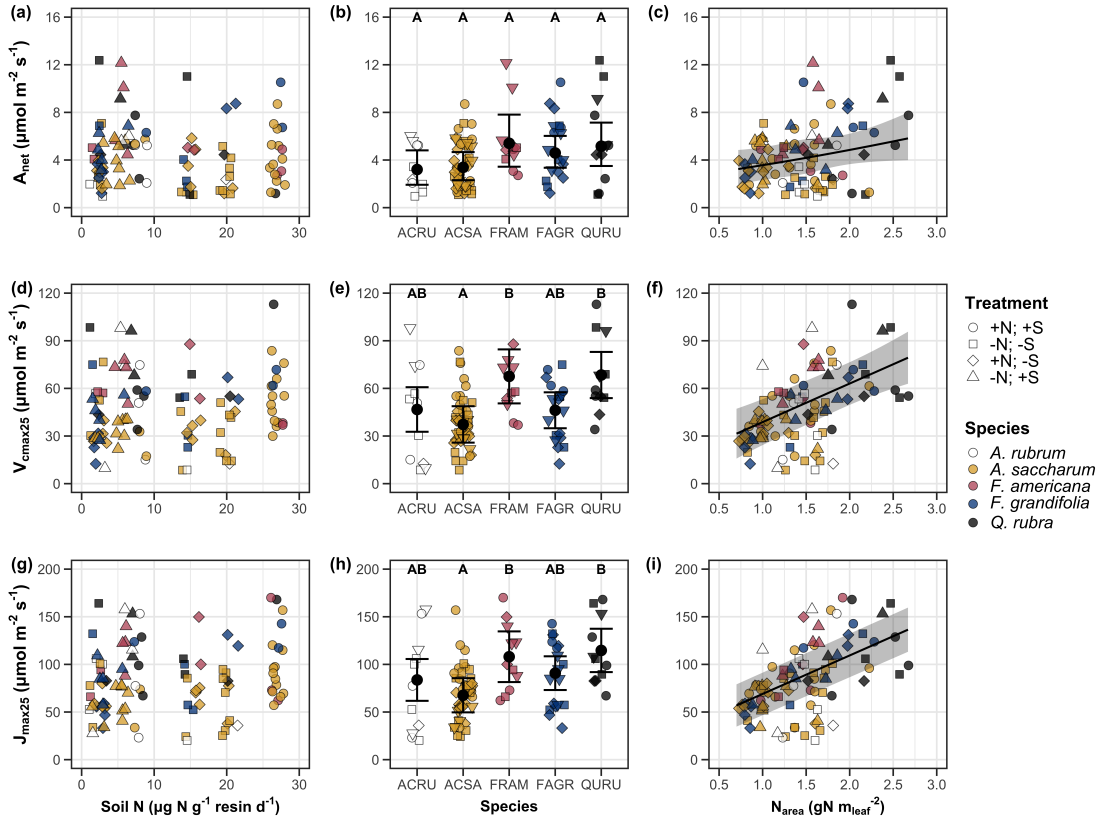
**Table 3.2.** Effects of soil N availability, soil pH, species, and  $N_{\text{area}}$  on leaf biochemistry

	$A_{\text{net}}$			$V_{\text{cmax25}}$			$J_{\text{max25}}$			
	df	Coefficient	$\chi^2$	p	Coefficient	$\chi^2$	p	Coefficient	$\chi^2$	p
(Intercept)	-	3.29E+00 <sup>b</sup>	-	-	6.38E+01	-	-	1.12E+02	-	-
Soil N	1	-1.23E-03 <sup>b</sup>	1.798	0.180	-3.84E-01	1.745	0.187	-6.70E-01	2.172	0.141
Soil pH	1	-3.09E-01 <sup>b</sup>	3.312	0.069	-4.91E+00	0.655	0.418	-8.18E+00	0.742	0.389
Species	4	-	11.838	<b>0.019</b>	-	31.748	<0.001	-	27.291	<0.001
( $N_{\text{area}}$ int.)	-	6.59E-01 <sup>b</sup>	-	-	1.45E-01	-	-	2.86E+01	-	-
$N_{\text{area}}$	4	3.13E-01 <sup>b</sup>	4.790	<b>0.029</b>	2.43E+01	22.616	<0.001	4.04E+01	28.259	<0.001

	$J_{\text{max25}}:V_{\text{cmax25}}$			
	df	Coefficient	$\chi^2$	p
(Intercept)	-	6.59E-01 <sup>a</sup>	-	-
Soil N	1	7.04E-04 <sup>a</sup>	0.088	0.767
Soil pH	1	-7.84E-03 <sup>a</sup>	0.025	0.874
Species	4	-	12.745	<b>0.013</b>
( $N_{\text{area}}$ int.)	-	6.69E-01 <sup>a</sup>	-	-
$N_{\text{area}}$	4	-4.69E-02 <sup>a</sup>	1.142	0.285

940 \*Significance determined using Type II Wald  $\chi^2$  tests ( $\alpha = 0.05$ ). P-values  $< 0.05$  are in bold, while p-values between  
 941 0.05 and 0.1 are italicized. Superscript letters indicate model coefficients fit to natural-log (<sup>a</sup>) or square-root (<sup>b</sup>)  
 942 transformed data. Relationships between  $N_{\text{area}}$  and each response variable were fit using the second series of bivariate  
 943 mixed-effects models, so model coefficients and results are independent of model coefficients and results reported  
 944 for relationships between soil N, soil pH, and species for each response variable. Key:  $A_{\text{net}}$  – light saturated net  
 945 photosynthesis rate;  $V_{\text{cmax25}}$  – maximum rate of Rubisco carboxylation at 25°C;  $J_{\text{max25}}$  – maximum rate of electron  
 946 transport for RuBP regeneration at 25°C,  $J_{\text{max25}}:V_{\text{cmax25}}$  – the ratio of  $J_{\text{max25}}$  to  $V_{\text{cmax25}}$ .



**Figure 3.2.** Effects of soil N availability (left column of panels), species (middle column of panels), and leaf N content per unit leaf area (right column of panels) on net photosynthesis (a-c), maximum Rubisco carboxylation rate (d-f), and maximum RuBP regeneration rate (g-i). Soil N availability is represented on the x-axis in the left column of panels, species is represented on the x-axis in the middle column of panels, and leaf N content per unit leaf area is represented continuously on the x-axis in the right column of panels. Species abbreviations and position along the x-axis in the middle column of panels, colored points, shapes, and trendlines are as explained in Figure 3.1.

**947** 3.3.3 *Leaf N allocation*

**948** Neither soil N availability nor soil pH affected the proportion of leaf N  
**949** allocated to Rubisco or bioenergetics (Table 3.3; Fig. 3.3a, Fig. 3.3c), nor was  
**950** there any subsequent effect on the proportion of leaf N allocated to photosynthesis  
**951** (Table 3.3; Fig. 3.3f). We also found no effect of soil N availability or soil pH on  
**952** the proportion of leaf N allocated to structure (Table 3.3; Fig 3.3g). Species varied  
**953** in the proportion of leaf N allocated to Rubisco, photosynthesis, and structure (Fig  
**954** 3.3b, Fig. 3.3d, Fig 3.3h), with no detectable species effect on the proportion of  
**955** leaf N allocated to bioenergetics (Table 3.3).

**Table 3.3.** Effects of soil N availability, soil pH, and species on the proportion of leaf nitrogen content allocated to photosynthesis, Rubisco, bioenergetics, and structure

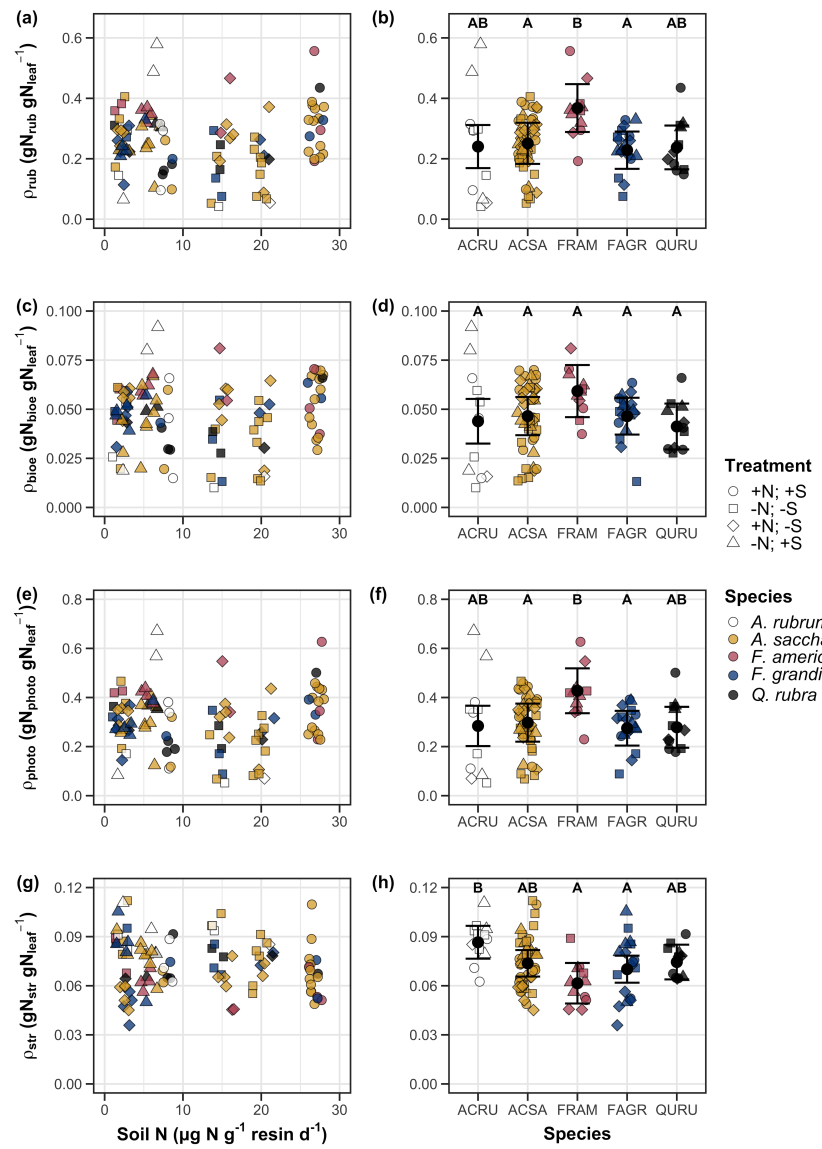
	$\rho_{\text{photo}}$			$\rho_{\text{rub}}$			$\rho_{\text{bioe}}$			
	df	Coefficient	$\chi^2$	p	Coefficient	$\chi^2$	p	Coefficient	$\chi^2$	p
Intercept	-	4.93E-01	-	-	4.17E-01	-	-	7.64E-02	-	-
Soil N	1	-1.23E-03	0.521	0.470	-1.04E-03	0.501	0.479	-1.77E-04	0.557	0.455
Soil pH	1	-4.37E-02	1.581	0.209	-3.70E-02	1.511	0.219	-6.84E-03	1.941	0.164
Species	4	-	13.106	<b>0.011</b>	-	14.152	<b>0.007</b>	-	7.300	0.121

	$\rho_{\text{str}}$			
	df	Coefficient	$\chi^2$	p
Intercept	-	9.77E-02	-	-
Soil N	1	-2.29E-04	1.165	0.280
Soil pH	1	-1.87E-03	0.179	0.672
Species	4	-	16.428	<b>0.002</b>

58

956 \*Significance determined using Type II Wald  $\chi^2$  tests ( $\alpha = 0.05$ ). P-values  $< 0.05$  are in bold. Key:  $\rho_{\text{photo}}$  -  
 957 proportion of leaf nitrogen content allocated to photosynthesis;  $\rho_{\text{rub}}$  - proportion of leaf nitrogen content allocated  
 958 to Rubisco;  $\rho_{\text{bioe}}$  - proportion of leaf nitrogen content allocated to bioenergetics;  $\rho_{\text{str}}$  - proportion of leaf nitrogen  
 959 content allocated to structure.



**Figure 3.3.** Effects of soil nitrogen availability and species on the proportion of leaf nitrogen content allocated to Rubisco (a-b), bioenergetics (c-d), photosynthesis (e-f), and structure (g-h). Soil nitrogen availability is represented on the x-axis in the left column of panels and species are represented on the x-axis in the right column of panels. Species abbreviations and position along the x-axis in the middle column of panels, colored points, shapes, trendlines, error bars, and compact lettering are as explained in Figure 3.1.

**960** 3.3.4 *Tradeoffs between nitrogen and water use*

**961** Although soil N availability did not affect  $\chi$  (Table 3.4; Fig. 3.4a), increasing  
**962** soil N availability decreased PNUE (Table 3.4; Fig. 3.4d) and increased the  
**963** ratio of  $N_{\text{area}}:\chi$  (Table 3.4; Fig. 3.4f). Specifically, this response yielded a 26%  
**964** reduction in PNUE and 37% stimulation in  $N_{\text{area}}:\chi$  across the soil nitrogen avail-  
**965** ability gradient. There was no apparent effect of soil N availability on  $V_{\text{cmax25}}:\chi$   
**966** (Table 3.4; Fig. 3.4h). Increasing soil pH had a weak marginal negative effect  
**967** on PNUE, but did not influence  $\chi$ ,  $N_{\text{area}}:\chi$ , or  $V_{\text{cmax25}}:\chi$  (Table 3.4). We also  
**968** observed differences in  $\chi$  (Fig. 3.4b), PNUE (Fig. 3.4e),  $N_{\text{area}}:\chi$  (Fig. 3.4g), and  
**969**  $V_{\text{cmax25}}:\chi$  (Fig. 3.4i) between species (Table 3.4). Finally, increasing  $N_{\text{area}}$  had a  
**970** strong negative effect on  $\chi$  (Table 3.4; Fig. 3.4c) and a strong positive effect on  
**971**  $V_{\text{cmax25}}:\chi$  (Table 3.4; Fig. 3.4j).

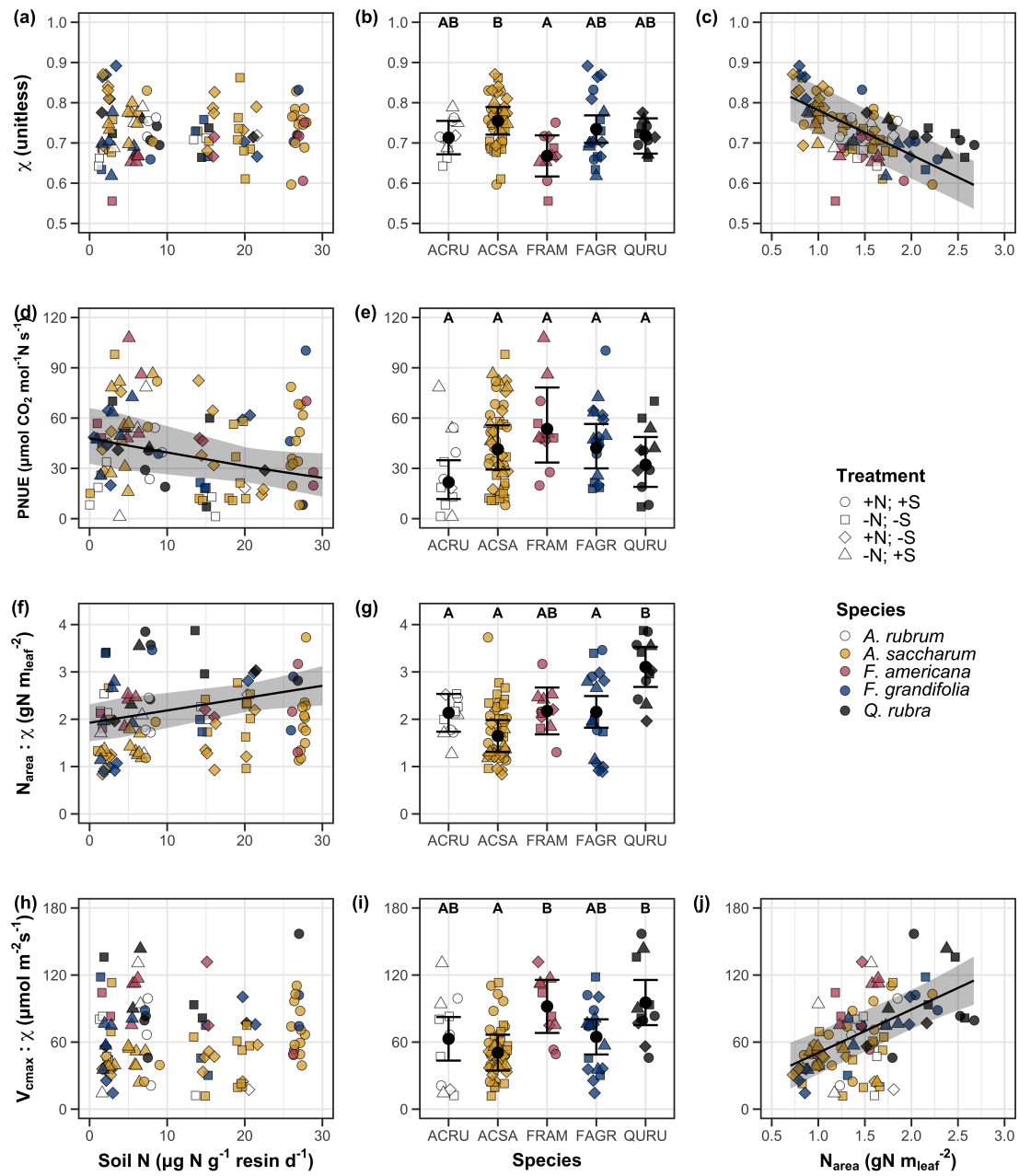
**Table 3.4.** Effects of soil N availability, soil pH, species, and  $N_{\text{area}}$  on tradeoffs between nitrogen and water use

	$\chi$	PNUE				$N_{\text{area}}:\chi$				
	df	Coefficient	$\chi^2$	p	Coefficient	$\chi^2$	p	Coefficient	$\chi^2$	p
(Intercept)	-	8.12E-01	-	-	9.57E+00	-	-	9.19E-01	-	-
Soil N	1	-1.14E-03	1.698	0.193	-6.63E-02	6.396	<b>0.011</b>	2.60E-02	9.533	<b>0.002</b>
Soil pH	1	-1.91E-02	1.087	0.297	-9.25E-01	2.843	<i>0.092</i>	2.03E-01	1.321	0.250
Species	4	-	18.843	<b>0.001</b>	-	13.454	<b>0.009</b>	-	52.983	<b>&lt;0.001</b>
$(N_{\text{area}} \text{ int.})$	-	8.93E-01	-	-	-	-	-	-	-	-
$N_{\text{area}}$	1	-1.11E-01	80.606	<b>&lt;0.001</b>	-	-	-	-	-	-

	$V_{\text{cmax25}}:\chi$			
	df	Coefficient	$\chi^2$	p
(Intercept)	-	7.20E+01	-	-
Soil N	1	3.99E-01	0.963	0.326
Soil pH	1	-3.12E+00	0.138	0.711
Species	4	-	31.450	<b>&lt;0.001</b>
$(N_{\text{area}} \text{ int.})$	-	1.18E+01	-	-
$N_{\text{area}}$	4	3.87E+01	32.797	<b>&lt;0.001</b>

\*Significance determined using Type II Wald  $\chi^2$  tests ( $\alpha = 0.05$ ).  $P$ -values  $< 0.05$  are in bold, while  $p$ -values between 0.05 and 0.1 are italicized. Superscript letters indicate model coefficients fit to natural-log <sup>(a)</sup> or square-root <sup>(b)</sup> transformed data. Relationships between  $N_{\text{area}}$  and each response variable were fit using the second series of bivariate mixed-effects models, so model coefficients and results are independent of model coefficients and results reported for relationships between soil N, soil pH, and species for each response variable. Key:  $\chi$  - isotope-derived estimate of the  $C_i:C_a$ ; PNUE - photosynthetic N use efficiency, ratio of net photosynthesis to leaf N content per unit leaf area;  $N_{\text{area}}:\chi$  - ratio of  $N_{\text{area}}$  to  $\chi$ ;  $V_{\text{cmax25}}:\chi$  - ratio of  $V_{\text{cmax25}}$  to  $\chi$ .



**Figure 3.4.** Effects of soil nitrogen availability and species on the proportion of leaf nitrogen content allocated to Rubisco (a-b), bioenergetics (c-d), photosynthesis (Rubisco + bioenergetics; e-f), and structure (g-h). Soil nitrogen availability is represented on the x-axis in the left column of panels and species are represented on the x-axis in the right column of panels. Species abbreviations and position along the x-axis in the middle column of panels, colored points, shapes, trendlines, error bars, and compact lettering are as explained in Figure 3.1.

**979** 3.4 Discussion

**980** Photosynthetic least-cost theory provides an explanation for understand-  
**981** ing relationships between soil nutrient availability, leaf nutrient allocation, and  
**982** photosynthetic capacity. The theory suggests that plants acclimate to a given  
**983** environment by optimizing leaf photosynthesis rates at the lowest summed cost  
**984** of using nutrients and water Prentice et al. (2014), Wang et al. (2017), Smith  
**985** et al. (2019), Paillassa et al. (2020). The theory predicts that an increase in  
**986** soil nutrient availability should allow similar photosynthesis rates to be achieved  
**987** with increased leaf nutrient content and photosynthetic capacity (i.e.,  $V_{cmax25}$  and  
**988**  $J_{max25}$ ) at lower leaf  $C_i:C_a$  ( $\chi$ ), resulting in an increase in water use efficiency,  
**989** decrease in nutrient use efficiency, and increase in both leaf nutrient content and  
**990** photosynthetic capacity per unit  $\chi$ . The theory predicts similar leaf responses to  
**991** increasing soil pH under acidic conditions, presumably due to generally faster nu-  
**992** trient cycle dynamics and consequent reductions in the cost of acquiring nutrients  
**993** relative to water with increasing soil pH (Wang et al. 2017; Paillassa et al. 2020;  
**994** Dong et al. 2020).

**995** Supporting the theory, we showed that increasing soil N availability was  
**996** associated with increased leaf N content (Fig 3.1a, 3.1c), a pattern that reduced  
**997** photosynthetic N use efficiency (Fig 3.4d) and increased leaf N content per unit  
**998**  $\chi$  (Fig 3.4f). Increasing soil N coincided with slight, but non-significant decreases  
**999** in  $\chi$  and increases in  $V_{cmax25}$  and  $J_{max25}$  ( $p < 0.2$ , Table 3.2). The positive trend  
**1000** between soil N availability and photosynthetic capacity was supported by the con-  
**1001** current strong increase in leaf N content with increasing soil N availability, which  
**1002** resulted in no change in the proportion of leaf N content allocated to photosynthe-

1003 sis across the soil N availability gradient. Additionally, leaf N content exhibited a  
1004 strong negative correlation with  $\chi$ , indicative of strong nitrogen-water use trade-  
1005 offs at the leaf level. Responses tended to vary more due to soil N availability  
1006 than soil pH. Overall, these findings are consistent with the nutrient-water use  
1007 tradeoffs predicted from theory.

1008 3.4.1 *Soil nitrogen availability modifies tradeoffs between nitrogen and water use*

1009 In support of expected least-cost outcomes and past environmental gradient  
1010 studies (Dong et al. 2017; Paillassa et al. 2020), we found that increasing soil N  
1011 availability was associated with increased leaf N content. Soil N availability had  
1012 smaller impacts on measures of net photosynthesis and  $\chi$ , which led to reductions  
1013 in PNUE and increases in leaf N content per unit  $\chi$ , as expected from theory.  
1014 Photosynthetic least-cost theory suggests that reductions in PNUE should be  
1015 driven by an increase in the proportion of leaf N allocated to photosynthetic tissue,  
1016 a pattern that should allow plants to achieve optimal photosynthetic rates with  
1017 greater photosynthetic capacity to make better use of available light. Contrasting  
1018 theory predictions, we found no effect of soil N availability on photosynthetic  
1019 capacity. However, photosynthetic capacity did tend to increase with increasing  
1020 soil N availability ( $p < 0.20$ ; Table 3.2) resulting in no effect of soil N availability on  
1021 the relative fraction of leaf N allocated to photosynthesis, Rubisco, or bioenergetics  
1022 (Fig. 3.3). These lines of evidence support the idea that trees use additional N  
1023 to support increased leaf N allocation toward photosynthetic tissue and enhance  
1024 photosynthetic capacity (Wright et al. 2003).

1025 Soil N availability had a stronger effect on leaf N than photosynthetic ca-

1026 pacity. This pattern suggests that additional plant N uptake due to increased  
1027 soil N availability was also being used to support non-photosynthetic N pools,  
1028 possibly to structural tissue or stress-induced amino acid and polyamine synthe-  
1029 sis (Minocha et al. 2000; Onoda et al. 2004; Bubier et al. 2011). While we  
1030 found no change in the proportion of leaf N allocated to leaf structural tissue, the  
1031 overall stimulation in leaf N content with increasing soil N availability suggests an  
1032 increase in the net amount of N invested in leaf structural tissue along the N avail-  
1033 ability gradient. Importantly, leaf N allocated to structure was calculated using  
1034 an empirical relationship between  $M_{\text{area}}$  and the amount of leaf N allocated to cell  
1035 walls (Onoda et al. 2017). As the generality of relationships between  $M_{\text{area}}$  and  
1036 the amount of leaf N allocated to cell walls has been called into question (Harrison  
1037 et al. 2009), future work should consider explicitly measuring N allocation to cell  
1038 wall tissue and stress-induced amino acid synthesis to confirm these patterns.

1039 In opposition to patterns expected from least-cost theory, increasing soil  
1040 N availability had no apparent effect on  $\chi$  (Fig. 3.4a). Interestingly, despite  
1041 the null effect of soil N availability on  $\chi$ , we observed a strong negative effect of  
1042 increasing  $N_{\text{area}}$  on  $\chi$  (Fig. 3.4c), consistent with the nitrogen-water use tradeoffs  
1043 expected from theory. The null response of  $\chi$  to increasing soil N availability may  
1044 have been due to a lack of water limitation in the system, given that the area  
1045 received approximately 20% more precipitation (1167 mm) during the 12-month  
1046 period leading up to our measurement period than normally expected (972 mm).  
1047 However, droughts can and do occur in temperate forests of the northeastern  
1048 United States (Sweet et al. 2017), so the observed increase in leaf N content  
1049 with increasing soil N availability could be a strategy that allows trees to hedge

**1050** bets against drier than normal growing seasons (Onoda et al. 2004; Onoda et al.  
**1051** 2017; Hallik et al. 2009). As was suggested in Paillassa et al. (2020), and more  
**1052** recently by Querejeta et al. (2022), negative effects of soil N availability on  $\chi$  may  
**1053** increase with increasing aridity. This strategy would be especially advantageous if  
**1054** it allows individuals growing in arid regions to maintain carbon assimilation rates  
**1055** with reduced water loss. Future work should attempt to quantify interactive roles  
**1056** of climate and soil nitrogen availability on nitrogen-water use tradeoffs, which  
**1057** could be done by leveraging coordinated and multifactor nutrient (Borer et al.  
**1058** 2014) and water (Knapp et al. 2017) manipulation experiments across broad  
**1059** climatic gradients.

**1060** 3.4.2 *Soil pH did not modify tradeoffs between nitrogen and water usage*

**1061** While the primary purpose of this study was to examine the role of soil N  
**1062** availability on nitrogen-water use tradeoffs, our experimental design manipulated  
**1063** both soil N and pH, providing an opportunity to isolate the roles of these variables.  
**1064** Previous correlational studies along environmental gradients identified soil pH as  
**1065** a particularly important factor that can modify tradeoffs between nutrient and  
**1066** water use (Smith et al. 2019; Paillassa et al. 2020; Westerband et al. 2023)  
**1067** and the proportion of leaf nitrogen allocated to photosynthesis (Luo et al. 2021).  
**1068** Such studies implied that these patterns may be driven by reductions in the cost of  
**1069** acquiring nutrients relative to water with increasing pH, which may be exacerbated  
**1070** in acidic soils.

**1071** Consistent with theory (Wright et al. 2003; Prentice et al. 2014), our  
**1072** results indicate that increasing soil pH was negatively associated with PNUE.

1073 However, there was no effect of soil pH on leaf N content,  $\chi$ , or leaf N content per  
1074 unit  $\chi$ , most likely because the experimental N additions increased soil N sup-  
1075 ply while both increasing (sodium nitrate) and decreasing (ammonium sulfate)  
1076 soil pH. These results suggest that soil pH did not play a major role in modify-  
1077 ing expected photosynthetic least-cost theory patterns, contrasting findings from  
1078 Paillassa et al. (2020) and other gradient studies that note positive effects of in-  
1079 creasing soil pH on leaf N content, Rubisco carboxylation, and  $\chi$  (Viet et al. 2013;  
1080 Cornwell et al. 2018; Luo et al. 2021). Instead, null responses to soil pH show  
1081 that leaf photosynthetic parameters depend more on soil N availability than pH  
1082 per se, and that inferences from gradient studies might be confounding covariation  
1083 between N availability and soil acidity.

1084 3.4.3 *Species identity explains a large amount of variation in leaf and whole*  
1085 *plant traits*

1086 Species generally explained a larger amount of variation in measured leaf  
1087 traits than soil N availability or soil pH. Interspecies variation is an important  
1088 factor to consider when deducing mechanisms that drive photosynthetic least-  
1089 cost theory, particularly for species that form distinct mycorrhizal associations or  
1090 have different photosynthetic pathways, growth forms, or leaf habit (Espelta et al.  
1091 2005; Adams et al. 2016; Bialic-Murphy et al. 2021; Scott and Smith 2022). The  
1092 need to consider species may also be important when comparing nutrient-water  
1093 use tradeoffs in early and late successional species, or in species with different  
1094 resource economic strategies (Abrams and Mostoller 1995; Ellsworth and Reich  
1095 1996; Wright et al. 2004; Reich 2014; Onoda et al. 2017; Ziegler et al. 2020).

1096        A strength of the study design and sampling effort is that it controls for  
1097 many species differences that should modify nitrogen-water use tradeoffs expected  
1098 from theory. All tree species measured in this study shared the leaf habit of decid-  
1099 uous broadleaves, were growing in forests of similar successional stage, but differed  
1100 in mycorrhizal association and consequent resource economic strategies. As stands  
1101 tended to be dominated by trees that associate with arbuscular mycorrhizae (*Frax-*  
1102 *inus* and both *Acer* species made up 70% of total aboveground biomass across  
1103 stands), ecosystem biogeochemical cycle dynamics may be more closely aligned  
1104 to the inorganic nutrient economy proposed in Phillips et al. (2013), which may  
1105 promote stronger nitrogen-water use tradeoffs in tree species that associate with  
1106 arbuscular mycorrhizae. This result was not observed here, as photosynthetic  
1107 properties varied as much within as across the two mycorrhizal associations rep-  
1108 resented. Given the high variability in measured photosynthetic traits within  
1109 and across species, effects of mycorrhizal association likely require more intensive  
1110 sampling efforts to detect than were possible here.

1111 3.4.4 *Implications for photosynthetic least-cost theory model development*

1112        In the field, soil nutrient availability is heterogeneous across time and space  
1113 (Table S4). Unaccounted within-plot heterogeneity may have contributed to the  
1114 low amount of variation explained by soil N availability in our statistical mod-  
1115 els, as resin bags are a coarse surrogate for soil N availability. Despite this, we  
1116 still observed evidence for nutrient-water use tradeoffs, suggesting that observed  
1117 responses reported here may be an underestimate toward the net effect of soil  
1118 N availability on these tradeoffs. While we urge caution in the interpretation of

1119 these results, they do provide a promising baseline for future studies investigating  
1120 patterns expected from photosynthetic least-cost theory at finer spatiotemporal  
1121 resolutions.

1122 The general stronger relationship between leaf N content and photosyn-  
1123 thetic parameters versus between leaf N content and soil N availability suggests  
1124 that leaf N content is more directly tied to photosynthesis than soil N availabil-  
1125 ity. While this could be due to the high spatiotemporal heterogeneity of soil N  
1126 availability, principles from photosynthetic least-cost theory suggest that leaf N  
1127 content is the downstream product of leaf nutrient demand to build and maintain  
1128 photosynthetic machinery, which is set by aboveground environmental conditions  
1129 such as light availability, CO<sub>2</sub>, temperature, or vapor pressure deficit (Smith  
1130 et al. 2019; Paillassa et al. 2020; Peng et al. 2021; Westerband et al. 2023). The  
1131 stronger relationship between leaf N and photosynthetic parameters paired with  
1132 the strong negative relationship between leaf N and  $\chi$  could indicate a relatively  
1133 stronger effect of climate on leaf N-photosynthesis relationships than soil resource  
1134 availability. However, the short distance between plots and across sites limited  
1135 our ability to test this mechanism.

1136 Variation in soil pH affected least cost responses less than variations in  
1137 soil N availability, in part because experimental treatments directly increased soil  
1138 N and affected soil pH in opposite directions. While soil pH has been shown  
1139 to drive nitrogen-water tradeoffs in global gradient analyses (Viet et al. 2013;  
1140 Paillassa et al. 2020), these responses may be due to covariations between soil pH  
1141 and nutrient cycling rather than a role of pH per se. The direct manipulations  
1142 of soil pH and soil N availability in this study allowed us to partly disentangle

**1143** these factors and show that variation in N availability matters more for least-cost  
**1144** tradeoffs than pH alone.

**1145** 3.4.5 *Conclusions*

**1146** Increasing soil N availability generally increased leaf N content (both area-  
**1147** and mass-based), but did not significantly influence  $\chi$ . This shift in leaf N led  
**1148** to a reduction in PNUE, and an increase in leaf N per unit  $\chi$  with increasing  
**1149** soil N availability. Despite null effects of soil N availability on  $\chi$ , we observed a  
**1150** strong negative relationship between leaf N content and  $\chi$ . These results provide  
**1151** empirical support for the nutrient-water use tradeoffs expected from photosyn-  
**1152** thetic least-cost theory in response to soil nutrient availability, but suggest that  
**1153** all tenets of the theory may not hold in every environment. These results exper-  
**1154** imentially test previous work suggesting that leaf water-nitrogen economies vary  
**1155** across gradients of soil nutrient availability and pH, and show that variations in  
**1156** nutrient availability matter more for determining variation in leaf photosynthetic  
**1157** traits than soil pH.

1158

## Chapter 4

1159 The relative cost of resource use for photosynthesis drives variance in  
1160 leaf nitrogen content across climate and soil resource availability  
1161 gradients

1162 4.1 Introduction

1163 Terrestrial biosphere models, which comprise the land surface component of  
1164 Earth system models, are sensitive to the formulation of photosynthetic processes  
1165 (Knorr 2000; Ziehn et al. 2011; Booth et al. 2012). This is because photosynthe-  
1166 sis is the largest carbon flux between the atmosphere and terrestrial biosphere,  
1167 and is constrained by ecosystem carbon and nutrient cycles (Hungate et al. 2003;  
1168 LeBauer and Treseder 2008; IPCC 2021; Fay et al. 2015). Many terrestrial bio-  
1169 sphere models formulate photosynthesis by parameterizing photosynthetic capac-  
1170 ity within plant functional groups through empirical linear relationships between  
1171 area-based leaf nitrogen content ( $N_{\text{area}}$ ) and the maximum carboxylation rate  
1172 of Ribulose-1,5-bisphosphate carboxylase/oxygenase (Kattge et al. 2009; Rogers  
1173 2014; Rogers et al. 2017). Models are also beginning to include connected carbon-  
1174 nitrogen cycles (Wieder et al. 2015; Shi et al. 2016; Davies-Barnard et al. 2020;  
1175 Braghieri et al. 2022), which allows leaf photosynthesis to be predicted directly  
1176 through changes in  $N_{\text{area}}$  and indirectly through changes in soil nitrogen avail-  
1177 ability (e.g., LPJ-GUESS, Smith et al., 2014; CLM5.0, Lawrence et al., 2019).  
1178 Despite recent model developments, open questions remain regarding the gen-  
1179 erality of ecological relationships between soil nitrogen availability, leaf nitrogen  
1180 content, and leaf photosynthesis across edaphic and climatic gradients.  
1181 Empirical support for positive relationships between soil nitrogen avail-

ability and  $N_{\text{area}}$  is abundant (Firn et al. 2019; Liang et al. 2020), and is a result often attributed to the high nitrogen cost of building and maintaining Rubisco (Evans 1989; Evans and Seemann 1989; Onoda et al. 2004; Onoda et al. 2017; Dong et al. 2020). Such patterns imply that positive relationships between soil nitrogen availability and  $N_{\text{area}}$  should cause an increase in leaf photosynthesis and photosynthetic capacity by increasing the maximum rate of Rubisco carboxylation through increased investments to Rubisco construction and maintenance. This integrated  $N_{\text{area}}$ -photosynthesis response to soil nitrogen availability has been observed both in manipulative experiments and across environmental gradients (Field and Mooney 1986; Evans 1989; Walker et al. 2014; Li et al. 2020), and is thought to be driven by ecosystem nitrogen limitation, which limits its primary productivity globally (LeBauer and Treseder 2008; Fay et al. 2015). However, this response is not consistently observed, as recent studies note variable  $N_{\text{area}}$ -photosynthesis relationships across soil nitrogen availability gradients (Liang et al. 2020; Luo et al. 2021) and that aboveground growing conditions (e.g., light availability, temperature, vapor pressure deficit) or species identity traits (e.g., photosynthetic pathway, nitrogen acquisition strategy) may be more important for explaining variance in  $N_{\text{area}}$  and photosynthetic capacity across time and space (Adams et al. 2016; Dong et al. 2017; Dong et al. 2020; Dong et al. 2022; Smith et al. 2019; Peng et al. 2021; Westerband et al. 2023).

One hypothesized mechanism to explain variance in  $N_{\text{area}}$  across environmental gradients has been proposed via photosynthetic least-cost theory (Wright et al. 2003; Prentice et al. 2014; Paillassa et al. 2020; Harrison et al. 2021). The theory predicts that plants acclimate to environments by optimizing photo-

**1206** synthetic assimilation rates at the lowest summed cost of nitrogen and water use  
**1207** (Wright et al. 2003; Prentice et al. 2014). In a given environment, the theory  
**1208** proposes that nitrogen and water use can be substituted for each other to main-  
**1209** tain the lowest summed cost to satisfy leaf resource demand, such that optimal  
**1210** photosynthetic rates are achieved with less efficient use of the more abundant  
**1211** and less costly resource to acquire in exchange for more efficient use of the less  
**1212** abundant and more costly resource to acquire.

**1213** Photosynthetic least-cost theory predicts that, all else equal, an increase  
**1214** in soil nitrogen availability should decrease the cost of acquiring and using nitro-  
**1215** gen relative to water ( $\beta$ ), resulting in optimal photosynthetic rates achieved with  
**1216** greater  $N_{\text{area}}$  at lower stomatal conductance and lower leaf  $C_i:C_a$  ( $\chi$ ) (Wright et al.  
**1217** 2003; Prentice et al. 2014). Alternatively, an increase in soil moisture should re-  
**1218** duce costs of water acquisition and use, increasing  $\beta$ , stomatal conductance, and  
**1219**  $\chi$ , resulting in optimal photosynthetic rates achieved with decreased  $N_{\text{area}}$ . The  
**1220** theory also predicts variability in stomatal conductance and  $N_{\text{area}}$  in response to  
**1221** climatic factors, suggesting that the optimal response to increased vapor pressure  
**1222** deficit (VPD) should be a reduction in stomatal conductance and  $\chi$  that is coun-  
**1223** terbalanced by an increase in  $N_{\text{area}}$  to support the higher photosynthetic capacity  
**1224** needed to maintain high assimilation at lower conductance (Grossiord et al. 2020;  
**1225** Dong et al. 2020; Westerband et al. 2023).

**1226** Leaf nitrogen allocation responses to changing climates or soil resource  
**1227** availability may also depend on their mode of nutrient acquisition or photo-  
**1228** synthetic pathway. For example, species that form associations with symbiotic  
**1229** nitrogen-fixing bacteria (referred as “N-fixing species” from this point forward)

1230 should, in theory, have access to a less finite nitrogen supply, which may result in  
1231 lower  $\beta$  values than species not capable of forming such associations (referred as  
1232 “non-fixing species” from this point forward). This result was previously shown  
1233 in a greenhouse experiment, where a leguminous species generally had lower costs  
1234 of nitrogen acquisition compared to a non-leguminous species, although these dif-  
1235 ferences were generally stronger under increased nitrogen limitation (Fig. 2.1)  
1236 (Perkowski et al. 2021). Lower  $\beta$  values could be a possible explanation for  
1237 why N-fixing species commonly have higher leaf nitrogen content than non-fixing  
1238 species (Adams et al. 2016; Dong et al. 2017).

1239 Similarly, leaf nitrogen allocation patterns across environmental gradients  
1240 may be dependent on photosynthetic pathway. General lower  $\chi$  values in C<sub>4</sub>  
1241 species suggests that C<sub>4</sub> species should have lower  $\beta$  values than C<sub>3</sub> species, a  
1242 pattern that could be the result of increased costs associated with water acquisition  
1243 and use or reduced costs associated with nutrient acquisition and use relative to  
1244 C<sub>3</sub> species. No study to date has directly quantified  $\chi$  in C<sub>4</sub> species aside from the  
1245 dataset used to initially parameterize an optimality model for C<sub>4</sub> species (Scott  
1246 and Smith 2022).

1247 While photosynthetic least-cost theory provides a unified hypothesis for  
1248 understanding effects of climate and soil resource availability on  $N_{\text{area}}$ , empiri-  
1249 cal tests of the theory are sparse. Increasing soil nitrogen availability has been  
1250 previously shown to decrease the cost of acquiring nutrients (Bae et al. 2015; Lu  
1251 et al. 2022; Eastman et al. 2021), which can induce predictable nutrient-water use  
1252 tradeoffs expected from the theory across broad environmental gradients (Paillassa  
1253 et al. 2020; Querejeta et al. 2022; Westerband et al. 2023) and in manipulation

1254 experiments (Bialic-Murphy et al. 2021). Additionally, increasing VPD has been  
1255 shown to have a positive effect on  $N_{\text{area}}$  (Dong et al. 2017; Dong et al. 2020; Firn  
1256 et al. 2019). However, studies have been restricted to exploring these patterns  
1257 with C<sub>3</sub> species and, while previous studies have shown that variance in  $N_{\text{area}}$   
1258 across environmental gradients is driven by strong negative relationships with  $\chi$   
1259 (Fig 3.4c)(Dong et al. 2017; Paillassa et al. 2020; Westerband et al. 2023),  
1260 no study to date has explicitly investigated effects of soil resource availability or  
1261 plant functional group on  $N_{\text{area}}$  using  $\beta$  as a direct predictor of  $\chi$ . Additionally, as  
1262  $N_{\text{area}}$  can be broken down into structural (leaf mass per area;  $M_{\text{area}}$ ; g m<sup>-2</sup>) and  
1263 metabolic (mass-based leaf nitrogen content;  $N_{\text{mass}}$ ; gN g<sup>-1</sup>) components (Dong et  
1264 al. 2017), no study has investigated which component of  $N_{\text{area}}$  drives the hypothe-  
1265 sized response of  $N_{\text{area}}$  to  $\chi$ , which would be useful for detecting whether changes  
1266 in  $N_{\text{area}}$  due to  $\chi$  are driven by changes in leaf morphology or stoichiometry.

1267 Here, I measured  $N_{\text{area}}$ ,  $N_{\text{mass}}$ ,  $M_{\text{area}}$ , leaf δ<sup>13</sup>C-derived estimates of  $\chi$ , and  
1268 leaf δ<sup>13</sup>C-derived estimates of  $\beta$  in 520 individuals spanning 57 species scattered  
1269 across 24 grassland sites in Texas, USA (Table S1). Texas contains a diverse  
1270 climatic gradient, indicated by 2006-2020 mean annual precipitation totals ranging  
1271 from 204 to 1803 mm and 2006-2020 mean annual temperature ranging from  
1272 11.8° to 24.6°C. Variability in soil nitrogen availability and soil moisture was  
1273 expected across sites, owing to differences in soil texture and aboveground climate  
1274 that would drive differential rates of water retention and nitrogen transformations  
1275 to plant-available substrate. I leveraged the expected climatic and soil resource  
1276 variability across sites to test the following hypotheses:

1277 1. Soil nitrogen availability will decrease  $\beta$  through a reduction in costs of

1278 nitrogen acquisition and use, while soil moisture will increase  $\beta$  through a  
1279 reduction in costs of water acquisition and use. We expected that N-fixing  
1280 species would have lower  $\beta$  values due to their ability to minimize costs  
1281 of nitrogen acquisition under low nitrogen availability and that C<sub>4</sub> species  
1282 would have lower  $\beta$  values due to increased costs of water acquisition and  
1283 use or reduced costs of nitrogen acquisition and use.

1284 2.  $\chi$  will be positively related to  $\beta$ , a pattern that will result in a negative  
1285 indirect effect of increasing soil nitrogen availability, positive indirect effect  
1286 of increasing soil moisture on  $\chi$ , and lower  $\chi$  in both N-fixing species and  
1287 C<sub>4</sub> species. We also expected that  $\chi$  would be negatively related to VPD,  
1288 as increasing atmospheric dryness should cause plants to close stomata to  
1289 minimize water loss.

1290 3.  $N_{\text{area}}$  will be negatively related to  $\chi$ . This response will result in an indi-  
1291 rect positive effect of increasing soil nitrogen availability, a negative effect of  
1292 increasing soil moisture on  $N_{\text{area}}$ , and generally larger  $N_{\text{area}}$  values in both N-  
1293 fixing species. We expected these patterns to be mediated through a positive  
1294 relationship between  $\beta$  and  $\chi$ . While theory predicts that negative relation-  
1295 ships between  $N_{\text{area}}$  and  $\chi$  should yield generally larger  $N_{\text{area}}$  in C<sub>4</sub> species,  
1296 we expected that C<sub>4</sub> species would have lower  $N_{\text{area}}$  due to generally greater  
1297 nitrogen use efficiency in C<sub>4</sub> species than C<sub>3</sub> species. Additionally, VPD  
1298 was expected to increase  $N_{\text{area}}$ , a pattern that would be directly mediated  
1299 through the reduction in  $\chi$  with increasing VPD.

**1300** 4.2 Methods

**1301** 4.2.1 *Site descriptions and sampling methodology*

**1302** I collected leaf and soil samples from 24 open grassland sites across cen-  
**1303** tral and eastern Texas in summer 2020 and summer 2021 (Fig. 4.1). Twelve  
**1304** sites were visited between June and July 2020 and 14 sites (11 unique from 2020)  
**1305** were visited between May and June 2021 (Table 1). I explicitly chose sites that  
**1306** maximized variability in precipitation and edaphic variability between sites while  
**1307** minimizing temperature variability across the environmental gradient (Table 1).  
**1308** No site with personally communicated or anecdotal evidence of grazing or distur-  
**1309** bance (e.g., mowing, feral hog activity, etc.) were used. I collected leaf material  
**1310** from three individuals each of the five most abundant species at random locations  
**1311** at each site, only selecting species that were broadly classified as graminoid or  
**1312** forb/herb growth habits per the USDA PLANTS database (USDA NRCS 2022).  
**1313** All collected leaves were fully expanded with no visible herbivory or other external  
**1314** damage and also free from shading by nearby shrubs or trees. Five soil samples  
**1315** were collected from 0-15cm below the soil surface at each site near the leaf collec-  
**1316** tion sample locations. Soil samples were later mixed together by hand to create  
**1317** one composite soil sample per site.

**1318** 4.2.2 *Leaf trait measurements*

**1319** Images of each leaf were taken immediately following each site visit using  
**1320** a flat-bed scanner. Fresh leaf area was determined from each image using the  
**1321** 'LeafArea' R package (Katabuchi 2015), which automates leaf area calculations  
**1322** using ImageJ software (Schneider et al. 2012). Each leaf was dried at 65°C for at

**1323** least 48 hours to a constant mass, weighed, and manually ground in a mortar and  
**1324** pestle until homogenized. Leaf mass per area ( $M_{\text{area}}$ ; g m<sup>-2</sup>) was calculated as the  
**1325** ratio of dry leaf biomass to fresh leaf area. Subsamples of dried and homogenized  
**1326** leaf tissue were used to measure leaf nitrogen content ( $N_{\text{mass}}$ ; gN g<sup>-1</sup>) through el-  
**1327** emental combustion analysis (Costech-4010, Costech Instruments, Valencia, CA).  
**1328** Leaf nitrogen content per unit leaf area ( $N_{\text{area}}$ ; gN m<sup>-2</sup>) was then calculated as  
**1329** the product of  $N_{\text{mass}}$  and  $M_{\text{area}}$ .

**1330** Subsamples of dried and homogenized leaf tissue were sent to the University  
**1331** of California-Davis Stable Isotope Facility to determine leaf  $\delta^{13}\text{C}$ . Leaf  $\delta^{13}\text{C}$  values  
**1332** were determined using an elemental analyzer (PDZ Europa ANCA-GSL; Sercon  
**1333** Ltd., Chestshire, UK) interfaced to an isotope ratio mass spectrometer (PDZ  
**1334** Europa 20-20 Isotope Ratio Mass Spectrometer, Sercon Ltd., Chestshire, UK).  
**1335** I used leaf  $\delta^{13}\text{C}$  values (‰; relative to Vienna Pee Dee Belemnite international  
**1336** reference standard) to estimate the ratio of intercellular ( $C_i$ ) to extracellular ( $C_a$ )  
**1337** CO<sub>2</sub> ratio (leaf  $C_i:C_a$ ,  $\chi$ ; unitless) following the approach of Farquhar et al. (1989)  
**1338** described in Cernusak et al. (2013). Specifically, I derived  $\chi$  as:

$$\chi = \frac{C_i}{C_a} = \frac{\Delta^{13}\text{C} - a}{b - a} \quad (4.1)$$

**1339** where  $\Delta^{13}\text{C}$  represents the relative difference between leaf  $\delta^{13}\text{C}$  (‰) and air  $\delta^{13}\text{C}$   
**1340** (‰), and is calculated as:

$$\Delta^{13}\text{C} = \frac{\delta^{13}\text{C}_{\text{air}} - \delta^{13}\text{C}_{\text{leaf}}}{1 + \delta^{13}\text{C}_{\text{leaf}}} \quad (4.2)$$

**1341**  $\delta^{13}\text{C}_{\text{air}}$ , traditionally assumed to be -8‰ (Keeling et al. 1979; Farquhar et al.

**1342** 1989), was calculated as a function of calendar year  $t$  using an empirical equation  
**1343** derived in Feng (1999):

$$\delta^{13}C_{air} = -6.429 - 0.006e^{0.0217(t-1740)} \quad (4.3)$$

**1344** This calculation resulted in  $\delta^{13}C_{air}$  values for 2020 and 2021 as -9.04 and -9.09,  
**1345** respectively.  $a$  represents the fractionation between  $^{12}C$  and  $^{13}C$  due to diffusion  
**1346** in air, assumed to be 4.4‰, and  $b$  represents the fractionation caused by Rubisco  
**1347** carboxylation, assumed to be 27‰ (Farquhar et al. 1989). For  $C_4$  species,  $b$  in  
**1348** Eqn. 4.1 was set to 6.3‰, and was derived from:

$$b = c + (d \cdot \phi) \quad (4.4)$$

**1349** Where  $c$  was set to -5.7‰ and  $d$  was set to 30‰ (Farquhar et al. 1989).  $\phi$ , which  
**1350** is the bundle sheath leakiness term, was set to 0.4. All  $\chi$  values less than 0.2 and  
**1351** greater than 1.0 were assumed to be incorrect and removed.

**1352** I derived the unit cost of resource use ( $\beta$ ) using leaf  $\chi$  and site climate data  
**1353** with equations first described in Prentice et al. (2014) and simplified in Lavergne  
**1354** et al. (2020):

$$\beta = 1.6\eta^*D \frac{\chi - (\frac{\Gamma^*}{C_a})^2}{(1 - \chi)^2(K_m + \Gamma^*)} \quad (4.5)$$

**1355** where  $\eta^*$  is the viscosity of water relative to 25°C, calculated using elevation and  
**1356** mean air temperature of the seven days leading up to each site visit following  
**1357** equations in Huber et al. (2009).  $D$  represents vapor pressure deficit (Pa), set

**1358** to the mean vapor pressure deficit of the seven days leading up to each site visit,  
**1359**  $C_a$  represents atmospheric CO<sub>2</sub> concentration, arbitrarily set to 420  $\mu\text{mol mol}^{-1}$   
**1360** CO<sup>2</sup>.  $K_m$  (Pa) is the Michaelis-Menten coefficient for Rubisco affinity to CO<sub>2</sub> and  
**1361** O<sub>2</sub>, calculated as:

$$K_m = K_c \cdot \left(1 + \frac{O_i}{K_o}\right) \quad (4.6)$$

**1362** where  $K_c$  (Pa) and  $K_o$  (Pa) are the Michaelis-Menten coefficients for Rubisco  
**1363** affinity to CO<sub>2</sub> and O<sub>2</sub>, respectively, and  $O_i$  is the intercellular O<sub>2</sub> concentration.  
**1364**  $\Gamma^*$  (Pa) is the CO<sub>2</sub> compensation point in the absence of dark respiration.  $K_c$ ,  $K_o$ ,  
**1365** and  $\Gamma^*$  were determined using equations described in Medlyn et al. (2002) and  
**1366** derived in Bernacchi et al. (2001), invoking an elevation correction for atmospheric  
**1367** pressure as explained in Stocker et al. (2020).

**Table 4.1.** Site locality information, sampling year(s), 2006-2020 mean annual precipitation (MAP; mm), mean annual temperature (MAT; °C), and water holding capacity (WHC; mm)\*

Site	Latitude	Longitude	Sampling year	MAP	MAT	WHC
Edwards_2019_17	29.95	-100.36	2020	563.5	19.0	224.7
Uvalde_2020_02	29.59	-100.09	2020, 2021	648.5	19.5	224.7
Menard_2020_01	30.91	-99.59	2020	641.9	18.3	220.2
Kerr_2020_03	30.06	-99.34	2021	672.4	18.3	237.5
Bandera_2020_03	29.85	-99.30	2021	789.4	18.8	235.1
Sansaba_2020_01	31.29	-98.62	2020	733.0	18.8	234.3
Comal_2020_21	29.79	-98.43	2020	878.5	19.9	220.7
Blanco_2019_16	29.99	-98.43	2020	833.0	19.2	222.2
Bexar_2019_13	29.24	-98.43	2020	759.3	21.5	206.0
Burnet_2020_14	30.84	-98.34	2021	763.3	19.5	217.8
Comal_2020_19	30.01	-98.32	2021	845.0	19.3	220.4
Hays_2020_54	29.96	-98.17	2021	861.3	20.0	225.6
Burnet_2020_12	30.82	-98.06	2021	815.1	19.4	245.3
Williamson_2019_09	30.71	-97.86	2020	867.7	19.7	270.2
Williamson_2019_10	30.54	-97.77	2020	819.5	19.9	239.8
Bell_2021_08	31.06	-97.55	2021	937.3	19.6	232.3
Fayette_2021_12	29.86	-97.21	2021	985.7	20.4	165.6
Fayette_2019_04	30.09	-96.78	2020	1017.4	20.6	226.9
Fayette_2020_09	29.86	-96.71	2021	1002.7	20.8	187.6
Washington_2020_08	30.28	-96.41	2021	1077.4	20.4	203.9
Austin_2020_03	29.78	-96.24	2021	1108.7	20.6	253.0
Brazos_2020_16	30.93	-96.23	2021	1078.0	20.1	202.2
Brazos_2020_18	30.52	-96.21	2020, 2021	1099.4	20.4	233.5
Harris_2020_03	29.88	-95.31	2020, 2021	1492.0	21.6	265.6

**1368** \*Rows are arranged by longitude to visualize precipitation variability across sites

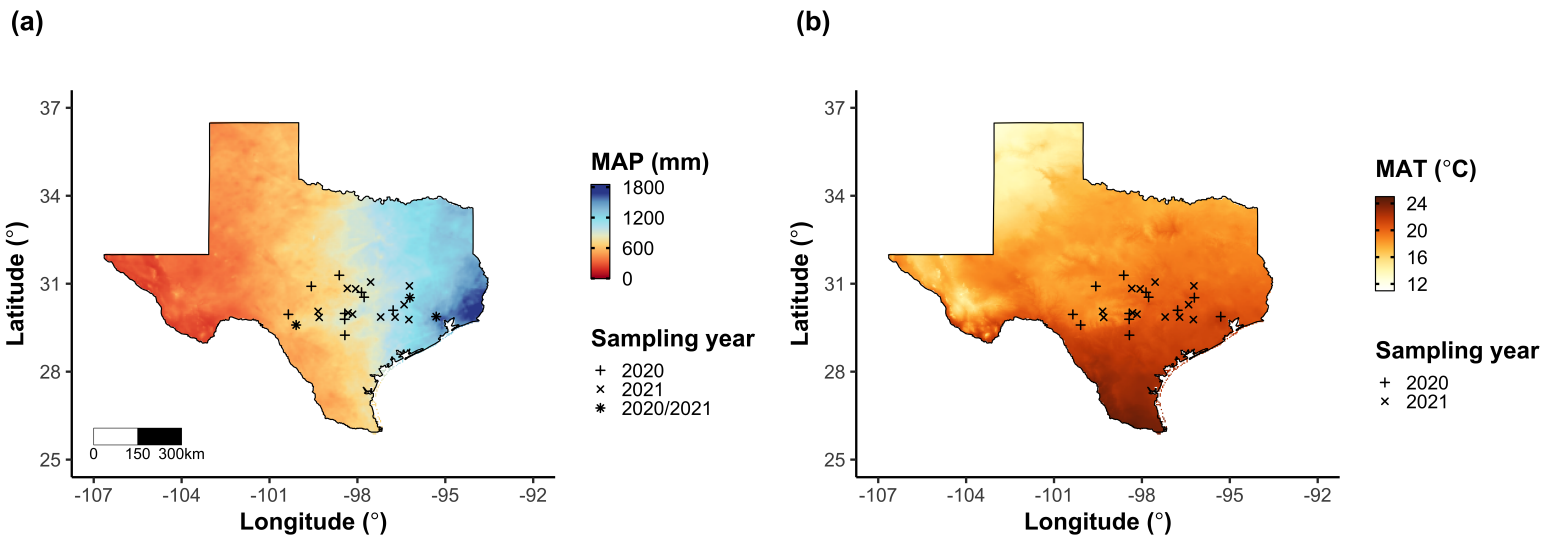


**Figure 4.1.** Maps that detail site locations along 2006-2020 mean annual precipitation (a) and mean annual temperature (b) gradients in Texas, USA. Precipitation and temperature data were plotted at a 4-km grid resolution and are masked to include only grid cells that occur in the Texas state boundary in the United States. In both panels, open circles refer to sites visited in 2020, open triangles to sites visited in 2021, and closed circles to sites visited in 2020 and 2021. The scale bar in panel A also applies to panel B.

**1369** 4.2.3 *Site climate data*

**1370** I used the Parameter-elevation Regressions on Independent Slopes Model  
**1371** (PRISM) (Daly et al. 2008)climate product to access gridded daily temperature  
**1372** and precipitation data for the coterminous United States at a 4-km grid resolution  
**1373** between January 1, 2006 and July 31, 2021 (PRISM Climate Group, Oregon State  
**1374** University, <https://prism.oregonstate.edu>, data created 4 Feb 2014, accessed 24  
**1375** Mar 2022). Daily mean air temperature, mean VPD, and total precipitation  
**1376** data were extracted from the grid cell that contained the latitude and longitude  
**1377** of each property using the ‘extract’ function in the ‘terra’ R package (Hijmans  
**1378** 2022). PRISM data were used in lieu of local weather station data because several  
**1379** rural sites did not have a local weather station present within a 20-km radius of  
**1380** the site. Daily site climate data were used to estimate mean annual precipitation  
**1381** and mean annual temperature for each site between 2006 and 2020 (Table 1). I  
**1382** calculated total precipitation and mean daily VPD for the prior 1, 2, 3, 4, 5, 6, 7,  
**1383** 8, 9, 10, 15, 20, 25, 30, 60, and 90 days leading up to each site visit.

**1384** 4.2.4 *Site edaphic characteristics*

**1385** Subsamples of composited soil samples were sent to the Texas A & M  
**1386** Soil, Water and Forage Laboratory to quantify soil nitrate concentration (NO<sub>3</sub>-N;  
**1387** ppm). Soil NO<sub>3</sub>-N was determined by extracting composite soil samples in 1 M  
**1388** KCl, measuring absorbance values of extracts at 520 nm using the end product of  
**1389** a NO<sub>3</sub>-N to NO<sub>2</sub>-N cadmium reduction reaction (Kachurina et al. 2000). Soil tex-  
**1390** ture data from 0-15cm below the soil surface were accessed using the SoilGrids2.0  
**1391** data product (Poggio et al. 2021) through the ‘fetchSoilGrids’ function in the

**1392** ‘soilDB’ R package (Beaudette et al. 2022). I used SoilGrids2.0 to access soil  
**1393** texture data in lieu of analyses using the collected composite soil sample due to  
**1394** a lack of soil material from some sites after sending samples for soil NO<sub>3</sub>-N.

**1395** Soil moisture was not measured in the field, but was estimated using  
**1396** the ‘Simple Process-Led Algorithms for Simulating Habitats’ model (‘SPLASH’)  
**1397** (Davis et al. 2017). This model, derived from the STASH model (Cramer and  
**1398** Prentice 1988), spins up a bucket model using Priestley-Taylor equations (Priest-  
**1399** ley and Taylor 1972) to calculate daily soil moisture ( $W_n$ ; mm) as a function  
**1400** of the previous day’s soil moisture ( $W_{n-1}$ ; mm), daily precipitation ( $P_n$ ; mm),  
**1401** condensation ( $C_n$ ; mm), actual evapotranspiration ( $E_n^a$ ; mm), and runoff (RO;  
**1402** mm):

$$W_n = W_{n-1} + P_n + C_n - E_n^a - RO \quad (4.7)$$

**1403** Models were spun up by equilibrating the previous day’s soil moisture using  
**1404** successive model iterations with daily mean air temperature, daily precipitation  
**1405** total, the number of daily sunlight hours, and latitude as model inputs (Davis et al.  
**1406** 2017). Daily sunlight hours were estimated for each day at each site using the  
**1407** ‘getSunlightTimes’ function in the ‘suncalc’ R package, which estimated sunrise  
**1408** and sunset times of each property using date and site coordinates (Thieurmel and  
**1409** Elmarhraoui 2019). Water holding capacity (mm), or bucket size, was estimated  
**1410** as a function of soil texture using pedotransfer equations explained in Saxton and  
**1411** Rawls (2006), as done in Stocker et al. (2020) and Bloomfield et al. (2023). A  
**1412** summary of these equations is included in the Supplemental Information.

1413 Daily soil moisture outputs from the SPLASH model for each site were  
1414 used to calculate mean daily soil moisture for the prior 1, 2, 3, 4, 5, 6, 7, 8, 9,  
1415 10, 15, 20, 25, 30, 60, and 90 days leading up to each site visit. Mean daily  
1416 soil moisture values were then expressed as a fraction of water holding capacity  
1417 to normalize across sites with different bucket depths, as done in Stocker et al.  
1418 (2018).

1419 4.2.5 *Plant functional group assignments*

1420 Plant functional group was assigned to each species and used as the pri-  
1421 mary descriptor of species identity. Specifically, I assigned plant functional groups  
1422 based on photosynthetic pathway ( $C_3$ ,  $C_4$ ) and ability to form associations with  
1423 symbiotic nitrogen-fixing bacteria. The ability to form associations with symbi-  
1424 otic nitrogen-fixing bacteria was assigned based on whether species were in the  
1425 *Fabaceae* family, and photosynthetic pathway of each species was determined from  
1426 past literature and confirmed through leaf  $\delta^{13}\text{C}$  values. We chose these plant func-  
1427 tional groups based on *a priori* hypotheses regarding the functional role of nitrogen  
1428 fixation and photosynthetic pathway on the sensitivity of plant nitrogen uptake  
1429 and leaf nitrogen allocation to soil nutrient availability and aboveground growing  
1430 conditions. These plant functional group classifications resulted in three distinct  
1431 plant functional groups within our dataset:  $C_3$  legumes ( $n = 53$ ),  $C_3$  non-legumes  
1432 ( $n = 350$ ), and  $C_4$  non-legumes ( $n = 117$ ).

**1433** 4.2.6 *Data analysis*

**1434** All analyses and plotting were conducted in R version 4.1.1 (R Core Team  
**1435** 2021). I constructed a series of separate linear mixed-effects models to investigate  
**1436** environmental drivers of  $\beta$ ,  $\chi$ ,  $N_{\text{area}}$ ,  $N_{\text{mass}}$ , and  $M_{\text{area}}$ , followed by a path analysis  
**1437** using a piecewise structural equation model to investigate direct and indirect  
**1438** effects of climate and soil resource availability on  $N_{\text{area}}$ .

**1439** To explore environmental drivers of  $\beta$ , I built a linear mixed-effects model  
**1440** that included soil moisture, soil nitrogen availability, and plant functional group  
**1441** as fixed effect coefficients. Species were designated as a random intercept term.  
**1442** Interaction coefficients between all possible combinations of the three fixed effect  
**1443** coefficients were also included.  $\beta$  was natural log transformed to linearize data.  
**1444** I used an information-theoretic model selection approach to determine whether  
**1445** 90-, 60-, 30-, 20-, 15-, 10-, 9-, 8-, 7-, 6-, 5-, 4-, 3-, 2-, or 1-day mean daily soil  
**1446** moisture conferred the best model fit for  $\beta$ . To do this, I constructed 16 separate  
**1447** linear mixed-effects models where log-transformed  $\beta$  was included as the response  
**1448** variable and each soil moisture time step was separately included as a single  
**1449** continuous fixed effect. Species were included as a random intercept term for all  
**1450** models. I used corrected Akaike Information Criterion (AICc) to select the soil  
**1451** moisture timescale that conferred the best model fit, indicated by the model with  
**1452** the lowest AICc score (Table S2; Fig. S2).

**1453** To explore environmental drivers of  $\chi$ , I constructed a second linear mixed  
**1454** effects model that included VPD, soil moisture, soil nitrogen availability, and plant  
**1455** functional group as fixed effect coefficients. Two-way interactions between plant  
**1456** functional group and VPD, soil nitrogen availability, or soil moisture were also

1457 included as fixed effect coefficients, in addition to a three-way interaction between  
1458 soil moisture, soil nitrogen availability, and plant functional group. Species were  
1459 included as a random intercept term. I used an information-theoretic model se-  
1460 lection approach to determine whether 90-, 60-, 30-, 20-, 15-, 10-, 9-, 8-, 7-, 6-,  
1461 5-, 4-, 3-, 2-, or 1-day mean daily VPD conferred the best model fit for  $\chi$  using  
1462 the same approach explained above for the soil moisture effect on  $\beta$ . The soil  
1463 moisture timescale was set to the same timescale that conferred the best fit for  $\beta$ .

1464 To explore environmental drivers of  $N_{\text{area}}$ ,  $N_{\text{mass}}$ , and  $M_{\text{area}}$ , I constructed  
1465 three separate linear mixed effects model that each included  $\chi$ , soil nitrogen avail-  
1466 ability, soil moisture, and plant functional group as fixed effect coefficients. Two-  
1467 way interactions between plant functional group and  $\beta$ ,  $\chi$ , soil nitrogen availability,  
1468 or soil moisture were included as additional fixed effect coefficients, in addition to  
1469 a three-way interaction between soil nitrogen availability, soil moisture, and plant  
1470 functional group. Species were included as a random intercept term, with the soil  
1471 moisture timescale set to the same timescale that conferred the best fit for  $\beta$ .

1472 In all linear mixed-effects models explained above, including those to select  
1473 relevant timescales, I used the 'lmer' function in the 'lme4' R package (Bates et al.  
1474 2015) to fit each model and the 'Anova' function in the 'car' R package (Fox and  
1475 Weisberg 2019) to calculate Type II Wald's  $\chi^2$  and determine the significance  
1476 level ( $\alpha = 0.05$ ) of each fixed effect coefficient. I used the 'emmeans' R package  
1477 (Lenth 2019) to conduct post-hoc comparisons using Tukey's tests, where degrees  
1478 of freedom were approximated using the Kenward-Roger approach (Kenward and  
1479 Roger 1997). Trendlines and error ribbons for all plots were drawn using a series  
1480 of 'emmeans' outputs across the range in plotted x-axis values.

Finally, I conducted a path analysis using a piecewise structural equation model to examine direct and indirect pathways that determined variance in  $N_{\text{area}}$ . Seven separate linear mixed effects models were loaded into the piecewise structural equation model. Models were constructed per our *a priori* hypotheses following patterns expected from photosynthetic least-cost theory. The first model regressed  $N_{\text{area}}$  against  $\chi$ ,  $N_{\text{mass}}$ , and  $M_{\text{area}}$ . The second model regressed  $M_{\text{area}}$  against  $\chi$ . The third model regressed  $N_{\text{mass}}$  against  $\chi$  and  $M_{\text{area}}$  (Dong et al. 2017; Dong et al. 2020). The fourth model regressed  $\chi$  against  $\beta$  and VPD. The fifth model regressed  $\beta$  against soil nitrogen availability, soil moisture, ability to associate with symbiotic nitrogen-fixing bacteria, and photosynthetic pathway. The sixth model regressed soil nitrogen availability against soil moisture, while the seventh model regressed VPD against soil moisture (Novick et al. 2016; Sulman et al. 2016). All models included the relevant timescale selected in the individual linear mixed effect models explained above (2-day soil moisture, 4-day vapor pressure deficit). Models also included species as a random intercept term, were built using the ‘lme’ function in the ‘nlme’ R package (Pinheiro and Bates 2022), and subsequently loaded into the piecewise structural equation model using the ‘psem’ function in the ‘piecewiseSEM’ R package (Lefcheck 2016).

## 1499 4.3 Results

### 1500 4.3.1 Cost to acquire nitrogen relative to water ( $\beta$ )

Model selection indicated that 2-day soil moisture was the timescale that conferred the best model fit for  $\beta$  (AICc = 1227.83; Table S2; Fig. S1). Increasing soil nitrogen availability generally decreased  $\beta$  ( $p < 0.001$ ; Table 4.2), a pattern

1504 driven by a negative effect of increasing soil nitrogen availability on  $\beta$  in C<sub>3</sub> non-  
1505 legumes (Tukey:  $p < 0.001$ ) and C<sub>3</sub> legumes (Tukey:  $p = 0.004$ ; Fig. 4.2a). C<sub>4</sub>  
1506 nonlegumes also demonstrated a negative trend in the effect of increasing soil ni-  
1507 trogen availability on  $\beta$ , but this pattern was not significantly different from zero  
1508 (Tukey:  $p = 0.307$ ; Fig. 4.2a). There was no apparent effect of soil moisture on  
1509  $\beta$  ( $p = 0.264$ ; Table 4.2; Fig. 4.2b). A functional group effect ( $p < 0.001$ ; Table  
1510 4.2) indicated that C<sub>4</sub> nonlegumes generally had lower  $\beta$  values than both C<sub>3</sub>  
1511 legumes and C<sub>3</sub> non-legumes when averaged across soil moisture and soil nitrogen  
1512 availability values (Tukey:  $p < 0.001$  in both cases), while average  $\beta$  values in C<sub>3</sub>  
1513 legumes did not differ from C<sub>3</sub> nonlegumes (Tukey:  $p = 0.691$ ).

**Table 4.2.** Effects of soil moisture, soil nitrogen availability, and plant functional group on  $\beta$ 

	df	Coefficient	$\chi^2$	p
Intercept	-	3.20E+00	-	-
Soil moisture ( $SM_2$ )	1	2.19E-01	1.244	0.265
Soil N (N)	1	-1.70E-02	26.823	<b>&lt;0.001</b>
PFT	2	-	199.617	<b>&lt;0.001</b>
$SM_2*N$	1	1.77E-03	0.438	0.508
$SM_2*PFT$	2	-	2.038	0.361
$N*PFT$	2	-	7.668	<b>0.022</b>
$SM_2*N*PFT$	2	-	0.127	0.939

**1514** \*Significance determined using Type II Wald  $\chi^2$  tests ( $\alpha = 0.05$ ). P-values  $< 0.05$

**1515** are in bold. Model coefficients are expressed on the natural-log scale and are only

**1516** included for continuous fixed effects. Key: df = degrees of freedom,  $\chi^2$  = Wald

**1517** Type II chi-square test statistic

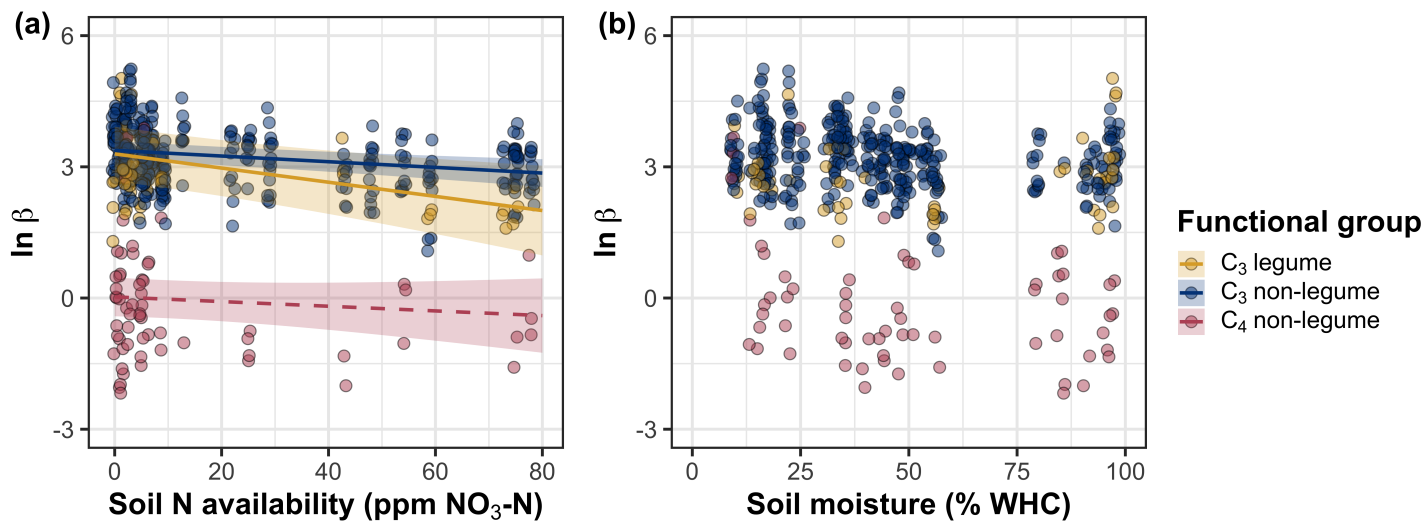


**Figure 4.2.** Effects of soil nitrogen availability (a) and soil moisture (b) on the unit cost ratio  $\beta$ . In (b), soil moisture is represented as a percent of site water holding capacity. Yellow shading and trendlines indicate C<sub>3</sub> legumes, blue shading and trendlines indicate C<sub>3</sub> non-legumes, and red shading and trendlines indicate C<sub>4</sub> non-legumes. Points are jittered for visibility. Variably colored trendlines are only included if there is an interaction between the x-axis and plant functional group, where solid trendlines indicate slopes that are different from zero ( $p < 0.05$ ) and dashed trendlines indicate slopes that are not different from zero ( $p > 0.05$ ). Error ribbons represent the upper and lower 95% confidence intervals of each fitted trendline.

1518 4.3.2 Leaf  $C_i:C_a$  ( $\chi$ )

1519 Model selection indicated that 4-day daily VPD was the timescale that  
1520 conferred the best model fit for  $\chi$  (AICc = -883.97; Table S1; Fig. S2).

1521 Variance in  $\chi$  was driven by a series of two-way interactions between func-  
1522 tional group and VPD ( $p = 0.006$ ; Table 3), soil moisture ( $p = 0.033$ , Table 3.3),  
1523 and soil nitrogen availability ( $p = 0.022$ ; Table 3). The interaction between 4-day  
1524 VPD and functional group revealed that the general negative effect of increasing  
1525 VPD ( $p < 0.001$ ; Table 3) was driven by a negative effect of increasing VPD  
1526 on  $\chi$  in C<sub>3</sub> nonlegumes (Tukey:  $p < 0.001$ ) and marginal negative effect in C<sub>3</sub>  
1527 legumes (Tukey:  $p = 0.074$ ) paired with a positive trending, but insignificant  
1528 effect of increasing VPD in C<sub>4</sub> nonlegumes (Tukey:  $p = 0.130$ ; Fig. 3a). The  
1529 interaction between 2-day soil moisture and functional group indicated that the  
1530 general negative effect of increasing soil moisture on  $\chi$  was driven by a positive  
1531 effect of increasing soil moisture on  $\chi$  in C<sub>4</sub> nonlegumes (Tukey:  $p = 0.009$ ) de-  
1532 spite a positive trending but insignificant effect of increasing soil moisture on  $\chi$   
1533 in C<sub>3</sub> legumes (Tukey:  $p = 0.116$ ) and a null effect of soil moisture on  $\chi$  in C<sub>3</sub>  
1534 nonlegumes (Tukey:  $p = 0.693$ ; Fig. 3c). The interaction between soil nitrogen  
1535 availability and plant functional group revealed a weak negative effect of increas-  
1536 ing soil nitrogen availability on  $\chi$  in C<sub>3</sub> legumes (Tukey:  $p = 0.045$ ), with no  
1537 apparent effect in C<sub>3</sub> nonlegumes (Tukey:  $p = 0.706$ ) or C<sub>4</sub> nonlegumes (Tukey:  
1538  $p = 0.757$ ). Finally, an individual effect of functional group ( $p < 0.001$ ; Table 3)  
1539 revealed that C<sub>4</sub> nonlegumes generally had lower  $\chi$  than C<sub>3</sub> legumes and C<sub>3</sub> non-  
1540 legumes (Tukey:  $p < 0.001$  in both cases), with no apparent difference between  
1541 C<sub>3</sub> legumes and C<sub>3</sub> nonlegumes (Tukey:  $p = 0.831$ ).

**Table 4.3.** Effects of soil moisture, soil nitrogen availability, and plant functional group on  $\chi^*$ 

	df	Coefficient	$\chi^2$	p
Intercept	-	9.33E-01	-	-
Vapor pressure deficit ( $VPD_4$ )	1	-1.78E-01	20.792	<b>&lt;0.001</b>
Soil moisture ( $SM_2$ )	1	4.53E-02	1.972	0.160
Soil N (N)	1	-1.30E-03	0.168	0.682
PFT	2	-	172.624	<b>&lt;0.001</b>
$SM_2^*N$	1	7.40E-04	0.849	0.357
$VPD_4^*PFT$	2	-	10.241	<b>0.006</b>
$SM_2^*PFT$	2	-	6.806	<b>0.033</b>
$N^*PFT$	2	-	7.602	<b>0.022</b>
$SM_2^*N^*PFT$	2	-	0.732	0.694

**1542** \*Significance determined using Type II Wald  $\chi^2$  tests ( $\alpha = 0.05$ ). *P*-values less

**1543** than 0.05 are in bold and *p*-values where  $0.05 < p < 0.1$  are italicized.  $\chi$  was

**1544** not transformed prior to model fitting, so model coefficients are reported on the

**1545** response scale. Model coefficients are only included for continuous fixed effects.

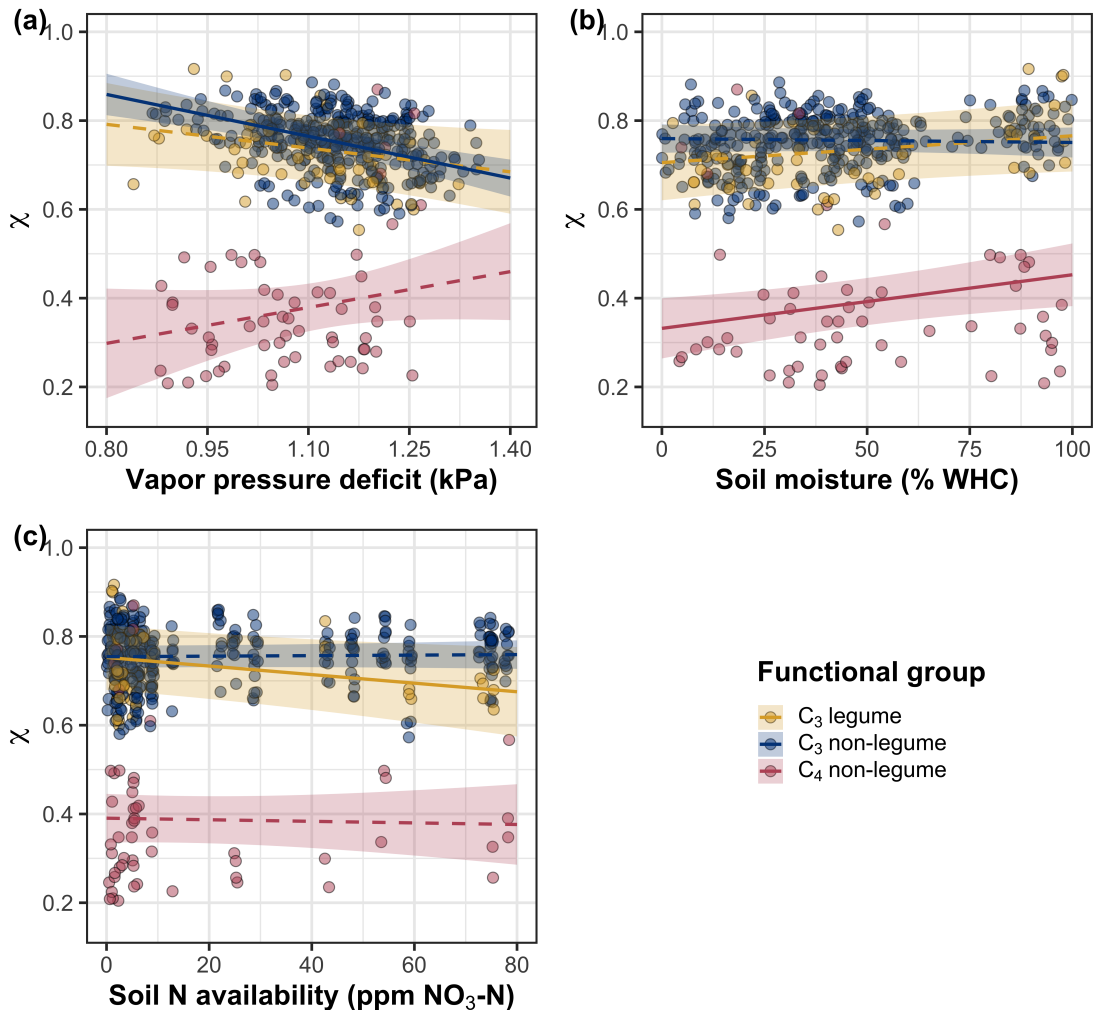


**Figure 4.3.** Effects of 4-day mean vapor pressure deficit (a), 2-day soil moisture (per water holding capacity; b), and soil nitrogen availability (c) on  $\chi$ . Shading and trendlines are as explained in Figure 2. Points are jittered for visibility. Variably colored trendlines are only included if there is an interaction between the x-axis and plant functional group, where solid trendlines indicate slopes that are different from zero ( $p < 0.05$ ) and dashed trendlines indicate slopes that are not different from zero ( $p < 0.05$ ). Error ribbons represent the upper and lower 95% confidence intervals of each fitted trendline.

**1546** 4.3.3 *Leaf nitrogen content*

**1547** An interaction between  $\chi$  and plant functional group ( $p < 0.001$ ; Table  
**1548** 4) revealed that the general negative effect of increasing  $\chi$  on  $N_{\text{area}}$  ( $p < 0.001$ ;  
**1549** Table 4) was driven by a negative effect of increasing  $\chi$  on  $N_{\text{area}}$  in C<sub>3</sub> nonlegumes  
**1550** (Tukey:  $p < 0.001$ ) and C<sub>3</sub> legumes (Tukey:  $p = 0.002$ ) despite a null effect of  $\chi$   
**1551** on  $N_{\text{area}}$  in C<sub>4</sub> nonlegumes (Tukey:  $p = 0.795$ ; Fig. 4a). An interaction between  
**1552** soil nitrogen availability and soil moisture ( $p = 0.028$ ; Table 4) indicated that the  
**1553** marginal positive effect of increasing soil nitrogen availability on  $N_{\text{area}}$  ( $p = 0.091$ ;  
**1554** Table 4) decreased with increasing soil moisture, despite no apparent individual  
**1555** effect of soil moisture on  $N_{\text{area}}$  ( $p = 0.692$ ; Table 4). Finally, a plant functional  
**1556** group effect ( $p < 0.001$ ; Table 4) indicated that C<sub>4</sub> nonlegumes had lower  $N_{\text{area}}$   
**1557** values on average compared to C<sub>3</sub> legumes (Tukey:  $p < 0.001$ ) and C<sub>3</sub> nonlegumes  
**1558** (Tukey:  $p = 0.001$ ), while C<sub>3</sub> legumes had lower average  $N_{\text{area}}$  values compared  
**1559** to C<sub>3</sub> nonlegumes (Tukey:  $p = 0.012$ ).

**1560** A marginal interaction between  $\chi$  and plant functional group ( $p = 0.088$ ;  
**1561** Table 4) revealed that, despite no apparent general effect of  $\chi$  on  $N_{\text{mass}}$  ( $p = 0.273$ ;  
**1562** Table 4), increasing  $\chi$  decreased  $N_{\text{mass}}$  in C<sub>3</sub> nonlegumes (Tukey:  $p = 0.021$ ), but  
**1563** this effect was not apparent in C<sub>4</sub> nonlegumes (Tukey:  $p = 0.693$ ) or C<sub>3</sub> legumes  
**1564** (Tukey:  $p = 0.477$ ). An interaction between soil nitrogen availability and soil  
**1565** moisture ( $p < 0.001$ ; Table 4) indicated that the general positive effect of increas-  
**1566** ing soil nitrogen availability on  $N_{\text{mass}}$  ( $p < 0.001$ ; Table 4) generally decreased  
**1567** with increasing soil moisture, despite an apparent general positive effect of in-  
**1568** creasing soil moisture on  $N_{\text{mass}}$  ( $p < 0.001$ ; Table 4). This interaction indicated  
**1569** that the positive effect of increasing soil nitrogen availability on  $N_{\text{mass}}$  was only

1570 apparent when soil moisture was less than 70% the maximum water holding ca-  
1571 pacity (Tukey:  $p < 0.05$  in all cases) despite a positive effect of increasing soil  
1572 moisture on  $N_{\text{mass}}$  ( $p < 0.001$ ; Table 4). Finally, a plant functional group effect  
1573 ( $p < 0.001$ ; Table 4) indicated that C<sub>4</sub> nonlegumes had lower  $N_{\text{mass}}$  values on  
1574 average compared to C<sub>3</sub> legumes (Tukey:  $p = 0.002$ ) and C<sub>3</sub> nonlegumes (Tukey:  
1575  $p = 0.019$ ), while  $N_{\text{mass}}$  did not differ between C<sub>3</sub> legumes and C<sub>3</sub> nonlegumes  
1576 (Tukey:  $p = 0.149$ ).

1577 An interaction between  $\chi$  and functional group ( $p = 0.005$ ; Table 4) indi-  
1578 cated that the general negative effect of increasing  $\chi$  on  $M_{\text{area}}$  ( $p < 0.001$ ; Table  
1579 4; Fig. 4c) was driven by a negative effect of increasing  $\chi$  on  $M_{\text{area}}$  in C<sub>3</sub> legumes  
1580 and C<sub>3</sub> nonlegumes (Tukey:  $p < 0.001$  in both cases) despite a nonsignificant  
1581 effect of increasing  $\chi$  on  $M_{\text{area}}$  in C<sub>4</sub> nonlegumes (Tukey:  $p = 0.724$ ). An in-  
1582 teraction between soil nitrogen and soil moisture ( $p < 0.001$ ; Table 4) indicated  
1583 that the general negative effect of increasing soil nitrogen availability on  $M_{\text{area}}$  ( $p$   
1584  $< 0.001$ ; Table 4) decreased with increasing soil moisture, despite an apparent  
1585 general negative effect of increasing soil moisture on  $M_{\text{area}}$  ( $p = 0.002$ ; Table 4).  
1586 Specifically, the negative effect of increasing soil nitrogen availability on  $M_{\text{area}}$  was  
1587 only apparent when soil moisture was less than 65% the maximum water holding  
1588 capacity (Tukey:  $p < 0.05$  in all cases). An additional interaction between soil  
1589 nitrogen availability and functional group ( $p = 0.034$ ; Table 4) indicated that the  
1590 general negative effect of increasing soil nitrogen availability on  $M_{\text{area}}$  was driven  
1591 by decreases in C<sub>3</sub> nonlegumes (Tukey:  $p < 0.001$ ) and C<sub>4</sub> nonlegumes (Tukey:  
1592  $p = 0.003$ ), with no apparent effect of soil nitrogen availability on  $M_{\text{area}}$  in C<sub>3</sub>  
1593 legumes (Tukey:  $p = 0.997$ ).

**Table 4.4.** Effects of soil nitrogen fertilization, inoculation, and CO<sub>2</sub> treatments on  $N_{\text{area}}$ ,  $N_{\text{mass}}$ , and  $M_{\text{area}}$ 

	df	$N_{\text{area}}$			$N_{\text{mass}}$			$M_{\text{area}}$		
		Coefficient	$\chi^2$	p	Coefficient	$\chi^2$	p	Coefficient	$\chi^2$	p
(Intercept)	-	2.78E+00	-	-	4.42E-01	-	-	6.97E+00	-	-
$\chi$	1	-2.53E+00	15.771	<b>&lt;0.001</b>	4.56E-01	1.201	0.273	-3.10E+00	20.620	<b>&lt;0.001</b>
Soil N (N)	1	1.08E-02	2.855	<i>0.091</i>	1.37E-02	54.531	<b>&lt;0.001</b>	-2.87E-03	29.759	<b>&lt;0.001</b>
Soil moisture (SM <sub>2</sub> )	1	3.61E-01	0.157	0.692	5.04E-01	16.255	<b>&lt;0.001</b>	-1.26E-01	9.282	<b>0.002</b>
PFT	1	-	60.641	<b>&lt;0.001</b>	-	21.539	<b>&lt;0.001</b>	-	11.520	<b>0.003</b>
SM <sub>2</sub> *N	1	-1.09E-02	4.779	<b>0.029</b>	-1.76E-02	41.784	<b>&lt;0.001</b>	6.35E-03	14.111	<b>&lt;0.001</b>
$\chi^*PFT$	1	-	15.188	<b>&lt;0.001</b>	-	4.864	<i>0.088</i>	-	17.032	<b>0.025</b>
N*PFT	1	-	2.289	<i>0.318</i>	-	0.914	0.633	-	6.760	<b>0.034</b>
SM <sub>2</sub> *PFT	1	-	0.978	0.613	-	0.128	0.938	-	2.121	0.346
SM <sub>2</sub> *N*PFT	1	-	1.289	0.525	-	2.180	0.336	-	0.629	0.730

<sup>9</sup>  
**1594** \*Significance determined using Type II Wald  $\chi^2$  tests ( $\alpha = 0.05$ ).  $P$ -values less than 0.05 are in bold and  $p$ -values  
**1595** where  $0.05 < p < 0.1$  are italicized. Coefficients are reported on the natural-log scale and are only included for  
**1596** continuous fixed effects.

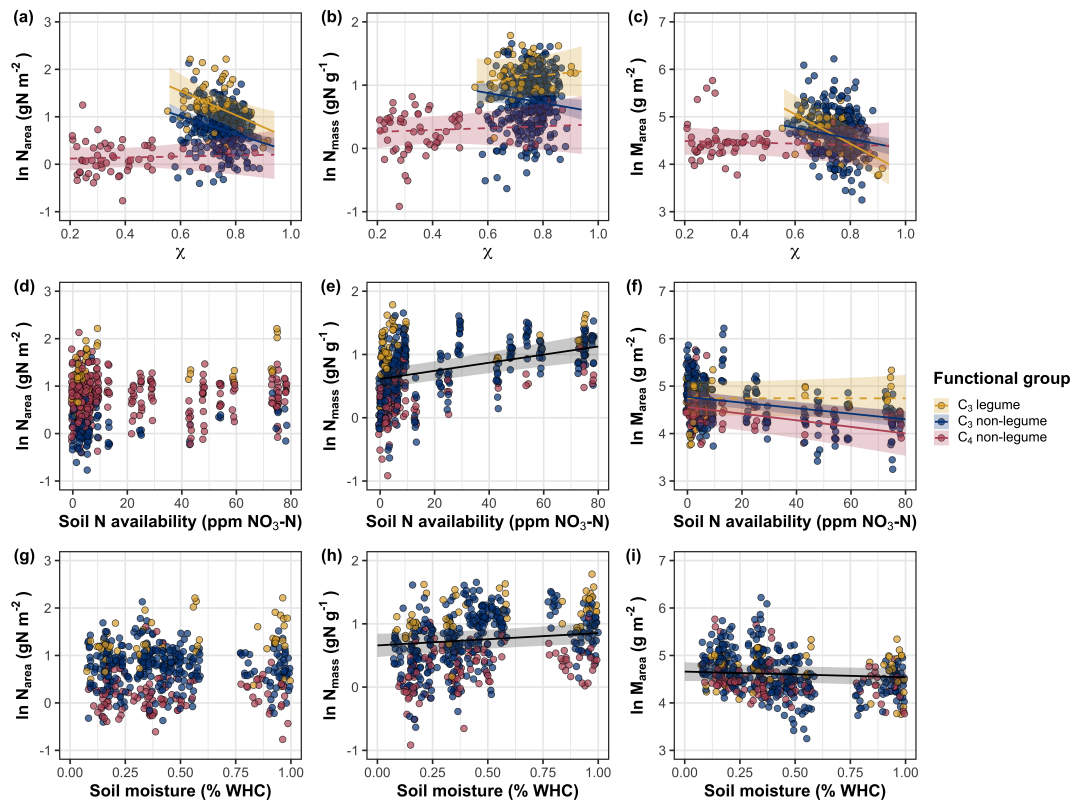


**Figure 4.4.** Effects of  $\chi$  (a-c), soil nitrogen availability (d-f), and soil moisture (g-i) on leaf nitrogen content per unit leaf area (a, d, g), leaf nitrogen content per unit leaf biomass (b, e, h), and leaf mass per area (c, f, i). A solid black trendline indicates the bivariate relationship between the fixed effect the x-axis and response variable on the y-axis and is only included when there is no interaction between the x-axis and plant functional group.

**1597** 4.3.4 *Structural equation model*

**1598** The piecewise structural equation model explained 90%, 54%, 80%, 92%,  
**1599** and 41% of variance in  $N_{\text{area}}$ ,  $N_{\text{mass}}$ ,  $M_{\text{area}}$ ,  $\chi$ , and  $\beta$ , respectively (Table 5; Fig.  
**1600** 5). Variance in  $N_{\text{area}}$  was driven by a negative effect of increasing  $\chi$  ( $p < 0.001$ ;  
**1601** Table 5) paired with positive effects of increasing  $N_{\text{mass}}$  and  $M_{\text{area}}$  ( $p < 0.001$  in  
**1602** both cases; Table 5; Fig. 5). Model results indicated that the negative effect  
**1603** of  $\chi$  on  $N_{\text{area}}$  was driven by a strong reduction in  $M_{\text{area}}$  with increasing  $\chi$  ( $p <$   
**1604** 0.001; Table 5) paired with no change in  $\chi$  due to  $N_{\text{mass}}$  ( $p = 0.150$ ; Table 5).  
**1605** However, there was a strong negative effect of increasing  $M_{\text{area}}$  on  $N_{\text{mass}}$  ( $p <$   
**1606** 0.001; Table 5; Fig. 5).  $\chi$  generally increased with increasing  $\beta$  ( $p < 0.001$ ; Table  
**1607** 5) and decreased with increasing VPD ( $p < 0.001$ ; Table 5; Fig. 5). Variance in  $\beta$   
**1608** was driven by a negative effect of increasing soil nitrogen availability ( $p < 0.001$ ;  
**1609** Table 5) and was generally higher in C<sub>3</sub> species ( $p < 0.001$ ; Table 5; Fig. 5).  
**1610** However,  $\beta$  did not change with soil moisture ( $p = 0.332$ ; Table 5) or with ability  
**1611** to acquire nitrogen via symbiotic nitrogen fixation ( $p = 0.546$ ; Table 5). Finally,  
**1612** soil nitrogen availability was positively associated with increasing soil moisture ( $p$   
**1613**  $< 0.001$ ; Table 5; Fig. 5), while VPD was negatively associated with increasing  
**1614** soil moisture ( $p < 0.001$ ; Table 5; Fig. 5).

**Table 4.5.** Structural equation model results investigating direct effects of climatic and soil resource availability on  $N_{\text{area}}$ ,  $N_{\text{mass}}$ ,  $M_{\text{area}}$ ,  $\chi$ , and  $\beta$ 

Predictor	Coefficient	<i>p</i>
$N_{\text{area}} (R^2_c) = 0.90$		
$\chi$	-0.140	<b>&lt;0.001</b>
$M_{\text{area}}$	0.807	<b>&lt;0.001</b>
$N_{\text{mass}}$	0.795	<b>&lt;0.001</b>
$N_{\text{mass}} (R^2_c) = 0.54$		
$\chi$	0.097	<b>&lt;0.001</b>
$M_{\text{area}} (R^2_c) = 0.80$		
$\chi$	-0.372	0.150
$M_{\text{area}}$	-0.303	<b>&lt;0.001</b>
$\chi (R^2_c) = 0.92$		
$\beta$	0.261	<b>&lt;0.001</b>
$\text{VPD}_4$	-0.122	<b>&lt;0.001</b>
$\beta (R^2_c) = 0.41$		
Soil N	-0.201	<b>&lt;0.001</b>
$\text{SM}_2$	-0.048	0.332
Photo. pathway	0.490	<b>&lt;0.001</b>
N-fixing ability	-0.053	0.546
Soil N ( $R^2_c$ ) = 0.39		
$\text{SM}_2$	0.410	<b>&lt;0.001</b>

**1615** \*Reported coefficients are standardized across the structural equation model. *P*-  
**1616** values less than 0.05 are noted in bold. Positive coefficients for photosynthetic  
**1617** pathway indicate generally larger values in C<sub>3</sub> species, while positive coefficients  
**1618** for N-fixing ability indicate generally larger values in N-fixing species. Key:  
**1619**  $N_{\text{area}}$ =leaf nitrogen content per unit leaf area,  $M_{\text{area}}$ =leaf mass per unit leaf dry  
**1620** biomass,  $N_{\text{mass}}$ =leaf nitrogen content per unit leaf dry biomass,  $\beta$ =cost of acquiring  
**1621** nitrogen relative to water,  $\chi$ =isotope-derived estimate of the leaf Ci:Ca ratio,  
**1622**  $\text{VPD}_4$ = 4-day mean vapor pressure deficit,  $\text{SM}_2$ =2-day mean soil moisture,  $R^2_c$   
**1623** = conditional R<sup>2</sup> value

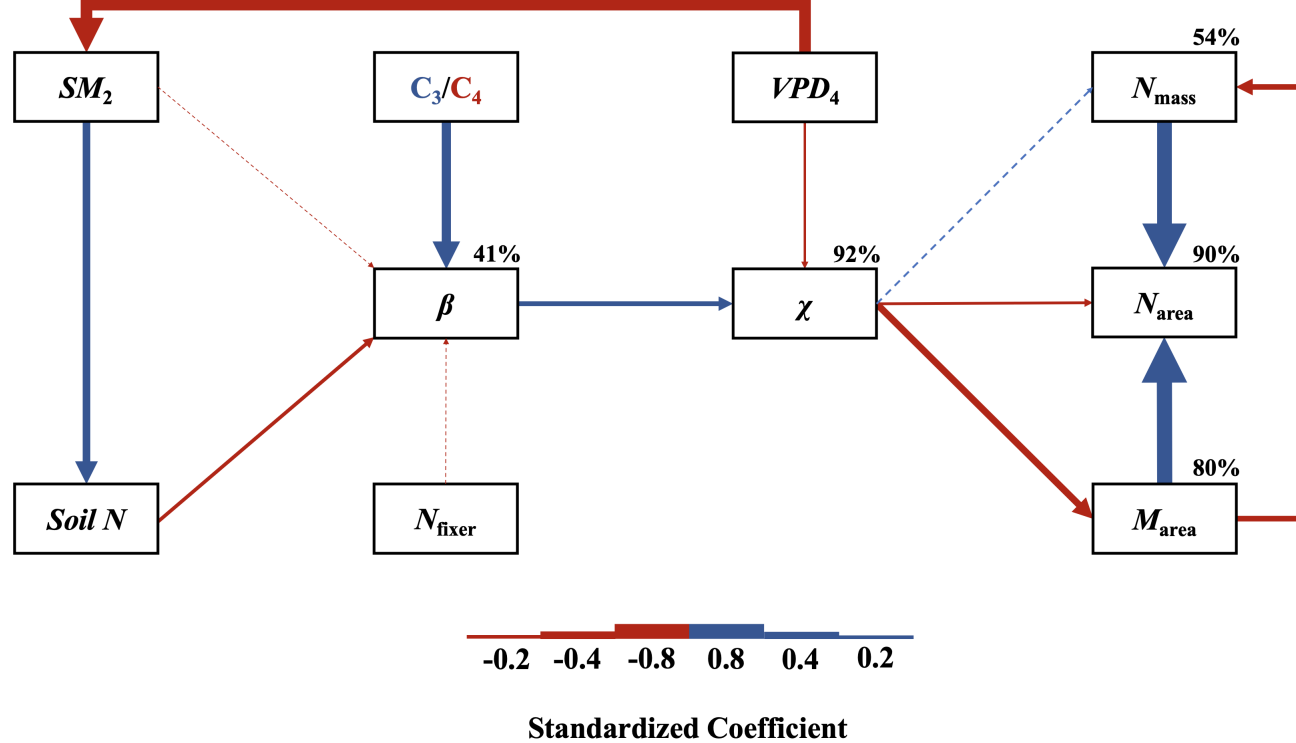


**Figure 4.5.** Structural equation model results exploring direct and indirect drivers of  $N_{area}$ . Boxes indicate measured edaphic factors, climatic factors, and leaf traits. Percentages above boxes indicate conditional  $R^2$  values of each respective leaf trait. Solid arrows indicate bivariate relationships where  $p < 0.05$ , while dashed arrows indicate bivariate relationships where  $p > 0.05$ . Positive model coefficients are indicated through blue arrows, while negative model coefficients are indicated through red arrows. Arrow thickness scales with the standardized model coefficient of each bivariate relationship. A positive coefficient for photosynthetic pathway indicates generally larger values in  $C_3$  species, while a positive coefficient for  $N_{fixer}$  indicates generally larger values in N-fixing species. Standardized model coefficients and associated  $p$ -values are reported in Table 5.

**1624** 4.4 Discussion

**1625** In this study, we quantified direct and indirect effects of soil resource avail-  
**1626** ability, climate,  $\chi$ , and  $\beta$  on  $N_{\text{area}}$  and components of  $N_{\text{area}}$  ( $N_{\text{mass}}$  and  $M_{\text{area}}$ ) in  
**1627** 520 individuals spanning across a soil resource availability and climate gradient  
**1628** in Texas, USA. We found consistent support for patterns expected from photo-  
**1629** synthetic least-cost theory, a result driven by a strong direct negative relationship  
**1630** between the relative costs to acquire nitrogen versus water ( $\beta$ ) on  $N_{\text{area}}$  as medi-  
**1631** ated through changes in the leaf C<sub>i</sub>:C<sub>a</sub> ratio ( $\chi$ ). In further support of patterns  
**1632** expected from theory, increasing soil nitrogen availability had a strong negative  
**1633** effect on  $\beta$ , resulting in an indirect stimulation in  $N_{\text{area}}$ . Increasing VPD also  
**1634** indirectly increased  $N_{\text{area}}$  through a direct negative effect of increasing VPD on  
**1635**  $\chi$ . Interestingly, we found a strong positive association between soil moisture and  
**1636** soil nitrogen availability resulted in an indirect positive effect of increasing soil  
**1637** moisture on  $N_{\text{area}}$  despite an apparent null direct effect of soil moisture on  $N_{\text{area}}$ .  
**1638** Overall, results provide strong and consistent support for patterns expected from  
**1639** photosynthetic least-cost theory, showing that both soil resource availability and  
**1640** climate drive variance in  $N_{\text{area}}$  through changes in  $\chi$ .

**1641** 4.4.1 *Negative effects of  $\chi$  on  $N_{\text{area}}$  are driven by reductions in  $M_{\text{area}}$ , not  $N_{\text{mass}}$*

**1642** A strong negative effect of increasing  $\chi$  on  $N_{\text{area}}$  was detected in both  
**1643** the linear mixed effect and piecewise structural equation models. The negative  
**1644** response of  $N_{\text{area}}$  to increasing  $\chi$  is consistent with previous environmental gra-  
**1645** dient (Dong et al. 2017; Querejeta et al. 2022) and manipulation experiments  
**1646** (Perkowski et al. n.d.), showing strong support for the nitrogen-water use trade-

1647 offs expected from photosynthetic least cost theory (Wright et al. 2003; Prentice  
1648 et al. 2014). Negative effects of increasing  $\chi$  on  $N_{\text{area}}$  were driven by a strong  
1649 negative effect of increasing  $\chi$  on  $M_{\text{area}}$ , with no apparent effect of  $\chi$  on  $N_{\text{mass}}$ , sug-  
1650 gesting that changes in  $N_{\text{area}}$  were driven by changes in leaf structure and not leaf  
1651 chemistry. Interestingly, increasing  $M_{\text{area}}$  was negatively associated with  $N_{\text{mass}}$ ,  
1652 indicating that an increase in  $N_{\text{mass}}$  was associated with larger, thinner leaves (i.e.  
1653 lower  $M_{\text{area}}$ ). These results are consistent with patterns reported from previous  
1654 studies indicating that variance in  $N_{\text{area}}$  is driven by changes in  $M_{\text{area}}$  across envi-  
1655 ronmental gradients, and that part of this response is due to negative covariance  
1656 between  $M_{\text{area}}$  and  $N_{\text{mass}}$  associated with tradeoffs between leaf longevity and leaf  
1657 productivity (Wright et al. 2004; Dong et al. 2017; Dong et al. 2022; Wang et al.  
1658 2023; Querejeta et al. 2022).

1659 The negative relationship between  $\chi$  and  $M_{\text{area}}$  could be also response that  
1660 allows leaves to maximize productivity in shorter-lived leaves. Tradeoffs between  
1661 leaf longevity and leaf productivity are commonly observed and are included in  
1662 a continuum of coordinated leaf traits that position individuals along a fast- or  
1663 slow-growing leaf economics spectrum (Wright et al. 2004; Onoda et al. 2004;  
1664 Onoda et al. 2017; Reich 2014; Wang et al. 2023). Negative relationships be-  
1665 tween  $\chi$  and  $M_{\text{area}}$  indicate that increased stomatal conductance and reduced  
1666 water use efficiency were associated with thinner, larger leaves (i.e., lower  $M_{\text{area}}$ ).  
1667 These patterns, combined with the negative relationship between  $M_{\text{area}}$  and  $N_{\text{mass}}$   
1668 mentioned above, likely allowed individuals to maximize light interception and  
1669 productivity by exploiting high light environments, though this may come at the  
1670 expense of increased water loss and decreased water-use efficiency. This strategy

1671 may be especially advantageous for fast-growing species in open canopy systems.  
1672 In this study, C<sub>3</sub> legumes and C<sub>3</sub> nonlegumes dominated the dataset (78% of total  
1673 sampling effort), of which 22% (17% of total sampling effort) were classified as  
1674 annual species with short growing seasons. We observed no effect of  $\chi$  on  $N_{\text{area}}$   
1675 or  $M_{\text{area}}$  in C<sub>4</sub> nonlegumes, which made up 22% of the sampling effort and were  
1676 generally classified as warm season graminoid species with slower growth rates and  
1677 longer growing seasons. These patterns indicate that stronger tradeoffs between  
1678 nitrogen and water use may be more apparent in fast-growing species with high  
1679 demand for building and maintaining productive leaf tissues.

1680 4.4.2 *Soil nitrogen availability increases  $N_{\text{area}}$  through changes in the cost to  
1681 acquire nitrogen*

1682 The null effect of soil nitrogen availability on  $N_{\text{area}}$  was driven by positive  
1683 and negative respective effects of increasing soil nitrogen availability on  $N_{\text{mass}}$  and  
1684  $M_{\text{area}}$  that were equal in magnitude. The null response of  $N_{\text{area}}$  to soil nitrogen  
1685 availability occurred alongside a negative effect of increasing soil nitrogen avail-  
1686 ability on  $\beta$ , which, paired with the negative relationship between  $\chi$  and  $N_{\text{area}}$ ,  
1687 suggests a general positive effect of increasing soil nitrogen availability on  $N_{\text{area}}$ ,  
1688 but only when mediated through changes in  $\beta$ . This result is consistent with our  
1689 hypotheses and patterns expected from photosynthetic least-cost theory. These  
1690 results suggest that positive direct effects of increasing soil nitrogen availability  
1691 on  $N_{\text{area}}$  are not ubiquitous across environmental gradients. Instead, as predicted  
1692 by our hypotheses and patterns expected from theory, positive responses of  $N_{\text{area}}$   
1693 to increasing soil nitrogen availability are a deterministic acclimation response to

1694 shifts in climate-related demand to build and maintain photosynthetic enzymes,  
1695 which allows plants to optimize photosynthetic processes and resource use to a  
1696 given environment (Paillassa et al. 2020; Peng et al. 2021; Dong et al. 2022;  
1697 Westerband et al. 2023).

1698 4.4.3 *Soil moisture increases  $N_{\text{area}}$  by facilitating increases in soil nitrogen  
1699 availability*

1700 Increasing soil moisture generally had no effect on  $N_{\text{area}}$ , a response that  
1701 was associated with a null effect of soil moisture on  $\beta$ . These results contrast  
1702 patterns expected from theory, where increasing soil moisture is expected to indi-  
1703 rectly decrease  $N_{\text{area}}$  through an increase in  $\beta$  due to a reduction in costs associated  
1704 with water acquisition and use (Wright et al. 2003; Prentice et al. 2014; Lavergne  
1705 et al. 2020). Interestingly, structural equation model results revealed a strong  
1706 positive association between soil moisture and soil nitrogen availability, indicat-  
1707 ing an indirect positive effect of increasing soil moisture on  $N_{\text{area}}$  mediated by the  
1708 negative effect of increasing soil nitrogen availability on  $\beta$ . In Texan grasslands,  
1709 productivity and nutrient uptake are often co-limited by precipitation and nutrient  
1710 availability (Yahdjian et al. 2011; Wang et al. 2017). Thus, increases in soil mois-  
1711 ture may have facilitated more favorable and productive environments for soil  
1712 microbial communities, thereby stimulating the accumulation of plant-available  
1713 nitrogen substrate through increased ammonification or nitrification rates (Reich-  
1714 man et al. 1966; Stark and Firestone 1995; Paul et al. 2003). Alternatively, soil  
1715 moisture may have facilitated greater nitrogen mobility through soil solution. As  
1716 discussed above, the positive indirect response of  $N_{\text{area}}$  to increasing soil nitrogen

1717 availability as mediated through reductions in  $\beta$  follow patterns expected from  
1718 theory.

1719 4.4.4 *Indirect effects of climate on  $N_{\text{area}}$  are mediated through changes in leaf  
1720  $C_i:C_a$  and  $\beta$*

1721 In support of our hypothesis and patterns expected from theory, increasing  
1722 VPD indirectly increased  $N_{\text{area}}$ , mediated through the negative effect of increasing  
1723 VPD on  $\chi$ . These responses are consistent with previous work noting strong reduc-  
1724 tions in stomatal conductance with increasing VPD (Oren et al. 1999; Novick et al.  
1725 2016; Sulman et al. 2016; Grossiord et al. 2020), a response that allows plants  
1726 to minimize water loss as a result of high atmospheric water demand. Results  
1727 also support findings from previous experiments across environmental gradients,  
1728 where increasing VPD generally increases  $N_{\text{area}}$  at lower stomatal conductance  
1729 across environmental gradients (Dong et al. 2017; Dong et al. 2022; Paillassa  
1730 et al. 2020; Westerband et al. 2023).

1731 4.4.5 *Species identity traits modify effects of the environment on  $\beta$ ,  $\chi$ , and  $N_{\text{area}}$*   
1732 N-fixing species generally had higher  $N_{\text{area}}$  values on average compared to  
1733 non-fixing species, a pattern driven by a stronger stimulation in  $N_{\text{mass}}$  in N-fixing  
1734 species coupled with no change in  $M_{\text{area}}$  between species with different N-fixation  
1735 ability. We found no evidence to suggest that N-fixing species had different  $\beta$  or  
1736  $\chi$  values compared to non-fixing species across the environmental gradient. These  
1737 results follow patterns from previous environmental gradient experiments that  
1738 investigate variance in leaf nitrogen allocation in N-fixing species (Adams et al.

1739 2016; Dong et al. 2017; Dong et al. 2020), and that increases in  $N_{\text{mass}}$  and  $N_{\text{area}}$  in  
1740 N-fixing species are not necessarily correlated to increases in water use efficiency  
1741 or reductions in  $\chi$  (Adams et al. 2016). While our results are consistent with  
1742 results from previous environmental gradient experiments, they do not necessarily  
1743 support our hypothesis or patterns expected from theory, which predicts that  
1744 stimulations in  $N_{\text{area}}$  by N-fixing species should be driven by a reduction in  $\beta$   
1745 relative to non-fixing species, and that this response should decrease stomatal  
1746 conductance and  $\chi$ .

1747 C<sub>4</sub> species generally had lower  $\beta$ ,  $\chi$ , and  $N_{\text{area}}$  values than C<sub>3</sub> species.  
1748 Reduced  $\beta$  and  $\chi$  values in C<sub>4</sub> species follow our hypothesis, a pattern that could  
1749 be the result of either reduced costs of nitrogen acquisition and use or increased  
1750 costs of water acquisition and use or both (Wright et al. 2003; Prentice et al.  
1751 2014). Results also indicate that  $\beta$  in C<sub>4</sub> nonlegumes was unresponsive to changes  
1752 in soil nitrogen availability despite an apparent negative effect of increasing soil  
1753 nitrogen availability on  $\beta$  in C<sub>3</sub> legumes and C<sub>3</sub> nonlegumes. Combined with a  
1754 general null response of  $\beta$  to soil moisture regardless of plant functional group,  
1755 these patterns imply that reduced  $\beta$  values in C<sub>4</sub> species may be the result of lower  
1756 costs of nitrogen acquisition and use relative to C<sub>3</sub> species. While lower  $\beta$  values  
1757 in C<sub>4</sub> species provides a possible explanation for why C<sub>4</sub> species often have lower  
1758  $\chi$  and greater water use efficiency, theory predicts that this response should cause  
1759 C<sub>4</sub> species to have greater  $N_{\text{area}}$  values compared to C<sub>3</sub> species, though C<sub>4</sub> species  
1760 commonly exhibit lower  $N_{\text{area}}$  and higher nitrogen use efficiency than C<sub>3</sub> species  
1761 (Schmitt and Edwards 1981; Sage and Pearcy 1987; Ghannoum et al. 2011). We  
1762 speculate that lowered costs of nitrogen acquisition and use in C<sub>4</sub> species could be

**1763** driven by more efficient Rubisco carboxylation efficiency in C<sub>4</sub> species associated  
**1764** with CO<sub>2</sub> concentrating mechanisms that eliminate photorespiration (Ghannoum  
**1765** et al. 2011), which could reduce or eliminate the need to sacrifice inefficient  
**1766** nitrogen use for efficient water use to achieve optimal photosynthesis rates.

**1767** 4.4.6 *Next steps for optimality model development*

**1768** Optimality models for both C<sub>3</sub> and C<sub>4</sub> species have been developed using  
**1769** principles from photosynthetic least-cost theory (Prentice et al. 2014; Wang et al.  
**1770** 2017; Smith et al. 2019; Stocker et al. 2020; Scott and Smith 2022). In both C<sub>3</sub>  
**1771** and C<sub>4</sub> model variants,  $\beta$  values are held constant using global datasets of leaf  $\delta^{13}\text{C}$   
**1772** (Wang et al. 2017; Cornwell et al. 2018). Specifically, the C<sub>3</sub> optimality model  
**1773** initially assumed a constant  $\beta$  value of 240 (Wang et al. 2017), later corrected to  
**1774** 146 (Stocker et al. 2020), while the C<sub>4</sub> optimality model assumes a constant  $\beta$   
**1775** value of 166 (Scott and Smith 2022). Our results, which build on findings from  
**1776** Paillassa et al. (2020), demonstrate high variability in calculated  $\beta$  values across  
**1777** environmental gradients. Specifically,  $\beta$  values in C<sub>3</sub> species ranged from 1.7 to  
**1778** 188.0 (mean: 30.2; median: 23.1; standard deviation: 25.4), while ranged from 0.1  
**1779** to 110.6 in C<sub>4</sub> species (mean: 7.2; median: 0.7; standard deviation: 18.6). Mean  
**1780**  $\beta$  values in both C<sub>3</sub> and C<sub>4</sub> species were consistently lower than values currently  
**1781** implemented in optimality models, though this was likely the result of increased  
**1782** water limitation across our sites relative to global averages. Regardless, the high  
**1783** degree of  $\beta$  variability across this environmental gradient, together with findings  
**1784** from Lavergne et al. (2020) and Paillassa et al. (2020), suggests that the use of  
**1785** constant  $\beta$  values may contribute to erroneous errors when conducting optimality

**1786** model simulations. We therefore build on suggestions from Wang et al. (2017),  
**1787** recommending future photosynthetic least-cost model developments to consider  
**1788** the use of dynamic  $\beta$  values.

**1789** 4.4.7 *Conclusions*

**1790** To summarize, variability in Narea across an environmental gradient in  
**1791** Texan grasslands was driven by indirect effects of climate and soil resource avail-  
**1792** ability mediated. Results from this experiment provide strong and consistent sup-  
**1793** port for patterns expected from photosynthetic least-cost theory, demonstrating  
**1794** that negative relationships between  $\chi$  and  $N_{\text{area}}$  unify expected effects of climatic  
**1795** and edaphic characteristics on Narea across environmental gradients. Our results  
**1796** also demonstrate a need to consider the dynamic nature of the relative cost of  
**1797** nitrogen versus water uptake ( $\beta$ ) across environmental gradients in optimality  
**1798** models that leverage principles of photosynthetic least-cost theory.

**1799**

## Chapter 5

**1800** Optimal resource investment to photosynthetic capacity maximizes  
**1801** nutrient allocation to whole plant growth under elevated CO<sub>2</sub>

**1802** 5.1 Introduction

**1803** Terrestrial ecosystems are regulated by complex carbon and nitrogen cy-  
**1804** cles. As a result, terrestrial biosphere models, which are beginning to include  
**1805** coupled carbon and nitrogen cycles (Shi et al. 2016; Davies-Barnard et al. 2020;  
**1806** Braghieri et al. 2022), must accurately represent these cycles under different  
**1807** environmental scenarios to reliably simulate carbon and nitrogen atmosphere-  
**1808** biosphere fluxes (Hungate et al. 2003; Prentice et al. 2015). While the inclusion  
**1809** of coupled carbon and nitrogen cycles tends to reduce model uncertainty (Arora  
**1810** et al. 2020), large uncertainty in role of soil nitrogen availability and nitrogen ac-  
**1811** quisition strategy on leaf and whole plant acclimation responses to CO<sub>2</sub> remains  
**1812** (Smith and Dukes 2013; Terrer et al. 2018; Smith and Keenan 2020). This source  
**1813** of uncertainty likely contributes to the widespread divergence in future carbon  
**1814** and nitrogen flux simulations across terrestrial biosphere models (Friedlingstein  
**1815** et al. 2014; Zaehle et al. 2014; Meyerholt et al. 2020).

**1816** Plants grown under elevated CO<sub>2</sub> generally have less leaf nitrogen content  
**1817** than those grown under ambient CO<sub>2</sub>, a response that often corresponds with  
**1818** reductions in photosynthetic capacity and stomatal conductance at the leaf-level  
**1819** and biomass stimulation over time at the whole plant level (Curtis 1996; Drake  
**1820** et al. 1997; Ainsworth et al. 2002; Makino 2003; Morgan et al. 2004; Ainsworth  
**1821** and Long 2005; Ainsworth and Rogers 2007; Smith and Dukes 2013; Poorter et al.  
**1822** 2022). As net primary productivity is generally limited by nitrogen availability

1823 (Vitousek and Howarth 1991; LeBauer and Treseder 2008; Fay et al. 2015), and  
1824 soil nitrogen availability is often positively correlated with leaf nitrogen content  
1825 and photosynthetic capacity (Field and Mooney 1986; Evans and Seemann 1989;  
1826 Evans 1989; Walker et al. 2014; Firn et al. 2019; Liang et al. 2020), some  
1827 have hypothesized that leaf and whole plant acclimation responses to CO<sub>2</sub> are  
1828 constrained by soil nitrogen availability. The progressive nitrogen limitation hy-  
1829 pothesis predicts that elevated CO<sub>2</sub> will increase plant nitrogen demand, which  
1830 will increase plant nitrogen uptake and progressively deplete soil nitrogen if soil  
1831 nitrogen supply does not exceed plant nitrogen demand (Luo et al. 2004). The  
1832 hypothesis predicts that this response should result in strong acute stimulations in  
1833 whole plant growth and primary productivity that diminish over time as nitrogen  
1834 becomes more limiting. Assuming a positive relationship between soil nitrogen  
1835 availability, leaf nitrogen content, and photosynthetic capacity, this hypothesis  
1836 also implies that progressive reductions in soil nitrogen availability should be the  
1837 mechanism that drives the downregulation in leaf nitrogen content and photosyn-  
1838 thetic capacity under elevated CO<sub>2</sub>. This hypothesis has received some support  
1839 from free air CO<sub>2</sub> enrichment experiments (Reich et al. 2006; Norby et al. 2010),  
1840 although is not consistently observed across experiments (Finzi et al. 2006; Moore  
1841 et al. 2006; Liang et al. 2016).

1842 While possible that progressive nitrogen limitation may determine leaf and  
1843 whole plant acclimation responses to CO<sub>2</sub>, growing evidence indicates that leaf ni-  
1844 trogen and photosynthetic capacity are more strongly determined through above-  
1845 ground growing conditions than by soil resource availability (Dong et al. 2017;  
1846 Dong et al. 2020; Dong et al. 2022; Smith et al. 2019; Smith and Keenan 2020;

1847 Paillassa et al. 2020; Peng et al. 2021; Querejeta et al. 2022; Westerband et al.  
1848 2023), and satellite-derived chlorophyll fluorescence data indicate that increasing  
1849 atmospheric CO<sub>2</sub> may decrease leaf and canopy demand for nitrogen (Dong et al.  
1850 2022). Together, results from these studies suggest that the downregulation in  
1851 leaf nitrogen content and photosynthetic capacity due to increasing CO<sub>2</sub> may not  
1852 be as tightly linked to progressive nitrogen limitation as previously hypothesized.

1853 A unification of optimal coordination and photosynthetic least-cost the-  
1854 ories predicts that leaves acclimate to elevated CO<sub>2</sub> by downregulating nitrogen  
1855 allocation to Ribulose-1,5-bisphosphate (RuBP) carboxylase/oxygenase (Rubisco)  
1856 to optimize resource use efficiencies at the leaf level, which allows for greater re-  
1857 source allocation to whole plant growth (Drake et al. 1997; Wright et al. 2003;  
1858 Prentice et al. 2014; Smith et al. 2019). The theory predicts that the downregu-  
1859 lation in nitrogen allocation to Rubisco results in a stronger downregulation in the  
1860 maximum rate of Rubisco carboxylation ( $V_{cmax}$ ) than the maximum rate of RuBP  
1861 regeneration ( $J_{max}$ ), which maximizes photosynthetic efficiency by allowing net  
1862 photosynthesis rates to be equally co-limited by Rubisco carboxylation and RuBP  
1863 regeneration (Chen et al. 1993; Maire et al. 2012). This acclimation response  
1864 allows plants to make more efficient use of available light while avoiding overin-  
1865 vestment in Rubisco, which has high nitrogen and energetic costs of building and  
1866 maintaining (Evans 1989; Evans and Clarke 2019). Instead, additional acquired  
1867 resources not needed to optimize leaf photosynthesis are allocated to the mainte-  
1868 nance of structures that support whole plant growth (e.g., total leaf area, whole  
1869 plant biomass, etc.) or to allocation processes not related to leaf photosynthesis  
1870 or growth, such as plant defense mechanisms or leaf structural tissue. Regardless,

**1871** optimized resource allocation at the leaf level should allow for greater resource  
**1872** allocation to whole plant growth. The theory indicates that leaf acclimation re-  
**1873** sponses to CO<sub>2</sub> should be independent of changes in soil nitrogen availability.  
**1874** While this leaf acclimation response maximizes nitrogen allocation to structures  
**1875** that support whole plant growth, the theory suggests that the positive effect of  
**1876** elevated CO<sub>2</sub> on whole plant growth may be further stimulated by soil nitrogen  
**1877** availability through a reduction in the cost of acquiring nitrogen (Bae et al. 2015;  
**1878** Perkowski et al. 2021; Lu et al. 2022).

**1879** Plants acquire nitrogen by allocating photosynthetically derived carbon be-  
**1880** lowground in exchange for nitrogen through different nitrogen acquisition strate-  
**1881** gies. These nitrogen acquisition strategies can include direct uptake pathways  
**1882** such as mass flow or diffusion (Barber 1962), symbioses with mycorrhizal fungi or  
**1883** symbiotic nitrogen-fixing bacteria (Vance and Heichel 1991; Marschner and Dell  
**1884** 1994; Smith and Read 2008; Udvardi and Poole 2013), or through the release  
**1885** of root exudates that prime free-living soil microbial communities (Phillips et al.  
**1886** 2011; Wen et al. 2022). Plants cannot acquire nitrogen without first allocating  
**1887** carbon belowground, which implies an inherent carbon cost to the plant for acquir-  
**1888** ing nitrogen regardless of nitrogen acquisition strategy. Carbon costs to acquire  
**1889** nitrogen often vary in species with different nitrogen acquisition strategies and  
**1890** are dependent on external environmental factors such as atmospheric CO<sub>2</sub>, light  
**1891** availability, and soil nitrogen availability (Brzostek et al. 2014; Terrer et al. 2016;  
**1892** Terrer et al. 2018; Allen et al. 2020; Perkowski et al. 2021; Lu et al. 2022), which  
**1893** suggests that acquisition strategy may be an important factor in determining ef-  
**1894** fects of soil nitrogen availability on leaf and whole plant acclimation responses to

1895 elevated CO<sub>2</sub>.

1896 A recent meta-analysis using data across 20 grassland and forest CO<sub>2</sub> en-  
1897 richment experiments suggested that species which acquire nitrogen from sym-  
1898 biotic nitrogen-fixing bacteria had reduced costs of nitrogen acquisition under  
1899 elevated CO<sub>2</sub> (Terrer et al. 2018). Findings from this meta-analysis indicated  
1900 that reductions in costs of nitrogen acquisition in species that form associations  
1901 with symbiotic nitrogen-fixing bacteria under elevated CO<sub>2</sub> may drive stronger  
1902 stimulations in whole plant growth and downregulations in  $V_{cmax}$  than species that  
1903 associate with arbuscular mycorrhizal fungi (Smith and Keenan 2020), which gen-  
1904 erally have higher costs of nitrogen acquisition under elevated CO<sub>2</sub> (Terrer et al.  
1905 2018). However, plant investments in symbiotic nitrogen fixation generally de-  
1906 cline with increasing nitrogen availability (Dovrat et al. 2018; Perkowski et al.  
1907 2021), a response that has been previously inferred to be the result of a shift in  
1908 the dominant mode of nitrogen acquisition to direct uptake pathways as costs of  
1909 direct uptake decrease with increasing soil nitrogen availability (Rastetter et al.  
1910 2001; Perkowski et al. 2021). Thus, effects of symbiotic nitrogen fixation on plant  
1911 acclimation responses to CO<sub>2</sub> should decline with increasing soil nitrogen avail-  
1912 ability, although manipulative experiments that directly test these patterns are  
1913 rare.

1914 Here, I conducted a 7-week growth chamber experiment using *Glycine max*  
1915 L. (Merr.) to examine the effects of soil nitrogen fertilization and inoculation with  
1916 symbiotic nitrogen-fixing bacteria on leaf and whole plant acclimation responses  
1917 to elevated CO<sub>2</sub>. Following patterns expected from theory, I hypothesized that in-  
1918 dividual leaves should acclimate to elevated CO<sub>2</sub> by more strongly downregulating

1919  $V_{cmax}$  relative to  $J_{max}$ , allowing leaf photosynthesis to approach optimal coordi-  
1920 nation. I expected this response to correspond with a stronger downregulation in  
1921 leaf nitrogen content than  $V_{cmax}$  and  $J_{max}$ , which would increase the fraction of  
1922 leaf nitrogen content allocated to photosynthesis and photosynthetic nitrogen use  
1923 efficiency. At the whole-plant level, I hypothesized that plants would acclimate  
1924 to elevated CO<sub>2</sub> by stimulating whole plant growth and productivity, a response  
1925 that would be driven by a strong positive response of total leaf area and above-  
1926 ground biomass to elevated CO<sub>2</sub>. I predicted that leaf acclimation responses to  
1927 elevated CO<sub>2</sub> would be independent of soil nitrogen fertilization and inoculation  
1928 with symbiotic nitrogen-fixing bacteria; however, I expected that increasing soil  
1929 nitrogen fertilization would increase the positive effect of elevated CO<sub>2</sub> on mea-  
1930 sures of whole plant growth due to a stronger reduction in the cost of acquiring  
1931 nitrogen under elevated CO<sub>2</sub> with increasing fertilization. I also expected stronger  
1932 stimulations in whole plant growth due to inoculation, but that this effect would  
1933 only be apparent under low fertilization due to a reduction in root nodulation  
1934 with increasing fertilization.

1935 5.2 Methods

1936 5.2.1 *Seed treatments and experimental design*

1937 *Glycine max* L. (Merr) seeds were planted in 144 6-liter surface sterilized  
1938 pots (NS-600, Nursery Supplies, Orange, CA, USA) containing a steam-sterilized  
1939 70:30 v:v mix of Sphagnum peat moss (Premier Horticulture, Quakertown, PA,  
1940 USA) to sand (Pavestone, subsidiary of Quikrete Companies, Atlanta, GA, USA).  
1941 Before planting, all *G. max* seeds were surface sterilized in 2% sodium hypochlorite

1942 for 3 minutes, followed by three separate 3-minute washes with ultrapure water  
1943 (MilliQ 7000; MilliporeSigma, Burlington, MA USA). A subset of surface steril-  
1944 ized seeds were inoculated with *Bradyrhizobium japonicum* (Verdesian N-Dure™  
1945 Soybean, Cary, NC, USA) in a slurry following manufacturer recommendations  
1946 (3.12 g inoculant and 241 g deionized water per 1 kg seed).

1947 Seventy-two pots were randomly planted with surface-sterilized seeds inoc-  
1948 ulated with *B. japonicum*, while the remaining 72 pots were planted with surface-  
1949 sterilized uninoculated seeds. Thirty-six pots within each inoculation treatment  
1950 were randomly placed in one of two atmospheric CO<sub>2</sub> treatments (ambient and  
1951 1000 μmol mol<sup>-1</sup> CO<sub>2</sub>). Pots within each unique inoculation-by-CO<sub>2</sub> treatment  
1952 combination randomly received one of nine soil nitrogen fertilization treatments  
1953 equivalent to 0, 35, 70, 105, 140, 210, 280, 350, or 630 ppm N. Nitrogen fertil-  
1954 ization treatments were created using a modified Hoagland solution (Hoagland  
1955 and Arnon 1950) designed to keep concentrations of other macronutrients and  
1956 micronutrients equivalent across treatments (Table S1). Pots received the same  
1957 fertilization treatment throughout the entire duration experiment, which were ap-  
1958 plied twice per week in 150 mL doses as topical agents to the soil surface through-  
1959 out the duration of the experiment. This experimental design yielded a fully  
1960 factorial experiment with four replicates per unique fertilization-by-inoculation-  
1961 by-CO<sub>2</sub> combination.

### 1962 5.2.2 *Growth chamber conditions*

1963 Upon experiment initiation, pots were randomly placed in one of six Per-  
1964 cival LED-41L2 growth chambers (Percival Scientific Inc., Perry, IA, USA) over

1965 two experimental iterations due to chamber space limitation. Two iterations were  
1966 conducted such that one iteration included all elevated CO<sub>2</sub> pots and the second  
1967 iteration included all ambient CO<sub>2</sub> pots. Average ( $\pm$  SD) CO<sub>2</sub> concentrations  
1968 across chambers throughout the experiment were  $439 \pm 5 \mu\text{mol mol}^{-1}$  for the  
1969 ambient CO<sub>2</sub> treatment and  $989 \pm 4 \mu\text{mol mol}^{-1}$  for the elevated CO<sub>2</sub> treatment.

1970 Daytime growing conditions were simulated using a 16-hour photoperiod,  
1971 with incoming light radiation set to chamber maximum (mean  $\pm$  SD:  $1240 \pm 32$   
1972  $\mu\text{mol m}^{-2} \text{s}^{-1}$  across chambers), air temperature set to 25°C, and relative humid-  
1973 ity set to 50%. The remaining 8 hours simulated nighttime growing conditions,  
1974 with incoming light radiation set to 0  $\mu\text{mol m}^{-2} \text{s}^{-1}$ , chamber temperature set  
1975 to 17°C, and relative humidity set to 50%. Transitions between daytime and  
1976 nighttime growing conditions were simulated by ramping incoming light radiation  
1977 in 45-minute increments and temperature in 90-minute increments over a 3-hour  
1978 period (Table S2).

1979 Including the two, 3-hour ramping periods, pots grew under average ( $\pm$   
1980 SD) daytime light intensity of  $1049 \pm 27 \mu\text{mol m}^{-2} \text{s}^{-1}$ . In the elevated CO<sub>2</sub>  
1981 iteration, pots grew under  $24.0 \pm 0.2^\circ\text{C}$  during the day,  $16.4 \pm 0.8^\circ\text{C}$  during the  
1982 night, and  $51.6 \pm 0.4\%$  relative humidity. In the ambient CO<sub>2</sub> iteration, pots grew  
1983 under  $23.9 \pm 0.2^\circ\text{C}$  during the day,  $16.0 \pm 1.4^\circ\text{C}$  during the night, and  $50.3 \pm 0.2\%$   
1984 relative humidity. We accounted for climatic differences across the six chambers  
1985 by shuffling the same group of pots daily throughout the growth chambers. This  
1986 process was done by iteratively moving the group of pots on the top rack of a  
1987 chamber to the bottom rack of the same chamber, while simultaneously moving  
1988 the group of pots on the bottom rack of a chamber to the top rack of the adjacent

1989 chamber. I moved pots within and across chambers every day throughout the  
1990 course of each experiment iteration.

1991 5.2.3 *Leaf gas exchange measurements*

1992 Gas exchange measurements were collected for all individuals on the sev-  
1993 enth week of development. All gas exchange measurements were collected on  
1994 the center leaf of the most recent fully expanded trifoliate leaf set. Specifi-  
1995 cally, I measured net photosynthesis ( $A_{\text{net}}$ ;  $\mu\text{mol m}^{-2} \text{s}^{-1}$ ), stomatal conductance  
1996 ( $g_{\text{sw}}$ ;  $\text{mol m}^{-2} \text{s}^{-1}$ ), and intercellular CO<sub>2</sub> ( $C_i$ ;  $\mu\text{mol mol}^{-1}$ ) concentrations across  
1997 a range of atmospheric CO<sub>2</sub> concentrations (i.e., an  $A_{\text{net}}/C_i$  curve) using the  
1998 Dynamic Assimilation Technique™. The Dynamic Assimilation Technique™ has  
1999 been shown to correspond well with traditional steady-state CO<sub>2</sub> response curves  
2000 in *G. max* (Saathoff and Welles 2021).  $A_{\text{net}}/C_i$  curves were generated along a  
2001 reference CO<sub>2</sub> ramp down from 420  $\mu\text{mol mol}^{-1}$  CO<sub>2</sub> to 20  $\mu\text{mol mol}^{-1}$  CO<sub>2</sub>, fol-  
2002 lowed by a ramp up from 420  $\mu\text{mol mol}^{-1}$  CO<sub>2</sub> to 1620  $\mu\text{mol mol}^{-1}$  CO<sub>2</sub> after  
2003 a 90-second wait period at 420  $\mu\text{mol mol}^{-1}$  CO<sub>2</sub>. The ramp rate for each curve  
2004 was set to 200  $\mu\text{mol mol}^{-1} \text{min}^{-1}$ , logging every five seconds, which generated 96  
2005 data points per response curve. All  $A_{\text{net}}/C_i$  curves were generated after  $A_{\text{net}}$  and  
2006  $g_{\text{sw}}$  stabilized in a LI-6800 cuvette set to a 500  $\text{mol s}^{-1}$ , 10,000 rpm mixing fan  
2007 speed, 1.5 kPa vapor pressure deficit, 25°C leaf temperature, 2000  $\mu\text{mol m}^{-2} \text{s}^{-1}$   
2008 incoming light radiation, and initial reference CO<sub>2</sub> set to 420  $\mu\text{mol mol}^{-1}$ .

2009 With the same focal leaf used to generate  $A_{\text{net}}/C_i$  curves, I measured dark  
2010 respiration ( $R_{\text{d25}}$ ;  $\mu\text{mol m}^{-2} \text{s}^{-1}$ ) following at least a 30-minute period of darkness.  
2011 Measurements were collected on a 5-second log interval for 60 seconds after stabi-

2012 lizing in a LI-6800 cuvette set to a  $500 \text{ mol s}^{-1}$ , 10,000 rpm mixing fan speed, 1.5  
2013 kPa vapor pressure deficit, 25°C leaf temperature, and  $420 \mu\text{mol mol}^{-1}$  reference  
2014 CO<sub>2</sub> concentration (for both CO<sup>2</sup> concentrations), with incoming light radiation  
2015 set to  $0 \mu\text{mol m}^{-2} \text{ s}^{-1}$ . A single dark respiration value was determined for each  
2016 focal leaf by calculating the mean dark respiration value (i.e. the absolute value  
2017 of  $A_{\text{net}}$  during the logging period) across the logging interval.

2018 5.2.4 *Leaf trait measurements*

2019 The focal leaf used to generate  $A_{\text{net}}/C_i$  curves and dark respiration was  
2020 harvested immediately following gas exchange measurements. Images of each focal  
2021 leaf were curated using a flat-bed scanner to determine wet leaf area using the  
2022 'LeafArea' R package (Katabuchi 2015), which automates leaf area calculations  
2023 using ImageJ software (Schneider et al. 2012). Each leaf was dried at 65°C for  
2024 at least 48 hours, and subsequently weighed and ground until homogenized. Leaf  
2025 mass per area ( $M_{\text{area}}$ ; g m<sup>-2</sup>) was calculated as the ratio of dry leaf biomass  
2026 to fresh leaf area. Using subsamples of ground and homogenized leaf tissue, I  
2027 measured leaf nitrogen content ( $N_{\text{mass}}$ ; gN g<sup>-1</sup>) through elemental combustion  
2028 analysis (Costech-4010, Costech, Inc., Valencia, CA, USA). Leaf nitrogen content  
2029 per unit leaf area ( $N_{\text{area}}$ ; gN m<sup>-2</sup>) was calculated by multiplying  $N_{\text{mass}}$  and  $M_{\text{area}}$ .

2030 I extracted chlorophyll content from a second leaf in the same trifoliolate  
2031 leaf set as the focal leaf used to generate  $A_{\text{net}}/C_i$  curves. Prior to chlorophyll  
2032 extraction, I used a cork borer to punch between 3 and 5 0.6 cm<sup>2</sup> disks from the  
2033 leaf. Separate images of each punched leaf and set of leaf disks were curated using  
2034 a flat-bed scanner to determine wet leaf area, again quantified using the 'LeafArea'

**2035** R package (Katabuchi 2015). The punched leaf was dried and weighed after at  
**2036** least 65°C in the drying oven to determine  $M_{\text{area}}$  of the chlorophyll leaf.

**2037** Leaf disks were shuttled into a test tube containing 10mL dimethyl sul-  
**2038** foxide, vortexed, and incubated at 65degreeC for 120 minutes (Barnes et al.  
**2039** 1992). Incubated test tubes were vortexed again before loaded in 150  $\mu\text{L}$  trip-  
**2040** licate aliquots to a 96-well plate. Dimethyl sulfoxide was also loaded in a 150  
**2041**  $\mu\text{L}$  triplicate aliquot as a blank. Absorbance measurements at 649.1 nm ( $A_{649.1}$ )  
**2042** and 665.1 nm ( $A_{665.1}$ ) were read in each well using a plate reader (Biotek Synergy  
**2043** H1; Biotek Instruments, Winooski, VT USA) (Wellburn 1994), with triplicates  
**2044** subsequently averaged and corrected by the mean of the blank absorbance value.  
**2045** Blank-corrected absorbance values were used to estimate  $Chl_a$  ( $\mu\text{g mL}^{-1}$ ) and  
**2046**  $Chl_b$  ( $\mu\text{g mL}^{-1}$ ) following equations from Wellburn (1994):

$$Chl_a = 12.47A_{665.1} - 3.62A_{649.1} \quad (5.1)$$

**2047** and

$$Chl_b = 25.06A_{665.1} - 6.50A_{649.1} \quad (5.2)$$

**2048**  $Chl_a$  and  $Chl_b$  were converted to mmol  $\text{mL}^{-1}$  using the molar mass of chlorophyll a  
**2049** (893.51 g  $\text{mol}^{-1}$ ) and the molar mass of chlorophyll b (907.47 g  $\text{mol}^{-1}$ ), then added  
**2050** together to calculate total chlorophyll content in the dimethyl sulfoxide extractant  
**2051** (mmol  $\text{mL}^{-1}$ ). Total chlorophyll content was multiplied by the volume of the  
**2052** dimethyl sulfoxide extractant (10 mL) and converted to area-based chlorophyll  
**2053** content by dividing by the total area of the leaf disks ( $Chl_{\text{area}}$ ; mmol  $\text{m}^{-2}$ ). Mass-  
**2054** based chlorophyll content ( $Chl_{\text{mass}}$ ; mmol  $\text{g}^{-1}$ ) was calculated by dividing  $Chl_{\text{area}}$

**2055** by the leaf mass per area of the punched leaf.

**2056** 5.2.5 *A/C<sub>i</sub> curve fitting and parameter estimation*

**2057** I fit  $A_{\text{net}}/C_i$  curves of each individual using the ‘fitaci’ function in the  
**2058** ‘plantecophys’ R package (Duursma 2015). This function estimates the maxi-  
**2059** mum rate of Rubisco carboxylation ( $V_{\text{cmax}}$ ;  $\mu\text{mol m}^{-2} \text{s}^{-1}$ ) and maximum rate  
**2060** of electron transport for RuBP regeneration ( $J_{\text{max}}$ ;  $\mu\text{mol m}^{-2} \text{s}^{-1}$ ) based on the  
**2061** Farquhar biochemical model of C<sub>3</sub> photosynthesis (Farquhar et al. 1980). Triose  
**2062** phosphate utilization (TPU) limitation was included in all curve fits, and all curve  
**2063** fits included measured dark respiration values. As  $A_{\text{net}}/C_i$  curves were generated  
**2064** using a common leaf temperature, curves were fit using Michaelis-Menten coeffi-  
**2065** cients for Rubisco affinity to CO<sub>2</sub> ( $K_c$ ;  $\mu\text{mol mol}^{-1}$ ) and O<sub>2</sub> ( $K_o$ ;  $\mu\text{mol mol}^{-1}$ ), and  
**2066** the CO<sub>2</sub> compensation point ( $\Gamma^*$ ;  $\mu\text{mol mol}^{-1}$ ) reported in Bernacchi et al. (2001).  
**2067** Specifically,  $K_c$  was set to 404.9  $\mu\text{mol mol}^{-1}$ ,  $K_o$  was set to 278.4  $\mu\text{mol mol}^{-1}$ , and  
**2068**  $\Gamma^*$  was set to 42.75  $\mu\text{mol mol}^{-1}$ . The use of a common leaf temperature across  
**2069** curves and dark respiration measurements also eliminated the need to manually  
**2070** temperature standardize rate estimates. For clarity, I reference  $V_{\text{cmax}}$ ,  $J_{\text{max}}$ , and  
**2071**  $R_d$  estimates throughout the rest of the paper as  $V_{\text{cmax}25}$ ,  $J_{\text{max}25}$ , and  $R_{d25}$ .

**2072** 5.2.6 Stomatal limitation

**2073** I quantified the extent by which stomatal conductance limited photosynthe-  
**2074** sis (l; unitless) following equations originally described in Farquhar and Sharkey  
**2075** (1982). Stomatal limitation was calculated as:

$$l = 1 - \frac{A_{net}}{A_{mod}} \quad (5.3)$$

**2076** where  $A_{mod}$  represents the photosynthetic rate where  $C_i = C_a$ .  $A_{mod}$  was calcu-

**2077** lated as:

$$A_{mod} = V_{cmax25} - \frac{420 - \Gamma^*}{420 + K_m} - R_{d25} \quad (5.4)$$

**2078**  $K_m$  is the Michaelis-Menten coefficient for Rubisco-limited photosynthesis, calcu-

**2079** lated as:

$$K_m = K_c \cdot \left(1 + \frac{O_i}{K_o}\right) \quad (5.5)$$

**2080** where  $O_i$  refers to leaf intercellular  $O_2$  concentrations, set to  $210 \mu\text{mol mol}^{-1}$ .

**2081** 5.2.7 *Proportion of leaf nitrogen allocated to photosynthesis and structure*

**2082** I used equations from Niinemets and Tenhunen (1997) to estimate the

**2083** proportion of leaf N content allocated to Rubisco bioenergetics, and light harvest-

**2084** ing proteins. The proportion of leaf N allocated to Rubisco ( $\rho_{rub}$ ;  $\text{gN gN}^{-1}$ ) was

**2085** calculated as a function of  $V_{cmax25}$  and  $N_{area}$ :

$$\rho_{rubisco} = \frac{V_{cmax25} N_r}{V_{cr} N_{area}} \quad (5.6)$$

**2086** where  $N_r$  is the amount of nitrogen in Rubisco, set to  $0.16 \text{ gN (gN in Rubisco)}^{-1}$

**2087** and  $V_{cr}$  is the maximum rate of RuBP carboxylation per unit Rubisco protein,

**2088** set to  $20.5 \mu\text{mol CO}_2 (\text{g Rubisco})^{-1}$ . The proportion of leaf nitrogen allocated to

**2089** bioenergetics ( $\rho_{bioe}$ ;  $\text{gN gN}^{-1}$ ) was similarly calculated as a function of  $J_{max25}$  and

**2090**  $N_{\text{area}}$ :

$$\rho_{\text{bioe}} = \frac{J_{\text{max}25} N_b}{J_{\text{mc}} N_{\text{area}}} \quad (5.7)$$

**2091** where  $N_b$  is the amount of nitrogen in cytochrome f, set to 0.12407 gN ( $\mu\text{mol}$  cytochrome f) $^{-1}$  assuming a constant 1: 1: 1.2 cytochrome f: ferredoxin NADP reductase: coupling factor molar ratio (Evans and Seemann 1989; Niinemets and Tenhunen 1997), and  $J_{\text{mc}}$  is the capacity of electron transport per cytochrome f, set to 156  $\mu\text{mol}$  electron ( $\mu\text{mol}$  cytochrome f) $^{-1}\text{s}^{-1}$ .

**2096** The proportion of leaf nitrogen allocated to light harvesting proteins was  
**2097** calculated as a function of  $Chl_{\text{mass}}$  and  $N_{\text{mass}}$ :

$$\rho_{\text{light}} = \frac{Chl_{\text{mass}}}{N_{\text{mass}} c_b} \quad (5.8)$$

**2098** where  $c_b$  is the stoichiometry of the light-harvesting chlorophyll complexes of  
**2099** photosystem II, set to 2.75 mmol chlorophyll (gN in chlorophyll) $^{-1}$ . We used the  
**2100**  $N_{\text{mass}}$  value of the focal leaf used to generate  $A_{\text{net}}/C_i$  curves instead of the leaf  
**2101** used to extract chlorophyll content, as the two leaves are from the same trifoliolate  
**2102** leaf set and are highly correlated with each other (Figure SX).

**2103** The proportion of leaf nitrogen content allocated to photosynthetic tissue  
**2104** ( $\rho_{\text{photo}}$ ; gN gN $^{-1}$ ) was estimated as the sum of  $\rho_{\text{rubisco}}$ ,  $\rho_{\text{bioe}}$ , and  $\rho_{\text{light}}$ .

**2105** Finally, the proportion of leaf N content allocated to structural tissue ( $\rho_{\text{str}}$ ;  
**2106** gN gN $^{-1}$ ) was estimated as:

$$\rho_{\text{structure}} = \frac{N_{\text{cw}}}{N_{\text{area}}} \quad (5.9)$$

2107 where  $N_{cw}$  is the leaf N content allocated to cell walls ( $\text{gN m}^{-2}$ ), calculated as a  
2108 function of  $M_{area}$  using an empirical equation from Onoda et al. (2017):

$$N_{cw} = 0.000355 * M_{area}^{1.39} \quad (5.10)$$

2109 5.2.8 *Whole plant traits*

2110 Seven weeks after experiment initiation and immediately following gas ex-  
2111 change measurements, I harvested all experimental individuals and separated  
2112 biomass of each experimental individual into major organ types (leaves, stems,  
2113 roots, and nodules when present). Fresh leaf area of all harvested leaves was mea-  
2114 sured using an LI-3100C (Li-COR Biosciences, Lincoln, Nebraska, USA). Total  
2115 fresh leaf area ( $\text{cm}^2$ ) was calculated as the sum of all leaf areas, including the focal  
2116 leaf used to collect gas exchange data and the focal leaf used to extract chlorophyll  
2117 content. All harvested material was dried in an oven set to 65°C for at least 48  
2118 hours, weighed, and ground to homogeneity. Leaves and nodules were manually  
2119 ground either with a mortar and pestle, while stems and roots were ground using  
2120 a Wiley mill (E3300 Mini Mill; Eberbach Corp., MI, USA). Total dry biomass (g)  
2121 was calculated as the sum of dry leaf (including focal leaf for both the  $A_{net}/C_i$   
2122 curve and leaf used to extract chlorophyll content), stem, root, and root nodule  
2123 biomass. I quantified carbon and nitrogen content of each respective organ type  
2124 through elemental combustion (Costech-4010, Costech, Inc., Valencia, CA, USA)  
2125 using subsamples of ground and homogenized organ tissue.

2126 Following the approach explained in the first experimental chapter, I calcu-  
2127 lated structural carbon costs to acquire nitrogen as the ratio of total belowground

**2128** carbon biomass to whole plant nitrogen biomass ( $N_{\text{cost}}$ ; gC gN<sup>-1</sup>). Belowground  
**2129** carbon biomass ( $C_{\text{bg}}$ ; gC) was calculated as the sum of root carbon biomass  
**2130** and root nodule carbon biomass. Root carbon biomass and root nodule carbon  
**2131** biomass was calculated as the product of the organ biomass and the respective  
**2132** organ carbon content. Whole plant nitrogen biomass ( $N_{\text{wp}}$ ; gN) was similarly  
**2133** calculated as the sum of total leaf, stem, root, and root nodule nitrogen biomass,  
**2134** including the focal leaf used for  $A_{\text{net}}/C_i$  curve and chlorophyll extractions. Leaf,  
**2135** stem, root, and root nodule nitrogen biomass was calculated as the product of  
**2136** the organ biomass and the respective organ nitrogen content. This calculation  
**2137** only quantifies plant structural carbon costs to acquire nitrogen and does not  
**2138** include any additional costs of nitrogen acquisition associated with respiration,  
**2139** root exudation, or root turnover. An explicit explanation of the limitations for  
**2140** interpreting this calculation can be found in Perkowski et al. (2021) and Terrer  
**2141** et al. (2018).

**2142** Finally, plant investments in nitrogen fixation were calculated as the ra-  
**2143** tio of root nodule biomass to root biomass, where increasing values indicate an  
**2144** increase in plant investments to nitrogen fixation (Dovrat et al. 2018; Dovrat  
**2145** et al. 2020; Perkowski et al. 2021). I also calculated the percent of leaf nitrogen  
**2146** acquired from the atmosphere (% $N_{\text{dfa}}$ ) using leaf  $\delta^{15}\text{N}$  and the following equation  
**2147** from Andrews et al. (2011):

$$\%N_{\text{dfa}} = \frac{\delta^{15}N_{\text{reference}} - \delta^{15}N_{\text{sample}}}{\delta^{15}N_{\text{reference}} - B} \quad (5.11)$$

**2148** where  $\delta^{15}\text{N}_{\text{reference}}$  refers to a reference plant that exclusively acquires nitrogen via

2149 direct uptake,  $\delta^{15}\text{N}_{\text{sample}}$  refers to an individual's leaf  $\delta^{15}\text{N}$ , and B refers to individuals  
2150 that are entirely reliant on nitrogen fixation. Within each unique nitrogen  
2151 fertilization treatment-by-CO<sub>2</sub> treatment combination, I calculated the mean leaf  
2152  $\delta^{15}\text{N}$  for individuals growing in the non-inoculated treatment for  $\delta^{15}\text{N}_{\text{reference}}$ . Any  
2153 individuals with visual confirmation of root nodule formation or nodule initiation  
2154 were omitted from the calculation of  $\delta^{15}\text{N}_{\text{reference}}$ . Following recommendations  
2155 from Andrews et al. (2011) I calculated B within each CO<sub>2</sub> treatment using  
2156 the mean leaf  $\delta^{15}\text{N}$  of inoculated individuals that received 0 ppm N. I did not  
2157 calculate B within each unique soil nitrogen-by-CO<sub>2</sub> treatment combination, as  
2158 previous studies suggest decreased reliance on nitrogen fixation with increasing  
2159 soil nitrogen availability (Perkowski et al. 2021). This approach for estimating  
2160 nitrogen fixation standardizes values such that approaching 1 indicates increasing  
2161 reliance on nitrogen fixation.

2162 5.2.9 *Statistical analyses*

2163 Any uninoculated pots that had substantial root nodule formation (nodule  
2164 biomass: root biomass values greater than 0.05 g g<sup>-1</sup>) were removed from analyses.  
2165 This was because they were assumed to have been colonized by symbiotic nitrogen-  
2166 fixing bacteria from outside sources. This decision resulted in the removal of  
2167 sixteen pots from our analysis: two pots in the elevated CO<sub>2</sub> treatment that  
2168 received 35 ppm N, three pots in the elevated CO<sub>2</sub> treatment that received 70  
2169 ppm N, one pot in the elevated CO<sub>2</sub> treatment that received 210 ppm N, two pots  
2170 in the elevated CO<sub>2</sub> treatment that received 280 ppm N, two pots in the ambient  
2171 CO<sub>2</sub> treatment that received 0 ppm N, three pots in the ambient CO<sub>2</sub> treatment

2172 that received 70 ppm N, two pots in the ambient CO<sub>2</sub> treatment that received  
2173 105 ppm N, and one pot in the ambient CO<sub>2</sub> treatment that received 280 ppm N.

2174 I built a series of linear mixed effects models to investigate the impacts of  
2175 CO<sub>2</sub> concentration, soil nitrogen fertilization, and inoculation with *B. japonicum*  
2176 on *G. max* gas exchange, tradeoffs between nitrogen and water use, whole plant  
2177 growth, and investment in nitrogen fixation. All models included CO<sub>2</sub> treatment  
2178 as a categorical fixed effect, inoculation treatment as a categorical fixed effect,  
2179 soil nitrogen fertilization as a continuous fixed effect, with interaction terms be-  
2180 tween all three fixed effects. All models also accounted for climatic difference  
2181 between chambers across experiment iterations by including a random intercept  
2182 term that nested starting chamber rack by CO<sub>2</sub> treatment. Models with this  
2183 independent variable structure were created for each of the following dependent  
2184 variables:  $N_{\text{area}}$ ,  $M_{\text{area}}$ ,  $N_{\text{mass}}$ ,  $Chl_{\text{area}}$ ,  $V_{\text{cmax25}}$ ,  $J_{\text{max25}}$ ,  $J_{\text{max25}}:V_{\text{cmax25}}$ ,  $R_{\text{d25}}$ ,  $g_{\text{sw}}$ ,  
2185 stomatal limitation,  $\rho_{\text{rubisco}}$ ,  $\rho_{\text{bioe}}$ ,  $\rho_{\text{light}}$ ,  $\rho_{\text{photo}}$ ,  $\rho_{\text{structure}}$ ,  $N_{\text{cost}}$ ,  $C_{\text{bg}}$ ,  $N_{\text{wp}}$ , total  
2186 biomass, total leaf area, nodule biomass, and the ratio of nodule biomass to root  
2187 biomass.

2188 I used Shapiro-Wilk tests of normality to determine whether linear mixed  
2189 effects models satisfied residual normality assumptions. If residual normality as-  
2190 sumptions were not met (Shapiro-Wilk:  $p < 0.05$ ), then models were fit using  
2191 dependent variables that were natural log transformed. All residual normality  
2192 assumptions that did not originally satisfy residual normality assumptions were  
2193 met with either a natural log or square root data transformation (Shapiro-Wilk:  
2194  $p > 0.05$  in all cases). Specifically, models for  $N_{\text{area}}$ ,  $N_{\text{mass}}$ ,  $Chl_{\text{area}}$ ,  $V_{\text{cmax25}}$ ,  
2195  $J_{\text{max25}}$ ,  $J_{\text{max25}}:V_{\text{cmax25}}$ ,  $g_{\text{sw}}$ , stomatal limitation,  $\rho_{\text{rubisco}}$ ,  $\rho_{\text{bioe}}$ ,  $\rho_{\text{light}}$ ,  $\rho_{\text{photo}}$ , and to-

**2196** tal leaf area satisfied residual normality assumptions without data transformation.  
**2197** Models for  $M_{\text{area}}$ ,  $\rho_{\text{structure}}$ ,  $N_{\text{cost}}$ ,  $C_{\text{bg}}$ ,  $N_{\text{wp}}$ , and total biomass satisfied residual  
**2198** normality assumptions with a natural log data transformation, while models for  
**2199** nodule biomass and nodule biomass: root biomass satisfied residual normality  
**2200** assumptions with a square root data transformation.

**2201** In all statistical models, I used the 'lmer' function in the 'lme4' R package  
**2202** (Bates et al. 2015) to fit each model and the 'Anova' function in the 'car' R  
**2203** package (Fox and Weisberg 2019) to calculate Type II Wald's  $\chi^2$  and determine  
**2204** the significance ( $\alpha = 0.05$ ) of each fixed effect coefficient. I used the 'emmeans'  
**2205** R package (Lenth 2019) to conduct post-hoc comparisons using Tukey's tests,  
**2206** where degrees of freedom were approximated using the Kenward-Roger approach  
**2207** (Kenward and Roger 1997). All analyses and plots were conducted in R version  
**2208** 4.2.0 (R Core Team 2021).

**2209** 5.3 Results

**2210** 5.3.1 *Leaf nitrogen and chlorophyll content*

**2211** Elevated CO<sub>2</sub> reduced  $N_{\text{area}}$ ,  $N_{\text{mass}}$ , and  $Chl_{\text{area}}$  by 29%, 50%, and 31%,  
**2212** respectively, and stimulated  $M_{\text{area}}$  by 44% ( $p < 0.001$  in all cases; Table 5.1). An  
**2213** interaction between fertilization and CO<sub>2</sub> (CO<sub>2</sub>-by-fertilization interaction:  $p_{N_{\text{area}}}$   
**2214** = 0.017,  $p_{N_{\text{mass}}} < 0.001$ ,  $p_{M_{\text{area}}} = 0.006$ ,  $p_{Chl_{\text{area}}} = 0.083$ ; Table 5.1) indicated  
**2215** that the general positive effect of increasing fertilization on  $N_{\text{area}}$ ,  $N_{\text{mass}}$ , and  
**2216**  $Chl_{\text{area}}$  ( $p < 0.001$  in all cases; Table 5.1) was generally stronger under ambient  
**2217** CO<sub>2</sub> (Tukey <sub>$N_{\text{area}}$</sub> :  $p = 0.026$ ; Tukey <sub>$N_{\text{mass}}$</sub> :  $p < 0.001$ ; Tukey <sub>$M_{\text{area}}$</sub> :  $p = 0.009$ ;  
**2218** Tukey <sub>$Chl_{\text{area}}$</sub> :  $p = 0.065$ ; Table 5.1; Figs. 5.1a-d). This pattern resulted in a

**2219** stronger reduction in  $N_{\text{area}}$ ,  $N_{\text{mass}}$ , and  $Chl_{\text{area}}$  as well as a stronger stimulation  
**2220** in  $M_{\text{area}}$  under elevated CO<sub>2</sub> with increasing fertilization. An additional interac-  
**2221** tion between inoculation and CO<sub>2</sub> on  $N_{\text{area}}$  (CO<sub>2</sub>-by-inoculation interaction:  $p =$   
**2222** 0.030; Table 5.1) indicated that the general positive effect of inoculation on  $N_{\text{area}}$   
**2223** ( $p < 0.001$ ; Table 5.1) was stronger under elevated CO<sub>2</sub> (45% increase; Tukey:  $p$   
**2224**  $< 0.001$ ) than under ambient CO<sub>2</sub> (18% increase; Tukey:  $p < 0.001$ ), a result that  
**2225** increased the reduction in  $N_{\text{area}}$  in inoculated pots under elevated CO<sub>2</sub>. Inocula-  
**2226** tion treatment did not modify the downregulation in  $N_{\text{mass}}$  (CO<sub>2</sub>-by-inoculation  
**2227** interaction:  $p = 0.148$ ; Table 5.1) and  $Chl_{\text{area}}$  ( $p = 0.147$ ; Table 5.1) or the stimu-  
**2228** lation in  $M_{\text{area}}$  ( $p = 0.866$ ; Table 5.1) under elevated CO<sub>2</sub>. However, interactions  
**2229** between fertilization and inoculation on  $N_{\text{area}}$  (fertilization-by-inoculation inter-  
**2230** action:  $p < 0.001$ ; Table 5.1; Fig. 5.1a),  $N_{\text{mass}}$  ( $p = 0.001$ ; Table 5.1; Fig. 5.1b),  
**2231**  $M_{\text{area}}$  ( $p = 0.025$ ; Table 5.1; Fig. 5.1c), and  $Chl_{\text{area}}$  ( $p < 0.001$ ; Table 5.1; Fig.  
**2232** 5.1d) indicated that the general positive effect of increasing fertilization on each  
**2233** trait was stronger in uninoculated pots (Tukey <sub>$N_{\text{area}}$</sub> :  $p < 0.001$ ; Tukey <sub>$N_{\text{mass}}$</sub> :  $p =$   
**2234** 0.001; Tukey <sub>$M_{\text{area}}$</sub> :  $p = 0.031$ ; Tukey <sub>$Chl_{\text{area}}$</sub> :  $p < 0.001$ ).

**Table 5.1.** Effects of soil nitrogen fertilization, inoculation, and CO<sub>2</sub> treatments on  $N_{\text{area}}$ ,  $N_{\text{mass}}$ ,  $M_{\text{area}}$ , and  $Chl_{\text{area}}$ 

	$N_{\text{area}}$			$N_{\text{mass}}$			$M_{\text{area}}^a$			
	df	Coefficient	$\chi^2$	p	Coefficient	$\chi^2$	p	Coefficient	$\chi^2$	p
(Intercept)	-	1.10E+00	-	-	3.05E-02	-	-	3.64E+00	-	-
CO <sub>2</sub>	1	-5.67E-01	155.908	<0.001	-1.80E-02	272.362	<0.001	3.04E-01	151.319	<0.001
Inoculation (I)	1	6.21E-01	86.029	<0.001	7.54E-03	15.576	<0.001	1.81E-01	19.158	<0.001
Fertilization (N)	1	3.06E-03	316.408	<0.001	5.78E-05	106.659	<0.001	3.10E-04	21.440	<0.001
CO <sub>2</sub> *I	1	2.63E-01	4.729	<b>0.030</b>	3.96E-03	2.025	0.155	-3.37E-02	0.029	0.866
CO <sub>2</sub> *N	1	-3.68E-04	5.723	<b>0.017</b>	-2.85E-05	22.542	<0.001	2.80E-04	7.619	<b>0.006</b>
I*N	1	-1.36E-03	43.381	<0.001	-2.00E-05	11.137	<b>0.001</b>	-3.36E-04	5.022	<b>0.025</b>
CO <sub>2</sub> *I*N	1	-3.23E-04	0.489	0.484	-2.59E-06	0.041	0.839	1.15E-04	0.208	0.649
	$Chl_{\text{area}}$									
	df	Coefficient	$\chi^2$	p						
(Intercept)	-	2.13E-02	-	-						
CO <sub>2</sub>	1	-1.33E-02	69.233	<0.001						
Inoculation (I)	1	1.24E-01	136.341	<0.001						
Fertilization (N)	1	3.35E-04	163.111	<0.001						
CO <sub>2</sub> *I	1	-3.18E-02	2.102	0.147						
CO <sub>2</sub> *N	1	-8.79E-05	2.999	<i>0.083</i>						
I*N	1	-2.65E-04	75.769	<0.001						
CO <sub>2</sub> *I*N	1	7.68E-05	2.144	0.147						

130

2235 \*Significance determined using Type II Wald  $\chi^2$  tests ( $\alpha = 0.05$ ).  $P$ -values  $< 0.05$  are in bold, while  $p$ -values between  
 2236 0.05 and 0.1 are italicized. A superscript “a” is included after trait labels to indicate if models were fit with natural  
 2237 log transformed response variables. Key: df = degrees of freedom,  $N_{\text{area}}$  = leaf nitrogen content per unit leaf area,  
 2238  $N_{\text{mass}}$  = leaf nitrogen content,  $M_{\text{area}}$  = leaf mass per unit leaf area.

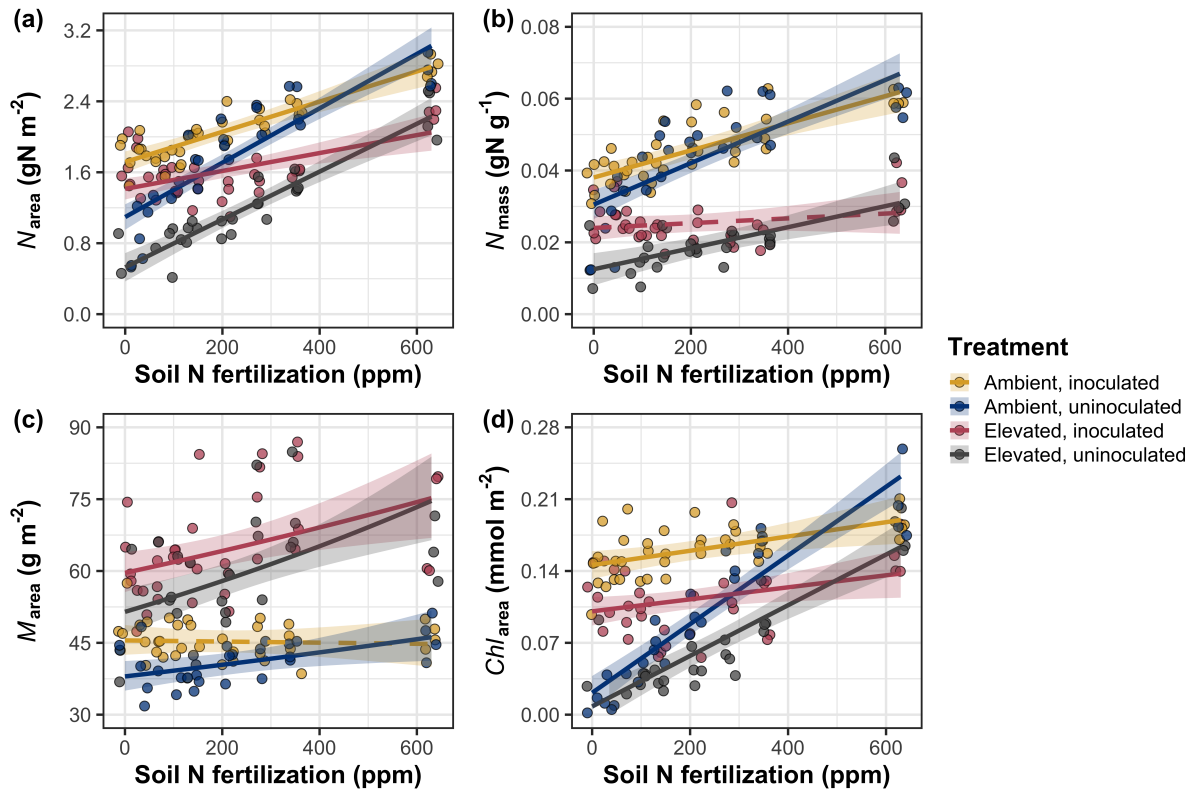


**Figure 5.1.** Effects of  $\text{CO}_2$ , fertilization, and inoculation on leaf nitrogen per unit leaf area (a), leaf nitrogen content (b), leaf mass per unit leaf area (c), and chlorophyll content per unit leaf area (d). Soil nitrogen fertilization is represented on the x-axis in all panels. Yellow points and trendlines indicate inoculated individuals grown under ambient  $\text{CO}_2$ , blue points and trendlines indicate uninoculated individuals grown under ambient  $\text{CO}_2$ , red points and trendlines indicate inoculated individuals grown under elevated  $\text{CO}_2$ , and grey points indicate uninoculated individuals grown under elevated  $\text{CO}_2$ . Solid trendlines indicate regression slopes that are different from zero ( $p < 0.05$ ), while dashed trendlines indicate slopes that are not distinguishable from zero ( $p > 0.05$ ).

**2239** 5.3.2 *Leaf biochemistry and stomatal conductance*

**2240** Elevated CO<sub>2</sub> resulted in plants with 16% lower  $V_{cmax25}$  ( $p < 0.001$ ; Table  
**2241** 5.2) and 10% lower  $J_{max25}$  ( $p = 0.014$ ; Table 5.2) as compared to those grown under  
**2242** ambient CO<sub>2</sub>. However, CO<sub>2</sub> concentration did not influence  $R_{d25}$  ( $p = 0.613$ ;  
**2243** Table 5.2). A relatively stronger downregulation in  $V_{cmax25}$  than  $J_{max25}$  resulted  
**2244** in an 8% stimulation in  $J_{max25}:V_{cmax25}$  under elevated CO<sub>2</sub> ( $p < 0.001$ ; Table 5.2;  
**2245** Fig. 2E). The downregulatory effect of CO<sub>2</sub> on  $V_{cmax25}$  and  $J_{max25}$  was not modified  
**2246** across the fertilization gradient (CO<sub>2</sub>-by-fertilization interaction:  $p = 0.185$ ,  $p =$   
**2247** 0.389 for  $V_{cmax25}$  and  $J_{max25}$ , respectively; Table 5.2; Fig. 5.2a-b) or between  
**2248** inoculation treatments (CO<sub>2</sub>-by-inoculation interaction:  $p = 0.799$  and  $p = 0.714$   
**2249** for  $V_{cmax25}$  and  $J_{max25}$ , respectively; Table 5.2). However, a strong interaction  
**2250** between fertilization and inoculation (fertilization-by-inoculation interaction:  $p \leq$   
**2251** 0.001 in all cases; Table 5.2) indicated that the general positive effect of increasing  
**2252** fertilization on  $V_{cmax25}$  ( $p < 0.001$ ; Table 5.2),  $J_{max25}$  ( $p < 0.001$ ; Table 5.2), and  
**2253**  $R_{d25}$  ( $p = 0.015$ ; Table 2) was only observed in uninoculated pots (Tukey:  $p$   
**2254**  $\leq 0.001$  in all cases), as there was no apparent effect of fertilization on  $V_{cmax25}$   
**2255** (Tukey:  $p = 0.456$ ),  $J_{max25}$  (Tukey:  $p = 0.180$ ), or  $R_{d25}$  (Tukey:  $p = 0.443$ ) in  
**2256** inoculated pots (Figs. 5.2a-d). A relatively stronger positive effect of increasing  
**2257** fertilization on  $V_{cmax25}$  than  $J_{max25}$  resulted in a general reduction in  $J_{max25}:V_{cmax25}$   
**2258** with increasing fertilization ( $p < 0.001$ ), though this pattern was only seen in  
**2259** uninoculated pots (Tukey:  $p = 0.003$ ) and not inoculated plants (Tukey:  $p >$   
**2260** 0.05).

**2261** Elevated CO<sub>2</sub> reduced stomatal conductance by 20% ( $p < 0.001$ ; Table  
**2262** 5.2; Fig. 5.2e) compared to ambient CO<sub>2</sub>, but this downregulation did not influ-

ence stomatal limitation of photosynthesis ( $p = 0.355$ ; Table 5.2; Fig. 5.2f). As with  $V_{cmax25}$  and  $J_{max25}$ , the downregulation of stomatal conductance due to elevated CO<sub>2</sub> was not modified across the fertilization gradient (CO<sub>2</sub>-by-fertilization interaction:  $p = 0.141$ ; Table 5.2) or between inoculation treatments (CO<sub>2</sub>-by-inoculation interaction:  $p = 0.179$ ; Table 5.2). Fertilization also did not modify the general null effect of CO<sub>2</sub> on stomatal limitation (CO<sub>2</sub>-by-fertilization interaction:  $p = 0.554$ ; Table 5.2), although an interaction between CO<sub>2</sub> and inoculation (CO<sub>2</sub>-by-inoculation interaction:  $p = 0.043$ ; Table 5.2) indicated that inoculation increased stomatal limitation under ambient CO<sub>2</sub> (Tukey:  $p = 0.021$ ), but not under elevated CO<sub>2</sub> (Tukey:  $p > 0.999$ ). An interaction between inoculation and fertilization on stomatal conductance (fertilization-by-inoculation interaction:  $p < 0.001$ ; Table 5.2) indicated that increasing fertilization increased stomatal conductance in uninoculated pots (Tukey:  $p = 0.003$ ) but decreased stomatal conductance in inoculated pots (Tukey:  $p = 0.021$ ). The similar in magnitude, but opposite direction, trend in the effect of increasing fertilization on stomatal conductance between inoculation treatments likely drove a null general response of stomatal conductance to increasing fertilization ( $p = 0.642$ ; Table 5.2).

**Table 5.2.** Effects of soil nitrogen fertilization, inoculation, and CO<sub>2</sub> on leaf biochemistry

	<i>V<sub>cmax25</sub></i>			<i>J<sub>max25</sub></i>			<i>R<sub>d25</sub></i>			
	df	Coefficient	$\chi^2$	p	Coefficient	$\chi^2$	p	Coefficient	$\chi^2$	p
(Intercept)	-	4.36E+01	-	-	8.30E+01	-	-	1.69E+00	-	-
CO <sub>2</sub>	1	-7.05E+00	18.039	<0.001	-9.11E+00	6.042	<b>0.014</b>	4.53E-01	0.256	0.613
Inoculation (I)	1	5.87E+01	98.579	<0.001	9.62E+01	85.064	<0.001	1.04E+00	3.094	0.079
Fertilization (N)	1	1.32E-01	37.053	<0.001	2.09E-01	25.356	<0.001	2.86E-03	5.965	<b>0.015</b>
CO <sub>2</sub> *I	1	-4.65E+00	0.065	0.799	7.84E-01	0.667	0.414	-5.71E-01	2.563	0.109
CO <sub>2</sub> *N	1	-3.58E-02	1.758	0.185	-4.33E-02	0.742	0.389	-1.55E-03	2.675	0.102
I*N	1	-1.35E-01	60.394	<0.001	-2.30E-01	57.410	<0.001	-2.84E-03	12.083	<b>0.001</b>
CO <sub>2</sub> *I*N	1	2.73E-02	0.748	0.387	3.46E-02	0.377	0.539	7.21E-04	0.244	0.622

	<i>J<sub>max25</sub>:V<sub>cmax25</sub></i>			<i>g<sub>sw</sub></i>			Stomatal limitation			
	df	Coefficient	$\chi^2$	p	Coefficient	$\chi^2$	p	Coefficient	$\chi^2$	p
(Intercept)	-	1.92E+00	-	-	1.95E-01	-	-	2.12E-01	-	-
CO <sub>2</sub>	1	5.71E-02	92.010	<0.001	-6.23E-02	9.718	<b>0.002</b>	3.91E-02	0.856	0.355
Inoculation (I)	1	-1.79E-01	27.768	<0.001	1.30E-01	22.351	<0.001	7.87E-02	4.582	<b>0.032</b>
Fertilization (N)	1	-4.61E-04	28.147	<0.001	2.50E-04	0.066	0.797	2.60E-04	32.218	<0.001
CO <sub>2</sub> *I	1	8.94E-02	2.916	0.088	6.69E-02	1.810	0.179	-7.84E-02	4.093	<b>0.043</b>
CO <sub>2</sub> *N	1	2.35E-04	3.210	0.073	-8.50E-05	2.165	0.141	-1.24E-04	0.350	0.554
I*N	1	3.27E-04	9.607	<b>0.002</b>	-3.09E-04	14.696	<0.001	-1.67E-04	2.547	0.110
CO <sub>2</sub> *I*N	1	-1.66E-04	1.102	0.294	-8.89E-05	0.234	0.629	1.67E-04	2.231	0.135

134

2280 \*Significance determined using Type II Wald  $\chi^2$  tests ( $\alpha = 0.05$ ). *P*-values  $< 0.05$  are in bold, while *p*-values between  
 2281 0.05 and 0.1 are italicized. Key: *V<sub>cmax25</sub>* = maximum rate of Rubisco carboxylation at 25°C; *J<sub>max25</sub>* = maximum rate  
 2282 of electron transport for RuBP regeneration at 25°C, *R<sub>d25</sub>* = dark respiration at 25°C; *J<sub>max25</sub>:V<sub>cmax25</sub>* = the ratio of  
 2283 *J<sub>max25</sub>* to *V<sub>cmax25</sub>*; *g<sub>sw</sub>* = stomatal conductance.

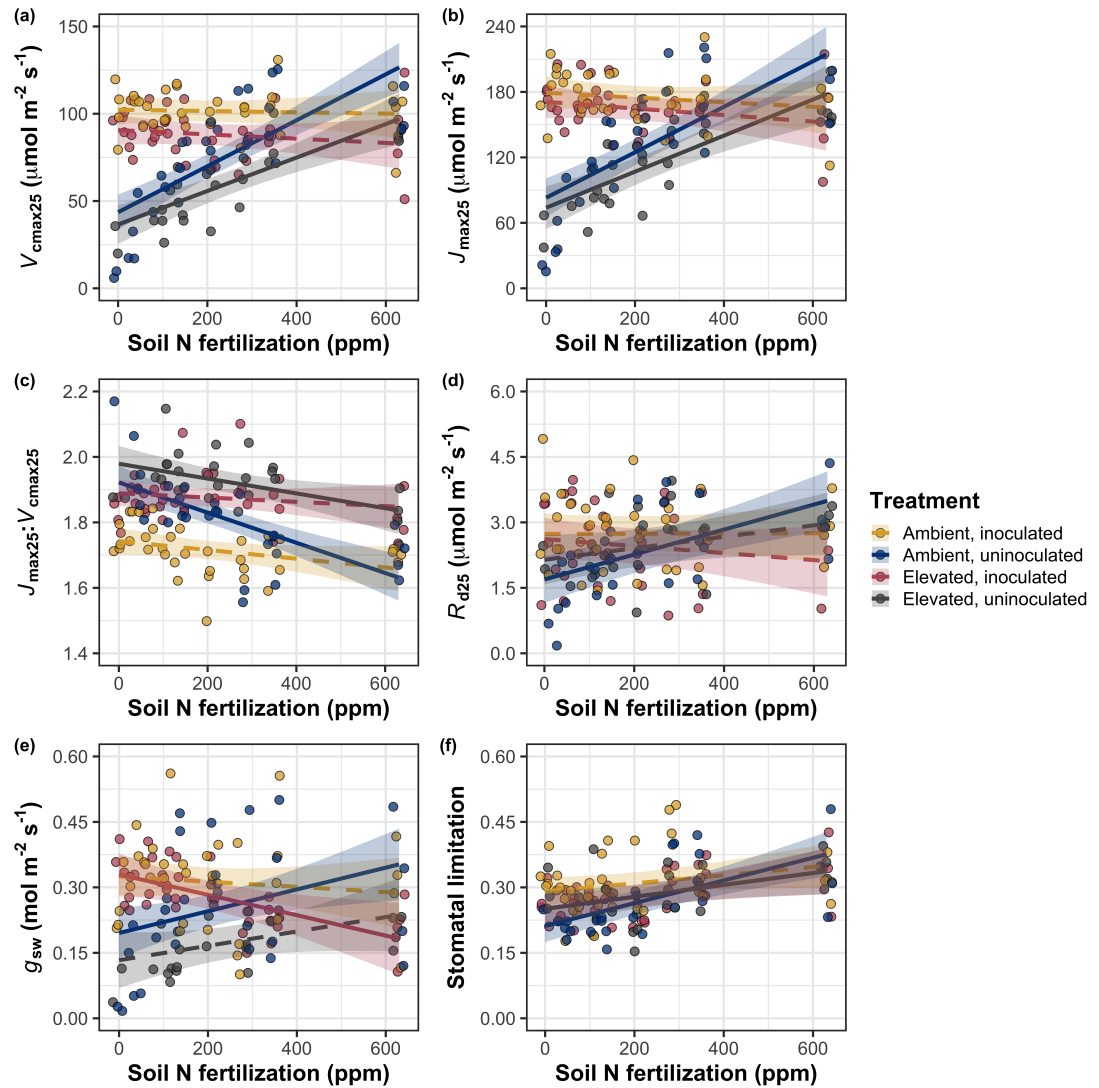


**Figure 5.2.** Effects of CO<sub>2</sub>, fertilization, and inoculation on maximum rate of Rubisco carboxylation (a), the maximum rate of RuBP regeneration (b), and the ratio of the maximum rate of RuBP regeneration to the maximum rate of Rubisco carboxylation leaf mass per unit leaf area (c), dark respiration (d), stomatal conductance (e), and stomatal limitation (f). Soil nitrogen fertilization is represented on the x-axis in all panels. Colored points and trendlines are as explained in Figure 1.

**2284** 5.3.3 *Leaf nitrogen allocation*

**2285** A relatively stronger downregulation in  $N_{\text{area}}$  than  $V_{\text{cmax}25}$  or  $J_{\text{max}25}$  resulted  
**2286** in an 20% and 29% respective stimulation in  $\rho_{\text{rubisco}}$  and  $\rho_{\text{bioe}}$  under elevated CO<sub>2</sub>  
**2287** ( $p < 0.001$  in both cases; Table 5.3). There was no apparent CO<sub>2</sub> effect on  $\rho_{\text{light}}$   
**2288** ( $p = 0.700$ ; Table 5.3), but the strong stimulation in  $\rho_{\text{rubisco}}$  and  $\rho_{\text{bioe}}$  resulted  
**2289** in a 21% stimulation of  $\rho_{\text{photo}}$  under elevated CO<sub>2</sub> ( $p < 0.001$ ; Table 5.3; Fig.  
**2290** 5.3a). The stimulation of  $\rho_{\text{rubisco}}$ ,  $\rho_{\text{bioe}}$ , and  $\rho_{\text{photo}}$  due to elevated CO<sub>2</sub> was not  
**2291** modified across the fertilization gradient (CO<sub>2</sub>-by-fertilization interaction:  $p_{\text{rubisco}}$   
**2292** = 0.269,  $p_{\text{bioe}} = 0.298$ ,  $p_{\text{photo}} = 0.281$ ; Table 5.3). A marginal interaction between  
**2293** inoculation and CO<sub>2</sub> on  $\rho_{\text{rubisco}}$  and  $\rho_{\text{photo}}$  (CO<sub>2</sub>-by-inoculation interaction:  $p_{\text{rubisco}}$   
**2294** = 0.057,  $p_{\text{photo}} = 0.057$ ; Table 5.3) indicated that the general positive effect of  
**2295** inoculation on  $\rho_{\text{rubisco}}$  and  $\rho_{\text{photo}}$  ( $p < 0.001$  in both cases; Table 5.3) was only  
**2296** apparent under ambient CO<sub>2</sub> (Tukey:  $p < 0.001$  in both cases), with no apparent  
**2297** effect of inoculation under elevated CO<sub>2</sub> (Tukey<sub>rubisco</sub>:  $p = 0.200$ ; Tukey<sub>photo</sub>:  $p$   
**2298** = 0.147). Inoculation did not modify the stimulation of  $\rho_{\text{bioe}}$  under elevated CO<sub>2</sub>  
**2299** (CO<sub>2</sub>-by-inoculation interaction:  $p = 0.122$ ; Table 5.3) or the null effect of CO<sub>2</sub> on  
**2300**  $\rho_{\text{bioe}}$  (CO<sub>2</sub>-by-inoculation interaction:  $p = 0.298$ ; Table 5.3). Strong interactions  
**2301** between fertilization and inoculation on  $\rho_{\text{rubisco}}$ ,  $\rho_{\text{bioe}}$ , and  $\rho_{\text{photo}}$  (fertilization-  
**2302** by-inoculation interaction:  $p < 0.001$  in all cases; Table 5.3) indicated that the  
**2303** general negative effect of increasing fertilization ( $p < 0.001$  in all cases; Table  
**2304** 5.3) was only observed in inoculated pots (Tukey:  $p < 0.001$  in all cases), with  
**2305** no apparent effect of fertilization on  $\rho_{\text{rubisco}}$  (Tukey:  $p = 0.612$ ),  $\rho_{\text{bioe}}$  (Tukey:  
**2306**  $p = 0.544$ ), or  $\rho_{\text{photo}}$  (Tukey:  $p = 0.521$ ; Fig 5.3a) in uninoculated pots. An  
**2307** additional interaction between fertilization and inoculation on  $\rho_{\text{light}}$  (fertilization-

**2308** by-inoculation interaction:  $p < 0.001$ ; Table 5.3) indicated a negative effect of  
**2309** increasing fertilization on  $\rho_{\text{light}}$  in inoculated pots (Tukey:  $p = 0.041$ ), but a  
**2310** positive effect of increasing fertilization in uninoculated pots (Tukey:  $p < 0.001$ ).  
  
**2311** The stimulation in  $M_{\text{area}}$  resulted in an 133% stimulation of  $\rho_{\text{structure}}$  under  
**2312** elevated CO<sub>2</sub> ( $p < 0.001$ ; Table 5.3; Fig 5.3b). An interaction between fertiliza-  
**2313** tion and CO<sub>2</sub> (CO<sub>2</sub>-by-fertilization interaction:  $p = 0.039$ ; Table 5.3) indicated  
**2314** that the general negative effect of increasing fertilization ( $p < 0.001$ ; Table 5.3) on  
**2315**  $\rho_{\text{structure}}$  was marginally stronger under ambient CO<sub>2</sub> (Tukey:  $p = 0.055$ ), resulting  
**2316** in a stronger stimulation in  $\rho_{\text{structure}}$  under elevated CO<sub>2</sub> with increasing fertiliza-  
**2317** tion. A marginal interaction between inoculation and CO<sub>2</sub> (CO<sub>2</sub>-by-inoculation  
**2318** interaction:  $p = 0.057$ ; Table 5.3) indicated that the general positive effect of  
**2319** inoculation on  $\rho_{\text{structure}}$  ( $p < 0.001$ ; Table 5.3) was only observed under elevated  
**2320** CO<sub>2</sub> (Tukey:  $p < 0.001$ ), with no apparent inoculation effect observed under am-  
**2321** bient CO<sub>2</sub> (Tukey:  $p = 0.513$ ). Finally, an interaction between fertilization and  
**2322** inoculation (fertilization-by-inoculation interaction:  $p < 0.001$ ; Table 5.3) indi-  
**2323** cated that, while increasing fertilization generally increased  $\rho_{\text{structure}}$  ( $p < 0.001$ ;  
**2324** Table 5.3), this response was generally stronger in uninoculated pots (Tukey:  $p$   
**2325** = 0.001; Fig. 5.3b).

**Table 5.3.** Effects of soil N availability, soil pH, species, and  $N_{\text{area}}$  on leaf nitrogen allocation

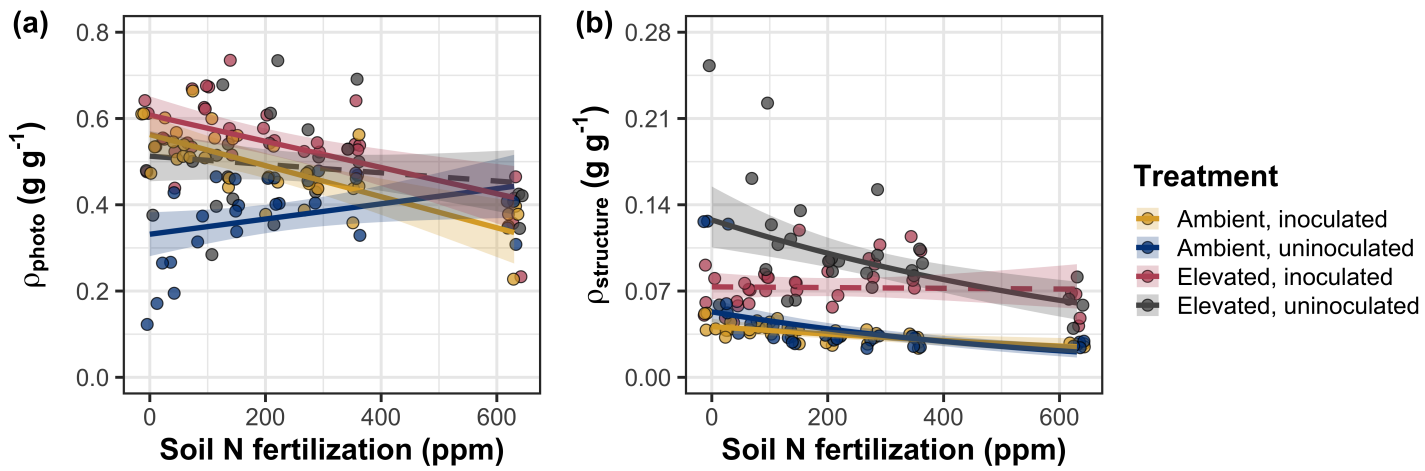
		$\rho_{\text{rubisco}}$			$\rho_{\text{bioe}}$			$\rho_{\text{light}}$		
	df	Coefficient	$\chi^2$	p	Coefficient	$\chi^2$	p	Coefficient	$\chi^2$	p
(Intercept)	-	2.70E-01	-	-	5.26E-02	-	-	8.48E-03	-	-
CO <sub>2</sub>	1	1.42E-01	23.510	<0.001	3.00E-02	53.899	<0.001	2.03E-03	0.149	0.700
Inoculation (I)	1	1.83E-01	23.475	<0.001	2.80E-02	13.860	<0.001	2.04E-02	147.234	<0.001
Fertilization (N)	1	1.35E-04	16.609	<0.001	1.22E-05	26.827	<0.001	3.22E-05	19.378	<0.001
CO <sub>2</sub> *I	1	-1.07E-01	3.629	0.057	-1.67E-02	2.390	0.122	-5.33E-03	0.684	0.408
CO <sub>2</sub> *N	1	-2.16E-04	1.223	0.269	-3.59E-05	1.085	0.298	-7.01E-06	0.351	0.553
I*N	1	-4.26E-04	20.045	<0.001	-6.87E-05	15.458	<0.001	-4.37E-05	64.042	<0.001
CO <sub>2</sub> *I*N	1	2.50E-04	3.327	0.068	4.08E-05	2.651	0.103	1.74E-05	3.735	0.053

		$\rho_{\text{photo}}$			$\rho_{\text{structure}}^a$					
	df	Coefficient	$\chi^2$	p	Coefficient	$\chi^2$	p			
(Intercept)	-	3.32E-01	-	-	-2.93E+00	-	-			
CO <sub>2</sub>	1	1.81E-01	27.651	<0.001	8.77E-01	229.571	<0.001			
Inoculation (I)	1	2.31E-01	26.238	<0.001	-2.55E-01	13.872	<0.001			
Fertilization (N)	1	1.76E-04	15.899	<0.001	-1.51E-03	38.128	<0.001			
CO <sub>2</sub> *I	1	-1.36E-01	3.671	0.055	-2.99E-01	3.622	0.057			
CO <sub>2</sub> *N	1	-2.72E-04	1.163	0.281	3.14E-04	4.266	0.039			
I*N	1	-5.37E-04	21.355	<0.001	7.00E-04	11.025	0.001			
CO <sub>2</sub> *I*N	1	3.29E-04	4.009	0.045	4.52E-04	0.669	0.413			

138

2326 \*Significance determined using Type II Wald  $\chi^2$  tests ( $\alpha = 0.05$ ). P-values  $< 0.05$  are in bold, while p-values  
 2327 between 0.05 and 0.1 are italicized. A superscript “a” is included after trait labels to indicate if models were fit with  
 2328 natural log transformed response variables. Key: df=degrees of freedom,  $\rho_{\text{rubisco}}$  = proportion of leaf N allocated  
 2329 to photosynthesis,  $\rho_{\text{bioe}}$  = proportion of leaf N allocated to bioenergetics,  $\rho_{\text{light}}$  = proportion of leaf N allocated to  
 2330 light harvesting proteins,  $\rho_{\text{photo}}$  = proportion of leaf N allocated to photosynthesis,  $\rho_{\text{structure}}$  = proportion of leaf N  
 2331 allocated to cell wall structural tissue



**Figure 5.3.** Effects of  $\text{CO}_2$ , fertilization, and inoculation on the relative fraction of leaf nitrogen allocated to photosynthesis (a) and the fraction of leaf nitrogen allocated to structure (b). Soil nitrogen fertilization is represented on the x-axis in both panels. Colored points and trendlines are as explained in Figure 1.

**2332** 5.3.4 *Whole plant traits*

**2333** Total leaf area was 51% greater and total biomass was 102% greater under  
**2334** elevated CO<sub>2</sub> ( $p < 0.001$  in both cases; Table 5.4), a pattern that was enhanced  
**2335** by fertilization (CO<sub>2</sub>-by-fertilization interaction:  $p < 0.001$  in both cases; Table  
**2336** 5.4; Figs. 5.4a-b) but was not modified across inoculation treatments (CO<sub>2</sub>-by-  
**2337** inoculation interaction:  $p_{total\_leaf\_area} = 0.151$ ,  $p_{total\_biomass} = 0.472$ ; Table 5.4).  
**2338** Specifically, the general positive effect of increasing fertilization on total leaf area  
**2339** and whole plant biomass ( $p < 0.001$  in both cases; Table 5.4) was stronger under  
**2340** elevated CO<sub>2</sub> (Tukey:  $p < 0.001$  in both cases). The general positive effect of  
**2341** increasing fertilization on total leaf area was modified by inoculation treatment  
**2342** (fertilization-by-inoculation interaction:  $p < 0.001$  in both cases; Table 5.4), in-  
**2343** dicating a stronger positive effect of increasing fertilization in uninoculated pots  
**2344** (Tukey:  $p_{total\_leaf\_area} = 0.002$ ,  $p_{total\_biomass} = 0.001$ , Fig. 5.4a).

**2345** A 62% stimulation in  $N_{cost}$  under elevated CO<sub>2</sub> was modified through a  
**2346** strong three-way interaction between CO<sub>2</sub>, fertilization, and inoculation (CO<sub>2</sub>-  
**2347** by-inoculation-by-fertilization interaction:  $p < 0.001$ ; Table 5.4; Fig. 5.4). This  
**2348** interaction revealed a general negative effect of increasing fertilization on  $N_{cost}$   
**2349** ( $p < 0.001$ ; Table 5.4) that was observed in all treatment combinations (Tukey:  
**2350**  $p < 0.001$  in all cases) except for inoculated pots grown under elevated CO<sub>2</sub>  
**2351** (Tukey:  $p = 0.779$ ; Fig. 5.4c). This response also resulted in generally stronger  
**2352** negative effects of increasing fertilization on  $N_{cost}$  in uninoculated pots grown  
**2353** under elevated CO<sub>2</sub> than uninoculated pots grown under ambient CO<sub>2</sub> (Tukey:  
**2354**  $p = 0.001$ ) and inoculated pots grown under either ambient CO<sub>2</sub> (Tukey:  $p <$   
**2355**  $0.001$ ) or elevated CO<sub>2</sub> (Tukey:  $p < 0.001$ ), while uninoculated pots grown under

**2356** ambient CO<sub>2</sub> had generally stronger negative effects of increasing fertilization on  
**2357**  $N_{\text{cost}}$  than inoculated pots grown under elevated CO<sub>2</sub> (Tukey:  $p = 0.002$ ), but  
**2358** not inoculated pots grown under ambient CO<sub>2</sub> (Tukey:  $p = 0.216$ ; Fig. 5.4).  
**2359** The general reduction in  $N_{\text{cost}}$  with increasing fertilization and in uninoculated  
**2360** pots were driven by a stronger positive effect of increasing fertilization on  $N_{\text{wp}}$   
**2361** (denominator of  $N_{\text{cost}}$ ) than  $C_{\text{bg}}$  (numerator of  $N_{\text{cost}}$ ), while the general stimulation  
**2362** in  $N_{\text{cost}}$  under elevated CO<sub>2</sub> was driven by a stronger positive effect of elevated  
**2363** CO<sub>2</sub> on  $C_{\text{bg}}$  than  $N_{\text{wp}}$  (Table 5.4).

**Table 5.4.** Effects of soil N availability, soil pH, species, and  $N_{\text{area}}$  on total leaf area, whole plant biomass, and carbon costs to acquire nitrogen

	Total leaf area			Total biomass			$N_{\text{cost}}$			
	df	Coefficient	$\chi^2$	p	Coefficient	$\chi^2$	p	Coefficient	$\chi^2$	p
(Intercept)	-	8.78E+01	-	-	9.96E-01	-	-	8.67E+00	-	-
$\text{CO}_2$	1	3.36E+01	69.291	<b>&lt;0.001</b>	5.07E-01	131.477	<b>&lt;0.001</b>	8.75E+00	88.189	<b>&lt;0.001</b>
Inoculation (I)	1	1.88E+02	35.715	<b>&lt;0.001</b>	7.96E-01	34.264	<b>&lt;0.001</b>	-1.68E+00	136.343	<b>&lt;0.001</b>
Fertilization (N)	1	9.35E-01	274.199	<b>&lt;0.001</b>	3.14E-03	269.046	<b>&lt;0.001</b>	-8.50E-03	80.501	<b>&lt;0.001</b>
$\text{CO}_2 * \text{I}$	1	6.44E+01	2.064	0.151	-7.69E-02	0.518	0.472	-8.38E+00	85.237	<b>&lt;0.001</b>
$\text{CO}_2 * \text{N}$	1	5.05E-01	18.655	<b>&lt;0.001</b>	1.61E-03	16.877	<b>&lt;0.001</b>	-9.17E-03	1.050	0.306
$\text{I} * \text{N}$	1	-3.84E-01	10.804	<b>0.001</b>	-1.45E-03	15.779	<b>&lt;0.001</b>	4.20E-03	46.489	<b>&lt;0.001</b>
$\text{CO}_2 * \text{I} * \text{N}$	1	-2.97E-03	<0.001	0.990	-1.14E-04	0.023	0.880	1.32E-02	18.125	<b>&lt;0.001</b>

	$C_{\text{bg}}$			$N_{\text{wp}}$			
	df	Coefficient	$\chi^2$	p	Coefficient	$\chi^2$	p
(Intercept)	-	-1.70E+00	-	-	1.24E-01	-	-
$\text{CO}_2$	1	9.21E-01	84.134	<b>&lt;0.001</b>	-3.41E-03	23.890	<b>&lt;0.001</b>
Inoculation (I)	1	1.18E+00	41.030	<b>&lt;0.001</b>	1.68E-01	134.460	<b>&lt;0.001</b>
N fertilization (N)	1	3.38E-03	152.248	<b>&lt;0.001</b>	6.69E-04	529.021	<b>&lt;0.001</b>
$\text{CO}_2 * \text{I}$	1	-6.18E-01	8.965	<b>0.003</b>	3.68E-02	1.190	0.275
$\text{CO}_2 * \text{N}$	1	-3.66E-05	1.188	0.276	1.58E-04	5.915	<b>0.015</b>
$\text{I} * \text{N}$	1	-2.22E-03	22.648	<b>&lt;0.001</b>	-3.20E-04	55.562	<b>&lt;0.001</b>
$\text{CO}_2 * \text{I} * \text{N}$	1	8.09E-04	1.109	0.292	-7.54E-05	0.620	0.431

142

2364 \*Significance determined using Type II Wald  $\chi^2$  tests ( $\alpha = 0.05$ ). P-values  $< 0.05$  are in bold, while p-values between  
 2365 0.05 and 0.1 are italicized. Key: df = degrees of freedom;  $N_{\text{cost}}$  = structural carbon cost to acquire nitrogen;  $C_{\text{bg}}$  =  
 2366 belowground carbon biomass;  $N_{\text{wp}}$  = whole plant nitrogen biomass

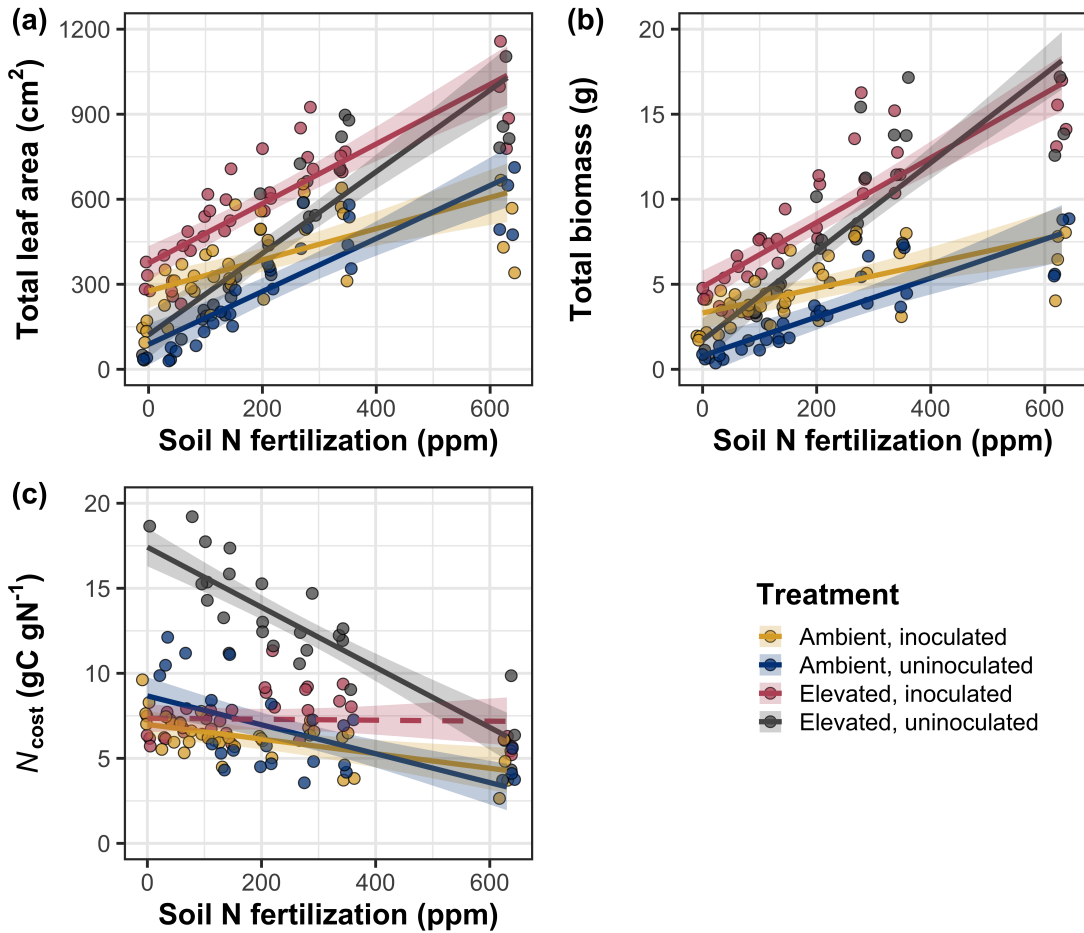


**Figure 5.4.** Effects of  $\text{CO}_2$ , fertilization, and inoculation on total leaf area (a), total biomass (b), and structural carbon costs to acquire nitrogen (c). Soil nitrogen fertilization is represented continuously on the x-axis in all panels. Colored points and trendlines are as explained in Figure 1.

**2367** 5.3.5 *Nitrogen fixation*

**2368** Nodule biomass was stimulated by 30% under elevated CO<sub>2</sub> ( $p < 0.001$ ;  
**2369** Table 5.5), a pattern that was modified across the fertilization gradient (CO<sub>2</sub>-  
**2370** by-fertilization interaction:  $p = 0.479$ ; Table 5.5), but not between inoculation  
**2371** treatments (CO<sub>2</sub>-by-inoculation interaction:  $p = 0.404$ ; Table 5.5). Specifically,  
**2372** the general negative effect of increasing fertilization on nodule biomass ( $p < 0.001$ ;  
**2373** Table 5.5) was stronger under elevated CO<sub>2</sub> than ambient CO<sub>2</sub> (Tukey:  $p <$   
**2374** 0.001; Fig. 5.5a), which reduced the stimulation in nodule biomass under elevated  
**2375** CO<sub>2</sub> with increasing fertilization. A strong interaction between fertilization and  
**2376** inoculation (fertilization-by-inoculation interaction:  $p < 0.001$ ; Table 5.5) was  
**2377** driven by a stronger negative effect of increasing fertilization in inoculated pots  
**2378** (Tukey:  $p < 0.001$ ; Fig. 5.5a).

**2379** There was no effect of CO<sub>2</sub> on nodule: root biomass ( $p = 0.767$ ; Table  
**2380** 5.5), although an interaction between CO<sub>2</sub> and inoculation (CO<sub>2</sub>-by-inoculation  
**2381** interaction:  $p < 0.001$ ; Table 5.5) indicated that the general positive effect of in-  
**2382** oculation on nodule: root biomass ( $p < 0.001$ ; Table 5.5) was stronger under am-  
**2383** bient CO<sub>2</sub> (3129% increase; Tukey:  $p < 0.001$ ) than elevated CO<sub>2</sub> (379% increase;  
**2384** Tukey:  $p < 0.001$ ; Fig. 5.5b). The null effect of CO<sub>2</sub> on nodule: root biomass  
**2385** was consistently observed across the fertilization gradient ( $p = 0.183$ ; Table 5.5;  
**2386** Fig. 5.5b). An interaction between fertilization and inoculation (fertilization-by-  
**2387** inoculation interaction:  $p < 0.001$ ; Table 5.5) indicated that the general negative  
**2388** effect of increasing fertilization on nodule: root biomass ( $p < 0.001$ ; Table 5.5)  
**2389** was stronger in inoculated pots (Tukey:  $p < 0.001$ ; Fig. 5.5b).

**2390** There was no effect of CO<sub>2</sub> on %N<sub>dfa</sub> ( $p = 0.472$ ; Table 5.5), a pattern

**2391** that was not modified by inoculation ( $\text{CO}_2$ -by-inoculation interaction:  $p = 0.156$ ;  
**2392** Table 5.5) or fertilization ( $\text{CO}_2$ -by-fertilization interaction:  $p = 0.099$ ; Table 5.5).  
**2393** An interaction between fertilization and inoculation (fertilization-by-inoculation  
**2394** interaction:  $p < 0.001$ ; Table 5.5) indicated that the general negative effect of  
**2395** increasing fertilization on  $\%N_{dfa}$  ( $p < 0.001$ ; Table 5.5) was only observed in  
**2396** inoculated pots (Tukey:  $p < 0.001$ ), with no apparent effect of fertilization on  
**2397**  $\%N_{dfa}$  in uninoculated pots (Tukey:  $p = 0.651$ ; Table 5.5; Fig. 5.5c).

**Table 5.5.** Effects of soil N availability, soil pH, species, and  $N_{\text{area}}$  on root nodule biomass and plant investments in symbiotic nitrogen fixation

	Root nodule biomass <sup>b</sup>			Root nodule: root biomass <sup>b</sup>			% $N_{\text{dfa}}^b$			
	df	Coefficient	$\chi^2$	p	Coefficient	$\chi^2$	p	Coefficient	$\chi^2$	p
(Intercept)	-	9.41E-03	-	-	1.33E-02	-	-	7.48E-01	-	-
CO <sub>2</sub>	1	1.20E-01	19.258	<b>&lt;0.001</b>	9.94E-02	0.087	0.768	-1.00E-01	0.518	0.472
Inoculation (I)	1	5.74E-01	755.020	<b>&lt;0.001</b>	5.40E-01	903.691	<b>&lt;0.001</b>	9.01E+00	955.570	<b>&lt;0.001</b>
Fertilization (N)	1	7.71E-06	84.376	<b>&lt;0.001</b>	-5.99E-06	258.099	<b>&lt;0.001</b>	3.64E-04	292.938	<b>&lt;0.001</b>
CO <sub>2</sub> *I	1	-4.68E-02	0.950	0.330	-1.38E-01	20.614	<b>&lt;0.001</b>	-1.44E-01	2.010	0.156
CO <sub>2</sub> *N	1	-1.59E-04	2.106	0.147	-1.73E-04	1.773	0.183	-6.21E-05	2.716	0.099
I*N	1	-5.82E-04	44.622	<b>&lt;0.001</b>	-7.45E-04	133.918	<b>&lt;0.001</b>	-1.58E-02	231.290	<b>&lt;0.001</b>
CO <sub>2</sub> *I*N	1	7.26E-05	0.196	0.658	1.76E-04	2.359	0.125	2.77E-03	2.119	0.145

2398 \*Significance determined using Type II Wald  $\chi^2$  tests ( $\alpha = 0.05$ ). P-values  $< 0.05$  are in bold, while p-values between  
 2399 0.05 and 0.1 are italicized. Superscript letters indicate model coefficients fit to square-root (<sup>b</sup>) transformed data.  
 2400 Key: df = degrees of freedom % $N_{\text{dfa}}$  = percent nitrogen fixed from the atmosphere.

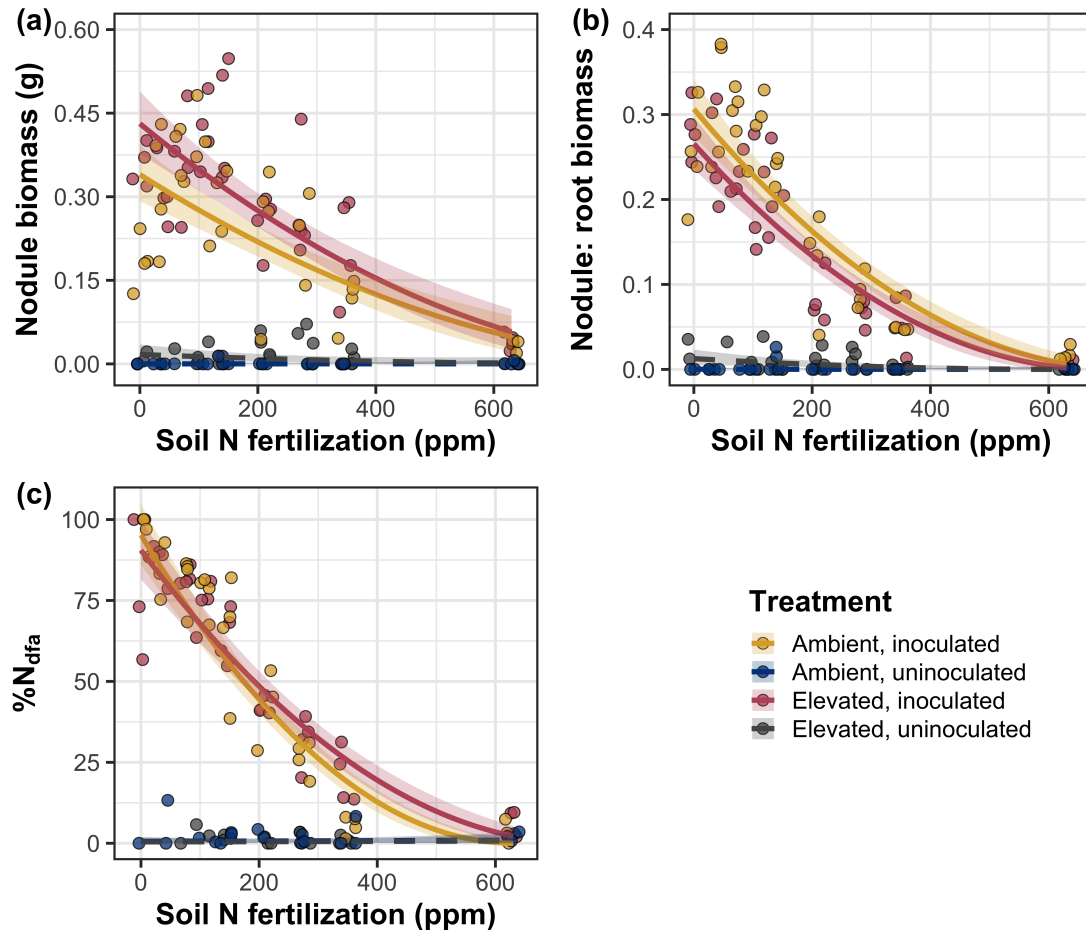


**Figure 5.5.** Effects of  $\text{CO}_2$ , fertilization, and inoculation on nodule biomass (a), nodule: root biomass (b), and percent nitrogen fixed from the atmosphere (c). Soil nitrogen fertilization is represented on the x-axis. Yellow points and trendlines indicate inoculated individuals grown under ambient  $\text{CO}_2$ , blue points and trendlines indicate uninoculated individuals grown under ambient  $\text{CO}_2$ , red points and trendlines indicate inoculated individuals grown under elevated  $\text{CO}_2$ , and grey points indicate uninoculated individuals grown under elevated  $\text{CO}_2$ . Solid trendlines indicate slopes that are different from zero ( $p < 0.05$ ), while dashed trendlines indicate slopes that are not different from zero ( $p > 0.05$ ). Curvilinear trendlines occur as a result of back-transforming models where response variables received either a natural log or square root transformation prior to fitting.

**2401** 5.4 Discussion

**2402** In this study, I determined leaf and whole plant acclimation responses of  
**2403** 7-week *G. max* seedlings grown under two CO<sub>2</sub> concentrations, two inoculation  
**2404** treatments, and nine soil nitrogen fertilization treatments in a full-factorial growth  
**2405** chamber experiment. In support of my hypotheses and patterns expected from  
**2406** theory, elevated CO<sub>2</sub> reduced  $N_{\text{area}}$ ,  $V_{\text{cmax25}}$ , and  $J_{\text{max25}}$ . The relatively stronger  
**2407** downregulation in  $V_{\text{cmax25}}$  than  $J_{\text{max25}}$  under elevated CO<sub>2</sub> resulted in a stimulation  
**2408** in  $J_{\text{max25}}:V_{\text{cmax25}}$  under elevated CO<sub>2</sub>. The downregulation of  $V_{\text{cmax25}}$  and  $J_{\text{max25}}$   
**2409** under elevated CO<sub>2</sub> was similar across fertilization and inoculation treatments,  
**2410** indicating that the CO<sub>2</sub> responses were not due to nitrogen limitation. Interest-  
**2411** ingly, results indicate that elevated CO<sub>2</sub> increased the fraction of leaf nitrogen  
**2412** allocated to photosynthesis and structure, leading to a stimulation in nitrogen  
**2413** use efficiency under elevated CO<sub>2</sub> despite the apparent downregulation in  $N_{\text{area}}$ ,  
**2414**  $V_{\text{cmax25}}$ , and  $J_{\text{max25}}$ . The downregulation in leaf photosynthetic processes under  
**2415** elevated CO<sub>2</sub> also corresponded with a strong stimulation in total leaf area and to-  
**2416** tal biomass. Strong stimulations in whole plant growth due to elevated CO<sub>2</sub> were  
**2417** generally enhanced with increasing fertilization and were negatively related to  
**2418** structural carbon costs to acquire nitrogen. Inoculation generally did not modify  
**2419** whole plant responses to elevated CO<sub>2</sub> across the fertilization gradient, likely due  
**2420** to a strong reduction in root nodulation with increasing fertilization. However,  
**2421** strong positive effects of inoculation on whole plant growth were observed under  
**2422** low fertilization, consistent with our hypothesis. Overall, observed leaf and whole  
**2423** plant acclimation responses to CO<sub>2</sub> support hypotheses and patterns expected  
**2424** from photosynthetic least-cost theory, showing that leaf acclimation responses to

2425 CO<sub>2</sub> were decoupled from soil nitrogen availability and ability to acquire nitro-  
2426 gen via symbiotic nitrogen fixation. Instead, leaf and whole plant acclimation  
2427 responses to CO<sub>2</sub> were driven by optimal resource investment to photosynthetic  
2428 capacity, where optimal resource investment at the leaf level maximized nitrogen  
2429 allocation to structures that support whole plant growth.

2430 5.4.1 *Soil nitrogen fertilization has divergent effects on leaf and whole plant  
2431 acclimation responses to CO<sub>2</sub>*

2432 Elevated CO<sub>2</sub> reduced  $N_{\text{area}}$ ,  $V_{\text{cmax25}}$ ,  $J_{\text{max25}}$ , and stomatal conductance by  
2433 29%, 16%, 10%, and 20%, respectively (Table 5.2). The larger downregulation in  
2434  $V_{\text{cmax25}}$  than  $J_{\text{max25}}$  led to an 8% stimulation in  $J_{\text{max25}}:V_{\text{cmax25}}$  (Table 5.2), while  
2435 the larger downregulation in  $N_{\text{area}}$  than  $V_{\text{cmax25}}$  resulted in a 21% stimulation  
2436 in the fraction of leaf nitrogen allocated to photosynthesis under elevated CO<sub>2</sub>.  
2437 These acclimation responses are directionally consistent with previous studies that  
2438 have investigated or reviewed leaf acclimation responses to CO<sub>2</sub> (Drake et al.  
2439 1997; Makino et al. 1997; Ainsworth et al. 2002; Ainsworth and Long 2005;  
2440 Ainsworth and Rogers 2007; Smith and Dukes 2013; Smith and Keenan 2020;  
2441 Poorter et al. 2022), and follow patterns expected from photosynthetic least-cost  
2442 theory (Wright et al. 2003; Prentice et al. 2014; Smith et al. 2019; Smith and  
2443 Keenan 2020). Together, the stimulation in  $J_{\text{max25}}:V_{\text{cmax25}}$  and the fraction of leaf  
2444 nitrogen allocated to photosynthesis, and nitrogen use efficiency under elevated  
2445 CO<sub>2</sub> provide strong support for the idea that leaves were downregulating  $V_{\text{cmax25}}$   
2446 in response to elevated CO<sub>2</sub> in order to optimally coordinate photosynthesis such  
2447 that net photosynthesis rates approached becoming equally co-limited by Rubisco

**2448** carboxylation and RuBP regeneration (Chen et al. 1993; Maire et al. 2012).

**2449** Increasing fertilization and inoculation induced strong positive effects on  
**2450**  $N_{\text{area}}$  (Fig. 1a),  $V_{\text{cmax}25}$  (Fig. 5.2a),  $J_{\text{max}25}$  (Fig. 5.2b). The general positive  
**2451** response of  $N_{\text{area}}$  to increasing fertilization and in inoculated pots was enhanced  
**2452** under ambient CO<sub>2</sub>, which, paired with the general downregulation in  $N_{\text{area}}$  un-  
**2453** der elevated CO<sub>2</sub>, resulted in a stronger downregulation of  $N_{\text{area}}$  under elevated  
**2454** CO<sub>2</sub> with increasing fertilization and in inoculated pots (Fig. 5.1a). These pat-  
**2455** terns suggest that  $N_{\text{area}}$  responses to CO<sub>2</sub> were at least partially dependent on  
**2456** soil nitrogen fertilization and nitrogen acquisition strategy. However, the general  
**2457** stimulation in the fraction of leaf nitrogen allocated to Rubisco, bioenergetics,  
**2458** or photosynthesis under elevated CO<sub>2</sub> was not modified across the fertilization  
**2459** gradient and was only marginally enhanced in inoculated pots. These patterns  
**2460** suggest that the increased downregulation of Narea under elevated CO<sub>2</sub> with in-  
**2461** creasing fertilization was not associated with a change in relative investment to  
**2462** photosynthetic tissue. Instead, a stronger downregulation in the fraction of leaf  
**2463** nitrogen allocated to structure under ambient CO<sub>2</sub> resulted in a stronger stim-  
**2464** ulation in  $\rho_{\text{structure}}$  under elevated CO<sub>2</sub> with increasing fertilization (Fig. 5.3b),  
**2465** indicating that fertilization shifted relative investment in leaf structural tissue un-  
**2466** der elevated CO<sub>2</sub>. These results, combined with a stimulation in PNUE (Fig. SX)  
**2467** and iWUE (Fig. SX) under elevated CO<sub>2</sub> that was independent of fertilization  
**2468** or inoculation treatment, provide additional support for the hypothesis that leaf  
**2469** acclimation photosynthetic responses to CO<sub>2</sub> were independent of fertilization;  
**2470** though fertilization may contribute to changes in leaf morphology under elevated  
**2471** CO<sub>2</sub> through shifts in  $M_{\text{area}}$  (Onoda et al. 2017; Wang et al. 2017; Dong et al.

**2472** 2022).

**2473** The downregulation in  $N_{\text{area}}$ ,  $V_{\text{cmax}25}$ , and  $J_{\text{max}25}$  under elevated CO<sub>2</sub> cor-  
**2474** responded with a respective 62% and 100% stimulation in total leaf area (Fig.  
**2475** 5.4a) and total biomass (Fig. 5.4b). The stimulation in total leaf area and total  
**2476** biomass under elevated CO<sub>2</sub> also corresponded with generally higher structural  
**2477** carbon costs to acquire nitrogen (Fig. 5.4c), a pattern driven by a stimulation  
**2478** in belowground carbon biomass and reduction in whole plant nitrogen biomass.  
**2479** Alone, this result suggests that elevated CO<sub>2</sub> reduces plant nitrogen uptake effi-  
**2480** ciency, which does not explain why plants grown under elevated CO<sub>2</sub> generally had  
**2481** higher biomass and total leaf area. However, a strong negative effect of increasing  
**2482** fertilization on structural carbon costs to acquire nitrogen, which were generally  
**2483** similar between CO<sub>2</sub> concentrations, was driven by a stronger increase in whole  
**2484** plant nitrogen biomass than belowground carbon biomass. Thus, increases in the  
**2485** positive response of whole plant growth and total leaf area under elevated CO<sub>2</sub>  
**2486** with increasing fertilization were likely driven by an increase in nitrogen uptake  
**2487** efficiency, allowing plants to satisfy any increase in whole plant nitrogen demand  
**2488** associated with increased CO<sub>2</sub>.

**2489** Interestingly, these results indicate that the general stimulation in total  
**2490** leaf area and whole plant growth under elevated CO<sub>2</sub> was not modified by inoc-  
**2491** ulation despite an apparent general negative effect of inoculation on  $N_{\text{cost}}$ . This  
**2492** response could have been due to strong negative effect of increasing fertilization on  
**2493** nodulation (Fig. 5.5), which may have caused the strong increase in the positive  
**2494** effect of elevated CO<sub>2</sub> on whole plant growth with increasing fertilization to mask  
**2495** any increase in the positive effect of elevated CO<sub>2</sub> on whole plant growth due to

2496 inoculation. Reductions in nodulation with increasing fertilization are commonly  
2497 observed patterns that have been inferred to be a response that allows species  
2498 optimize nitrogen uptake efficiency as costs to acquire nitrogen via direct uptake  
2499 become more similar (Fig. 5.4c) (Gibson and Harper 1985; Rastetter et al. 2001).  
2500 In this study, pairwise comparisons indicated strong positive effects of inocula-  
2501 tion on total leaf area and total biomass (158% increase in total leaf area, 119%  
2502 increase in total biomass) under elevated CO<sub>2</sub> at 0 ppm N, but no observable  
2503 inoculation effect on total leaf area or total biomass under elevated CO<sub>2</sub> at 350  
2504 ppm N or 630 ppm N. While these responses did not generally differ from those  
2505 observed under ambient CO<sub>2</sub>, they do confirm the hypothesis that positive effects  
2506 of inoculation on whole plant growth responses to elevated CO<sub>2</sub> would decrease  
2507 with increasing fertilization.

2508 Combined, results reported here suggest that soil nitrogen availability has  
2509 a divergent role in modifying leaf and whole plant acclimation responses to CO<sub>2</sub>.  
2510 Leaf acclimation responses were generally decoupled from fertilization, while whole  
2511 plant acclimation responses relied heavily on an increase in nitrogen uptake ef-  
2512 ficiency and consequent reduction in costs of acquiring nitrogen associated with  
2513 increasing fertilization. However, whole plant responses to CO<sub>2</sub> indicated that  
2514 fertilization may play a more important role in determining whole plant acclima-  
2515 tion responses to CO<sub>2</sub> than nitrogen acquisition strategy, although these patterns  
2516 were likely driven by reductions in nodulation with increasing fertilization. These  
2517 results suggest that plants acclimate to CO<sub>2</sub> in nitrogen-limited systems by mini-  
2518 mizing the number of optimally coordinated leaves, and that the downregulation  
2519 in leaf nitrogen content under elevated CO<sub>2</sub> is not a direct response to changes in

**2520** soil nitrogen availability as previously implied.

**2521** 5.4.2 *Implications for future model development*

**2522** Many terrestrial biosphere models predict photosynthetic capacity through  
**2523** plant functional group-specific linear regressions between  $N_{\text{area}}$  and  $V_{\text{cmax}}$  (Rogers  
**2524** 2014; Rogers et al. 2017), which assumes that leaf nitrogen-photosynthesis rela-  
**2525** tionships are constant across growing environments. Our results build on previ-  
**2526** ous work suggesting that leaf nitrogen-photosynthesis relationships dynamically  
**2527** change across growing environments (Luo et al. 2021; Dong et al. 2022). Specif-  
**2528** ically, results from this experiment indicate that  $\text{CO}_2$  concentration increased  
**2529** the fraction of leaf nitrogen content allocated to photosynthesis, while a general  
**2530** negative effect of increasing fertilization on the fraction of leaf nitrogen content  
**2531** allocated to photosynthesis was dependent on inoculation treatment. Similar in-  
**2532** creases in  $N_{\text{area}}$ ,  $V_{\text{cmax}25}$ , and  $J_{\text{max}25}$  with increasing fertilization resulted in no  
**2533** change in the fraction of leaf nitrogen allocated to photosynthesis in uninoculated  
**2534** pots, while larger increases in  $N_{\text{area}}$  than  $V_{\text{cmax}25}$  and  $J_{\text{max}25}$  with increasing fertil-  
**2535** ization decreased the fraction of leaf nitrogen allocated to photosynthesis in inoc-  
**2536** ulated pots (Fig. 5.3a). As inoculated pots were able to access less finite supply of  
**2537** nitrogen across the fertilization gradient, these patterns suggest that constant leaf  
**2538** nitrogen-photosynthesis relationships may only apply in environments where ni-  
**2539** trogen is limiting and will likely change with increasing  $\text{CO}_2$  concentrations. Thus,  
**2540** terrestrial biosphere models that parameterize photosynthetic capacity through  
**2541** linear relationships between  $N_{\text{area}}$  and  $V_{\text{cmax}}$  (Rogers 2014; Rogers et al. 2017)  
**2542** may be overestimating photosynthetic capacity in systems where nitrogen is not

2543 as limiting and may contribute to erroneous model simulations under future CO<sub>2</sub>  
2544 concentrations.

2545 These results also demonstrate that optimal resource investment to pho-  
2546 tosynthetic capacity defines leaf acclimation responses to elevated CO<sub>2</sub>, and that  
2547 these responses were independent of fertilization or inoculation treatment. Cur-  
2548 rent approaches for simulating photosynthetic responses to CO<sub>2</sub> generally invoke  
2549 patterns expected from progressive nitrogen limitation, where the downregulation  
2550 in  $N_{\text{area}}$ , and therefore photosynthetic capacity, due to elevated CO<sub>2</sub> are com-  
2551 monly a function of progressive reductions in soil nitrogen availability. Results  
2552 reported here contradict this formulation, suggesting that the leaf acclimation re-  
2553 sponse is driven by optimal resource investment to photosynthetic capacity and  
2554 is independent of soil resource supply. Optimality models that leverage prin-  
2555 ciples from optimal coordination and photosynthetic least-cost theories (Wang  
2556 et al. 2017; Stocker et al. 2020; Scott and Smith 2022) are capable of capturing  
2557 such acclimation responses to CO<sub>2</sub> (Smith and Keenan 2020), suggesting that the  
2558 implementation of these models may improve the simulation of photosynthetic  
2559 processes in terrestrial biosphere models under increasing CO<sub>2</sub> concentrations.

2560 5.4.3 *Study limitations and future directions*

2561 There are two study limitations that must be addressed to contextualize  
2562 patterns observed in this study. First, restricting the volume of belowground  
2563 substrate via a potted experiment does not adequately replicate belowground en-  
2564 vironments of natural systems, and therefore may modify effects of soil resource  
2565 availability and inoculation on plant nitrogen uptake, particularly if pot size limits

2566 whole plant growth (Poorter et al. 2012). I attempted to minimize the extent of  
2567 pot size limitation experienced in the first experimental chapters while account-  
2568 ing for the expected stimulation in whole plant growth under elevated CO<sub>2</sub> by  
2569 using 6-liter pots. Despite attempts to minimize growth limitation imposed by  
2570 pot volume, fertilization and CO<sub>2</sub> treatments increased the biomass: pot volume  
2571 ratio such that all treatment combinations to exceed 1 g L<sup>-1</sup> biomass: pot volume  
2572 under high fertilization. The 1 g L<sup>-1</sup> biomass: pot volume recommendation from  
2573 Poorter et al. (2012) was designated to avoid growth limitation imposed by pot  
2574 volume. However, if pot size limitation indeed limited whole plant growth, then  
2575 structural carbon costs to acquire nitrogen, belowground carbon biomass, whole  
2576 plant nitrogen biomass, and whole plant biomass should each exhibit strong sat-  
2577 uration points with increasing fertilization, which was not observed here. Addi-  
2578 tionally, a second set of photosynthetic measurements from one week prior to the  
2579 harvest (6 weeks post-germination) revealed ... As pot limitation is expected  
2580 to decrease net photosynthesis, and focal leaves were of similar ages between the  
2581 sixth and seventh week, one might expect growth limitation induced by constricted  
2582 pot volume to result in a dampened effect of inoculation and fertilization on net  
2583 photosynthesis,  $V_{cmax}$ , and  $J_{max25}$ . Analyses from the sixth week of development  
2584 revealed ... Additionally, analyses revealed a stronger/weaker downregulation in  
2585  $V_{cmax25}$  and  $J_{max25}$  on week 7, though disentangling the causality of this response  
2586 (i.e. whether due to pot size limitation or simply a stronger acclimation response)  
2587 would be difficult.

2588 Second, this study evaluated leaf and whole plant responses to CO<sub>2</sub> in 7-  
2589 week seedlings. Given the long-term scale of the progressive nitrogen limitation

2590 hypothesis, patterns observed here should be validated in longer-term nitrogen  
2591 manipulation experiments. Previous work in free air CO<sub>2</sub> enrichment experiments  
2592 show some support for patterns expected from the progressive nitrogen limitation  
2593 hypothesis (Reich et al. 2006; Norby et al. 2010), although results are not consis-  
2594 tent across experimental sites (Finzi et al. 2006; Moore et al. 2006; Liang et al.  
2595 2016). We found some support for patterns expected by the progressive nitrogen  
2596 limitation hypothesis, namely an increase in plant nitrogen uptake under elevated  
2597 CO<sub>2</sub> (Luo et al. 2004), though leaf acclimation responses to CO<sub>2</sub> were strongly  
2598 indicative of optimal resource investment to photosynthetic capacity as expected  
2599 from photosynthetic least-cost theory (Prentice et al. 2014; Smith et al. 2019;  
2600 Smith and Keenan 2020).

2601 5.4.4 *Conclusions*

2602 This study provides strong evidence suggesting that leaf acclimation re-  
2603 sponds to elevated CO<sub>2</sub> did not vary with soil nitrogen fertilization or ability  
2604 to acquire nitrogen through symbiotic nitrogen fixation. However, whole plant  
2605 acclimation responses to CO<sub>2</sub> were dependent on fertilization, where increasing  
2606 fertilization increased the positive effect of whole plant growth under elevated  
2607 CO<sub>2</sub>. Results also indicate that fertilization played a relatively more important  
2608 role in modifying whole plant responses to CO<sub>2</sub>, perhaps due to a reduction in  
2609 nodulation across the fertilization gradient. These patterns strongly support the  
2610 hypothesis that leaf and whole plant acclimation responses are driven by opti-  
2611 mal resource investment to photosynthetic capacity, and that leaf acclimation  
2612 responses to CO<sub>2</sub> were not modified by changes in soil nitrogen availability. Ad-

2613 ditionally, strong interactions between fertilization and inoculation on leaf and  
2614 whole plant traits indicated positive effects of fertilization on leaf and whole plant  
2615 traits in uninoculated pots, but null effects of fertilization on leaf and whole plant  
2616 traits in inoculated pots. These results build on previous work suggesting that  
2617 constant leaf nitrogen-photosynthesis relationships are dynamic and change across  
2618 growing environments, calling the use of constant relationships by terrestrial bio-  
2619 sphere models into question.

**2620**

## Chapter 6

**2621**

### Conclusions

**2622** Experiments included in this dissertation leverage patterns expected from  
**2623** photosynthetic least-cost theory to investigate effects of soil resource availability  
**2624** and aboveground climate on costs of nitrogen acquisition, leaf nitrogen-water use  
**2625** tradeoffs, and plant acclimation responses to elevated CO<sub>2</sub>. Photosynthetic least-  
**2626** cost theory provides a contemporary framework for understanding impacts of  
**2627** climatic and edaphic characteristics on plant ecophysiological processes, namely  
**2628** leaf nitrogen allocation and photosynthetic capacity. When I began planning  
**2629** experiments for this dissertation in August 2018,, empirical tests of the theory  
**2630** were sparse and model development was just beginning with a goal of eventually  
**2631** implementing the theory in terrestrial biosphere models. At the time, it was  
**2632** critical that experimentation be done to test underlying assumptions of the theory  
**2633** and validate its suitability for implementing in terrestrial biosphere models.

**2634** Early iterations of model development held the unit cost of acquiring ni-  
**2635** trogen relative to water constant (Wang et al. 2017), in part because limited data  
**2636** existed to evaluate how this parameter changes across spatiotemporal scales and  
**2637** different environmental gradients. However, the Fixation and Uptake of Nitrogen  
**2638** model (Fisher et al. 2010; Brzostek et al. 2014) indicates that costs of nitro-  
**2639** gen acquisition decreased with increasing soil nitrogen availability and varies in  
**2640** species with different nitrogen acquisition strategies, suggesting that the unit cost  
**2641** of acquiring nitrogen relative to water should change across nitrogen availability  
**2642** gradients. Additionally,

**2643** All experimental chapters in this dissertation provide strong and consist-  
**2644** ent support for patterns expected from the theory across different experimental  
**2645** approaches, spatiotemporal scales, and different plant functional groups. In this  
**2646** chapter, I first summarize experimental approaches and primary findings of each  
**2647** experimental chapter. Then, I use findings from the four experimental chapters  
**2648** to synthesize recommendations for future photosynthetic least-cost theory model  
**2649** development, and propose experiments that will allow for further understanding  
**2650** of mechanisms that drive patterns expected from photosynthetic least-cost theory  
**2651** across environmental gradients.

**2652**

## References

- 2653** Abrams, M. D. and S. A. Mostoller (1995). Gas exchange, leaf structure and  
**2654** nitrogen in contrasting successional tree species growing in open and under-  
**2655** story sites during a drought. *Tree Physiology* 15(6), 361–370.
- 2656** Adams, M. A., T. L. Turnbull, J. I. Sprent, and N. Buchmann (2016). Legumes  
**2657** are different: Leaf nitrogen, photosynthesis, and water use efficiency. *Pro-  
**2658** ceedings of the National Academy of Sciences of the United States of Amer-  
**2659** ica* 113(15), 4098–4103.
- 2660** Ainsworth, E. A., P. A. Davey, C. J. Bernacchi, O. C. Dermody, E. A. Heaton,  
**2661** D. J. Moore, P. B. Morgan, S. L. Naidu, H. S. Y. Ra, X. G. Zhu, P. S. Curtis,  
**2662** and S. P. Long (2002). A meta-analysis of elevated [CO<sub>2</sub>] effects on soybean  
**2663** (*Glycine max*) physiology, growth and yield. *Global Change Biology* 8(8),  
**2664** 695–709.
- 2665** Ainsworth, E. A. and S. P. Long (2005). What have we learned from 15 years of  
**2666** free-air CO<sub>2</sub> enrichment (FACE)? A meta-analytic review of the responses  
**2667** of photosynthesis, canopy properties and plant production to rising CO<sub>2</sub>.  
**2668** *New Phytologist* 165(2), 351–372.
- 2669** Ainsworth, E. A. and A. Rogers (2007). The response of photosynthesis and  
**2670** stomatal conductance to rising [CO<sub>2</sub>]: mechanisms and environmental in-  
**2671** teractions. *Plant, Cell and Environment* 30(3), 258–270.
- 2672** Allen, K., J. B. Fisher, R. P. Phillips, J. S. Powers, and E. R. Brzostek (2020).  
**2673** Modeling the carbon cost of plant nitrogen and phosphorus uptake across  
**2674** temperate and tropical forests. *Frontiers in Forests and Global Change* 3,

- 2675** 1–12.
- 2676** Allison, S. D., C. I. Czimczik, and K. K. Treseder (2008). Microbial activity  
**2677** and soil respiration under nitrogen addition in Alaskan boreal forest. *Global*  
**2678** *Change Biology* 14(5), 1156–1168.
- 2679** Andersen, M. K., H. Hauggaard-Nielsen, P. Ambus, and E. S. Jensen (2005).  
**2680** Biomass production, symbiotic nitrogen fixation and inorganic N use in dual  
**2681** and tri-component annual intercrops. *Plant and Soil* 266(1-2), 273–287.
- 2682** Andrews, M., E. K. James, J. I. Sprent, R. M. Boddey, E. Gross, and F. B. dos  
**2683** Reis (2011). Nitrogen fixation in legumes and actinorhizal plants in natural  
**2684** ecosystems: Values obtained using  $^{15}\text{N}$  natural abundance. *Plant Ecology*  
**2685** and *Diversity* 4(2-3), 117–130.
- 2686** Arndal, M. F., A. Tolver, K. S. Larsen, C. Beier, and I. K. Schmidt (2018). Fine  
**2687** root growth and vertical distribution in response to elevated CO<sub>2</sub>, warming  
**2688** and drought in a mixed heathland–grassland. *Ecosystems* 21(1), 15–30.
- 2689** Arnone, J. A. (1997). Indices of plant N availability in an alpine grassland under  
**2690** elevated atmospheric CO<sub>2</sub>. *Plant and Soil* 190(1), 61–66.
- 2691** Arora, V. K., A. Katavouta, R. G. Williams, C. D. Jones, V. Brovkin,  
**2692** P. Friedlingstein, J. Schwinger, L. Bopp, O. Boucher, P. Cadule, M. A.  
**2693** Chamberlain, J. R. Christian, C. Delire, R. A. Fisher, T. Hajima, T. Ilyina,  
**2694** E. Joetzjer, M. Kawamiya, C. D. Koven, J. P. Krasting, R. M. Law, D. M.  
**2695** Lawrence, A. Lenton, K. Lindsay, J. Pongratz, T. Raddatz, R. Séférian,  
**2696** K. Tachiiri, J. F. Tjiputra, A. Wiltshire, T. Wu, and T. Ziehn (2020).  
**2697** Carbon-concentration and carbon-climate feedbacks in CMIP6 models and  
**2698** their comparison to CMIP5 models. *Biogeosciences* 17(16), 4173–4222.

- 2699** Bae, K., T. J. Fahey, R. D. Yanai, and M. Fisk (2015). Soil nitrogen availability affects belowground carbon allocation and soil respiration in northern hardwood forests of New Hampshire. *Ecosystems* 18(7), 1179–1191.
- 2700**
- 2701**
- 2702** Barber, S. A. (1962). A diffusion and mass-flow concept of soil nutrient availability. *Soil Science* 93(1), 39–49.
- 2703**
- 2704** Barnes, J. D., L. Balaguer, E. Manrique, S. Elvira, and A. W. Davison (1992).
- 2705** A reappraisal of the use of DMSO for the extraction and determination
- 2706** of chlorophylls a and b in lichens and higher plants. *Environmental and*
- 2707** *Experimental Botany* 32(2), 85–100.
- 2708** Bates, D., M. Mächler, B. Bolker, and S. Walker (2015). Fitting linear mixed-
- 2709** effects models using lme4. *Journal of Statistical Software* 67(1), 1–48.
- 2710** Beaudette, D., J. Skovlin, S. Roeker, and A. Brown (2022). soilDB: Soil
- 2711** Database Interface.
- 2712** Bengtson, P., J. Barker, and S. J. Grayston (2012). Evidence of a strong cou-
- 2713** pling between root exudation, C and N availability, and stimulated SOM
- 2714** decomposition caused by rhizosphere priming effects. *Ecology and Evolu-*
- 2715** *tion* 93(8), 1843–1852.
- 2716** Bernacchi, C. J., E. L. Singsaas, C. Pimentel, A. R. Portis, and S. P. Long
- 2717** (2001). Improved temperature response functions for models of Rubisco-
- 2718** limited photosynthesis. *Plant, Cell and Environment* 24(2), 253–259.
- 2719** Bialic-Murphy, L., N. G. Smith, P. Voothuluru, R. M. McElderry, M. D.
- 2720** Roche, S. T. Cassidy, S. N. Kivlin, and S. Kalisz (2021). Invasion-induced
- 2721** root–fungal disruptions alter plant water and nitrogen economies. *Ecology*

- 2722** *Letters* 24(6), 1145–1156.
- 2723** Bloom, A. J., F. S. Chapin, and H. A. Mooney (1985). Resource limitation
- 2724** in plants - an economic analogy. *Annual Review of Ecology and Systematics* 16(1), 363–392.
- 2725**
- 2726** Bloomfield, K. J., B. D. Stocker, T. F. Keenan, and I. C. Prentice (2023).
- 2727** Environmental controls on the light use efficiency of terrestrial gross primary
- 2728** production. *Global Change Biology* 29(4), 0–2.
- 2729** Bonan, G. B., M. D. Hartman, W. J. Parton, and W. R. Wieder (2013). Evalu-
- 2730** ating litter decomposition in earth system models with long-term litter
- 2731** bag experiments: an example using the Community Land Model version 4
- 2732** (CLM4). *Global Change Biology* 19(3), 957–974.
- 2733** Bonan, G. B., P. J. Lawrence, K. W. Oleson, S. Levis, M. Jung, M. Reich-
- 2734** stein, D. M. Lawrence, and S. C. Swenson (2011). Improving canopy pro-
- 2735** cesses in the Community Land Model version 4 (CLM4) using global flux
- 2736** fields empirically inferred from FLUXNET data. *Journal of Geophysical Re-*
- 2737** *search* 116(G2), G02014.
- 2738** Booth, B. B. B., C. D. Jones, M. Collins, I. J. Totterdell, P. M. Cox, S. Sitch,
- 2739** C. Huntingford, R. A. Betts, G. R. Harris, and J. Lloyd (2012). High sen-
- 2740** sitivity of future global warming to land carbon cycle processes. *Environ-*
- 2741** *mental Research Letters* 7(2), 024002.
- 2742** Borer, E. T., W. S. Harpole, P. B. Adler, E. M. Lind, J. L. Orrock, E. W.
- 2743** Seabloom, and M. D. Smith (2014). Finding generality in ecology: A model
- 2744** for globally distributed experiments. *Methods in Ecology and Evolution* 5(1),
- 2745** 65–73.

- 2746** Braghieri, R. K., J. B. Fisher, K. Allen, E. Brzostek, M. Shi, X. Yang, D. M.
- 2747** Ricciuto, R. A. Fisher, Q. Zhu, and R. P. Phillips (2022). Modeling global
- 2748** carbon costs of plant nitrogen and phosphorus acquisition. *Journal of Ad-*
- 2749** *vances in Modeling Earth Systems* 14(8), 1–23.
- 2750** Brix, H. (1971). Effects of nitrogen fertilization on photosynthesis and respi-
- 2751** ration in Douglas-fir. *Forest Science* 17(4), 407–414.
- 2752** Brzostek, E. R., J. B. Fisher, and R. P. Phillips (2014). Modeling the carbon
- 2753** cost of plant nitrogen acquisition: Mycorrhizal trade-offs and multipath
- 2754** resistance uptake improve predictions of retranslocation. *Journal of Geo-*
- 2755** *physical Research: Biogeosciences* 119, 1684–1697.
- 2756** Bubier, J. L., R. Smith, S. Juutinen, T. R. Moore, R. Minocha, S. Long, and
- 2757** S. Minocha (2011). Effects of nutrient addition on leaf chemistry, morphol-
- 2758** ogy, and photosynthetic capacity of three bog shrubs. *Oecologia* 167(2),
- 2759** 355–368.
- 2760** Cernusak, L. A., N. Ubierna, K. Winter, J. A. M. Holtum, J. D. Marshall, and
- 2761** G. D. Farquhar (2013). Environmental and physiological determinants of
- 2762** carbon isotope discrimination in terrestrial plants. *New Phytologist* 200(4),
- 2763** 950–965.
- 2764** Chen, J.-L., J. F. Reynolds, P. C. Harley, and J. D. Tenhunen (1993). Coor-
- 2765** dination theory of leaf nitrogen distribution in a canopy. *Oecologia* 93(1),
- 2766** 63–69.
- 2767** Clark, D. B., L. M. Mercado, S. Sitch, C. D. Jones, N. Gedney, M. J. Best,
- 2768** M. Pryor, G. G. Rooney, R. L. H. Essery, E. Blyth, O. Boucher, R. J.
- 2769** Harding, C. Huntingford, and P. M. Cox (2011). The Joint UK Land Envi-

- 2770** ronment Simulator (JULES), model description. Part 2: Carbon fluxes and  
**2771** vegetation dynamics. *Geoscientific Model Development* 4(3), 701–722.
- 2772** Cornwell, W. K., J. H. C. Cornelissen, K. Amatangelo, E. Dorrepaal, V. T.  
**2773** Eviner, O. Godoy, S. E. Hobbie, B. Hoorens, H. Kurokawa, N. Pérez-  
**2774** Harguindeguy, H. M. Quested, L. S. Santiago, D. A. Wardle, I. J. Wright,  
**2775** R. Aerts, S. D. Allison, P. van Bodegom, V. Brovkin, A. Chatain, T. V.  
**2776** Callaghan, S. Díaz, E. Garnier, D. E. Gurvich, E. Kazakou, J. A. Klein,  
**2777** J. Read, P. B. Reich, N. A. Soudzilovskaia, M. V. Vaieretti, and M. Westoby  
**2778** (2008). Plant species traits are the predominant control on litter decompo-  
**2779** sition rates within biomes worldwide. *Ecology Letters* 11(10), 1065–1071.
- 2780** Cornwell, W. K., I. J. Wright, J. Turner, V. Maire, M. M. Barbour, L. A.  
**2781** Cernusak, T. E. Dawson, D. S. Ellsworth, G. D. Farquhar, H. Griffiths,  
**2782** C. Keitel, A. Knohl, P. B. Reich, D. G. Williams, R. Bhaskar, J. H. C. Cor-  
**2783** nelissen, A. Richards, S. Schmidt, F. Valladares, C. Körner, E.-D. Schulze,  
**2784** N. Buchmann, and L. S. Santiago (2018). Climate and soils together regulate  
**2785** photosynthetic carbon isotope discrimination within C<sub>3</sub> plants worldwide.  
**2786** *Global Ecology and Biogeography* 27(9), 1056–1067.
- 2787** Cramer, W. and I. C. Prentice (1988). Simulation of regional soil moisture  
**2788** deficits on a European scale. *Norsk Geografisk Tidsskrift - Norwegian Jour-  
**2789** nal of Geography* 42(2-3), 149–151.
- 2790** Curtis, P. S. (1996). A meta-analysis of leaf gas exchange and nitrogen in trees  
**2791** grown under elevated carbon dioxide. *Plant, Cell and Environment* 19(2),  
**2792** 127–137.
- 2793** Daly, C., M. Halbleib, J. I. Smith, W. P. Gibson, M. K. Doggett, G. H. Taylor,

- 2794** J. Curtis, and P. P. Pasteris (2008). Physiographically sensitive mapping  
**2795** of climatological temperature and precipitation across the conterminous  
**2796** United States. *International Journal of Climatology* 28(15), 2031–2064.
- 2797** Davies-Barnard, T., J. Meyerholt, S. Zaehle, P. Friedlingstein, V. Brovkin,  
**2798** Y. Fan, R. A. Fisher, C. D. Jones, H. Lee, D. Peano, B. Smith, D. Wårlind,  
**2799** and A. J. Wiltshire (2020). Nitrogen cycling in CMIP6 land surface models:  
**2800** progress and limitations. *Biogeosciences* 17(20), 5129–5148.
- 2801** Davis, T. W., I. C. Prentice, B. D. Stocker, R. T. Thomas, R. J. Whitley,  
**2802** H. Wang, B. J. Evans, A. V. Gallego-Sala, M. T. Sykes, and W. Cramer  
**2803** (2017). Simple process-led algorithms for simulating habitats (SPLASH  
**2804** v.1.0): robust indices of radiation, evapotranspiration and plant-available  
**2805** moisture. *Geoscientific Model Development* 10, 689–708.
- 2806** Delaire, M., E. Frak, M. Sigogne, B. Adam, F. Beaujard, and X. Le Roux  
**2807** (2005). Sudden increase in atmospheric CO<sub>2</sub> concentration reveals strong  
**2808** coupling between shoot carbon uptake and root nutrient uptake in young  
**2809** walnut trees. *Tree Physiology* 25(2), 229–235.
- 2810** Doane, T. A. and W. R. Horwáth (2003). Spectrophotometric determination of  
**2811** nitrate with a single reagent. *Analytical Letters* 36(12), 2713–2722.
- 2812** Dong, N., I. C. Prentice, B. J. Evans, S. Caddy-Retalic, A. J. Lowe, and I. J.  
**2813** Wright (2017). Leaf nitrogen from first principles: field evidence for adaptive  
**2814** variation with climate. *Biogeosciences* 14(2), 481–495.
- 2815** Dong, N., I. C. Prentice, I. J. Wright, B. J. Evans, H. F. Togashi, S. Caddy-  
**2816** Retalic, F. A. McInerney, B. Sparrow, E. Leitch, and A. J. Lowe (2020).  
**2817** Components of leaf-trait variation along environmental gradients. *New Phy-*

- 2818** *tologist* 228(1), 82–94.
- 2819** Dong, N., I. C. Prentice, I. J. Wright, H. Wang, O. K. Atkin, K. J. Bloomfield,  
**2820** T. F. Domingues, S. M. Gleason, V. Maire, Y. Onoda, H. Poorter, and N. G.  
**2821** Smith (2022). Leaf nitrogen from the perspective of optimal plant function.  
**2822** *Journal of Ecology* 110(11), 2585–2602.
- 2823** Dong, N., I. J. Wright, J. M. Chen, X. Luo, H. Wang, T. F. Keenan, N. G.  
**2824** Smith, and I. C. Prentice (2022). Rising CO<sub>2</sub> and warming reduce global  
**2825** canopy demand for nitrogen. *New Phytologist* 235(5), 1692–1700.
- 2826** Dovrat, G., H. Bakhshian, T. Masci, and E. Sheffer (2020). The nitrogen eco-  
**2827** nomic spectrum of legume stoichiometry and fixation strategy. *New Phytol-  
ogist* 227(2), 365–375.
- 2829** Dovrat, G., T. Masci, H. Bakhshian, E. Mayzlish Gati, S. Golan, and E. Shef-  
**2830** fer (2018). Drought-adapted plants dramatically downregulate dinitrogen  
**2831** fixation: Evidences from Mediterranean legume shrubs. *Journal of Ecol-  
ogy* 106(4), 1534–1544.
- 2833** Drake, B. G., M. A. Gonzàlez-Meler, and S. P. Long (1997). More efficient  
**2834** plants: a consequence of rising atmospheric CO<sub>2</sub>? *Annual Review of Plant  
Biology* 48, 609–639.
- 2836** Duursma, R. A. (2015). Plantecophys - An R Package for Analyzing and Mod-  
**2837** elling Leaf Gas Exchange Data. *PLOS ONE* 10(11), e0143346.
- 2838** Eastman, B. A., M. B. Adams, E. R. Brzostek, M. B. Burnham, J. E. Carrara,  
**2839** C. Kelly, B. E. McNeil, C. A. Walter, and W. T. Peterjohn (2021). Altered  
**2840** plant carbon partitioning enhanced forest ecosystem carbon storage after 25

- 2841 years of nitrogen additions. *New Phytologist* 230(4), 1435–1448.
- 2842 Ellsworth, D. S. and P. B. Reich (1996). Photosynthesis and leaf nitrogen in five
- 2843 Amazonian tree species during early secondary succession. *Ecology* 77(2),
- 2844 581–594.
- 2845 Espelta, J. M., P. Cortés, M. Mangirón, and J. Retana (2005). Differences in
- 2846 biomass partitioning, leaf nitrogen content, and water use efficiency d13C
- 2847 result in similar performance of seedlings of two Mediterranean oaks with
- 2848 contrasting leaf habit. *Ecoscience* 12(4), 447–454.
- 2849 Evans, J. R. (1989). Photosynthesis and nitrogen relationships in leaves of C<sub>3</sub>
- 2850 plants. *Oecologia* 78(1), 9–19.
- 2851 Evans, J. R. and V. C. Clarke (2019). The nitrogen cost of photosynthesis.
- 2852 *Journal of Experimental Botany* 70(1), 7–15.
- 2853 Evans, J. R. and H. Poorter (2001). Photosynthetic acclimation of plants to
- 2854 growth irradiance: the relative importance of specific leaf area and nitrogen
- 2855 partitioning in maximizing carbon gain. *Plant, Cell and Environment* 24(8),
- 2856 755–767.
- 2857 Evans, J. R. and J. R. Seemann (1989). The allocation of protein nitrogen in
- 2858 the photosynthetic apparatus: costs, consequences, and control. *Photosyn-*
- 2859 *thesis* 8, 183–205.
- 2860 Exbrayat, J.-F., A. A. Bloom, P. Falloon, A. Ito, T. L. Smallman, and
- 2861 M. Williams (2018). Reliability ensemble averaging of 21<sup>st</sup> century projec-
- 2862 tions of terrestrial net primary productivity reduces global and regional
- 2863 uncertainties. *Earth System Dynamics* 9(1), 153–165.

- 2864 Farquhar, G. D., J. R. Ehleringer, and K. T. Hubick (1989). Carbon Isotope  
2865 Discrimination and Photosynthesis. *Annual Review of Plant Physiology and*  
2866 *Plant Molecular Biology* 40(1), 503–537.
- 2867 Farquhar, G. D. and T. D. Sharkey (1982). Stomatal conductance and photo-  
2868 synthesis. *Annual Review of Plant Physiology* 33(1), 317–345.
- 2869 Farquhar, G. D., S. von Caemmerer, and J. A. Berry (1980). A biochemical  
2870 model of photosynthetic CO<sub>2</sub> assimilation in leaves of C<sub>3</sub> species.  
2871 *Planta* 149(1), 78–90.
- 2872 Fay, P. A., S. M. Prober, W. S. Harpole, J. M. H. Knops, J. D. Bakker, E. T.  
2873 Borer, E. M. Lind, A. S. MacDougall, E. W. Seabloom, P. D. Wragg, P. B.  
2874 Adler, D. M. Blumenthal, Y. M. Buckley, C. Chu, E. E. Cleland, S. L.  
2875 Collins, K. F. Davies, G. Du, X. Feng, J. Firn, D. S. Gruner, N. Hagenah,  
2876 Y. Hautier, R. W. Heckman, V. L. Jin, K. P. Kirkman, J. A. Klein, L. M.  
2877 Ladwig, Q. Li, R. L. McCulley, B. A. Melbourne, C. E. Mitchell, J. L. Moore,  
2878 J. W. Morgan, A. C. Risch, M. Schütz, C. J. Stevens, D. A. Wedin, and  
2879 L. H. Yang (2015). Grassland productivity limited by multiple nutrients.  
2880 *Nature Plants* 1(7), 15080.
- 2881 Feng, X. (1999). Trends in intrinsic water-use efficiency of natural trees for the  
2882 past 100-200 years: A response to atmospheric CO<sub>2</sub> concentration. *Geochim-  
2883 ica et Cosmochimica Acta* 63(13-14), 1891–1903.
- 2884 Field, C. B. and H. A. Mooney (1986). The photosynthesis-nitrogen relationship  
2885 in wild plants. In T. J. Givnish (Ed.), *On the Economy of Plant Form and*  
2886 *Function*, pp. 25–55. Cambridge: Cambridge University Press.
- 2887 Finzi, A. C., D. J. P. Moore, E. H. DeLucia, J. Lichter, K. S. Hofmockel, R. B.

- 2888 Jackson, H. S. Kim, R. Matamala, H. R. McCarthy, R. Oren, J. S. Pippen,  
2889 and W. H. Schlesinger (2006). Progressive nitrogen limitation of ecosystem  
2890 processes under elevated CO<sub>2</sub> in a warm-temperate forest. *Ecology* 87(1),  
2891 15–25.
- 2892 Firn, J., J. M. McGree, E. Harvey, H. Flores Moreno, M. Schutz, Y. M. Buckley,  
2893 E. T. Borer, E. W. Seabloom, K. J. La Pierre, A. M. MacDougall, S. M.  
2894 Prober, C. J. Stevens, L. L. Sullivan, E. Porter, E. Ladouceur, C. Allen,  
2895 K. H. Moromizato, J. W. Morgan, W. S. Harpole, Y. Hautier, N. Eisen-  
2896 hauer, J. P. Wright, P. B. Adler, C. A. Arnillas, J. D. Bakker, L. Biederman,  
2897 A. A. D. Broadbent, C. S. Brown, M. N. Bugalho, M. C. Caldeira, E. E. Cle-  
2898 land, A. Ebeling, P. A. Fay, N. Hagenah, A. R. Kleinhesselink, R. Mitchell,  
2899 J. L. Moore, C. Nogueira, P. L. Peri, C. Roscher, M. D. Smith, P. D. Wragg,  
2900 and A. C. Risch (2019). Leaf nutrients, not specific leaf area, are consistent  
2901 indicators of elevated nutrient inputs. *Nature Ecology and Evolution* 3(3),  
2902 400–406.
- 2903 Fisher, J. B., S. Sitch, Y. Malhi, R. A. Fisher, C. Huntingford, and S.-Y. Tan  
2904 (2010). Carbon cost of plant nitrogen acquisition: A mechanistic, globally  
2905 applicable model of plant nitrogen uptake, retranslocation, and fixation.  
2906 *Global Biogeochemical Cycles* 24(1), 1–17.
- 2907 Fox, J. and S. Weisberg (2019). *An R companion to applied regression* (Third  
2908 edit ed.). Thousand Oaks, California: Sage.
- 2909 Franklin, O., R. E. McMurtrie, C. M. Iversen, K. Y. Crous, A. C. Finzi, D. Tis-  
2910 sue, D. S. Ellsworth, R. Oren, and R. J. Norby (2009). Forest fine-root  
2911 production and nitrogen use under elevated CO<sub>2</sub>: contrasting responses

- 2912** in evergreen and deciduous trees explained by a common principle. *Global  
2913 Change Biology* 15(1), 132–144.
- 2914** Friedlingstein, P., M. Meinshausen, V. K. Arora, C. D. Jones, A. Anav, S. K.  
**2915** Liddicoat, and R. Knutti (2014). Uncertainties in CMIP5 climate projections  
**2916** due to carbon cycle feedbacks. *Journal of Climate* 27(2), 511–526.
- 2917** Friel, C. A. and M. L. Friesen (2019). Legumes modulate allocation to rhizobial  
**2918** nitrogen fixation in response to factorial light and nitrogen manipulation.  
**2919** *Frontiers in Plant Science* 10, 1316.
- 2920** Fujikake, H., A. Yamazaki, N. Ohtake, K. Sueoshi, S. Matsuhashi, T. Ito,  
**2921** C. Mizuniwa, T. Kume, S. Hoshimoto, N.-S. Ishioka, S. Watanabe, A. Osa,  
**2922** T. Sekine, H. Uchida, A. Tsuji, and T. Ohyama (2003). Quick and reversible  
**2923** inhibition of soybean root nodule growth by nitrate involves a decrease in  
**2924** sucrose supply to nodules. *Journal of Experimental Botany* 54(386), 1379–  
**2925** 1388.
- 2926** Ghannoum, O., J. R. Evans, and S. von Caemmerer (2011). Nitrogen and water  
**2927** use efficiency of C<sub>4</sub> plants. In A. S. Raghavendra and R. F. Sage (Eds.), *C<sub>4</sub>  
2928 Photosynthesis and Related CO<sub>2</sub> Concentrating Mechanisms*, Chapter 8, pp.  
**2929** 129–146. Springer.
- 2930** Ghimire, B., W. J. Riley, C. D. Koven, J. Kattge, A. Rogers, P. B. Reich, and  
**2931** I. J. Wright (2017). A global trait-based approach to estimate leaf nitrogen  
**2932** functional allocation from observations:. *Ecological Applications* 27(5),  
**2933** 1421–1434.
- 2934** Giardina, C. P., M. D. Coleman, J. E. Hancock, J. S. King, E. A. Lilleskov,  
**2935** W. M. Loya, K. S. Pregitzer, M. G. Ryan, and C. C. Trettin (2005). The

- 2936 response of belowground carbon allocation in forests to global change. In  
2937 D. Binkley and O. Manyailo (Eds.), *Tree Species Effects on Soils: Implications for Global Change* (Volume 55 ed.), Chapter Chapter 7, pp. 119–154.  
2938 Berlin/Heidelberg: Springer-Verlag.
- 2939
- 2940 Gibson, A. H. and J. E. Harper (1985). Nitrate effect on nodulation of soybean  
2941 by *Bradyrhizobium japonicum*. *Crop Science* 25(3), 497–501.
- 2942 Gill, A. L. and A. C. Finzi (2016). Belowground carbon flux links biogeochemical  
2943 cycles and resource-use efficiency at the global scale. *Ecology Letters* 19(12),  
2944 1419–1428.
- 2945 Goll, D. S., V. Brovkin, B. R. Parida, C. H. Reick, J. Kattge, P. B. Reich, P. M.  
2946 van Bodegom, and Ü. Niinemets (2012). Nutrient limitation reduces land  
2947 carbon uptake in simulations with a model of combined carbon, nitrogen  
2948 and phosphorus cycling. *Biogeosciences Discussions* 9(3), 3173–3232.
- 2949 Gregory, L. M., A. M. McClain, D. M. Kramer, J. D. Pardo, K. E. Smith, O. L.  
2950 Tessmer, B. J. Walker, L. G. Ziccardi, and T. D. Sharkey (2021, oct). The  
2951 triose phosphate utilization limitation of photosynthetic rate: Out of global  
2952 models but important for leaf models. *Plant, Cell and Environment* 44(10),  
2953 3223–3226.
- 2954 Grossiord, C., T. N. Buckley, L. A. Cernusak, K. A. Novick, B. Poulter, R. T. W.  
2955 Siegwolf, J. S. Sperry, and N. G. McDowell (2020). Plant responses to rising  
2956 vapor pressure deficit. *New Phytologist* 226(6), 1550–1566.
- 2957 Guerrieri, R., M. Mencuccini, L. J. Sheppard, M. Saurer, M. P. Perks, P. Levy,  
2958 M. A. Sutton, M. Borghetti, and J. Grace (2011). The legacy of enhanced  
2959 N and S deposition as revealed by the combined analysis of  $\delta^{13}\text{C}$ ,  $\delta^{18}\text{O}$  and

- 2960**  $\delta^{15}\text{N}$  in tree rings. *Global Change Biology* 17(5), 1946–1962.
- 2961** Gulmon, S. L. and C. C. Chu (1981). The effects of light and nitrogen on photo-
- 2962** synthesis, leaf characteristics, and dry matter allocation in the chaparral
- 2963** shrub, *<i>Diplacus aurantiacus</i>*. *Oecologia* 49(2), 207–212.
- 2964** Gutschick, V. P. (1981). Evolved strategies in nitrogen acquisition by plants.
- 2965** *The American Naturalist* 118(5), 607–637.
- 2966** Hallik, L., Ü. Niinemets, and I. J. Wright (2009). Are species shade and drought
- 2967** tolerance reflected in leaf-level structural and functional differentiation in
- 2968** Northern Hemisphere temperate woody flora? *New Phytologist* 184(1), 257–
- 2969** 274.
- 2970** Harrison, M. T., E. J. Edwards, G. D. Farquhar, A. B. Nicotra, and J. R.
- 2971** Evans (2009). Nitrogen in cell walls of sclerophyllous leaves accounts for
- 2972** little of the variation in photosynthetic nitrogen-use efficiency. *Plant, Cell*
- 2973** and *Environment* 32(3), 259–270.
- 2974** Harrison, S. P., W. Cramer, O. Franklin, I. C. Prentice, H. Wang,
- 2975** Å. Brännström, H. de Boer, U. Dieckmann, J. Joshi, T. F. Keenan,
- 2976** A. Lavergne, S. Manzoni, G. Mengoli, C. Morfopoulos, J. Peñuelas,
- 2977** S. Pietsch, K. T. Rebel, Y. Ryu, N. G. Smith, B. D. Stocker, and I. J.
- 2978** Wright (2021). Eco-evolutionary optimality as a means to improve vegeta-
- 2979** tion and land-surface models. *New Phytologist* 231(6), 2125–2141.
- 2980** Henneron, L., P. Kardol, D. A. Wardle, C. Cros, and S. Fontaine (2020). Rhizo-
- 2981** sphere control of soil nitrogen cycling: a key component of plant economic
- 2982** strategies. *New Phytologist* 228(4), 1269–1282.

- 2983** Hijmans, R. J. (2022). *terra: Spatial Data Analysis*.
- 2984** Hikosaka, K. and A. Shigeno (2009). The role of Rubisco and cell walls in the  
**2985** interspecific variation in photosynthetic capacity. *Oecologia* 160(3), 443–  
**2986** 451.
- 2987** Hoagland, D. R. and D. I. Arnon (1950). The water culture method for growing  
**2988** plants without soil. *California Agricultural Experiment Station: 347* 347(2),  
**2989** 1–32.
- 2990** Hobbie, E. A. (2006). Carbon allocation to ectomycorrhizal fungi correlates  
**2991** with belowground allocation in culture studies. *Ecology* 87(3), 563–569.
- 2992** Hobbie, E. A. and J. E. Hobbie (2008). Natural abundance of  $^{15}\text{N}$  in nitrogen-  
**2993** limited forests and tundra can estimate nitrogen cycling through mycorrhizal  
**2994** fungi: a review. *Ecosystems* 11(5), 815–830.
- 2995** Hoek, T. A., K. Axelrod, T. Biancalani, E. A. Yurtsev, J. Liu, and J. Gore  
**2996** (2016). Resource availability modulates the cooperative and competitive na-  
**2997** nature of a microbial cross-feeding mutualism. *PLOS Biology* 14(8), e1002540.
- 2998** Höglberg, M. N., M. J. I. Briones, S. G. Keel, D. B. Metcalfe, C. Campbell, A. J.  
**2999** Midwood, B. Thornton, V. Hurry, S. Linder, T. Näsholm, and P. Höglberg  
**3000** (2010). Quantification of effects of season and nitrogen supply on tree below-  
**3001** ground carbon transfer to ectomycorrhizal fungi and other soil organisms in  
**3002** a boreal pine forest. *New Phytologist* 187(2), 485–493.
- 3003** Höglberg, P., M. N. Höglberg, S. G. Göttlicher, N. R. Betson, S. G. Keel, D. B.  
**3004** Metcalfe, C. Campbell, A. Schindlbacher, V. Hurry, T. Lundmark, S. Linder,  
**3005** and T. Näsholm (2008). High temporal resolution tracing of photosynthate

- 3006** carbon from the tree canopy to forest soil microorganisms. *New Phytologist* 177(1), 220–228.
- 3007**
- 3008** Houlton, B. Z., Y.-P. Wang, P. M. Vitousek, and C. B. Field (2008). A unifying framework for dinitrogen fixation in the terrestrial biosphere. *Nature* 454(7202), 327–330.
- 3009**
- 3010**
- 3011** Huber, M. L., R. A. Perkins, A. Laesecke, D. G. Friend, J. V. Sengers, M. J.
- 3012** Assael, I. N. Metaxa, E. Vogel, R. Mareš, and K. Miyagawa (2009). New
- 3013** international formulation for the viscosity of H<sub>2</sub>O. *Journal of Physical and*
- 3014** *Chemical Reference Data* 38(2), 101–125.
- 3015** Hungate, B. A., J. S. Dukes, M. R. Shaw, Y. Luo, and C. B. Field (2003).
- 3016** Nitrogen and climate change. *Science* 302(5650), 1512–1513.
- 3017** IPCC (2021). *Climate Change 2021: The Physical Science Basis. Contribution*
- 3018** *of Working Group I to the Sixth Assessment Report of the Intergovernmental*
- 3019** *Panel on Climate Change*, Volume In Press. Cambridge, United Kingdom
- 3020** and New York, NY, USA: Cambridge University Press.
- 3021** Johnson, N. C., J. H. Graham, and F. A. Smith (1997). Functioning of mycor-
- 3022** rhizal associations along the mutualism-parasitism continuum. *New Phytologist* 135(4), 575–585.
- 3023**
- 3024** Kachurina, O. M., H. Zhang, W. R. Raun, and E. G. Krenzer (2000). Simulta-
- 3025** neous determination of soil aluminum, ammonium- and nitrate- nitrogen
- 3026** using 1 M potassium chloride. *Communications in Soil Science and Plant*
- 3027** *Analysis* 31(7-8), 893–903.
- 3028** Kaiser, C., M. R. Kilburn, P. L. Clode, L. Fuchslueger, M. Koranda, J. B. Cliff,

- 3029** Z. M. Solaiman, and D. V. Murphy (2015). Exploring the transfer of recent  
**3030** plant photosynthates to soil microbes: mycorrhizal pathway vs direct root  
**3031** exudation. *New Phytologist* 205(4), 1537–1551.
- 3032** Katabuchi, M. (2015). LeafArea: An R package for rapid digital analysis of leaf  
**3033** area. *Ecological Research* 30(6), 1073–1077.
- 3034** Kattge, J. and W. Knorr (2007). Temperature acclimation in a biochemical  
**3035** model of photosynthesis: a reanalysis of data from 36 species. *Plant, Cell*  
**3036** and *Environment* 30(9), 1176–1190.
- 3037** Kattge, J., W. Knorr, T. Raddatz, and C. Wirth (2009). Quantifying photosyn-  
**3038** thetic capacity and its relationship to leaf nitrogen content for global-scale  
**3039** terrestrial biosphere models. *Global Change Biology* 15(4), 976–991.
- 3040** Kayler, Z., A. Gessler, and N. Buchmann (2010). What is the speed of link  
**3041** between aboveground and belowground processes? *New Phytologist* 187(4),  
**3042** 885–888.
- 3043** Kayler, Z., C. Keitel, K. Jansen, and A. Gessler (2017). Experimental evi-  
**3044** dence of two mechanisms coupling leaf-level C assimilation to rhizosphere  
**3045** CO<sub>2</sub> release. *Environmental and Experimental Botany* 135,  
**3046** 21–26.
- 3047** Keeling, C. D., W. G. Mook, and P. P. Tans (1979, jan). Recent trends in the  
**3048** <sup>13</sup>C/<sup>12</sup>C ratio of atmospheric carbon dioxide.  
**3049** *Nature* 277(5692), 121–123.
- 3050** Kenward, M. G. and J. H. Roger (1997). Small sample inference for fixed effects  
**3051** from restricted maximum likelihood. *Biometrics* 53(3), 983.

- 3052** Knapp, A. K., M. L. Avolio, C. Beier, C. J. W. Carroll, S. L. Collins, J. S.  
**3053** Dukes, L. H. Fraser, R. J. Griffin-Nolan, D. L. Hoover, A. Jentsch, M. E.  
**3054** Loik, R. P. Phillips, A. K. Post, O. E. Sala, I. J. Slette, L. Yahdjian, and  
**3055** M. D. Smith (2017). Pushing precipitation to the extremes in distributed  
**3056** experiments: recommendations for simulating wet and dry years. *Global  
Change Biology* 23(5), 1774–1782.
- 3058** Knorr, W. (2000). Annual and interannual CO<sub>2</sub> exchanges of the  
**3059** terrestrial biosphere: process-based simulations and uncertainties. *Global  
3060 Ecology and Biogeography* 9(3), 225–252.
- 3061** Knorr, W. and M. Heimann (2001). Uncertainties in global terrestrial biosphere  
**3062** modeling: 1. A comprehensive sensitivity analysis with a new photosynthesis  
**3063** and energy balance scheme. *Global Biogeochemical Cycles* 15(1), 207–225.
- 3064** Kulmatiski, A., P. B. Adler, J. M. Stark, and A. T. Tredennick (2017). Water  
**3065** and nitrogen uptake are better associated with resource availability than  
**3066** root biomass. *Ecosphere* 8(3), e01738.
- 3067** Lavergne, A., D. Sandoval, V. J. Hare, H. Graven, and I. C. Prentice (2020).  
**3068** Impacts of soil water stress on the acclimated stomatal limitation of pho-  
**3069** tosynthesis: Insights from stable carbon isotope data. *Global Change Biol-  
ogy* 26(12), 7158–7172.
- 3071** Lawrence, D. M., R. A. Fisher, C. D. Koven, K. W. Oleson, S. C. Swen-  
**3072** son, G. B. Bonan, N. Collier, B. Ghimire, L. Kampenhout, D. Kennedy,  
**3073** E. Kluzek, P. J. Lawrence, F. Li, H. Li, D. L. Lombardozzi, W. J. Riley,  
**3074** W. J. Sacks, M. Shi, M. Vertenstein, W. R. Wieder, C. Xu, A. A. Ali,  
**3075** A. M. Badger, G. Bisht, M. Broeke, M. A. Brunke, S. P. Burns, J. Buzan,

- 3076** M. Clark, A. Craig, K. M. Dahlin, B. Drewniak, J. B. Fisher, M. Flanner,  
**3077** A. M. Fox, P. Gentine, F. M. Hoffman, G. Keppel-Aleks, R. Knox, S. Ku-  
**3078** mar, J. Lenaerts, L. R. Leung, W. H. Lipscomb, Y. Lu, A. Pandey, J. D.  
**3079** Pelletier, J. Perket, J. T. Randerson, D. M. Ricciuto, B. M. Sanderson,  
**3080** A. Slater, Z. M. Subin, J. Tang, R. Q. Thomas, M. Val Martin, and X. Zeng  
**3081** (2019). The Community Land Model Version 5: description of new features,  
**3082** benchmarking, and impact of forcing uncertainty. *Journal of Advances in*  
**3083** *Modeling Earth Systems* 11(12), 4245–4287.
- 3084** LeBauer, D. S. and K. K. Treseder (2008). Nitrogen limitation of net primary  
**3085** productivity. *Ecology* 89(2), 371–379.
- 3086** Lefcheck, J. S. (2016). piecewiseSEM: Piecewise structural equation modelling  
**3087** in r for ecology, evolution, and systematics. *Methods in Ecology and Evolu-*  
**3088** *tion* 7(5), 573–579.
- 3089** Lenth, R. (2019). emmeans: estimated marginal means, aka least-squares  
**3090** means.
- 3091** Li, W., H. Zhang, G. Huang, R. Liu, H. Wu, C. Zhao, and N. G. McDowell  
**3092** (2020). Effects of nitrogen enrichment on tree carbon allocation: A global  
**3093** synthesis. *Global Ecology and Biogeography* 29(3), 573–589.
- 3094** Liang, J., X. Qi, L. Souza, and Y. Luo (2016). Processes regulating progressive  
**3095** nitrogen limitation under elevated carbon dioxide: a meta-analysis. *Biogeosciences*  
**3096** 13(9), 2689–2699.
- 3097** Liang, X., T. Zhang, X. Lu, D. S. Ellsworth, H. BassiriRad, C. You, D. Wang,  
**3098** P. He, Q. Deng, H. Liu, J. Mo, and Q. Ye (2020). Global response patterns of  
**3099** plant photosynthesis to nitrogen addition: A meta-analysis. *Global Change*

- 3100** *Biology* 26(6), 3585–3600.
- 3101** Lu, J., J. Yang, C. Keitel, L. Yin, P. Wang, W. Cheng, and F. A. Dijkstra
- 3102** (2022). Belowground Carbon Efficiency for Nitrogen and Phosphorus Ac-
- 3103** quisition Varies Between *Lolium perenne* and *Trifolium repens* and Depends
- 3104** on Phosphorus Fertilization. *Frontiers in Plant Science* 13, 1–9.
- 3105** Luo, X., T. F. Keenan, J. M. Chen, H. Croft, I. C. Prentice, N. G. Smith,
- 3106** A. P. Walker, H. Wang, R. Wang, C. Xu, and Y. Zhang (2021). Global
- 3107** variation in the fraction of leaf nitrogen allocated to photosynthesis. *Nature*
- 3108** *Communications* 12(1), 4866.
- 3109** Luo, Y., W. S. Currie, J. S. Dukes, A. C. Finzi, U. A. Hartwig, B. A. Hungate,
- 3110** R. E. McMurtrie, R. Oren, W. J. Parton, D. E. Pataki, R. M. Shaw, D. R.
- 3111** Zak, and C. B. Field (2004). Progressive nitrogen limitation of ecosystem
- 3112** responses to rising atmospheric carbon dioxide. *BioScience* 54(8), 731–739.
- 3113** Maire, V., P. Martre, J. Kattge, F. Gastal, G. Esser, S. Fontaine, and J.-F.
- 3114** Soussana (2012). The coordination of leaf photosynthesis links C and N
- 3115** fluxes in C<sub>3</sub> plant species. *PLoS ONE* 7(6), e38345.
- 3116** Makino, A. (2003). Rubisco and nitrogen relationships in rice: leaf photosyn-
- 3117** thesis and plant growth. *Soil Science and Plant Nutrition* 49(3), 319–327.
- 3118** Makino, A., M. Harada, T. Sato, H. Nakano, and T. Mae (1997). Growth and N
- 3119** Allocation in Rice Plants under CO<sub>2</sub> Enrichment. *Plant Physiology* 115(1),
- 3120** 199–203.
- 3121** Markham, J. H. and C. Zekveld (2007). Nitrogen fixation makes biomass al-
- 3122** location to roots independent of soil nitrogen supply. *Canadian Journal of*

- 3123** *Botany* (9), 787–793.
- 3124** Marschner, H. and B. Dell (1994). Nutrient uptake in mycorrhizal symbiosis.
- 3125** *Plant and Soil* 159(1), 89–102.
- 3126** Matamala, R. and W. H. Schlesinger (2000). Effects of elevated atmospheric
- 3127** CO<sub>2</sub> on fine root production and activity in an intact tem-
- 3128** perate forest ecosystem. *Global Change Biology* 6(8), 967–979.
- 3129** Medlyn, B. E., E. Dreyer, D. S. Ellsworth, M. Forstreuter, P. C. Harley,
- 3130** M. U. F. Kirschbaum, X. Le Roux, P. Montpied, J. Strassmeyer, A. Wal-
- 3131** croft, K. Wang, and D. Loustau (2002). Temperature response of parameters
- 3132** of a biochemically based model of photosynthesis. II. A review of experimen-
- 3133** tal data. *Plant, Cell and Environment* 25(9), 1167–1179.
- 3134** Menge, D. N. L., S. A. Levin, and L. O. Hedin (2008). Evolutionary tradeoffs can
- 3135** select against nitrogen fixation and thereby maintain nitrogen limitation.
- 3136** *Proceedings of the National Academy of Sciences* 105(5), 1573–1578.
- 3137** Menne, M. J., I. Durre, R. S. Vose, B. E. Gleason, and T. G. Houston (2012).
- 3138** An overview of the global historical climatology network-daily database.
- 3139** *Journal of Atmospheric and Oceanic Technology* 29(7), 897–910.
- 3140** Meyerholt, J., K. Sickel, and S. Zaehle (2020). Ensemble projections elucidate
- 3141** effects of uncertainty in terrestrial nitrogen limitation on future carbon up-
- 3142** take. *Global Change Biology* 26(7), 3978–3996.
- 3143** Meyerholt, J., S. Zaehle, and M. J. Smith (2016). Variability of pro-
- 3144** jected terrestrial biosphere responses to elevated levels of atmospheric
- 3145** CO<sub>2</sub> due to uncertainty in biological nitrogen fixation. *Bio-*

- 3146** *geosciences* 13(5), 1491–1518.
- 3147** Minocha, R., S. Long, A. H. Magill, J. D. Aber, and W. H. McDowell (2000).
- 3148** Foliar free polyamine and inorganic ion content in relation to soil and soil solution chemistry in two fertilized forest stands at the Harvard Forest,
- 3149** Massachusetts. *Plant and Soil* 222(1-2), 119–137.
- 3150**
- 3151** Moore, D. J., S. Aref, R. M. Ho, J. S. Pippen, J. G. Hamilton, and E. H. De Lucia (2006). Annual basal area increment and growth duration of *Pinus taeda* in response to eight years of free-air carbon dioxide enrichment. *Global Change Biology* 12(8), 1367–1377.
- 3152**
- 3153**
- 3154**
- 3155** Morgan, J. A., D. E. Pataki, C. Körner, H. Clark, S. J. Del Gross, J. M. Grünzweig, A. K. Knapp, A. R. Mosier, P. C. D. Newton, P. A. Niklaus, J. B. Nippert, R. S. Nowak, W. J. Parton, H. W. Polley, and M. R. Shaw (2004). Water relations in grassland and desert ecosystems exposed to elevated atmospheric CO<sub>2</sub>. *Oecologia* 140(1), 11–25.
- 3156**
- 3157**
- 3158**
- 3159**
- 3160** Muñoz, N., X. Qi, M. W. Li, M. Xie, Y. Gao, M. Y. Cheung, F. L. Wong, and H.-M. Lam (2016). Improvement in nitrogen fixation capacity could be part of the domestication process in soybean. *Heredity* 117(2), 84–93.
- 3161**
- 3162**
- 3163** Nadelhoffer, K. J. and J. W. Raich (1992). Fine root production estimates and belowground carbon allocation in forest ecosystems. *Ecology* 73(4), 1139–1147.
- 3164**
- 3165**
- 3166** Niinemets, Ü. and J. D. Tenhunen (1997). A model separating leaf structural and physiological effects on carbon gain along light gradients for the shade-tolerant species *< i>Acer saccharum</i>*. *Plant, Cell and Environment* 20(7), 845–866.
- 3167**
- 3168**
- 3169**

- 3170** Norby, R. J., J. Ledford, C. D. Reilly, N. E. Miller, and E. G. O'Neill  
**3171** (2004). Fine-root production dominates response of a deciduous forest to  
**3172** atmospheric CO<sub>2</sub> enrichment. *Proceedings of the National Academy of Sci-  
ences* 101(26), 9689–9693.
- 3174** Norby, R. J., J. M. Warren, C. M. Iversen, B. E. Medlyn, and R. E. Mc-  
**3175** Murtrie (2010). CO<sub>2</sub> enhancement of forest productivity constrained by  
**3176** limited nitrogen availability. *Proceedings of the National Academy of Sci-  
ences* 107(45), 19368–19373.
- 3178** Novick, K. A., D. L. Ficklin, P. C. Stoy, C. A. Williams, G. Bohrer, A. C.  
**3179** Oishi, S. A. Papuga, P. D. Blanken, A. Noormets, B. N. Sulman, R. L.  
**3180** Scott, L. Wang, and R. P. Phillips (2016). The increasing importance of  
**3181** atmospheric demand for ecosystem water and carbon fluxes. *Nature Climate  
Change* 6(11), 1023–1027.
- 3183** Noyce, G. L., M. L. Kirwan, R. L. Rich, and J. P. Megonigal (2019). Asyn-  
**3184** chronous nitrogen supply and demand produce nonlinear plant allocation  
**3185** responses to warming and elevated CO<sub>2</sub>. *Proceedings of the  
National Academy of Sciences* 116(43), 21623–21628.
- 3187** Onoda, Y., K. Hikosaka, and T. Hirose (2004). Allocation of nitrogen to  
**3188** cell walls decreases photosynthetic nitrogen-use efficiency. *Functional Ecol-  
ogy* 18(3), 419–425.
- 3190** Onoda, Y., I. J. Wright, J. R. Evans, K. Hikosaka, K. Kitajima, Ü. Niinemets,  
**3191** H. Poorter, T. Tosens, and M. Westoby (2017). Physiological and structural  
**3192** trade-offs underlying the leaf economics spectrum. *New Phytologist* 214(4),  
**3193** 1447–1463.

- 3194** Oren, R., J. S. Sperry, G. G. Katul, D. E. Pataki, B. E. Ewers, N. Phillips,  
**3195** and K. V. R. Schäfer (1999). Survey and synthesis of intra- and interspecific  
**3196** variation in stomatal sensitivity to vapor pressure deficit. *Plant, Cell and*  
**3197** *Environment* 22(12), 1515–1526.
- 3198** Oreskes, N., K. Shrader-Frechette, and K. Belitz (1994). Verification, vali-  
**3199** dation, and confirmation of numerical models in the Earth sciences. *Sci-  
3200* *ence* 263(5147), 641–646.
- 3201** Paillassa, J., I. J. Wright, I. C. Prentice, S. Pepin, N. G. Smith, G. Ethier,  
**3202** A. C. Westerband, L. J. Lamarque, H. Wang, W. K. Cornwell, and V. Maire  
**3203** (2020). When and where soil is important to modify the carbon and water  
**3204** economy of leaves. *New Phytologist* 228(1), 121–135.
- 3205** Parvin, S., S. Uddin, S. Tausz Posch, R. Armstrong, and M. Tausz (2020). Car-  
**3206** bon sink strength of nodules but not other organs modulates photosynthesis  
**3207** of faba bean (*Vicia faba*) grown under elevated [CO<sub>2</sub>] and different  
**3208** water supply. *New Phytologist* 227(1), 132–145.
- 3209** Paul, K. I., P. J. Polglase, A. M. O'Connell, J. C. Carlyle, P. J. Smethurst, and  
**3210** P. K. Khanna (2003). Defining the relation between soil water content and  
**3211** net nitrogen mineralization. *European Journal of Soil Science* 54(1), 39–48.
- 3212** Peng, Y., K. J. Bloomfield, L. A. Cernusak, T. F. Domingues, and I. C. Pre-  
**3213** nttice (2021). Global climate and nutrient controls of photosynthetic capacity.  
**3214** *Communications Biology* 4(1), 462.
- 3215** Perkowski, E. A., E. F. Waring, and N. G. Smith (2021). Root mass carbon  
**3216** costs to acquire nitrogen are determined by nitrogen and light availabil-  
**3217** ity in two species with different nitrogen acquisition strategies. *Journal of*

- 3218** *Experimental Botany* 72(15), 5766–5776.
- 3219** Phillips, R. P., E. R. Brzostek, and M. G. Midgley (2013). The mycorrhizal-  
**3220** associated nutrient economy: a new framework for predicting carbon-  
**3221** nutrient couplings in temperate forests. *New Phytologist* 199(1), 41–51.
- 3222** Phillips, R. P., A. C. Finzi, and E. S. Bernhardt (2011). Enhanced root ex-  
**3223** udation induces microbial feedbacks to N cycling in a pine forest under  
**3224** long-term CO<sub>2</sub> fumigation. *Ecology Letters* 14(2), 187–194.
- 3225** Pinheiro, J. and D. Bates (2022). nlme: linear and nonlinear mixed effects  
**3226** models.
- 3227** Poggio, L., L. M. De Sousa, N. H. Batjes, G. B. M. Heuvelink, B. Kempen,  
**3228** E. Ribeiro, and D. Rossiter (2021). SoilGrids 2.0: Producing soil information  
**3229** for the globe with quantified spatial uncertainty. *Soil* 7(1), 217–240.
- 3230** Pons, T. L. and R. W. Pearcy (1994). Nitrogen reallocation and photosynthetic  
**3231** acclimation in response to partial shading in soybean plants. *Physiologia  
3232 Plantarum* 92(4), 636–644.
- 3233** Poorter, H., J. Bühler, D. Van Dusschoten, J. Climent, and J. A. Postma (2012).  
**3234** Pot size matters: A meta-analysis of the effects of rooting volume on plant  
**3235** growth. *Functional Plant Biology* 39(11), 839–850.
- 3236** Poorter, H., O. Knopf, I. J. Wright, A. A. Temme, S. W. Hogewoning, A. Graf,  
**3237** L. A. Cernusak, and T. L. Pons (2022). A meta-analysis of responses of C<sub>3</sub>  
**3238** plants to atmospheric CO<sub>2</sub>: dose–response curves for 85 traits ranging from  
**3239** the molecular to the whole-plant level. *New Phytologist* 233(4), 1560–1596.
- 3240** Prentice, I. C., N. Dong, S. M. Gleason, V. Maire, and I. J. Wright (2014).

- 3241** Balancing the costs of carbon gain and water transport: testing a new theo-  
**3242** retical framework for plant functional ecology. *Ecology Letters* 17(1), 82–91.
- 3243** Prentice, I. C., X. Liang, B. E. Medlyn, and Y.-P. Wang (2015). Reliable, ro-  
**3244** bust and realistic: The three R's of next-generation land-surface modelling.  
**3245** *Atmospheric Chemistry and Physics* 15, 5987–6005.
- 3246** Priestley, C. H. B. and R. J. Taylor (1972). On the Assessment of Surface  
**3247** Heat Flux and Evaporation Using Large-Scale Parameters. *Monthly Weather  
Review* 100(2), 81–92.
- 3249** Querejeta, J. I., I. Prieto, C. Armas, F. Casanoves, J. S. Diémé, M. Diouf,  
**3250** H. Yossi, B. Kaya, F. I. Pugnaire, and G. M. Rusch (2022). Higher leaf  
**3251** nitrogen content is linked to tighter stomatal regulation of transpiration  
**3252** and more efficient water use across dryland trees. *New Phytologist* 235(4),  
**3253** 1351–1364.
- 3254** R Core Team (2021). R: A language and environment for statistical computing.
- 3255** Raich, J. W., D. A. Clark, L. Schwendenmann, and T. E. Wood (2014). Above-  
**3256** ground tree growth varies with belowground carbon allocation in a tropical  
**3257** rainforest environment. *PLoS ONE* 9(6), e100275.
- 3258** Rastetter, E. B., P. M. Vitousek, C. B. Field, G. R. Shaver, D. Herbert, and  
**3259** G. I. Ågren (2001). Resource optimization and symbiotic nitrogen fixation.  
**3260** *Ecosystems* 4(4), 369–388.
- 3261** Reich, P. B. (2014). The world-wide 'fast-slow' plant economics spectrum: a  
**3262** traits manifesto. *Journal of Ecology* 102(2), 275–301.
- 3263** Reich, P. B., S. E. Hobbie, T. Lee, D. S. Ellsworth, J. B. West, D. Tilman,

- 3264 J. M. H. Knops, S. Naeem, and J. Trost (2006). Nitrogen limitation con-  
3265 strains sustainability of ecosystem response to CO<sub>2</sub>. *Nature* 440(7086), 922–925.
- 3267 Reichman, G. A., D. L. Grunes, and F. G. Viets (1966). Effect of Soil Mois-  
3268 ture on Ammonification and Nitrification in Two Northern Plains Soils. *Soil*  
3269 *Science Society of America Journal* 30(3), 363–366.
- 3270 Rhine, E. D., R. L. Mulvaney, E. J. Pratt, and G. K. Sims (1998). Improving  
3271 the Berthelot reaction for determining ammonium in soil extracts and water.  
3272 *Soil Science Society of America Journal* 62(2), 473.
- 3273 Rogers, A. (2014). The use and misuse of  $V_{\text{cmax}}$  in Earth System Models. *Pho-*  
3274 *tosynthesis Research* 119(1-2), 15–29.
- 3275 Rogers, A., B. E. Medlyn, J. S. Dukes, G. B. Bonan, S. Caemmerer, M. C.  
3276 Dietze, J. Kattge, A. D. B. Leakey, L. M. Mercado, Ü. Niinemets, I. C.  
3277 Prentice, S. P. Serbin, S. Sitch, D. A. Way, and S. Zaehle (2017). A roadmap  
3278 for improving the representation of photosynthesis in Earth system models.  
3279 *New Phytologist* 213(1), 22–42.
- 3280 Saathoff, A. J. and J. Welles (2021). Gas exchange measurements in the un-  
3281 steady state. *Plant Cell and Environment* 44(11), 3509–3523.
- 3282 Sage, R. F. and R. W. Pearcy (1987). The nitrogen use efficiency of C<sub>3</sub> and C<sub>4</sub>  
3283 plants: I. Leaf nitrogen, growth, and biomass partitioning in *Chenopodium*  
3284 *album* (L.) and *Amaranthus retroflexus* (L.). *Plant Physiology* 84(3), 954–  
3285 958.
- 3286 Saleh, A. M., M. Abdel-Mawgoud, A. R. Hassan, T. H. Habeeb, R. S. Yehia,

- 3287 and H. AbdElgawad (2020). Global metabolic changes induced by arbuscular  
3288 mycorrhizal fungi in oregano plants grown under ambient and elevated levels  
3289 of atmospheric CO<sub>2</sub>. *Plant Physiology and Biochemistry* 151, 255–263.
- 3290 Saxton, K. E. and W. J. Rawls (2006). Soil water characteristic estimates by  
3291 texture and organic matter for hydrologic solutions. *Soil Science Society of  
3292 America Journal* 70(5), 1569–1578.
- 3293 Schaefer, K., C. R. Schwalm, C. Williams, M. A. Arain, A. Barr, J. M. Chen,  
3294 K. J. Davis, D. Dimitrov, T. W. Hilton, D. Y. Hollinger, E. Humphreys,  
3295 B. Poulter, B. M. Racza, A. D. Richardson, A. Sahoo, P. Thornton, R. Var-  
3296 gas, H. Verbeeck, R. Anderson, I. Baker, T. A. Black, P. Bolstad, J. Chen,  
3297 P. S. Curtis, A. R. Desai, M. C. Dietze, D. Dragoni, C. M. Gough, R. F.  
3298 Grant, L. Gu, A. K. Jain, C. Kucharik, B. E. Law, S. Liu, E. Lokipitiya,  
3299 H. A. Margolis, R. Matamala, J. H. McCaughey, R. Monson, J. W. Munger,  
3300 W. Oechel, C. Peng, D. T. Price, D. Ricciuto, W. J. Riley, N. Roulet,  
3301 H. Tian, C. Tonitto, M. Torn, E. Weng, and X. Zhou (2012). A model-  
3302 data comparison of gross primary productivity: Results from the North  
3303 American Carbon Program site synthesis. *Journal of Geophysical Research:  
3304 Biogeosciences* 117(G3), G03010.
- 3305 Schmitt, M. R. and G. E. Edwards (1981). Photosynthetic capacity and nitrogen  
3306 use efficiency of maize, wheat, and rice: A comparison between C<sub>3</sub> and C<sub>4</sub>  
3307 photosynthesis. *Journal of Experimental Botany* 32(3), 459–466.
- 3308 Schneider, C. A., W. S. Rasband, and K. W. Eliceiri (2012). NIH Image to  
3309 ImageJ: 25 years of image analysis. *Nature Methods* 9(7), 671–675.
- 3310 Scott, H. G. and N. G. Smith (2022). A Model of C4 Photosynthetic Acclimation

- 3311** Based on Least-Cost Optimality Theory Suitable for Earth System Model  
**3312** Incorporation. *Journal of Advances in Modeling Earth Systems* 14(3), 1–16.
- 3313** Shi, M., J. B. Fisher, E. R. Brzostek, and R. P. Phillips (2016). Carbon cost  
**3314** of plant nitrogen acquisition: Global carbon cycle impact from an improved  
**3315** plant nitrogen cycle in the Community Land Model. *Global Change Biol-*  
**3316** *ogy* 22(3), 1299–1314.
- 3317** Shi, M., J. B. Fisher, R. P. Phillips, and E. R. Brzostek (2019). Neglecting  
**3318** plant–microbe symbioses leads to underestimation of modeled climate im-  
**3319** pacts. *Biogeosciences* 16(2), 457–465.
- 3320** Smith, B., D. Wärllind, A. Arneth, T. Hickler, P. Leadley, J. Siltberg, and  
**3321** S. Zaehle (2014). Implications of incorporating N cycling and N limitations  
**3322** on primary production in an individual-based dynamic vegetation model.  
**3323** *Biogeosciences* 11(7), 2027–2054.
- 3324** Smith, N. G. and J. S. Dukes (2013). Plant respiration and photosynthesis in  
**3325** global-scale models: incorporating acclimation to temperature and CO<sub>2</sub>.  
**3326** *Global Change Biology* 19(1), 45–63.
- 3327** Smith, N. G. and T. F. Keenan (2020). Mechanisms underlying leaf photosyn-  
**3328** thetic acclimation to warming and elevated CO<sub>2</sub> as inferred from least-cost  
**3329** optimality theory. *Global Change Biology* 26(9), 5202–5216.
- 3330** Smith, N. G., T. F. Keenan, I. C. Prentice, H. Wang, I. J. Wright, Ü. Niinemets,  
**3331** K. Y. Crous, T. F. Domingues, R. Guerrieri, F. oko Ishida, J. Kattge, E. L.  
**3332** Kruger, V. Maire, A. Rogers, S. P. Serbin, L. Tarvainen, H. F. Togashi,  
**3333** P. A. Townsend, M. Wang, L. K. Weerasinghe, and S.-X. Zhou (2019).  
**3334** Global photosynthetic capacity is optimized to the environment. *Ecology*

- 3335** *Letters* 22(3), 506–517.
- 3336** Smith, N. G., D. L. Lombardozzi, A. Tawfik, G. B. Bonan, and J. S. Dukes
- 3337** (2017). Biophysical consequences of photosynthetic temperature acclimation
- 3338** for climate. *Journal of Advances in Modeling Earth Systems* 9(1), 536–547.
- 3339** Smith, N. G., S. L. Malyshev, E. Shevliakova, J. Kattge, and J. S. Dukes
- 3340** (2016). Foliar temperature acclimation reduces simulated carbon sensitivity
- 3341** to climate. *Nature Climate Change* 6(4), 407–411.
- 3342** Smith, S. E. and D. J. Read (2008). *Mycorrhizal Symbiosis*. Academic Press.
- 3343** Soil Survey Staff (2022). Web Soil Survey.
- 3344** Soudzilovskaia, N. A., J. C. Douma, A. A. Akhmetzhanova, P. M. van Bode-
- 3345** gom, W. K. Cornwell, E. J. Moens, K. K. Treseder, and J. H. C. Cornelissen
- 3346** (2015). Global patterns of plant root colonization intensity by mycorrhizal
- 3347** fungi explained by climate and soil chemistry. *Global Ecology and Biogeog-*
- 3348** *raphy* 24(3), 371–382.
- 3349** Stark, J. M. and M. K. Firestone (1995). Mechanisms for soil moisture ef-
- 3350** fects on activity of nitrifying bacteria. *Applied and Environmental Microbi-*
- 3351** *ology* 61(1), 218–221.
- 3352** Stocker, B. D., H. Wang, N. G. Smith, S. P. Harrison, T. F. Keenan, D. San-
- 3353** doval, T. Davis, and I. C. Prentice (2020). P-model v1.0: An optimality-
- 3354** based light use efficiency model for simulating ecosystem gross primary pro-
- 3355** duction. *Geoscientific Model Development* 13(3), 1545–1581.
- 3356** Stocker, B. D., J. Zscheischler, T. F. Keenan, I. C. Prentice, J. Peñuelas, and
- 3357** S. I. Seneviratne (2018). Quantifying soil moisture impacts on light use

- 3358 efficiency across biomes. *New Phytologist* 218(4), 1430–1449.
- 3359 Sulman, B. N., D. T. Roman, K. Yi, L. Wang, R. P. Phillips, and K. A.  
3360 Novick (2016). High atmospheric demand for water can limit forest car-  
3361 bon uptake and transpiration as severely as dry soil. *Geophysical Research  
Letters* 43(18), 9686–9695.
- 3363 Sulman, B. N., E. Shevliakova, E. R. Brzostek, S. N. Kivlin, S. L. Malyshev,  
3364 D. N. L. Menge, and X. Zhang (2019). Diverse mycorrhizal associations  
3365 enhance terrestrial C storage in a global model. *Global Biogeochemical Cy-  
3366 cles* 33(4), 501–523.
- 3367 Sweet, S. K., D. W. Wolfe, A. DeGaetano, and R. Benner (2017). Anatomy  
3368 of the 2016 drought in the Northeastern United States: Implications for  
3369 agriculture and water resources in humid climates. *Agricultural and Forest  
3370 Meteorology* 247, 571–581.
- 3371 Taylor, B. N. and D. N. L. Menge (2018). Light regulates tropical symbiotic  
3372 nitrogen fixation more strongly than soil nitrogen. *Nature Plants* 4(9), 655–  
3373 661.
- 3374 Terrer, C., S. Vicca, B. A. Hungate, R. P. Phillips, and I. C. Prentice (2016).  
3375 Mycorrhizal association as a primary control of the CO<sub>2</sub> fertilization effect.  
3376 *Science* 353(6294), 72–74.
- 3377 Terrer, C., S. Vicca, B. D. Stocker, B. A. Hungate, R. P. Phillips, P. B. Reich,  
3378 A. C. Finzi, and I. C. Prentice (2018). Ecosystem responses to elevated CO<sub>2</sub>  
3379 governed by plant–soil interactions and the cost of nitrogen acquisition. *New  
3380 Phytologist* 217(2), 507–522.

- 3381 Thieurmel, B. and A. Elmarhraoui (2019). suncalc: Compute sun position,  
3382 sunlight phases, moon position, and lunar phase.
- 3383 Thomas, R. Q., E. N. J. Brookshire, and S. Gerber (2015). Nitrogen limita-  
3384 tion on land: how can it occur in Earth system models? *Global Change  
3385 Biology* 21(5), 1777–1793.
- 3386 Thomas, R. Q., S. Zaehle, P. H. Templer, and C. L. Goodale (2013). Global pat-  
3387 terns of nitrogen limitation: confronting two global biogeochemical models  
3388 with observations. *Global Change Biology* 19(10), 2986–2998.
- 3389 Thornton, P. E., J.-F. Lamarque, N. A. Rosenbloom, and N. M. Mahowald  
3390 (2007). Influence of carbon-nitrogen cycle coupling on land model response  
3391 to CO<sub>2</sub> fertilization and climate variability. *Global Bioge-  
3392 ochemical Cycles* 21(4), GB4018.
- 3393 Tingey, D. T., D. L. Phillips, and M. G. Johnson (2000). Elevated CO<sub>2</sub> and  
3394 conifer roots: effects on growth, life span and turnover. *New Phytolo-  
3395 gist* 147(1), 87–103.
- 3396 Udvardi, M. and P. S. Poole (2013). Transport and metabolism in legume-  
3397 rhizobia symbioses. *Annual Review of Plant Biology* 64, 781–805.
- 3398 USDA NRCS (2022). The PLANTS Database.
- 3399 Uselman, S. M., R. G. Qualls, and R. B. Thomas (2000). Effects of increased  
3400 atmospheric CO<sub>2</sub>, temperature, and soil N availability on root exudation  
3401 of dissolved organic carbon by an N-fixing tree (*Robinia pseudoacacia* L.).  
3402 *Plant and Soil* 222, 191–202.
- 3403 van Diepen, L. T. A., E. A. Lilleskov, K. S. Pregitzer, and R. M. Miller (2007).

- 3404** Decline of arbuscular mycorrhizal fungi in northern hardwood forests exposed to chronic nitrogen additions. *New Phytologist* 176(1), 175–183.
- 3405**
- 3406** Vance, C. P. and G. H. Heichel (1991). Carbon in N<sub>2</sub> fixation: Limitation or
- 3407** exquisite adaptation. *Annual Review of Plant Physiology and Plant Molecular Biology* 42(1), 373–392.
- 3408**
- 3409** Viet, H. D., J.-H. Kwak, K.-S. Lee, S.-S. Lim, M. Matsushima, S. X. Chang,
- 3410** K.-H. Lee, and W.-J. Choi (2013). Foliar chemistry and tree ring δ<sup>13</sup>C of
- 3411** *Pinus densiflora* in relation to tree growth along a soil pH gradient. *Plant*
- 3412** *and Soil* 363(1-2), 101–112.
- 3413** Vitousek, P. M., K. Cassman, C. C. Cleveland, T. Crews, C. B. Field, N. B.
- 3414** Grimm, R. W. Howarth, R. Marino, L. Martinelli, E. B. Rastetter, and
- 3415** J. I. Sprent (2002). Towards an ecological understanding of biological nitrogen fixation. In *The Nitrogen Cycle at Regional to Global Scales*, pp. 1–45.
- 3416** Springer Netherlands.
- 3417**
- 3418** Vitousek, P. M. and R. W. Howarth (1991). Nitrogen limitation on land and in
- 3419** the sea: How can it occur? *Biogeochemistry* 13(2), 87–115.
- 3420** Vitousek, P. M., S. Porder, B. Z. Houlton, and O. A. Chadwick (2010).
- 3421** Terrestrial phosphorus limitation: mechanisms, implications, and nitro-
- 3422** gen–phosphorus interactions. *Ecological Applications* 20(1), 5–15.
- 3423** Walker, A. P., A. P. Beckerman, L. Gu, J. Kattge, L. A. Cernusak, T. F.
- 3424** Domingues, J. C. Scales, G. Wohlfahrt, S. D. Wullschleger, and F. I. Woodward (2014). The relationship of leaf photosynthetic traits - V<sub>cmax</sub> and J<sub>max</sub> - to leaf nitrogen, leaf phosphorus, and specific leaf area: a meta-analysis
- 3425**
- 3426** and modeling study. *Ecology and Evolution* 4(16), 3218–3235.
- 3427**

- 3428** Wang, H., I. C. Prentice, T. F. Keenan, T. W. Davis, I. J. Wright, W. K.  
**3429** Cornwell, B. J. Evans, and C. Peng (2017). Towards a universal model for  
**3430** carbon dioxide uptake by plants. *Nature Plants* 3(9), 734–741.
- 3431** Wang, H., I. C. Prentice, I. J. Wright, D. I. Warton, S. Qiao, X. Xu, J. Zhou,  
**3432** K. Kikuzawa, and N. C. Stenseth (2023). Leaf economics fundamentals ex-  
**3433** plained by optimality principles. *Science Advances* 9(3), eadd566.
- 3434** Wang, J., J. M. Knops, C. E. Brassil, and C. Mu (2017). Increased productivity  
**3435** in wet years drives a decline in ecosystem stability with nitrogen additions  
**3436** in arid grasslands. *Ecology* 98(7), 1779–1786.
- 3437** Wang, W., Y. Wang, G. Hoch, Z. Wang, and J. Gu (2018). Linkage of root mor-  
**3438** phology to anatomy with increasing nitrogen availability in six temperate  
**3439** tree species. *Plant and Soil* 425(1-2), 189–200.
- 3440** Weatherburn, M. W. (1967). Phenol-hypochlorite reaction for determination of  
**3441** ammonia. *Analytical Chemistry* 39(8), 971–974.
- 3442** Wellburn, A. R. (1994). The spectral determination of chlorophylls a and b, as  
**3443** well as total carotenoids, using various solvents with spectrophotometers of  
**3444** different resolution. *Journal of Plant Physiology* 144(3), 307–313.
- 3445** Wen, Z., P. J. White, J. Shen, and H. Lambers (2022). Linking root exuda-  
**3446** tion to belowground economic traits for resource acquisition. *New Phytolo-*  
**3447** *gist* 233(4), 1620–1635.
- 3448** Westerband, A. C., I. J. Wright, V. Maire, J. Paillassa, I. C. Prentice, O. K.  
**3449** Atkin, K. J. Bloomfield, L. A. Cernusak, N. Dong, S. M. Gleason, C. Guil-  
**3450** herme Pereira, H. Lambers, M. R. Leishman, Y. Malhi, and R. H. Nolan

- 3451 (2023). Coordination of photosynthetic traits across soil and climate gradients. *Global Change Biology* 29(3), 1–29.
- 3452
- 3453 Wieder, W. R., C. C. Cleveland, W. K. Smith, and K. Todd-Brown (2015).
- 3454 Future productivity and carbon storage limited by terrestrial nutrient availability. *Nature Geoscience* 8(6), 441–444.
- 3455
- 3456 Wieder, W. R., D. M. Lawrence, R. A. Fisher, G. B. Bonan, S. J. Cheng, C. L.
- 3457 Goodale, A. S. Grandy, C. D. Koven, D. L. Lombardozzi, K. W. Oleson,
- 3458 and R. Q. Thomas (2019). Beyond static benchmarking: using experimental
- 3459 manipulations to evaluate land model assumptions. *Global Biogeochemical*
- 3460 *Cycles* 33(10), 1289–1309.
- 3461 Wright, I. J., P. B. Reich, and M. Westoby (2003). Least-cost input mixtures
- 3462 of water and nitrogen for photosynthesis. *The American Naturalist* 161(1),
- 3463 98–111.
- 3464 Wright, I. J., P. B. Reich, M. Westoby, D. D. Ackerly, Z. Baruch, F. Bongers,
- 3465 J. Cavender-Bares, T. Chapin, J. H. C. Cornelissen, M. Diemer, J. Flexas,
- 3466 E. Garnier, P. K. Groom, J. Gulias, K. Hikosaka, B. B. Lamont, T. Lee,
- 3467 W. Lee, C. Lusk, J. J. Midgley, M.-L. Navas, Ü. Niinemets, J. Oleksyn,
- 3468 N. Osada, H. Poorter, P. Poot, L. Prior, V. I. Pyankov, C. Roumet, S. C.
- 3469 Thomas, M. G. Tjoelker, E. J. Veneklaas, and R. Villar (2004). The world-
- 3470 wide leaf economics spectrum. *Nature* 428(6985), 821–827.
- 3471 Xu-Ri and I. C. Prentice (2017). Modelling the demand for new nitrogen fixation
- 3472 by terrestrial ecosystems. *Biogeosciences* 14(7), 2003–2017.
- 3473 Yahdjian, L., L. A. Gherardi, and O. E. Sala (2011). Nitrogen limitation in
- 3474 arid-subhumid ecosystems: A meta-analysis of fertilization studies. *Journal*

- 3475**      *of Arid Environments* 75(8), 675–680.
- 3476**      Zaehle, S., B. E. Medlyn, M. G. De Kauwe, A. P. Walker, M. C. Dietze, T. Hick-
- 3477**      ler, Y. Luo, Y. P. Wang, B. El-Masri, P. Thornton, A. Jain, S. Wang,
- 3478**      D. Warlind, E. Weng, W. Parton, C. M. Iversen, A. Gallet-Budynek, H. Mc-
- 3479**      carthy, A. C. Finzi, P. J. Hanson, I. C. Prentice, R. Oren, and R. J. Norby
- 3480**      (2014). Evaluation of 11 terrestrial carbon-nitrogen cycle models against
- 3481**      observations from two temperate Free-Air CO<sub>2</sub> Enrichment studies. *New*
- 3482**      *Phytologist* 202(3), 803–822.
- 3483**      Zaehle, S., S. Sitch, B. Smith, and F. Hatterman (2005). Effects of parame-
- 3484**      ter uncertainties on the modeling of terrestrial biosphere dynamics. *Global*
- 3485**      *Biogeochemical Cycles* 19(3), GB3020.
- 3486**      Zhu, Q., W. J. Riley, J. Tang, N. Collier, F. M. Hoffman, X. Yang, and G. Bisht
- 3487**      (2019). Representing nitrogen, phosphorus, and carbon interactions in the
- 3488**      E3SM land model: development and global benchmarking. *Journal of Ad-*
- 3489**      *vances in Modeling Earth Systems* 11(7), 2238–2258.
- 3490**      Ziegler, C., M. E. Dusenge, B. Nyirambangutse, E. Zibera, G. Wallin, and
- 3491**      J. Uddling (2020). Contrasting Dependencies of Photosynthetic Capacity
- 3492**      on Leaf Nitrogen in Early- and Late-Successional Tropical Montane Tree
- 3493**      Species. *Frontiers in Plant Science* 11, 1–12.
- 3494**      Ziehn, T., J. Kattge, W. Knorr, and M. Scholze (2011). Improving the pre-
- 3495**      dictability of global CO<sub>2</sub> assimilation rates under climate change. *Geophys-*
- 3496**      *ical Research Letters* 38(10), L10404.